

Switzerland

Swiss Geodetic Commission



Suisse

Commission Géodésique Suisse

**Swiss National Report on the
GEODETIC ACTIVITIES
in the years 2015 to 2019**

Presented to the XXVII General Assembly
of the International Union of Geodesy and Geophysics
in Montreal, Canada, July 2019



**Rapport National Suisse sur les
ACTIVITÉS GÉODÉSIQUES
exécutées de 2015 à 2019**

Présenté à la vingt-septième Assemblée générale
de l'Union Géodésique et Géophysique Internationale
tenue à Montréal, Canada, Juillet 2019

Zurich 2019

Swiss Geodetic Commission/Commission Géodésique Suisse

ETH Zurich

Robert-Gnehm-Weg 15

8093 Zurich

Switzerland

<http://www.sgc.ethz.ch/publications>

Edited by:

J. Mueller-Gantenbein

E. Brockmann

U. Marti

M. Rothacher

B. Merminod

Secretary of the SGC

(Commission 1)

(Commission 2)

(Commission 3)

(Commission 4)

In addition to the bibliographies at the end of each section we recommend the following
www-sites:

Astronomical Institute of the University of Bern (AIUB): <http://www.aiub.unibe.ch/>

Institute of Geodesy and Photogrammetry,
Eidgenössische Technische Hochschule, ETH Zurich: <http://www.igp.ethz.ch/>

Office federal de topographie (swisstopo)
Federal Office of Topography (swisstopo): <http://www.swisstopo.ch/>

Geodetic Engineering Laboratory,
École polytechnique fédérale de Lausanne EPFL: <http://topo.epfl.ch/>

Haute Ecole d'Ingénierie et de Gestion du Canton de Vaud: <http://www.heig-vd.ch/>

University of Applied Sciences Northwestern Switzerland,
Fachhochschule Nordwestschweiz: <http://www.fhnw.ch/>

ISBN 978-3-908440-48-2

Printed by: adag, Zurich

©2019 Swiss Geodetic Commission

PREFACE

The Swiss Geodetic Commission (SGC) is an organisation within the Swiss Academy of Sciences (SCNAT). It is devoted to research into scientific problems of geodesy including the transfer to practical applications in national surveying. Of particular importance is the promotion of international cooperation and national coordination. The SGC has close links to the Swiss Geophysical Commission, in particular in the field of gravimetry where research projects are being pursued jointly on an interdisciplinary basis.

For the compilation of the national report covering the scientific activities of the past 4 years it was decided to follow the structure of previous national reports and divide it into 4 commissions according to the structure of the International Association of Geodesy (IAG):

- 1 Reference Frames
- 2 Gravity Field
- 3 Earth Rotation and Geodynamics
- 4 Positioning & Applications

These main chapters were compiled by an editorial staff consisting of E. Brockmann (Commission 1), U. Marti (Commission 2), M. Rothacher (Commission 3), B. Merminod (Commission 4). Our special thanks go to J. Mueller-Gantenbein, secretary of SGC, for the careful editing and preparation of the layout. Without her efforts this report could not have been realized in due time.

The SGC expresses its appreciative thanks to all colleagues who have contributed to this report and who are promoting Geodetic Sciences in Switzerland. Financial support was provided by the SCNAT. Its valuable help is gratefully acknowledged.

On behalf of the Swiss Geodetic Commission, June 2019

Urs Marti
Vice-President of SGC

Alain Geiger
President of SGC

1	REFERENCE FRAMES	7
	SATELLITE LASER RANGING AT ZIMMERWALD	7
	<i>E. Cordelli¹, P. Lauber¹, T. Schildknecht¹, M. Prohaska¹, E. Brockmann², A. Jäggi¹</i>	
	CODE CONTRIBUTIONS TO THE IGS.....	10
	<i>S. Schaer^{1,2}, D. Arnold¹, R. Dach¹, L. Prange¹, D. Sidorov¹, P. Stebler¹, A. Sušnik^{1,3}, A. Villiger¹, A. Jäggi¹</i>	
	EUREF ACTIVITIES AT CODE	13
	<i>S. Schaer^{1,2}, D. Arnold¹, R. Dach¹, L. Prange¹, D. Sidorov¹, P. Stebler¹, A. Sušnik^{1,3}, A. Villiger¹, A. Jäggi¹</i>	
	GNSS REPROCESSING RESULTS IN THE FRAMEWORK OF THE EGSIM PROJECT	15
	<i>A. Sušnik^{1,2}, A. Grahs¹, D. Arnold¹, A. Villiger¹, R. Dach¹, A. Jäggi¹, G. Beutler¹</i>	
	CODE FIVE SYSTEM SOLUTION FOR THE IGS MGEX	19
	<i>L. Prange¹, D. Arnold¹, R. Dach¹, S. Schaer^{1,2}, D. Sidorov¹, P. Stebler¹, A. Sušnik^{1,3}, A. Villiger¹</i>	
	AIUB CONTRIBUTION TO THE GRSP	22
	<i>L. Prange, P. Stebler, A. Sušnik, E. Orliac, R. Dach</i>	
	THE SWISS OPTICAL GROUND STATION AND GEODYNAMICS OBSERVATORY ZIMMERWALD.....	24
	<i>E. Cordelli¹, T. Schildknecht¹, A. Jäggi¹, E. Brockmann²</i>	
	EVALUATION OF ITRF2014 SOLUTIONS	30
	<i>R. Dach¹, A. Sušnik^{1,2}, A. Grahs¹, A. Villiger¹, D. Arnold¹, A. Jäggi¹</i>	
	IMPROVING GLONASS ORBIT QUALITY BY RE-ESTIMATING SATELLITE ANTENNA OFFSETS	34
	<i>R. Dach¹, A. Sušnik^{1,2}, A. Grahs¹, A. Villiger¹, D. Arnold¹, L. Prange¹, S. Schaer^{1,3}, A. Jäggi¹</i>	
	ADVANCING THE ORBIT MODEL FOR GALILEO SATELLITES DURING THE ECLIPSE SEASONS.....	38
	<i>D. Sidorov, R. Dach, L. Prange, A. Jäggi</i>	
	VALIDATING THE USE OF A SCALABLE BOXWING MODEL FOR GNSS SATELLITES	40
	<i>L. McNair, A. Villiger, R. Dach, A. Jäggi</i>	
	AN EMPIRICAL SRP MODEL FOR THE ORBIT NORMAL ATTITUDE MODE.....	44
	<i>L. Prange¹, G. Beutler¹, R. Dach¹, D. Arnold¹, S. Schaer^{1,2}, A. Villiger¹, A. Jäggi¹</i>	
	SATELLITE LASER RANGING TO LOW EARTH ORBITERS – ORBIT AND NETWORK VALIDATION	46
	<i>D. Arnold¹, O. Montenbruck², S. Hackel², K. Sošnica³</i>	
	THE EFFECT OF SLR TRACKING SCENARIOS TO GNSS SATELLITES IN A COMBINED.....	49
	<i>F. Andritsch, U. Meyer, R. Dach, T. Schildknecht, A. Jäggi</i>	
	A SIMULATION TOOLKIT FOR SATELLITE LASER	51
	<i>M. Meindl, C. Lanegger, M. Rothacher</i>	
	ANALYSIS OF THE SHORT VLBI BASELINE AT THE WETTZELL OBSERVATORY	53
	<i>I. Herrera-Pinzón¹, M. Rothacher¹, J. Kodet², U. Schreiber²</i>	
	INVESTIGATIONS ON TIME DISSEMINATION FOR VLBI OBSERVATIONS AT THE WETTZELL OBSERVATORY	55
	<i>I. Herrera-Pinzón¹, M. Rothacher¹, J. Kodet², U. Schreiber²</i>	
	MULTI-YEAR ANALYSIS OF GNSS SHORT BASELINES AT CO-LOCATION SITES	57
	<i>I. Herrera-Pinzón and M. Rothacher</i>	
	GNSS ANTENNA PHASE CENTER MODELING AND ITS IMPACT ON PRECISE ORBIT DETERMINATION OF THE SWARM SATELLITES.....	59
	<i>K. Chen, M. Rothacher</i>	

ABSOLUTE FIELD CALIBRATION SYSTEM FOR MULTI-GNSS RECEIVER ANTENNAS	62
<i>D. Willi^{1,2}, D. Koch¹, M. Meindl¹, M. Rothacher¹</i>	
CALIBRATION OF AN INDUSTRIAL ROBOT.....	64
<i>D. Willi^{1,2}, S. Guillaume¹, T. Januth¹</i>	
ANALYSIS OF PERMANENT GNSS NETWORKS AT SWISSTOPO (PNAC)	66
<i>E. Brockmann, D. Ineichen, S. Lutz, S. Schaer</i>	
MAINTENANCE OF THE CHTRF REFERENCE	70
<i>E. Brockmann, D. Ineichen, S. Lutz</i>	
EUREF WORKING GROUP ON “EUROPEAN DENSE VELOCITIES”	73
<i>E. Brockmann, S. Lutz</i>	
MULTI-GNSS ACTIVITIES AT SWISSTOPO.....	77
<i>S. Lutz, E. Brockmann, D. Ineichen, S. Schaer</i>	
EXTENDED MONITORING OF THE PNAC-ANALYSIS KEY PARAMETERS	79
<i>D. Ineichen, E. Brockmann, S. Lutz</i>	
TRANSITION OF REFERENCE FRAMES LV03 → LV95 («BEZUGSRAHMENWECHSEL», «CHANGEMENT DE CADRE DE RÉFÉRENCE MN03 - MN95»).....	81
<i>A. Wiget</i>	
GEODETIC REFERENCE DATASETS AND GIS DATA OF THE SWISS GEODETIC SURVEY (SWISSTOPO) AVAILABLE ON THE FEDERAL GEOPORTAL AND THE MAP VIEWER MAP.GEO.ADMIN.CH	84
<i>A. Wiget and M. Kistler</i>	
CHTRF2016: 4 TH RE-OBSERVATION OF THE NATIONAL GNSS NETWORK LV95	86
<i>A. Wiget, St. Beckel, E. Brockmann, J. Carrel, M. Kistler, U. Marti, A. Schlatter and U. Wild</i>	
MEASUREMENTS FOR THE NATIONAL HEIGHT SYSTEM	89
<i>A. Schlatter, A. Wiget, U. Marti, B. Mattli</i>	
IMPACT OF THE MODELING OF STATION CLOCKS ON GEODETIC PARAMETERS	91
<i>K. Wang^{1,2}, M. Rothacher¹</i>	
GEOCENTER VARIATIONS DERIVED FROM A COMBINED PROCESSING OF LEO AND GROUND-BASED GPS OBSERVATIONS	93
<i>B. Männel^{1,2}, M. Rothacher¹</i>	
KINEMATIC DETERMINATION OF GNSS ORBITS INCLUDING CLOCK MODELING	94
<i>D. Koch¹, M. Rothacher¹, M. Meindl¹, K. Wang^{1,2}</i>	
BIBLIOGRAPHY COMMISSION 1	97
2 GRAVITY FIELD.....	105
ABSOLUTE AND RELATIVE GRAVITY MEASUREMENTS.....	105
<i>U. Marti¹, H. Baumann² and S. Guillaume³</i>	
GRAVITY MEASUREMENTS FOR THE VERTICAL NETWORK	107
<i>U. Marti and A. Schlatter</i>	
GEOID DETERMINATION	109
<i>U. Marti</i>	
EUROPEAN GRAVITY FIELD SERVICE FOR IMPROVED EMERGENCY MANAGEMENT (EGSIEM)	111

	<i>A. Jäggi¹, M. Weigelt², F. Flechtner³, A. Güntner³, T. Mayer-Gürr⁴, S. Martinis⁵, S. Bruinsma⁶, J. Flury², S. Bourgogne⁷</i>	
COMBINATION SERVICE FOR TIME-VARIABLE GRAVITY FIELDS (COST-G).....		113
	<i>U. Meyer, B. Jenny, Y. Jean, A. Jäggi</i>	
COMBINATION OF MONTHLY SWARM GRAVITY FIELD SOLUTIONS		115
	<i>U. Meyer¹, D. Arnold¹, L. Schreiter¹, C. Dahle², A. Jäggi¹</i>	
MITIGATING ARTIFACTS IN SWARM GPS DATA FOR IMPROVED RECONSTRUCTION OF THE TOPSIDE IONOSPHERE AND PLASMASPHERE.....		117
	<i>L. Schreiter, D. Arnold, A. Jäggi</i>	
LUNAR GRAVITY FIELD SOLUTIONS COMPUTED AT AIUB		120
	<i>S. Bertone, D. Arnold, V. Girardin, A. Jäggi</i>	
AIUB-RL02: AN IMPROVED TIME-SERIES OF MONTHLY GRAVITY FIELDS FROM GRACE DATA		123
	<i>U. Meyer, A. Jäggi</i>	
LOW-DEGREE TIME-VARIABLE GRAVITY FIELDS FROM SATELLITE LASER RANGING.....		125
	<i>U. Meyer, A. Grahl, R. Dach, A. Jäggi</i>	
DEFLECTIONS OF THE VERTICAL MEASUREMENT THROUGH ROCKY MOUNTAINS FOR THE NGS WITH THE CODIAC ETH ZURICH SYSTEM.....		127
	<i>S. Guillaume, A. Wolf, B. Bürki</i>	
DEFLECTIONS OF THE VERTICAL MEASUREMENTS IN PERTH BY TU MUNICH WITH THE ETH ZURICH QDAEDALUS SYSTEM		129
	<i>S. Guillaume</i>	
BIBLIOGRAPHY COMMISSION 2		131
3 EARTH ROTATION AND GEODYNAMICS.....		135
CODE CONTRIBUTIONS TO EARTH ROTATION MONITORING		135
	<i>S. Schaer², R. Dach¹, A. Villiger¹, A. Jäggi¹</i>	
DEPENDENCY OF GEODYNAMIC PARAMETERS ON THE GNSS CONSTELLATION		137
	<i>S. Scaramuzza^{1,2}, R. Dach¹, G. Beutler¹, D. Arnold¹, A. Sušnik^{1,3}, A. Jäggi¹</i>	
THE FUTURE OF NATIONAL GNSS-GEOMONITORING INFRASTRUCTURES IN SWITZERLAND		140
	<i>J. Clinton¹, A. Geiger², S. Häberling², F. Haslinger¹, M. Rothacher², A. Wiget³ and U. Wild³</i>	
INSTANTANEOUS DETECTION OF HAZARDOUS GROUND MOVEMENTS WITH GNSS		142
	<i>R. Hohensinn, A. Geiger, M. Meindl and D. Willi</i>	
DETECTION AND LOCALIZATION OF EARTHQUAKES BY GNSS		144
	<i>R. Hohensinn and A. Geiger</i>	
CONSISTENCY OF PPP GPS AND STRONG-MOTION RECORDS: CASE STUDY OF Mw9.0 TOHOKU-OKI 2011 EARTHQUAKE.....		146
	<i>P. Psimoulis^{1,2}, N. Houlié^{2,3}, M. Meindl², and M. Rothacher²</i>	
PERFORMANCE OF HIGH-RATE GPS WAVEFORMS AT LONG PERIODS: MOMENT TENSOR INVERSION OF THE 2003 Mw8.3 TOKACHI-OKI EARTHQUAKE		148
	<i>K. Kelevitz^{1,2}, N. Houlié^{1,2}, D. Giardini¹ and M. Rothacher²</i>	
USE OF A GPS-DERIVED TROPOSPHERE MODEL TO IMPROVE INSAR DEFORMATION ESTIMATES IN THE SAN GABRIEL VALLEY, CALIFORNIA.....		149
	<i>Nicolas Houlié^{1,2}, Gareth J. Funning³, and Roland Bürgmann⁴</i>	

VERTICAL TECTONICS AT AN ACTIVE CONTINENTAL MARGIN	151
<i>N. Houlié^{1,2} and T.A. Stern³</i>	
THE POTENTIAL OF HIGH-RATE GPS FOR STRONG GROUND MOTION ASSESSMENT	153
<i>C. Michel¹, K. Kelevitz², N. Houlié², B. Edwards³, P. Psimoulis⁴, Z. Su⁵, and D. Giardini²</i>	
REAL-TIME MAGNITUDE CHARACTERIZATION OF LARGE EARTHQUAKES USING THE PREDOMINANT PERIOD DERIVED FROM 1HZ GPS DATA	155
<i>P. Psimoulis¹, N. Houlié^{2,3}, and Y. Behr⁴</i>	
DETECTION OF GROUND MOTIONS USING HIGH-RATE GPS TIME-SERIES	157
<i>P. A. Psimoulis¹, N. Houlié^{2,3,4}, M. Habboub¹, C. Michel⁴, M. Rothacher²</i>	
BIBLIOGRAPHY COMMISSION 3	159
4 POSITIONING AND APPLICATIONS	161
DRAGON 4: SNOW DEPTH AND SNOW WATER EQUIVALENT ESTIMATION BY USING REFLECTED AND REFRACTED GPS SIGNALS.....	161
<i>L. Steiner¹, W. Li², M.Meindl¹, Y. Zhu², A. Geiger¹, D. Yongkai²</i>	
SNOW WATER EQUIVALENT OBSERVATIONS USING REFRACTED GPS SIGNALS	163
<i>L. Steiner¹, M. Meindl¹, C. Marty², C.Fierz², A. Geiger¹</i>	
SPACE ENVIRONMENTAL TESTS OF LOW-COST GNSS RECEIVERS	165
<i>M. Meindl, M. Rothacher</i>	
A GNSS PAYLOAD WITH LOW-COST COMMERCIAL-OF-THE-SHELF RECEIVERS.....	167
<i>M. Meindl, F. Kreiliger, K. Chen, M. Rothacher</i>	
VISIBILITY BASED ATTITUDE DETERMINATION FOR SATELLITES	169
<i>M. Meindl, G. Tagliaferro, M. Rothacher</i>	
ATTITUDE DETERMINATION FOR CUBE SATELLITES.....	171
<i>D. Willi^{1,2}, M. Rothacher¹</i>	
ESTIMATION OF ANTENNA HEIGHT ABOVE SNOW-COVERED GLACIER SURFACE USING GNSS-REFLECTOMETRY	173
<i>L. Steiner¹, M. Baumann¹, M. Huss², A. Geiger¹</i>	
GNSS FLIGHT PERFORMANCE ASSESSMENT OF ENHANCED ROTORCRAFT OPERATIONS	175
<i>M. Troller¹, M. Scaramuzza¹, H. Wipf¹, M. Nyffenegger¹, H. Leibundgut², M. Bertschi³</i>	
IMPACT OF THE NAVIGATION PERFORMANCE IN MOUNTAINOUS AREA DUE TO THE GPS CONSTELLATION VARIATION	176
<i>M. Troller¹, M. Scaramuzza¹, P. Truffer¹, A. Geiger²</i>	
ASSESSMENT OF ENVIRONMENTAL-FRIENDLY GNSS-BASED CURVED APPROACH FLIGHT PROCEDURE	177
<i>M. Troller¹, M. Scaramuzza¹, M. Nyffenegger¹, S. Rami², M. Bertschi²,</i>	
JAMMING OF AVIATION GPS RECEIVERS: INVESTIGATION OF FIELD TRIALS PERFORMED WITH CIVIL AND MILITARY AIRCRAFT.	178
<i>P. Truffer¹, M. Scaramuzza¹, M. Troller¹, M. Bertschi²,</i>	
C/NO BASED GNSS RFI DETECTION ON-BOARD OF HELICOPTERS	180
<i>M. Scaramuzza¹, H. Wipf¹, M. Troller¹, H. Leibundgut², S. Rami³, R. Wittwer⁴</i>	
ASSESSMENT OF RFI IMPACT ON AVIATION GPS/SBAS RECEIVER PERFORMANCE.....	181
<i>M. Scaramuzza¹, P. Truffer¹, M. Troller¹, H. Wipf¹, H. Leibundgut², M. Bertschi³, S. Rami³</i>	

COMPARISON OF GNSS PERFORMANCE SIMULATION RESULTS WITH DATA RECORDED ONBOARD OF HELICOPTERS	182
<i>M. Scaramuzza¹, P. Truffer¹, M. Troller¹, H. Leibundgut², M. Bertschi³</i>	
CONTRIBUTIONS OF SWISSTOPO TO GNSS METEOROLOGY AND GNSS CLIMATOLOGY	183
<i>E. Brockmann, D. Ineichen, S. Lutz</i>	
REPROCESSED GNSS TIME SERIES OF TROPOSPHERE ZENITH WET DELAYS FOR CLIMATE	193
<i>H. Su and M. Rothacher</i>	
SWISS POSITIONING SERVICE (SWIPOS).....	196
<i>U. Wild, D. Andrey, C. Biberstein-Pedroni, L. Kislig and J. Liechti</i>	
AIUB CONTRIBUTION TO THE COPERNICUS POD SERVICE	199
<i>D. Arnold, V. Girardin, A. Jäggi</i>	
REPROCESSING OF THE GOCE PRECISE SCIENCE ORBITS	201
<i>D. Arnold¹, V. Sterken¹, Th. Grombein², L. Schreiter¹, A. Jäggi¹</i>	
BERNESE GNSS SOFTWARE.....	204
<i>R. Dach, P. Fridez, F. Andritsch, D. Arnold, S. Bertone, A. Grahl, V. Girardin, Y. Jean, M. Lasser, S. McNair, L. Mervart, U. Meyer, L. Prange, S. Scaramuzza, S. Schaer, L. Schreiter, D. Sidorov, P. Stebler, A. Sušnik, A. Villiger, A. Jäggi</i>	
CODE CONTRIBUTIONS TO GLOBAL IONOSPHERE MONITORING.....	206
<i>S. Schaer^{1,2}, A. Villiger¹</i>	
AMBIGUITY RESOLUTION IN ZERO-DIFFERENCE SOLUTIONS AND FOR PPP.....	209
<i>S. Schaer^{1,2}, A. Villiger¹, D. Arnold¹, L. Prange¹, R. Dach¹, A. Jäggi¹</i>	
DETERMINATION OF GNSS PSEUDO-ABSOLUTE CODE BIASES AND CLASSIFICATION OF RECEIVER TRACKING TECHNOLOGY	212
<i>A. Villiger¹, S. Schaer^{1,2}, R. Dach¹, L. Prange¹, A. Sušnik^{1,3}, A. Jäggi¹</i>	
CONSISTENCY OF ANTENNA PRODUCTS IN THE MGEX ENVIRONMENT	215
<i>A. Villiger¹, L. Prange¹, R. Dach¹, F. Zimmermann², H. Kuhlmann², A. Jäggi¹</i>	
CONTRIBUTIONS OF THE NATIONAL GEODETIC SURVEY (SWISSTOPO) AND OF THE GGL/MPG OF ETH ZÜRICH TO THE ALPTRANSIT GOTTHARD BASE TUNNEL.....	218
<i>A. Wiget¹, B. Bürki², A. Geiger², S. Guillaume², U. Marti¹ and A. Schlatter¹</i>	
INTEGRATED SENSOR ORIENTATION ON MICRO AERIAL VEHICLES.....	219
<i>M. Rehak, J. Skaloud</i>	
VEHICLE DYNAMIC MODEL BASED NAVIGATION FOR UAVS.....	220
<i>M. Khaghani, J. Skaloud</i>	
CALIBRATION ASPECTS OF INS NAVIGATION.....	221
<i>P. Clausen, J. Skaloud</i>	
OPTIMIZED LOW LEVEL TRAJECTORIES FOR INSTRUMENT FLIGHT RULES IN ALPINE AREAS	222
<i>R. Pott¹, S. Guillaume^{1,2}, A. Geiger¹, and H. Wipf^{3,4}</i>	
BIBLIOGRAPHY COMMISSION 4.....	225

1 Reference Frames

Satellite Laser Ranging at Zimmerwald

E. Cordelli¹, P. Lauber¹, T. Schildknecht¹, M. Prohaska¹, E. Brockmann², A. Jäggi¹

¹Astronomical Institute, University of Bern

²Federal Office of Topography swisstopo

The Zimmerwald SLR stations is providing standard ILRS SLR services on a 24/7 basis. The SLR system is constantly improved and its performance in terms of target acquisition and tracking has been improved by means of a so-called Night-Tracking Camera. Building on the high flexibility of the SLR station, three very different types of measurements/experiments may be carried out and/or are currently under development: the ranging to space debris (with and without retroreflectors), the preparation for the European Laser Time Transfer experiment (ELT), and the collaboration with Institute of Applied Physics of University of Bern to set up a quantum physics experiment.

STANDARD ILRS SLR SERVICES

The Zimmerwald SLR station is part of the global tracking network of the International Laser Ranging (ILRS) and observes the ILRS satellites according to ILRS priorities on a 24/7 basis. Zimmerwald continues to be the most productive SLR station of the ILRS in the northern hemisphere second to Yarragadee only, a station in Australia. Current developments are focusing on the improvement of the accuracy of the delivered range measurements, both, in terms of achieving smaller observation rms, and reducing the biases. The latter includes the improvement of the calibration measurements.

Evaluations for replacing the current 100Hz laser system with a KHz laser are under way. At the same time, we should be able to shorten the pulse width of currently ~60ps by a factor of 10.

NIGHT-TRACKING CAMERA

Currently there are about 90 satellites tracked regularly by the SLR stations of the ILRS community. This amount of satellites together with the use of the SLR telescopes for different projects, requires the optimization of the station performance in terms of target acquisition and tracking. A first analysis after the integration of the night-tracking camera into ZIMLAT SLR system has shown an improvement in the observation efficiency thanks to the use of the tracking camera. The camera allows a faster satellite acquisition that results in an increased number of satellites tracked and an increased number of normal points acquired during an observation session.

The camera can be already used to acquire difficult targets like newly launched satellites and, in the frame of space debris studies, defunct and re-entering satellites whose ephemeris accuracy is poor.

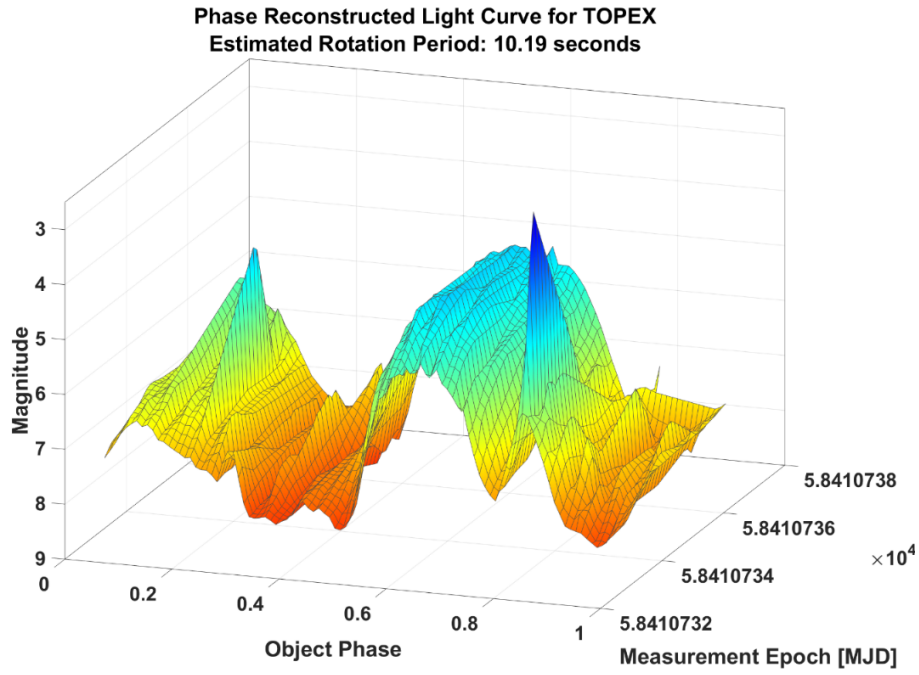


Figure 1. 1: Phase reconstructed light curve for a pass of TOPEX.

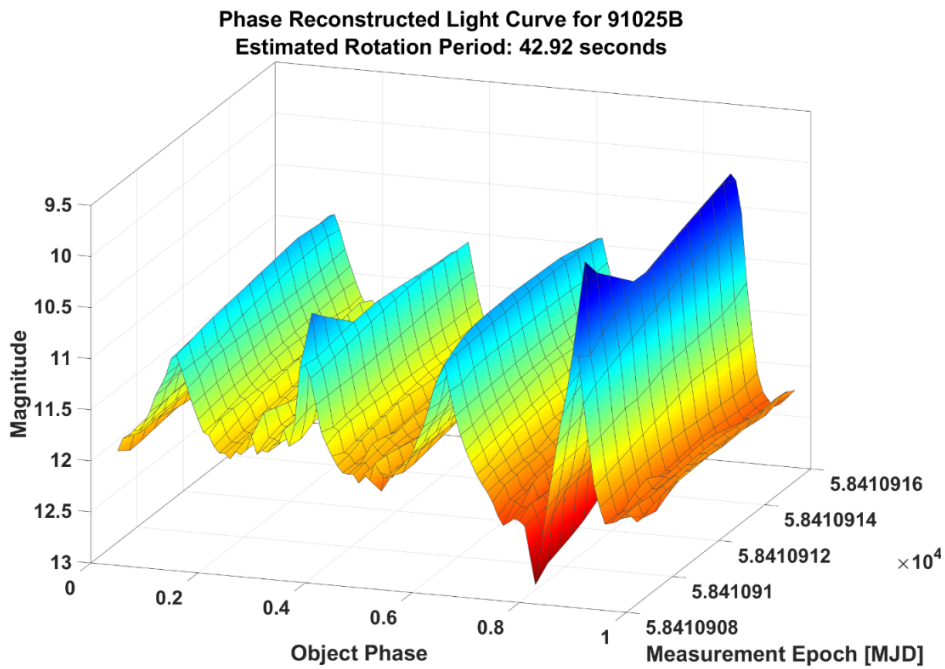


Figure 1. 2: Phase reconstructed light curve for a pass of defunct GLONASS satellite.

The camera, correcting the pointing of the telescope in real time, allows us to track LEO and MEO defunct satellites with our SLR system. The main outcomes of the tracking are the angular positions of the object in the sky (azimuth and elevation), its distance, and its brightness. All these measurements are acquired synchronously with the timing accuracy provided by the SLR system and can be used for both, the attitude, and the orbit determination of space debris. The angular measurements are obtained directly from the encoder readings of the telescope without any astrometric data reduction process, by applying a calibrated mount model. This does not produce the most accurate angular measurements but these measurements are extracted without requiring reference stars in the field of view, which is a big advantage when observing fast satellites with a telescope with a relatively small field of view.

Nevertheless, for the daily use of the tracking camera some automation steps are still needed. In particular, one could analyze the images and extract the object positions in real time so that the pointing corrections could be calculated and sent automatically to the telescope. Another improvement which can be added is the change of the correction type from azimuth and elevation to along- and cross-track corrections which will allow, in the case of poor ephemeris, the tracking of the object even once it is in the Earth shadow. Finally, one interesting aspect for which further investigations are needed is the possible application of the camera during daytime operations.

EUROPEAN LASER TIME TRANSFER (ELT)

For the ELT experiment in which we will participate in the future, it is required to fire laser pulses that are synchronized to UTC in order to hit the detector at the ISS during daytime with a small detector gate of 100 ns locked to the UTC time scale.

An ELT calibration procedure session together with the University of Prague has been carried out in order to determine one-way calibration constants, which are relevant for this one-way delay sensitive experiment. Significant one-way internal system calibration delays can now be expressed by ELT calibration constants and can in future be determined more easily using simple reproducible experiments without external calibration efforts.

To achieve a highly stable local time and frequency a maser has been installed.

To improve the UTC time scale precision from 100 ns to 15 ns, an additional GPS-receiver has been installed. The receiver is embedded into the system in such a way that the previously determined calibration constants should be preserved.

With the newly installed GPS-receiver and a time interval counter, the local time derived from the maser is now measured against GPS/UTC with a precision of 1 ns instead of 30 ns. SLR measurements provided to the ILRS are now tagged with epochs at 15 ns precision.

A very first source code part for the laser triggering software - which has not yet been implemented into the system - was written in order to consider the changing light travelling time to the ISS.

QUANTUM EXPERIMENT IN COLLABORATION WITH THE INSTITUTE OF APPLIED PHYSICS

Because the ZIMLAT SLR telescope optics are also prepared for infrared and the Institute of Applied Physics of the University Bern IAP has a CW entangled photon laser for infrared available, a quantum mechanics experiment was setup at the station as a starting point for the use of entangled photons in free space. The photon source was installed close to the telescope now. A retro reflector has been installed 659m from the telescope.

In the very near future for a very first experiment, the reflector should reflect back the entangled photons for coincidence tests at the telescope. The next step would be to extend this experiment to LEO satellites.

CODE Contributions to the IGS

S. Schaer^{1,2}, D. Arnold¹, R. Dach¹, L. Prange¹, D. Sidorov¹, P. Stebler¹, A. Sušnik^{1,3}, A. Villiger¹, A. Jäggi¹

¹ *Astronomical Institute, University of Bern*

² *Federal Office of Topography swisstopo*

³ *Now with: School of Civil Engineering and Geosciences, Newcastle University, Newcastle NE1 7RU, UK*

The consortium Center of Orbit Determination in Europe (CODE) consists of four institutions:

- Astronomical Institute of University Bern (AIUB), Switzerland
- Federal Office of Topography swisstopo, Switzerland
- Federal Agency of Cartography and Geodesy (BKG), Germany
- Ingenieurinstitut für Astronomische und Physikalische Geodäsie at Technische Universität München (IAPG/TUM), Germany

CODE is an Analysis Center (AC) of the International GNSS Service (IGS, Johnston et al., 2017) generating operationally series of Global Navigation Satellite System (GNSS) products since 1992. Since 2003, the contributions from CODE to the IGS are based on a rigorously combined analysis of GPS and GLONASS measurements in the legacy product chains. The major products are GNSS orbits, Earth orientation parameters (EOPs), receiver station coordinates, model parameters describing the troposphere and global ionosphere maps, phase-consistent satellite and receiver clock corrections (up to a time resolution of 5 seconds), and pseudo absolute code observable specific bias (OSB; former DCB: differential code biases). A complete list of all our products is available on our ftp server (ftp://ftp.aiub.unibe.ch/AIUB_AFTP.TXT).

We aim to deliver the best possible solutions to the IGS leading to a steady development of the processing routines and used software. Therefore, we use the development version of the Bernese GNSS Software (BSW, Dach et al., 2015), which is further developed and maintained at our institute. Because of this, we can benefit from the latest implementations and adapt the software in order to support the best possible processing strategies. A complete overview of the development steps during the covered reporting period can be obtained in the IGS technical reports (Dach et al. 2015, 2016, 2017, and 2018). The following improvements are a brief selection of the most important ones:

2015	<ul style="list-style-type: none"> • Rapid clock product extended from GPS only to GPS/GLONASS
2016	<ul style="list-style-type: none"> • Switch from a differential to pseudo absolute code observable specific bias parametrization (OSB) • RINEX 3 observation files are introduced for the final processing line
2017	<ul style="list-style-type: none"> • Redesign of CODEs IGS final clock product the clocks are now based on more than 300 stations including GPS and GLONASS • Switch from ITRF2008 to ITRF2014 • Multi-GNSS Extension (MGEX, Montenbruck et al., 2013) processing line including GPS, Galileo, GLONASS, Beidou and QZSS became operational (sampling of satellite positions in the orbit solution file 300 seconds; satellite clock corrections (30 second)
2018	<ul style="list-style-type: none"> • MGEX: Ambiguity resolution for Galileo and BeiDou (in addition to GPS) • RINEX 3 observation files are introduced for the Rapid and Ultra-rapid processing line • Enabled ambiguity-fixed clock products for all three processing lines (Rapid, Final, and MGEX)

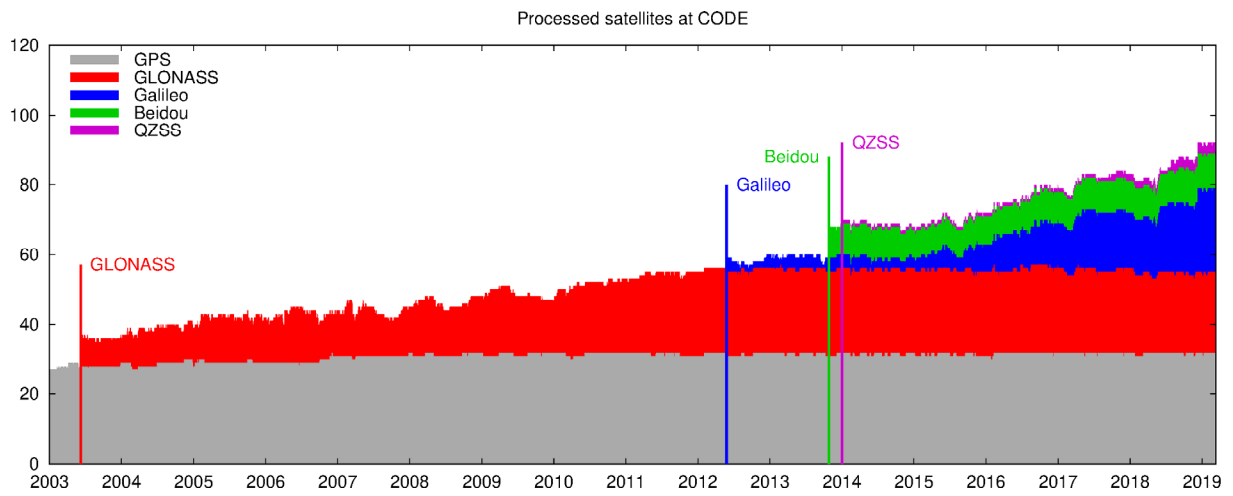


Figure 1. 3: Cumulative diagram of the processed satellites at CODE: Number of satellites which have been considered and delivered in the products for IGS final solutions and the MGEX project.

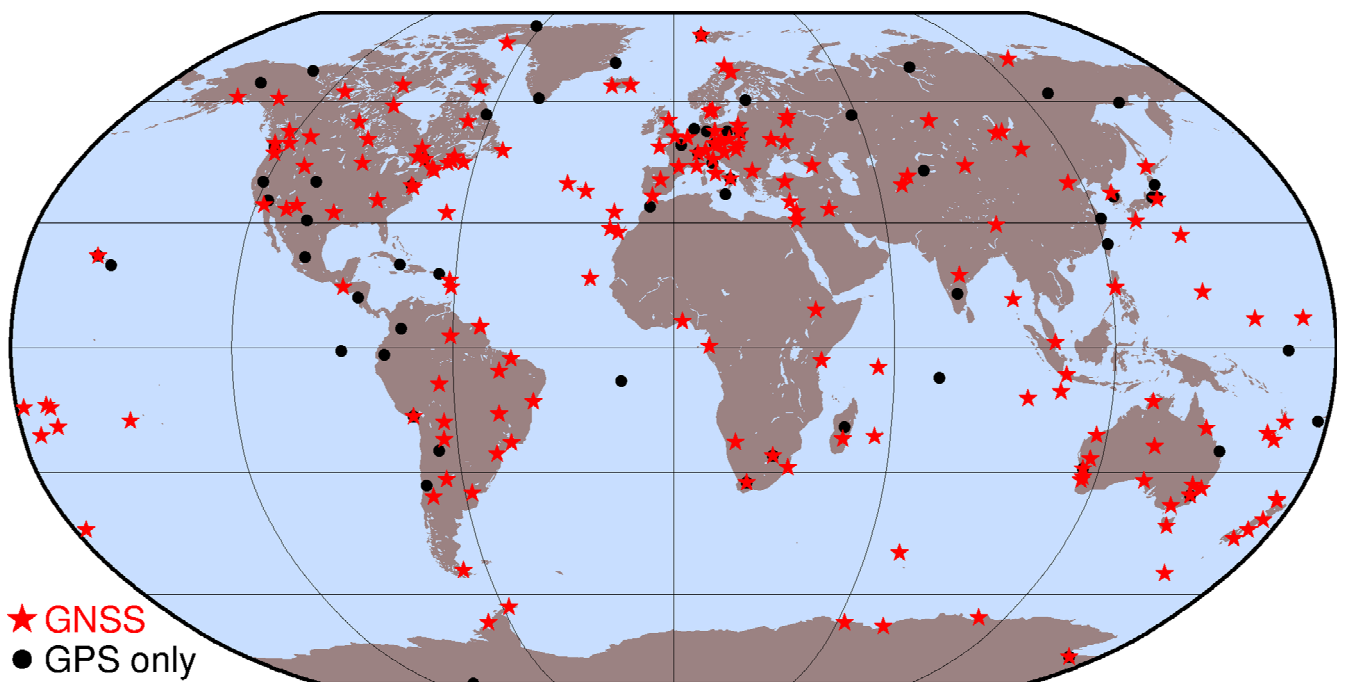


Figure 1. 4: IGS network processed at CODE (status of December 2019).

During the last four years our clock processing strategies for all IGS lines went under a major revision.

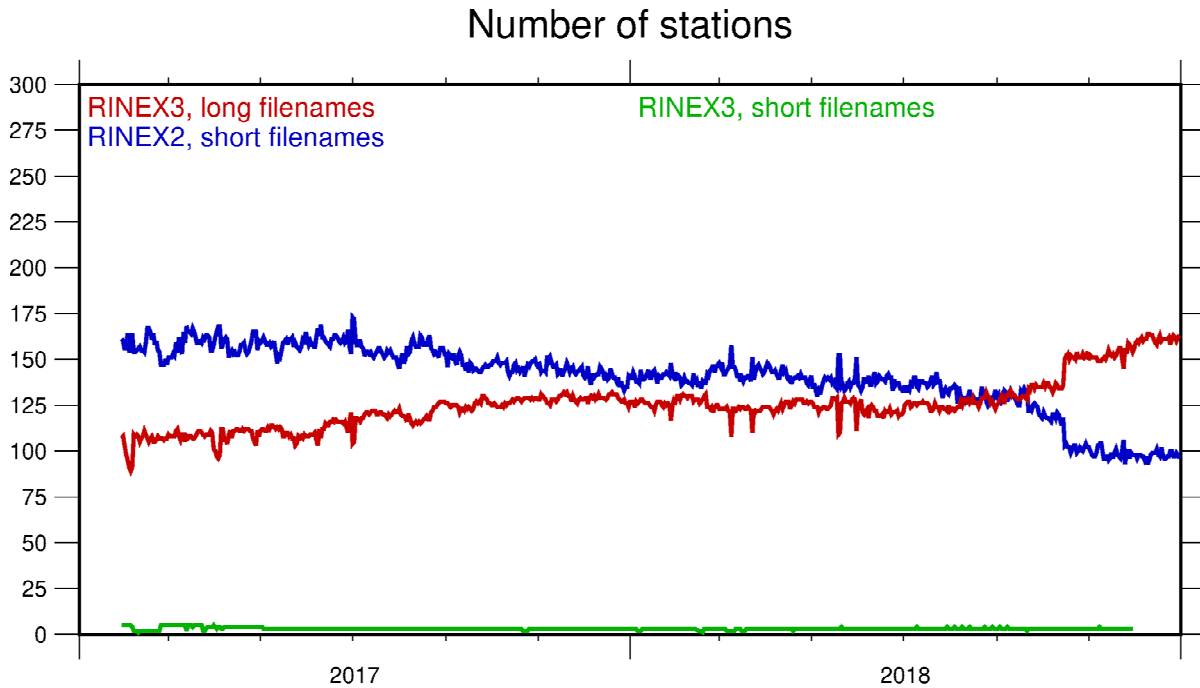


Figure 1. 5: Used observation data types for the IGS final product since 2017.

The clock product generations have been extended from a GPS only to a GPS/GLONASS solution for the Rapid and Final processing line. Since the switch from ITRF2008 to ITRF2014 the final clock product is based on more than 300 stations and includes also GLONASS whereas the Rapid clock products have already been extended with GLONASS in 2016. The next major improvement of our clock estimation was achieved in 2018. With the support of zero-difference ambiguity resolution CODE is now providing ambiguity fixed clock corrections for all of our product lines including MGEX. (Schaer et al., 2019).

In addition to our operational running processing lines for the IGS CODE was involved in the project EGSIM. In the framework of project EGSIM a dedicated reprocessing effort was carried out to estimate a consistent set of GNSS (GPS and GLONASS) orbits and clock from 1994 to 2015 (including 5 second clock densification for GPS and, for the first time, GLONASS) (Sušnik et al. 2019)

Another milestone was the transition of our MGEX solution from an experimental product into our regularly processing routine and is now processed regularly and is released with our final IGS products to the community (Prange et al., 2019). Figure 1. 3 shows the processed satellites at CODE in all our IGS and MGEX contributions since 2003.

Since the release of the RINEX 3 standards in 2013 the IGS stations slowly started to change the format of their observation file submissions from RINEX 2 to RINEX 3. In the last years the change from RINEX 2 to RINEX 3 was endorsed by the IGS and more and more stations are now submitting RINEX 3 data. At CODE we introduced RINEX 3 data for our operational IGS processing in 2017 and we see a continuously increasing number of stations providing observations in the new format. The benefit for the processing is that it is better specified how the observations are generated in the receiver. Figure 1. 5 shows the development of the data usage for CODE's final product generation.

EUREF Activities at CODE

S. Schaer^{1,2}, D. Arnold¹, R. Dach¹, L. Prange¹, D. Sidorov¹, P. Stebler¹, A. Sušnik^{1,3}, A. Villiger¹, A. Jäggi¹

¹*Astronomical Institute, University of Bern*

²*Federal Office of Topography swisstopo*

³*Now with: School of Civil Engineering and Geosciences, Newcastle University, Newcastle NE1 7RU, UK*

EUREF is an integrated component of the Subcommittee 1.3, Regional Reference Frames, of the IAG (International Association of Geodesy). A key component is the EUREF Permanent Network (EPN, Bruyninx 2004 and Bruyninx et al., 2012), consisting of more than 300 GNSS tracking stations (status of 10 January 2019). The data is analyzed in a distributed processing scheme between 19 Analysis Centers (ACs). It is worth mentioning that 16 out of 19 are using the Bernese GNSS Software (Dach et al., 2015) from version 5.2 up to the current development version at AIUB.

CODE, the Center for Orbit Determination in Europe, is one of the EUREF AC. It is a joint venture between the Astronomical Institute of the University of Bern (AIUB, Switzerland), the Swiss Federal Office of Topography (swisstopo, Wabern, Switzerland), the Federal Agency for Cartography and Geodesy (BKG, Frankfurt am Main, Germany), and the Ingenieurinstitut für Astronomische und Physikalische Geodäsie at Technische Universität München (IAPG, TUM, Munich, Germany).

CODE processes parts of the EPN network operationally using the development version of the Bernese GNSS Software package and delivers the results to the combination center. The weekly station coordinates are generated using a combined GPN/GLONASS solution. The precise orbits, used during the processing steps, are taken from CODE which are also submitted to the IGS for the final combination products. The contribution contains 58 stations (49 GPS/GLONASS and 9 GPS-only) as shown in Figure 1. 6. The EPN network has its focus on Europe; therefore, most stations are located on the western part of the Eurasian plate. The development of the processed network at CODE during the last four years is shown in Figure 1. 7.

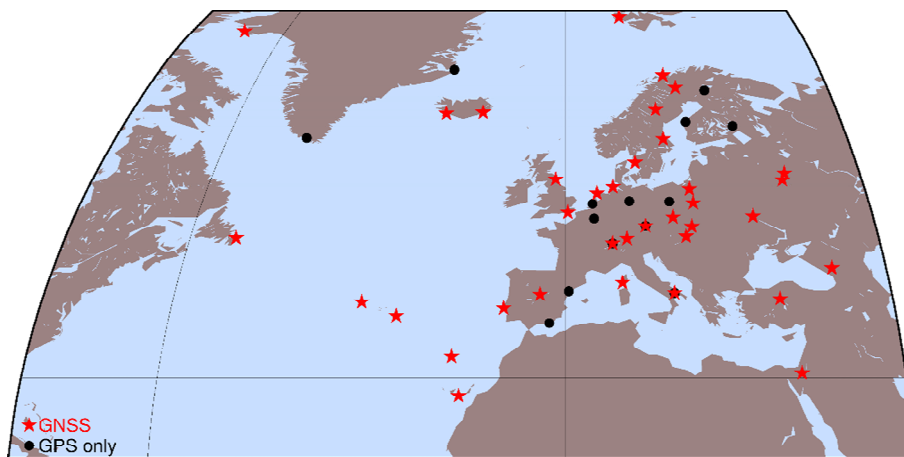


Figure 1. 6: GNSS network which is processed at AIUB and contributed to the EPN network.

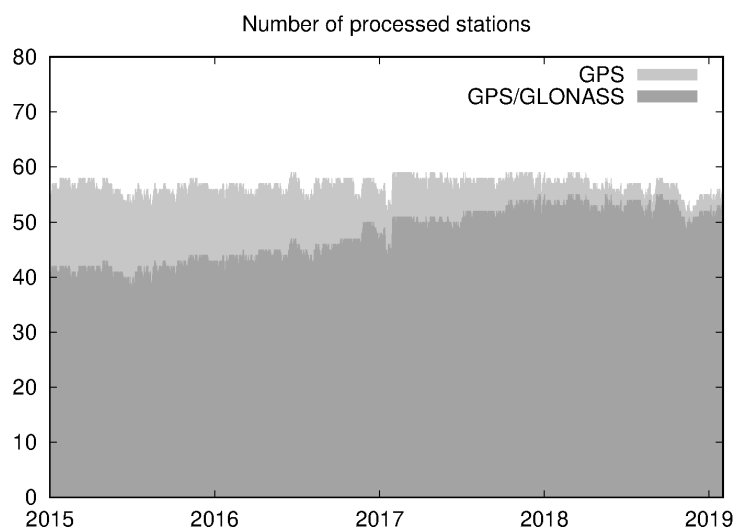


Figure 1. 7: EPN GPS and GPS/GLONASS receivers processed at CODE.

GNSS reprocessing results in the framework of the EGSiEM project

A. Sušnik^{1,2}, A. Grahs¹, D. Arnold¹, A. Villiger¹, R. Dach¹, A. Jäggi¹, G. Beutler¹

¹ Astronomical Institute, University of Bern

² Now with: School of Civil Engineering and Geosciences, Newcastle University, Newcastle NE1 7RU, UK.

In the framework of the European Gravity Service for Improved Emergency Management (EGSiEM, Jäggi et al., 2019) project, monthly gravity field solutions derived from the Gravity Recovery and Climate Experiment (GRACE) mission of different processing centers have been combined. Since a consistent reference frame is a prerequisite for precise orbit and related gravity field determination, a reprocessing campaign was initiated at AIUB (subsequently labelled as **repro15**) in the frame of the EGSiEM project. To get a consistent series of GNSS satellite clock corrections, GNSS orbits, Earth rotation parameters, and station coordinates, more than 250 globally distributed tracking stations of the IGS network were homogeneously reprocessed until end of 2014 following the processing standards from the CODE analysis center (status March 2015, Dach et al., 2016). Even if the precise orbit determination for GRACE only makes use of GPS satellites, the reprocessing activity considered GPS and GLONASS measurements. The interval of the reprocessing effort was also adjusted to the beginning of the IGS (International GNSS Service, Johnston et al, 2017) in 1994 instead of the launch date of GRACE in 2002.

In order to provide reference frame products using latest GNSS orbit modelling efforts, reprocessing of the GNSS data was performed using the extended Empirical CODE orbit model (Arnold et al., 2015), which significantly improves the accuracy of the GNSS orbits (in particular for the GLONASS satellites) and reduces the deficiencies in the geodynamical parameters. Since the reference frame for the reprocessing is still IGB08 the same station selection as in IGS-**repro2** from CODE (Steigenberger et al., 2015) was reused for the current repro15 effort. The processing started from the original GNSS observations in the RINEX files. As a priori orbit information the results from the repro2 campaign for the IGS were used and completed by alternative sources (e.g., broadcast orbits) in order to include as many satellites into the processing as possible. This effort resulted in a bigger number of satellites in the orbit solutions for the repro15 series than in the IGS-repro2 solution.

The resulting satellite-related products are listed in Table 1. 1. Station coordinates and Earth rotation parameters are also available during the entire period. They are accessible in the international standard as well as in the formats of the Bernese GNSS Software (Dach et al., 2015) package from ftp://ftp.aiub.unibe.ch/REPRO_2015/ (description in the file ftp://ftp.aiub.unibe.ch/AIUB_AFTP.TXT). The use of these products shall be referenced as:

Sušnik, Andreja; Dach, Rolf; Villiger, Arturo; Maier, Andrea; Arnold, Daniel; Schaer, Stefan; Jaeggi, Adrian (2016). CODE reprocessing product series. Published by Astronomical Institute, University of Bern. URL: http://www.aiub.unibe.ch/download/REPRO_2015; DOI: 10.7892/boris.80011.

Table 1. 1: Satellite-related products available from the EGSiEM reprocessing effort "repro15".

	GPS	GLONASS
GNSS satellite orbits	since 1994	since 2002
GNSS satellite clock corrections	since 2000	since 2008
sampling 30 s	since 2003	since 2010
sampling 5 s		

Product validation

Since all GLONASS and two of the GPS satellites are equipped with retro-reflector arrays, Satellite Laser Ranging (SLR) provides an independent tool to validate microwave-based GNSS orbits. Because the maximum angle of incidence of a laser pulse to a GNSS satellite does not exceed 14°, SLR residuals indicate mainly the radial accuracy of microwave-based GNSS orbits (Sośnica et al. 2015; Fritsche et al. 2014). Figure 1. 8 shows SLR residuals w.r.t. the

1-day GLONASS-M orbits – once using the old ECOM (IGS-repro2, left side) and once using the extended ECOM (repro15, right side). When the old ECOM model is used (left plot of Figure 1. 8), there is a clear dependency of the SLR residuals on the elongation angle: while the residuals to the satellite positions near solar beta angle 90° are scattered around zero, those to satellite positions of smaller absolute solar beta angle show a significant offset to zero. This behavior, as well as the dependency of the SLR residuals on the elongation angle is significantly reduced in the case of the new ECOM (right plot of Figure 1. 8).

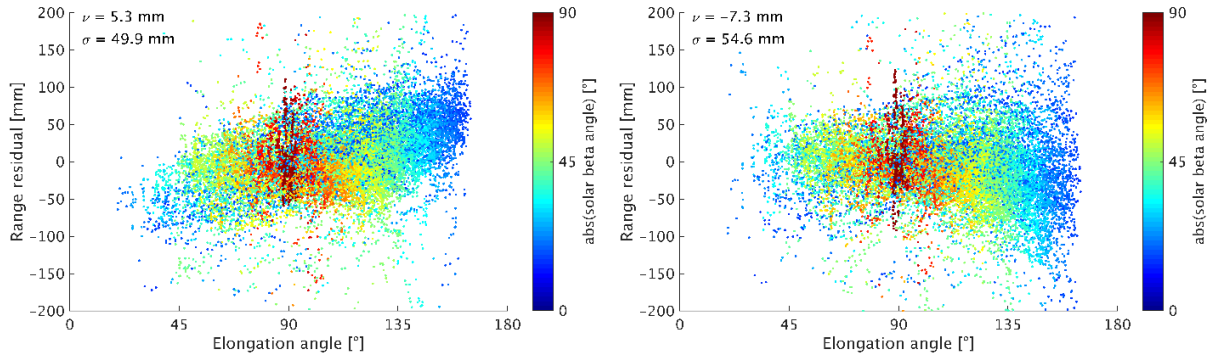


Figure 1. 8: SLR residuals w.r.t. GLONASS-M orbits using the original ECOM (left) and the extended ECOM (right). Mean value (ν) and standard deviation (σ) are based on all residuals whose absolute value is smaller than 150 mm. Observations to four GLONASS satellites (SVN 723, 725, 736, and 737) have been excluded due to anomalous patterns (see Dach et al, 2019). Furthermore, all residuals having an absolute beta angle smaller than 15° have not been taken into account due to unmodeled attitude during eclipses.

Precise Orbit Determination (POD) of GRACE is based on Precise Point Positioning (PPP), which requires precise GNSS satellite clock corrections which are consistent to the satellite orbits. Assuming 1 Hz sampling of GNSS data of LEOs, the GNSS satellite clock corrections are required with a sampling of at least 5 seconds (Bock et al. 2009). For the generation of 5 second clock products, GNSS observation files with a higher sampling than the common 30 seconds are needed. They are available from the IGS real-time service with a sampling of 1 Hz (Caissy et al. 2012). At least in the early years, the IGS real-time network was to a large extent independent from the legacy network. In this context, in particular for the generation of GLONASS satellite clock products, we were confronted with the limitation of available GLONASS tracking data in early years of the IGS real-time network. The number of available stations providing 5 s data is shown on the left side of Figure 1. 9, where grey color represents GPS only, green GPS/GLONASS and white no data available. As can be seen from Figure 1. 9, before the end of 2010 no high-rate RINEX observation files with GLONASS data are available. On the right side of the Figure 1. 9 the percentage of completeness of the GLONASS satellite clock products is shown for the 30 s sampling rate.

Figure 1. 10 shows the percentage of completeness of the satellite clock products with 30 s (left side) and 5 s sampling (right side) over an arbitrarily chosen period 2006–2007. It can be noticed that for the period shown, the overall completeness is generally 100% for both sampling rates, however there are some GPS satellites (namely G12, G15, G29, G31 and G32) for which both, 30 s and 5 s clock corrections are not complete. These data gaps are mainly due to reduced tracking of (unhealthy) satellites.

For validation purposes, the GRACE orbits for the year 2008 have been computed two times. One solution was generated using GPS orbits and 30 s GPS clock products from CODE’s contribution to IGS repro1 (no clock corrections have been computed by CODE in the frame of repro2), while the second set of orbits was generated using the corresponding products repro15. Results are shown in Figure 1. 11, where it can be noticed, that, when using repro15 products, the daily RMS values of the ionosphere-free carrier phase residuals are lower then when using repro1 products. In terms of the average values, calculated over the entire year, the improvement for the reduced-dynamic orbits is 0.40 mm while for the kinematic case 0.44 mm.

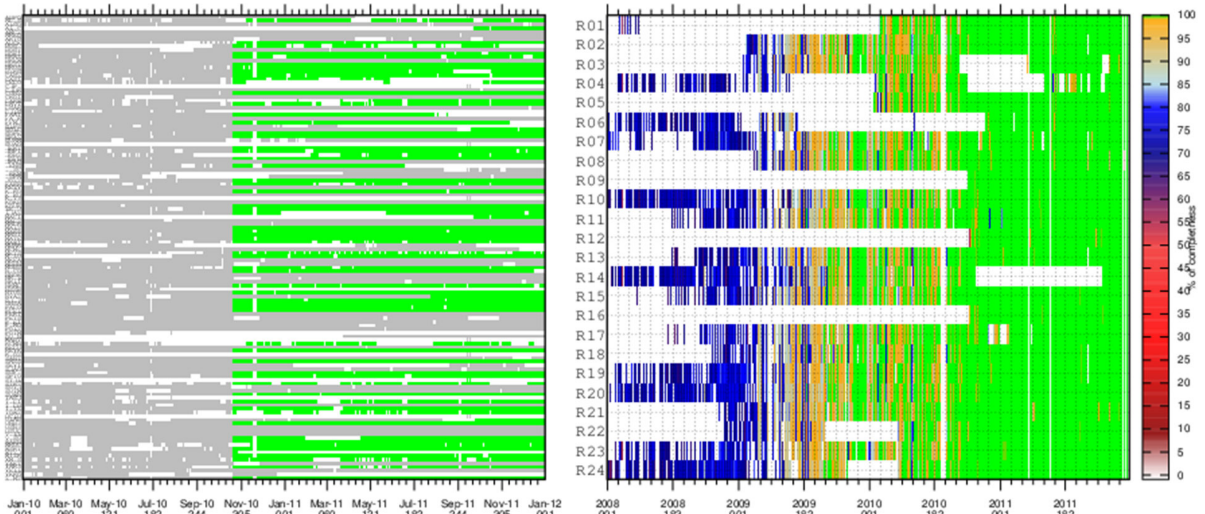


Figure 1. 9 (Left): number of stations delivering high-rate RINEX observation files, where grey color presents GPS-only, green GPS/GLONASS and white no data available. (Right): completeness of 30 s GLONASS clock corrections for the 2008-2011 period.

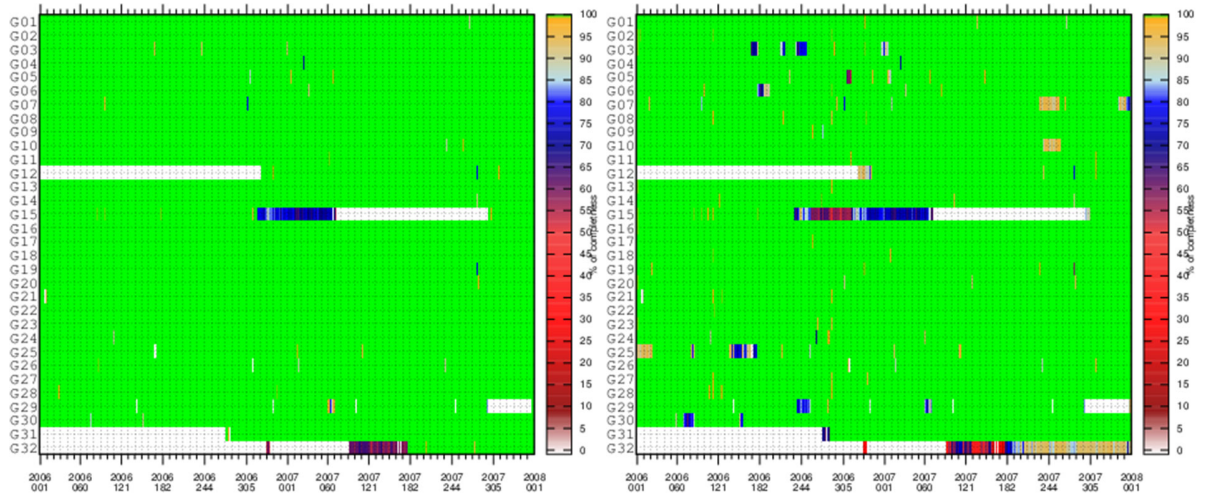


Figure 1. 10: Completeness of 30 s (left) and 5 s (right) GPS clock corrections for the time period between 2006 and 2007.

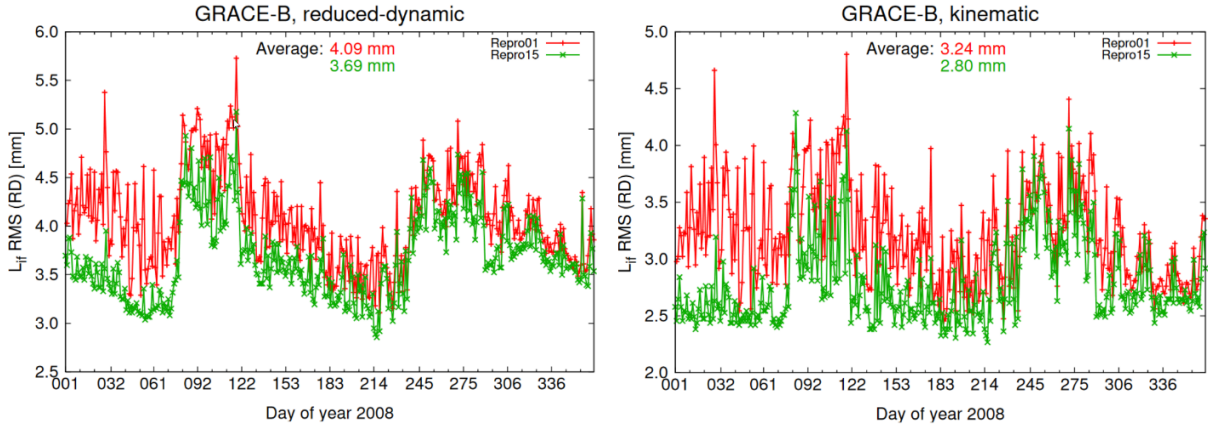


Figure 1. 11: Ionosphere-free carrier phase residuals of reduced-dynamic (left) and kinematic (right) POD for GRACE-B. The numbers indicate the average values over the entire year 2008.

Table 1. 2: Mean and standard deviation in mm of SLR residuals over the entire year 2008 for reduced-dynamic and kinematic GRACE orbits.

	Reduced-dynamic orbits				Kinematic Orbits			
	GRACE A		GRACE B		GRACE A		GRACE B	
repro15	-1.2	13.0	-2.6	14.2	-1.3	17.0	-2.1	19.8
repro1	-1.4	18.2	-3.2	18.6	-2.2	20.0	-2.9	23.0

Table 1. 2 documents the superiority of the repro15 over the repro1 products when applied to GRACE POD in terms of SLR residuals. For instance, the standard deviation of the SLR residuals for GRACE-B red-dynamic is 4.4 mm smaller, which correspond to a reduction by 25%. The ultra-precise inter-satellite K-band measurements of GRACE allow for a further independent orbit validation. When using repro15 instead of repro1 products, K-band range residuals are reduced from about 6.6 mm to 5.8 mm in the reduced-dynamic case and from 19.5 mm to 16.2 mm for the kinematic orbits in average over the entire year 2008.

Acknowledgment

This research was supported by the European Union's Horizon 2020 research and innovation program under the grant agreement No. 637010

CODE five system solution for the IGS MGEX

L. Prange¹, D. Arnold¹, R. Dach¹, S. Schaer^{1,2}, D. Sidorov¹, P. Stebler¹, A. Sušnik^{1,3}, A. Villiger¹

¹ Astronomical Institute, University of Bern

² Federal Office of Topography swisstopo

³ Now with: School of Civil Engineering and Geosciences, Newcastle University, Newcastle NE1 7RU, UK

The International GNSS service (IGS, Johnston et al. 2017) has been providing precise reference products for the Global Navigation Satellite Systems (GNSS) GPS and (starting later) GLONASS since about 25 years. These orbit, clock correction, coordinate reference frame, troposphere, and ionosphere products are freely distributed and widely used by scientific, administrative, and commercial users from all over the world. The IGS facilities needed for data collection, product generation, product combination, as well as data and product dissemination are well established. The Center for Orbit Determination in Europe (CODE, Dach et al., 2018) is one of the Analysis Centers (AC) of the IGS since the beginning. It generates the IGS products using the Bernese GNSS Software (BSW, Dach et al. 2015). In the current decade new GNSS (European Galileo and Chinese BeiDou) and regional complementary systems to GPS (Japanese QZSS and Indian IRNSS) were deployed. The existing GNSS are constantly under modernization, offering, among others, more stable satellite clocks and new signals. The additional systems and signals open new opportunities, but do also pose new challenges (Prange et al., 2017a).

In order to exploit the potential of the new GNSS and their signals and to prepare for their integration into the existing processing chains, the IGS has set up the Multi-GNSS EXperiment (MGEX, Montenbruck et al., 2013) in 2012 and has updated its standardized Receiver INdependent EXchange data format (RINEX3, MacLeod and Agrotis 2013). CODE has been participating in the MGEX with an own orbit and clock solution from the beginning (Prange et al., 2016). Originally, CODE's MGEX (COM) contribution considered GPS, GLONASS, and Galileo. The BeiDou2 (BDS2) data were added to the analysis in late 2013 and the QZSS data in early 2014 – making the COM a five-system solution (Prange et al. 2017a). Only satellites with medium Earth orbits (MEO) and inclined geosynchronous orbits (IGSO) are considered for COM. A map of the ground network station contributing to COM is shown in Figure 1. 12.

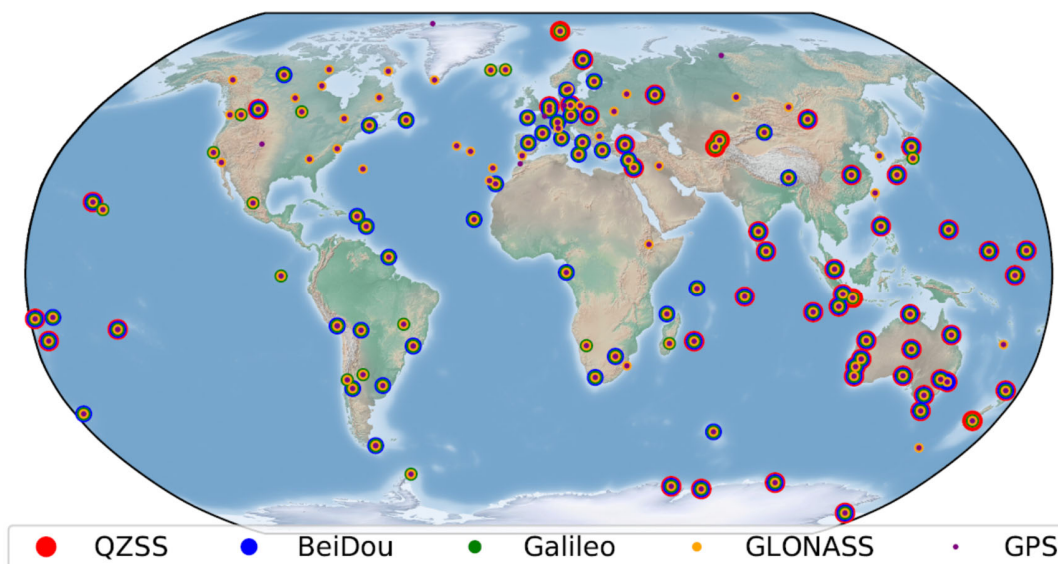


Figure 1. 12: Ground station network contributing to the COM solution.

In the first years of CODE's MGEX effort the focus was on enabling the BSW to accept data from the new GNSS, the new signals, the RINEX3 data format, to select observation types for a double-frequency processing, to set up prototype orbit and clock processing chains in a test environment, and to establish a batch-wise (not frequent) distribution of the results via the IGS products archive of the CDDIS. The results of this first stage of the COM processing were summarized and analyzed by Prange et al. (2017a), identifying potential points for improvements. Starting from early 2015 the COM products are generated in an operational scheme with a latency similar to that of the IGS Final products (about two weeks). In early 2017 the COM processing chains were migrated from the test environment to CODE's operational environment and adapted to the latest development version of the BSW. This major milestone allowed COM to benefit from the latest model, software, (RINEX3) data preparation, and processing developments introduced at CODE. On the other hand it allowed for a higher operability and an easier integration of the new GNSS into the legacy IGS routines – should such a decision be made. Further technical changes concern the sampling intervals of the orbits (15 min => 5 min) and satellite clocks (5 min => 30 s), the possibility to provide the orbits in the SP3-d format (if the number of satellites exceeds 85) from mid 2018 on, and the switch to the long product file name convention in August 2017 (see IGSMAIL-7515).

Besides these operational changes the modelling has improved, as well. The long-term goal is that the reference products based on data from the new GNSS shall have a quality comparable to those based on GPS and GLONASS. Considerable progress was made in the orbit modelling, in particular: At the beginning of 2015 the ECOM2 (Arnold et al. 2015) model replaced the ECOM1 (Springer et al. 1999) as the standard solar radiation pressure (SRP) model. According to Prange et al. (2017a) especially the orbits of Galileo and QZSS with their elongated satellite bodies benefit from this change. The extended analysis preceding this model change uncovered a high sensitivity of the higher order (4/rev) terms of the ECOM2 to the presence of modelling deficiencies - eventually resulting in a de-activation of the corresponding SRP model terms in all CODE solutions from July 2015 onwards. The comparison with older studies (Arnold et al. 2015) revealed issues concerning older GLONASS spacecraft - leading to an extended analysis by Dach et al. (2019a, 2019b). Since July 2018 the new empirical SRP model ECOM-TB is applied to BDS2 and QZS-1 satellites, while moving under orbit normal (ON) attitude (Prange et al. 2019a, 2019b).

While yaw steering (YS) attitude was assumed for all GNSS satellites in the past, the eclipse attitude laws proposed by Kouba (2009) and Dilssner (2011) were activated for GPS and GLONASS, respectively, in July 2016. The eclipse attitude laws disclosed by the GSA (2016) were activated for Galileo IOV and FOC satellites in August and November 2017, respectively. The ON attitude mode of QZS-1 and the BDS2 spacecraft has been correctly considered since July 2018.

Models for Earth albedo and transmit antenna thrust were implemented and activated for Galileo and QZSS spacecraft in August 2017 - significantly reducing the SLR offset for satellites of these systems (Prange et al. 2017b). The box-wing models used for the albedo modelling are based on the meta data disclosed by the GSA (2016) and CAO (2017). The transmit power used for the antenna thrust modelling is based on the meta data disclosed by the CAO (2017) in the case of QZSS and on a study performed by Steigenberger et al. (2018) in the case of Galileo. Finally, Prange et al. (2017a) identified that COM's Galileo (long-arc) orbits are heavily degraded during deep eclipse. Based on that Sidorov et al. (2018) analyzed the impact of the spacecraft's thermal re-radiation and developed models able to cover this effect (see also Sidorov et al. 2019 for details).

Since the phase center offsets (PCO) of the transmit antennas of Galileo and QZSS satellites have meanwhile been disclosed (see GSA 2016 and CAO 2017) and are provided in the igs14.atx file, we rely on these values in our COM solution in the case of QZSS. For Galileo the PCOs estimated by Steigenberger et al. (2016) are used. For the BDS2 transmit antennas we stick to the manufacturer PCO values, so far. For receiver antennas we still apply corrections copied from the GPS L1 and L2 values when analyzing data from Galileo, BDS2, and QZSS. The impact of the Galileo transmit and receiver antenna calibrations on the GNSS products is under investigation by Villiger et al. (2019c).

A major technical improvement concerns the change of the bias format from differential code biases (DCB) to observable-specific biases (OSB), accompanied by an update of the bias SINEX file format to version 1.00 and an improved bookkeeping of the observation types in April 2017 (see Villiger et al. 2019a, 2019b). These changes were the pre-condition for a revision of the ambiguity resolution strategy of Galileo, BDS2, and QZSS in the double-difference orbit and coordinate solution in June 2017, for the determination of fractional phase biases, and for the implementation of the zero-difference ambiguity resolution (for GPS, Galileo, and QZSS) active in the COM clock solution since June 2018. A detailed description of these changes and an analysis of its impact is provided by Schaer et al. (2018, 2019).

In summary, the COM orbit and clock solution has seen significant improvements in the recent years. It turned out to be a good testbed for the more complex multi-GNSS environment of the future. The COM products are made available for public use via the IGS data center CDDIS (<ftp://cddis.gsfc.nasa.gov/gnss/products/mgex>) (long file names) or the AIUB server (ftp://ftp.aiub.unibe.ch/CODE_MGEX/CODE/) (short file names) with a latency of about two weeks.

AIUB contribution to the GRSP

L. Prange, P. Stebler, A. Sušnik, E. Orliac, R. Dach

Astronomical Institute, University of Bern

GRSP (Geodetic Reference Service Provider) is a project related to the Galileo program - Europe's Global Navigation Satellite System (GNSS). GRSP is the successor of the projects GGSP (Galileo Geodetic Service Provider; 2005 - 2009) and TGVF-OVF (Time and Geodetic Validation Facility - Orbit Validation Facility; 2010 - 2018). Like its predecessors it is run by the GGSP consortium formed by the partner institutions ESOC (European Space Operations Centre), GFZ (Helmholtz-Zentrum Potsdam – Deutsches GeoForschungsZentrum), AIUB (Astronomical Institute of the University of Bern), BKG (Bundesamt für Kartographie und Geodäsie, Deutschland), and IGN (Institut national de l'information géographique et forestière).

GRSP's main tasks are:

- To define, realize and provide access to the GTRF - the Galileo Terrestrial Reference Frame. The GTRF is the geodetic basis for all other Galileo products and services and is tightly aligned to the ITRF (International Terrestrial Reference Frame).
- To produce a set of reference products (such as orbits, satellite clock corrections, hardware delays), which may serve the Galileo Mission Segment (GMS) as a reference for the validation of the navigation products it generates for uplink to the Galileo satellites.
- To provide the interface between the Galileo program and the space-geodetic science community.

The GRSP is organized in a similar way as the International GNSS Service (IGS) in the sense that the delivered products result from the combination of different solutions. These solutions are produced by three independent Processing Facilities (PF), with AIUB hosting one of them. The PFs are in charge of estimating the orbits of Galileo and GPS satellites, Earth Rotation Parameters (ERP), satellite and receiver clock corrections, Differential Code Biases (DCB), Inter-System Biases (ISB), ionosphere maps and troposphere delays. Each PF relies on its own GNSS analysis software package, namely the Bernese GNSS Software (Dach et al., 2015), EPOS (Angermann et al., 1997) and NAPEOS (Springer, 2010), and on its own analysis strategy. In contrast to the IGS, all PFs are requested to process the same dataset. The data is stemming from Galileo Sensor Stations (GSS) and a selected subset of IGS stations (see Figure 1. 13). The tracking network incorporates a significant amount of IGS stations (IGS-G) tracking GPS only in order to ensure a tight alignment between GTRF and ITRF. Receivers providing GPS and Galileo data from the IGS network are indicated by IGS-GE in Figure 1. 13.

GRSP offers two product lines:

- For the FINAL products all available raw data is post-processed in weekly batches in compliance with highest accuracy but relaxed latency (two weeks for combined products) requirements.
- The RAPID products are provided on a daily basis with a latency of just 12 hours. They are based on a subset of ground tracking stations.

Both product lines have in common that the products of the individual PFs are combined by a Combination Facility (CF) and later on verified by a Validation Facility (VF) before they are submitted to the GMS. The GTRF is based on the combination of a long time series of FINAL solutions.

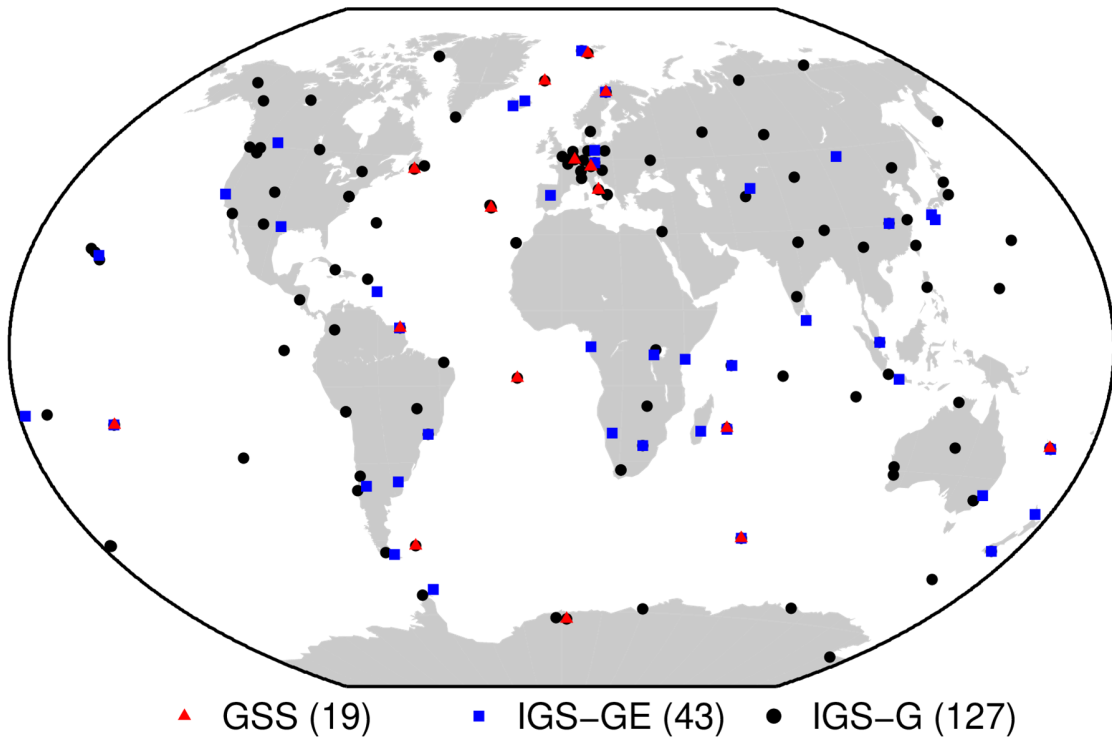


Figure 1. 13: Distribution of GSS, IGS multi-GNSS (MGEX), and IGS legacy (IGS) stations used by GRSP.

The Swiss Optical Ground Station and Geodynamics Observatory Zimmerwald

E. Cordelli¹, T. Schildknecht¹, A. Jäggi¹, E. Brockmann²

¹ *Astronomical Institute, University of Bern*

² *Federal Office of Topography swisstopo*

We will present a short summary of the main activities and recent achievements of the Zimmerwald observatory.

The Astronomical Institute of the University of Bern (AIUB) recently extended its observatory with two new domes and completed the renovation of an existing one (Figure 1. 14). This substantial extension was complemented by a series of new telescopes. Today, the observatory is equipped with six fully automated telescopes, which are used for tracking and survey applications, in particular to detect, catalogue, and characterize space debris. This will allow the Swiss Optical Ground Station and Geodynamics Observatory Zimmerwald (SwissOGS) to maintain and strengthen its leading role in space debris research.



Figure 1. 14: The 2 new domes of the Swiss Optical Ground Station and Geodynamics Observatory Zimmerwald.

Satellite Laser Ranging (SLR)

The Zimmerwald SLR station is part of the global tracking network of the International Laser Ranging (ILRS) since the foundation of this service in 1998. The SLR observations acquired with the monostatic 1-m Zimmerwald Laser and Astrometry Telescope are delivered in near real-time to the global ILRS data centers. The SLR activities at Zimmerwald are performed by the Astronomical Institute of the University of Bern (AIUB) and the Swiss Federal

Office of Topography (swisstopo). Zimmerwald continues to be the most productive SLR station of the ILRS in the northern hemisphere second to Yaragadee only, a station in Australia.

ZimTWIN – Observations to space debris

Survey

The Zimmerwald Twin Wide-field Instruments (ZimTWIN) was installed in September 2017 and consists of two ASA 16 inch f2.4 primary focus telescopes on the same mount. The primary focus produces a 2.14 x 2.14 degree field of View (FoV). Adjusting the relative pointing of the tubes a contiguous FoV of 4.28 x 2.14 degree, optimal for space debris and Near Earth Objects (NEO) surveys, can be obtained. Currently, the ZimTWIN is in test phase and is used for GEO surveys. One single tube produces ~1800 images over ~9.5 hours of observation time (based on October 2018 data). The ZimTWIN has a higher sensitiveness with respect to ZimSMART. shows the magnitude distribution of the tracklets from 2018. The second peak in the magnitude distribution visible for ~17 magnitude is characteristic of 0.4-0.5 meter-size object at GEO altitude. The cut-off of the telescope at 17 magnitude is due to the sensitivity limit given by the telescope aperture (40 cm) and the used exposure time (8 seconds).

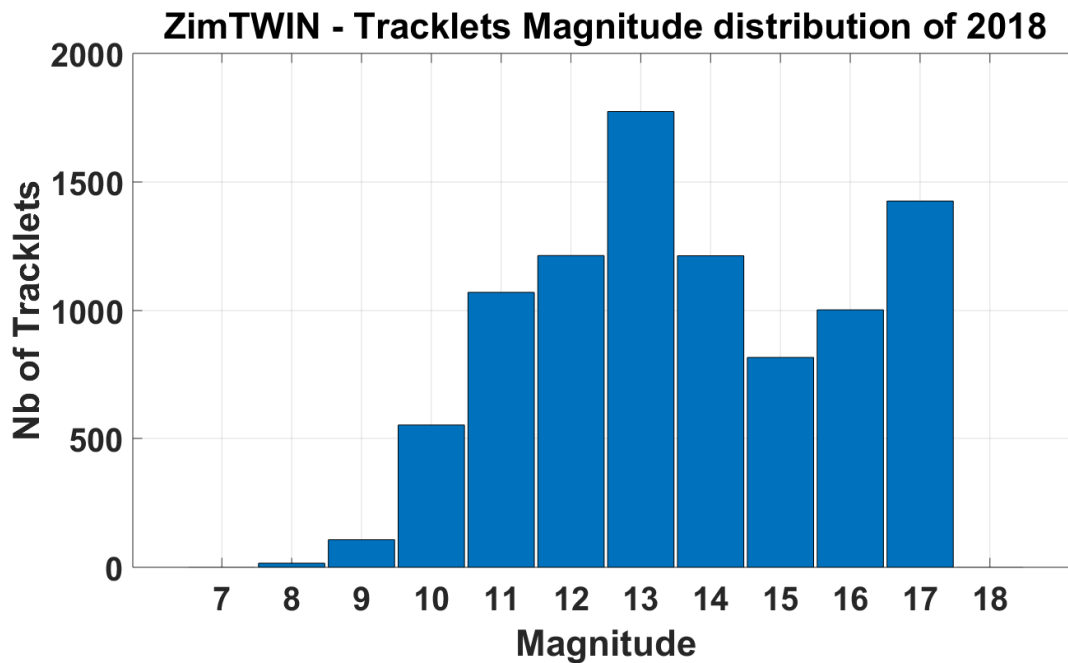


Figure 1. 15: ZimTWIN Tracklets Magnitude Distribution of 2018.

These are preliminary results. As soon as the test phase is completed, we will start using the second tube. Finally, the telescope will be used not only for GEO surveys, but also for MEO surveys such as for GNSS and Molniya orbits.

Simultaneous multi-color photometry

The ZimTWIN can be used also to characterize space debris. By overlapping the FoV of the two tubes and equipping them with different photometric filters, we can not only acquire color light curves, but we can also observe the same object with different filters at the same time under the same observations conditions. This allows us the extraction of

the time varying color index. An observation campaign was carried out during the summer of 2018 on active satellites, disposed upper stages, and on defunct Glonass satellites. An example of the synchronous light curves and the derived color index is reported below for a Delta 4 upper stage (11036B; Figure 1. 16). The color index shows only one minimum within one rotation period that can be used to discriminate which end of the rocket stage we are currently observing, either the adapter to the satellite or the nozzle.

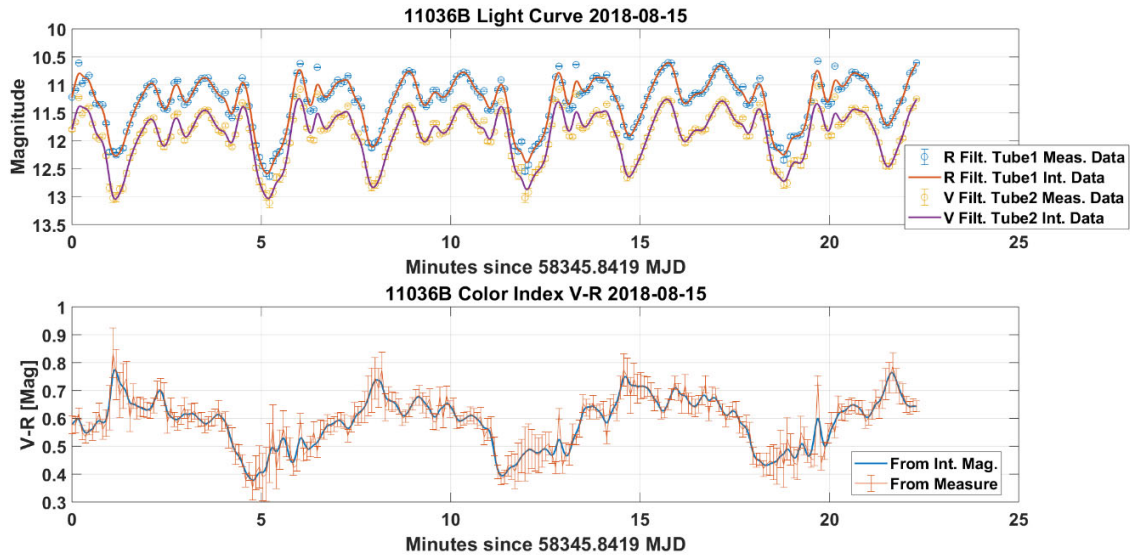


Figure 1. 16: Time-varying color index extracted from simultaneous color photometry observation performed with ZimTWIN.

In order to facilitate the switch between survey and photometric observation we plan to automate and control remotely the adjustment of the tubes relative pointing.

ZIMLAT – Optical Observations

Observation performance, number of observations, light curve database

During nighttime, the telescope is equally shared between SLR and CCD observations. The switch between observations mode is completely automatic, only photometric observations are performed manually.

The main targets of ZIMLAT are the faint area to mass ratio (HAMR) space debris objects of the AIUB internal catalog. ZIMLAT maintains a catalog of 85 objects (December 2018). As can be seen from Figure 1. 17, the sensitivity cut off for ZIMLAT (with 12 seconds of exposure time) is magnitude 19 which corresponds to 20-30 cm objects at GEO altitude.

ZIMLAT is also used for space debris characterization. Two hours per night are dedicated to the acquisition of light curves. The AIUB light curve database contains more than 3500 light curves for more than 520 objects.

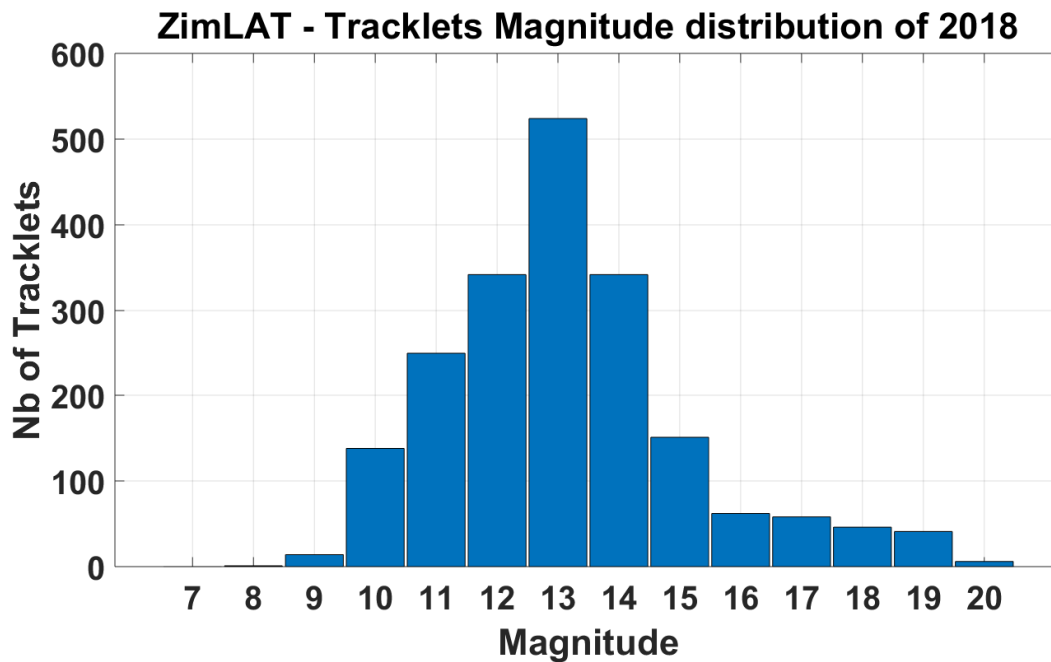


Figure 1. 17: ZIMLAT magnitude distribution of tracklets of 2018.

NEO observations

The ZIMLAT telescope is also used for “classical” astronomical observations as NEO. A special observation campaign was carried out for the asteroid 2012 TC4 during its close encounter to the Earth the night of 11th October 2017. 7 series of observations were performed over 140 minutes while the asteroid was visible over the Zimmerwald observatory. After the extraction of the light curve, the rotation period of the asteroid was determined and the phase diagram was reconstructed. The extracted rotation period of the asteroid is 735 ± 5 seconds (0.204 ± 0.001 hours). The obtained results are consistent with the values reported in Sonka, et al. 2017.

Night-tracking Camera

ZIMLAT was recently equipped with a night-tracking camera. The aim of the tracking camera is the correction of the offset in the pointing of the telescope given by ephemerides with poor accuracy. This correction is needed if we want to use the SLR system, which has a small FoV of <30 arcsec, to range to orbiting objects. The night-tracking camera provides measurements, at high temporal resolution (100 Hz for the ranges, and up to 30 Hz for the angular and brightness observations), for both, the orbit (measured azimuth, elevation and ranges) and the attitude determination (ranges and light curve) of the object within a single pass over the observatory. Finally, the tracking camera allows the extraction of angular measurements for the observed objects without performing astrometric data reduction, very important for LEO objects when the FoV of the instrument is relatively small and doesn't contain enough reference stars.

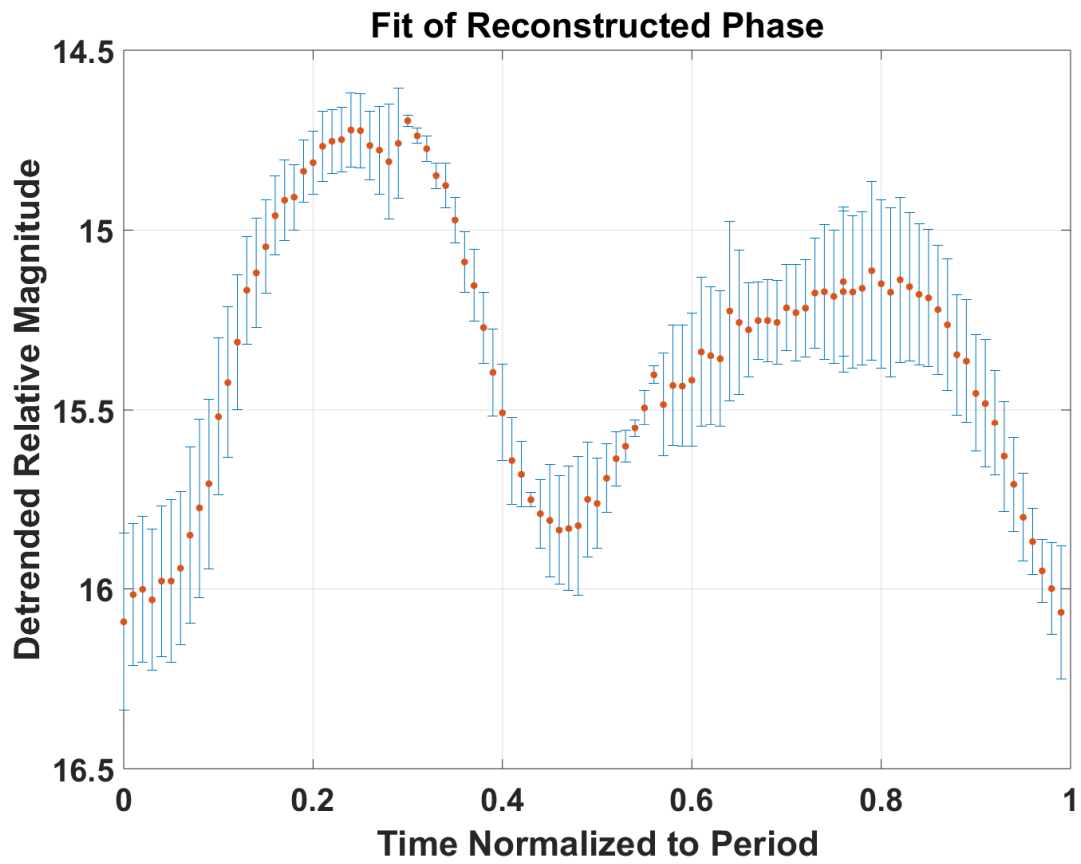


Figure 1. 18: Phase diagram of the asteroid 2012 TC4.

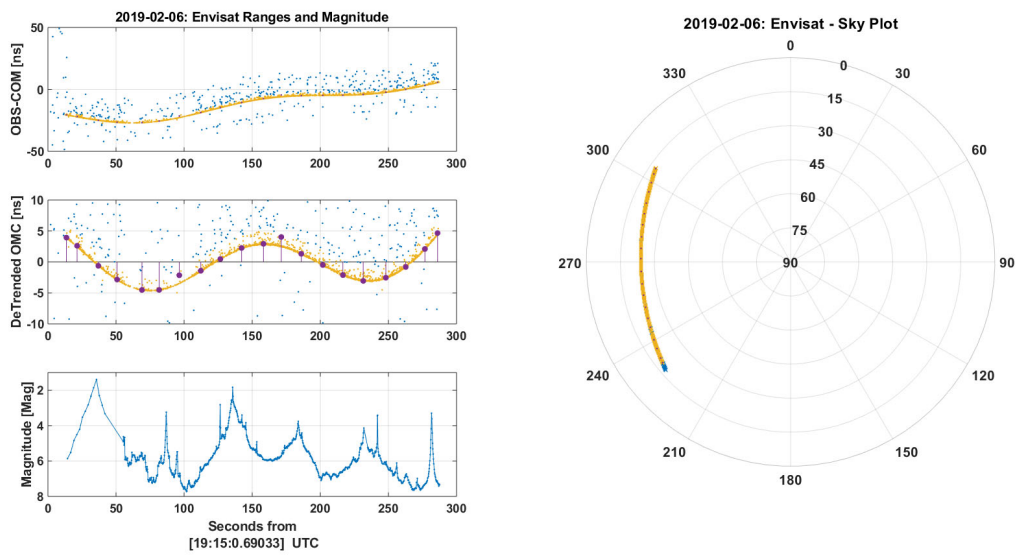


Figure 1. 19: Output measurements when using the night-tracking camera.

ZimMAIN and ZimSMART – Observations to space debris

The main purpose of the ZimSMART telescope is the discovery of space debris in the GEO region. ZimSMART is used to build up and maintain the AIUB internal catalog GEO of space debris. It produces ~1300 images and ~400 tracklets over 8 hours of observation time (based on September 2018 data). Its aperture allows the observation of 1 meter-size object at GEO altitude (cut off at 16 magnitude) with an exposure time of only 8 seconds. A refurbishment of the mount is foreseen in 2019, which will result in an improvement of the telescope performances.

The Zimmerwald Multiple Applications Instrument (ZimMAIN) is an 80 cm aperture Ritchey-Chrétien telescope with 22.5 x 22.5 arcmin FoV. The telescope was installed in February 2018 and is in the commissioning phase. The instrument is currently used for follow-up observations of the faint objects of AIUB's catalog (18-19 Magnitude) and the follow-up of faint fragments from recent breakup events in GEO and HEO. The telescope acquires an average of ~2200 images over 9.5 hours of observation time (based on October 2018 data). Improvement of the sensitiveness and number of tracklets are expected with the implementation of a more sensitive and larger CCD, which will allow us to double the effective FoV.

ZimNET – Status of collaboration with DLR

The Zimmerwald Network Telescope (ZimNET) is part of the SMARTnet project, a joint project between the German Aerospace Center (DLR) and the AIUB. The first ZimNET telescope (SMART 1) was deployed in South Africa and is operational since April 2017. The second (SMART 2) was recently shipped to DLR to be transported to its final destination in Australia. These telescopes were assembled, tested, and validated at the SwissOGS. The ZimNET telescopes consist of two tubes on the same mount, one Dall-Kirkham (50 cm aperture) and one Newtonian (20 cm and 30 cm aperture for SMART 1 and 2 respectively), used for the follow-up and the discovery of space debris.

Global Navigation Satellite Systems (GNSS)

GNSS receivers are operated at Zimmerwald by swisstopo and AIUB. Two permanent GNSS receivers mounted on 9-meter masts provide data to the data centers of the International GNSS Service (IGS), to the EUREF, and to the Automated GNSS Network for Switzerland (AGNES) of swisstopo.

Evaluation of ITRF2014 Solutions

R. Dach¹, A. Sušnik^{1,2}, A. Grahl¹, A. Villiger¹, D. Arnold¹, A. Jäggi¹

¹ Astronomical Institute, University of Bern

² Now with: School of Civil Engineering and Geosciences, Newcastle University, Newcastle NE1 7RU, UK.

For the most recent International Terrestrial Reference Frame (ITRF) realization three institutions have provided solutions. They significantly differ in the way how they have been generated and in their parametrizations:

- Deutsches Geodätisches Forschungsinstitut at TU Munich (DGFI-TUM, Germany; Seitz et al. 2016)
DTRF2014: based on a classical modelling of time series by station coordinates and linear velocities (after correcting for loading effects)
DTRF2014L: corrections for atmospheric pressure loading and hydrological effects are reapplied
- Institut national de l'information géographique et forestière (IGN, France; Altamimi et al. 2016)
ITRF2014: based on coordinate, linear velocities, and empirical post-seismic deformation corrections (together with annual/semi-annual periodic functions in the background)
ITRF2014P: periodic functions recovered
- Jet Propulsion Laboratory (JPL, USA; Wu et al. 2015)
JTRF2014: based on a filter approach

Coordinate sets for all days between 2000 and end of 2014 have been established following the instructions of the related TRF solutions.

Description of the Solution

The typical parameters for a global GNSS (Global Navigation Satellite Systems) solution have been estimated, namely station coordinate, troposphere zenith path delays with 2h-resolution as well as troposphere gradients with a daily resolution Earth rotation parameters (X- and Y-pole offset and rate as well as LOD; 1st UT-values taken from the C04 product), and GNSS satellite orbits with 7 dynamical orbit parameters according to the ECOM2 description (see Arnold et al. 2015) together with three empirical velocity changes of the satellites at noon as described in Beutler et al. (1994). All solution series are based on one and the same set of daily normal equations (generated in the frame of the EGSIEM reprocessing, Sušnik et al., 2019) to ensure full consistency regarding the GNSS processing.

For the datum definition a minimum constraint condition was applied including a NNR and NNT condition (no-net-rotation and no-net-translation) to all stations with given coordinates in the particular reference frame. Due to the NNT-condition the center of mass (relevant, e.g., for the satellite orbit modelling) is forced to coincide with the origin of the related reference frame – as typically done for the processing within the IGS. If the deviation of the center of mass from the origin is taken into account in the solution by estimating a translation vector (geocenter coordinates), the coordinates and GNSS orbits result in the same solution geometry – the differences can be fully absorbed by three translation and three rotation parameters. These solutions contain the usual pattern in the Z-component of the geocenter parameters (which is dominated by the orbit modelling, as reported for instance by Ray et al. 2008 or Meindl et al. 2013). This solution is labeled **datum-free solution** and is used for comparisons.

Station coordinates

In the datum-free solution the station network geometry is exclusively defined by the GNSS measurements. As soon as the center of mass of the solution is forced into the origin by applying a no-net-translation condition without estimating a geocenter vector, the network may become distorted. Any potential distortions may be verified for the five different reference frame solutions by a seven parameter Helmert transformation with respect to the datum-free coordinate solution. The magnitude of the network distortions is expressed by the RMS of the residuals, which is

displayed for the full time series in Figure 1. 20. The RMS is typically below 1 mm, which confirms only a marginal deformation of the station network geometry by this effect.

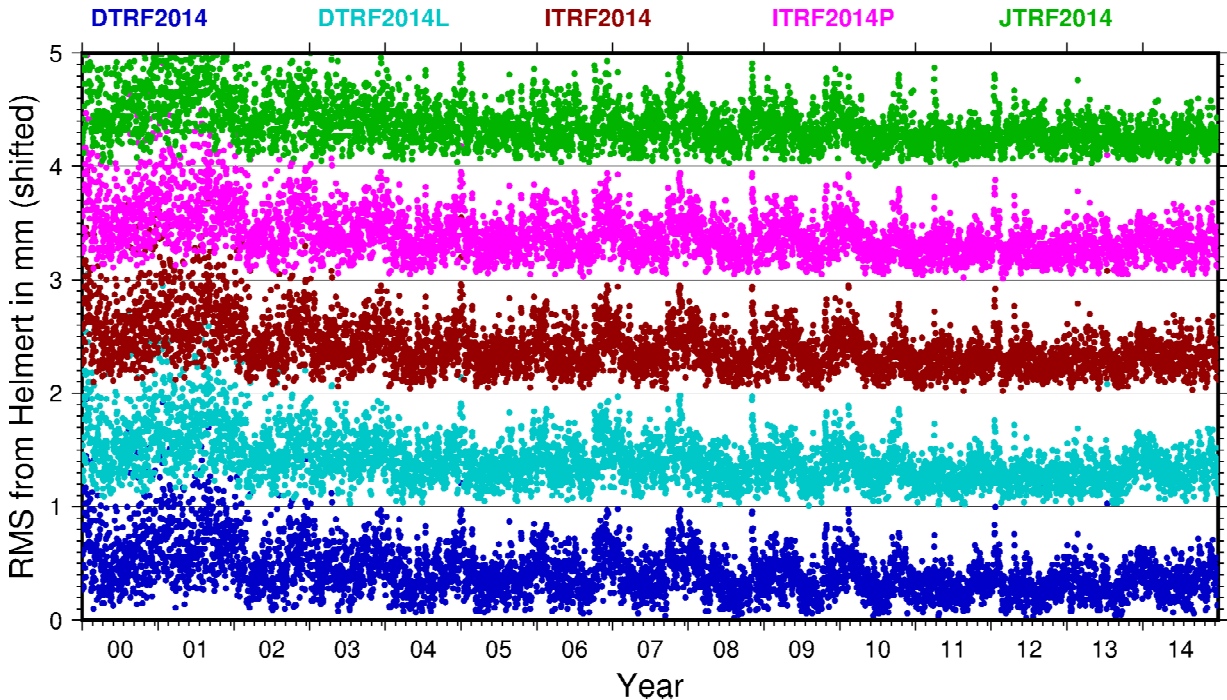


Figure 1. 20: RMS of the seven parameter Helmert transformation between the solutions fixed on the respective origin of the reference frame solutions and the datum-free solution; the datasets are shifted by 1 mm for plotting.

The statistical characteristics of the residuals of the Helmert transformation is very similar for all the solutions for each day. However, for most days the RMS of the individual solutions show the same order (with increasing RMS): JTRF2014, DTRF2014L, ITRF2014P, ITRF2014, and DTRF2014. In the same order, the magnitude of the annual variations in the total RMS as visible in Figure 1. 20 is decreasing. In the JTRF2014 solution the deterministic model for the long-term coordinate time series representation is adjusted by the filter approach. It can therefore follow the network geometry of the GNSS-data based coordinate time series best. On the other hand, with its coordinate and linear velocity parametrization the DTRF2014 solution shows the lowest flexibility. The solution DTRF2014L, where the loading effects are corrected based on models, got on average the second best fit after the JTRF2014 confirming the high quality of these background models. Of course, as stated above, the magnitude of these differences between the solutions is small.

Polar motion

The Earth rotation parameter are an important result from the GNSS data analysis for geodynamical purposes. In **Fehler! Verweisquelle konnte nicht gefunden werden.** the differences of the X pole with respect to the ITRF2014 solution (arbitrarily chosen) are displayed. The polar motion of the ITRF2014P (magenta curve) shows, as expected, periodic differences with respect to the ITRF2014 solution. This is because for the modelling of the station coordinate time series empirical periodic functions have been added. This confirms the sensitivity of the Earth rotation parameters on the stability of the reference frame solution regarding the orientation. The JTRF2014 solution is based on a filter approach with a weak long-term stability in the orientation of the reference frame. This is clearly visible in the green curve of **Fehler! Verweisquelle konnte nicht gefunden werden.** Even if this solution did coincide best with the coordinate estimates it has a disadvantage for the interpretation of the Earth rotation solution. The differences between

the DTRF2014 and DTRF2014L solutions (blue and cyan curves) may also be explained by the consideration of the loading corrections. They do not show such a clean periodic behavior like the differences between ITRF2014 and ITRF2014P. They are caused by the applied loading corrections instead of estimating periodic functions as in the ITRF2014P solution. The Y-component is not shown here but allows for the same conclusions.

The most interesting feature is the long-term stability of the two solutions ITRF2014 and DTRF2014. Even though both solutions are stable in the short-term by construction, they show a systematic difference in the long-term stability as clearly shown by the blue curve in **Fehler! Verweisquelle konnte nicht gefunden werden.**. This implies that both reference frame solutions do rotate with respect to each other influencing the obtained Earth rotation parameters.

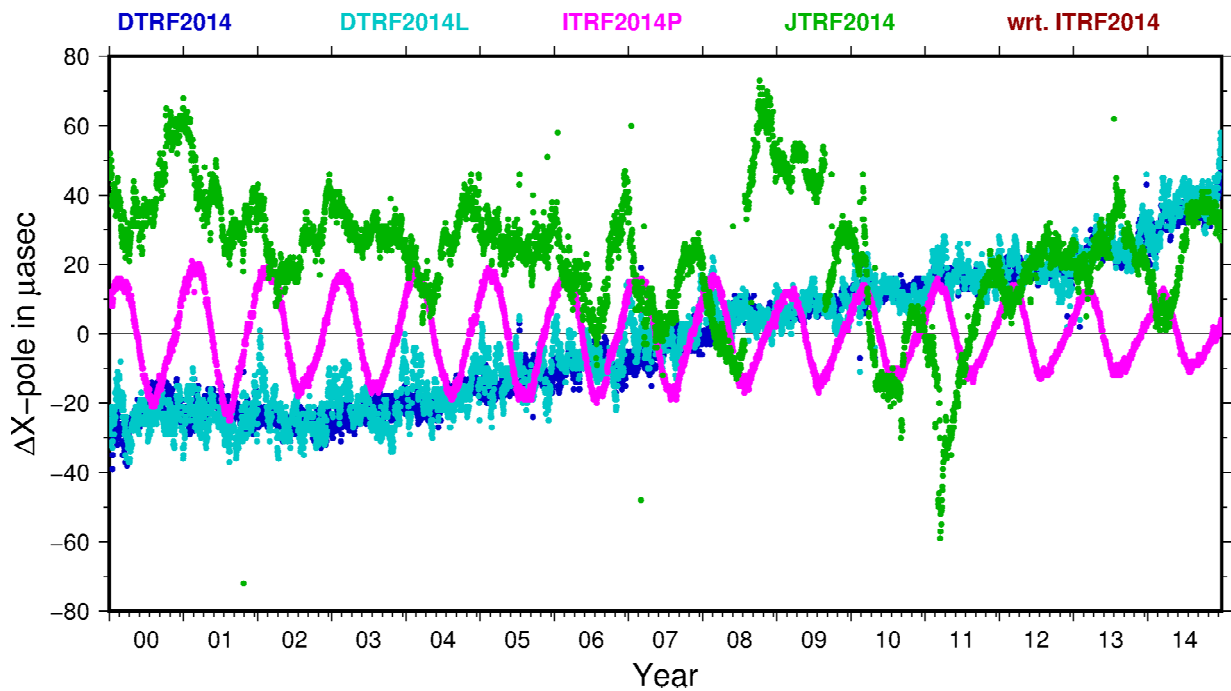


Figure 1. 21: Difference between the obtained polar motion X-components for the reference frame solutions with respect to the arbitrarily chosen solution ITRF2014.

SLR measurements

The coordinate series from all five reference frame solutions include not only GNSS stations but also Satellite Laser Ranging (SLR) stations. This allows to use SLR measurements to verify the consistency of the reference frames. For this purpose the positions of the GNSS satellites are extracted from the corresponding solution based on the GNSS microwave measurements. The resulting distances are directly compared with the SLR measurements after applying the usual corrections (e.g., for troposphere). No further parameters (e.g., SLR range biases or coordinates of the SLR tracking stations) were estimated. About 10 stations (in the early years even fewer) provide SLR measurements to GPS and GLONASS satellites whereas only sites with coordinates in the related reference frame solutions are considered (station 7406, San Juan, Argentina is not contained in the JTRF2014 solution for a certain interval).

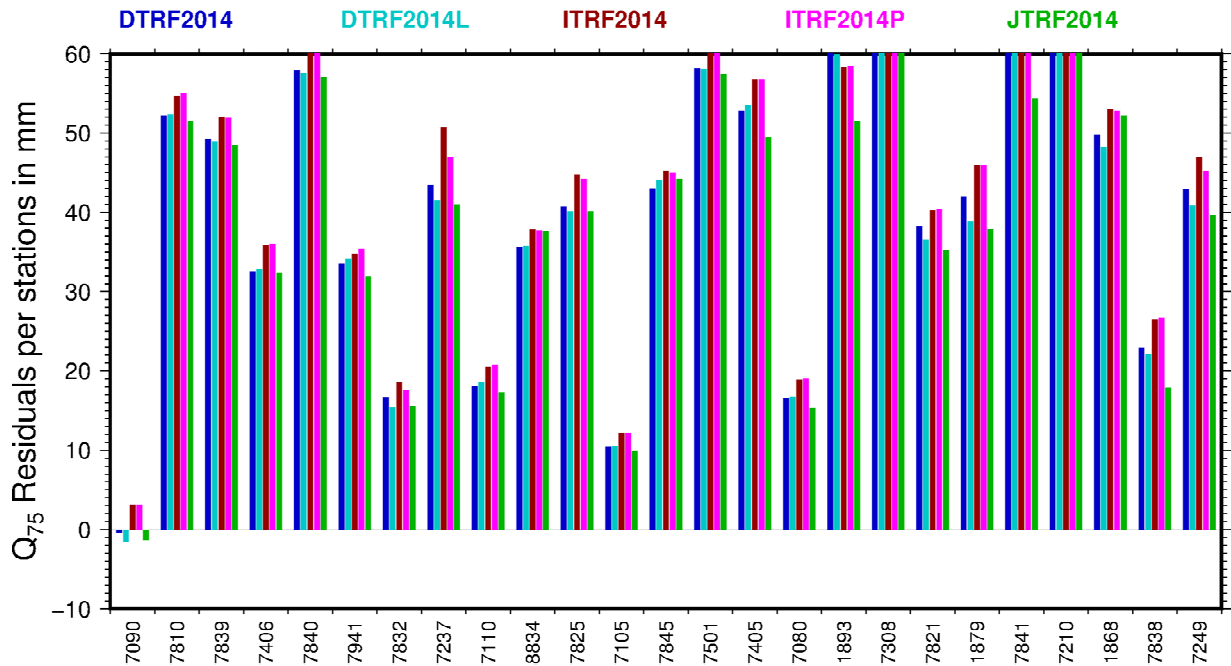


Figure 1. 22: Quantile 75% of all SLR residuals to GNSS satellites per station for each of the reference frame solutions.

The standard deviations of the SLR residuals per station are in the order of magnitude of 3 cm. Comparing the values between the reference frame solutions they are smallest for the JTRF2014 solutions followed in most cases by the DTRF2014L solution. This is consistent with the distortion of the network geometry in the GNSS solutions. The SLR residuals for the two ITRF2014 and ITRF2014P solutions are about 3 mm bigger than for the other solutions. This is visible also in Figure 1. 22 for most sites where the 75% quantile for the SLR residuals per station are shown. The smaller 75% quantile values in Figure 1. 22 are in general obtained for stations outside of Europe. A network effect, therefore, cannot be excluded.

Acknowledgment

The authors are grateful to the groups for providing their reference frame solutions and accompanying information used for this evaluation study. Thanks go in particular to Z. Altamimi (IGN, France), C. Abbondanza (JPL, USA) as well as M. Bloßfeld and M. Seitz (DGFI-TUM, Germany).

Improving GLONASS Orbit Quality by Re-estimating Satellite Antenna Offsets

R. Dach¹, A. Sušnik^{1,2}, A. Grahl¹, A. Villiger¹, D. Arnold¹, L. Prange¹, S. Schaer^{1,3}, A. Jäggi¹

¹ Astronomical Institute, University of Bern

² Now with: School of Civil Engineering and Geosciences, Newcastle University, Newcastle NE1 7RU, UK.

³ Federal Office of Topography swisstopo

While developing the extension of the Empirical CODE Orbit Model (ECOM) at CODE (Center for Orbit Determination in Europe) it was noticed that two of the GLONASS satellites showed an unexpected behavior. As a consequence the two satellites were excluded from the orbit validation using Satellite Laser Ranging (SLR) measurements (see Section 6 in Arnold et al., 2015). In a follow-up study conducted by Prange et al. (2017), the list of GLONASS satellites with specifically increased SLR residuals had to be further extended.

Such a behavior of a satellite can be interpreted as a deficiency of the related orbit model. However, this explanation seems to be unlikely regarding the figures provided for instance in Grahl et al. (2016). There is a number of GLONASS satellites where the differences to the independent Satellite Laser Ranging (SLR) measurements show the expected behavior only for the first years of their lifetime. Starting from a certain epoch, they become instantaneously larger by a factor of two or even more.

In the same context, the example of exchanging the space vehicles in the slot R21 in August 2014 is interesting (reported by Prange et al., 2017). The satellite with SVN 725 was launched in September 2008. In August 2014, this satellite was decommissioned and replaced by the new SVN 755 in the same slot. For the new space vehicle the magnitude of the SLR residuals becomes again much smaller. In case of a deficiency in the orbit model, the same behavior for both space vehicles (both are of the same GLONASS-M type) would have been expected. Because the geometry between the Sun, Earth, and the satellite directly before and after the satellite exchange is still comparable also potential weaknesses of an orbit model should have a similar effect on the obtained trajectory. Because the pattern in the SLR validation is changing with the exchange of the space vehicle, it is more likely that “something unexpected” happened at the satellite (which cannot be absorbed by the orbit model). Also in cases of an instantaneous increase of the SLR validation values (as described by Grahl et al., 2016) the geometry between Sun, Earth, and the satellites does not significantly change before and after the degradation of the satellite orbits.

Re-Estimating the satellite antenna offset corrections

Typically, one set of satellite antenna offset (SAO) corrections is estimated over the entire lifetime of each satellite. Afterwards, a weekly solution may be compared to the long-term solution in order to derive a quality measure for the stability of the obtained SAO corrections. Examples for two satellites are given in Figure 1. 23 where the long-term solution is shown as a horizontal line together with the weekly solutions (with their error bars). In particular for the GLONASS satellite in Figure 1. 23b large variations in the weekly solutions are visible that are related to significantly increased error bars. The variation of the formal errors and the pattern in the weekly solutions for the horizontal SAO-components is not limited to the GLONASS but also visible for the GPS satellites (see Figure 1. 23a). It is known and explained for instance in Schmid and Rothacher (2003) by the correlation with estimated orbital parameters.

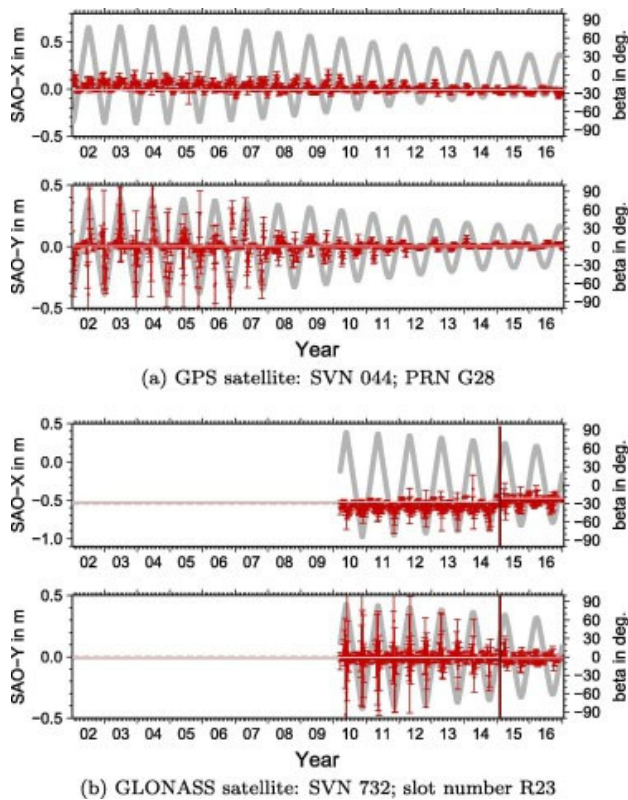


Figure 1. 23: Time series of estimated horizontal satellite antenna offset (SAO) where the nominal values that are used for the IGS processing are indicated by the dashed gray lines that are typically below the thick horizontal line indicating the long-term solution

Figure 1. 23b also shows a discontinuity in the estimated SAO-X parameters at the beginning of the year 2015 (indicated by the vertical line). Such discontinuities in the time series have been observed for a number of GLONASS satellites in the X- as well as in the Y-components. They do coincide also with the anomalies in the SLR residuals reported by Grahl et al. (2016). Interestingly, such events are not related to a change in the Z-component of the estimated SAOs. With a dedicated algorithm (see Dach et al., 2019) in total about 40 events have been detected in the processed time interval from 2002 to 2016. Some of the satellites showed two or even more changes of the estimated horizontal SAO correction series. There are also satellites where the estimated long-term SAO values deviate more than 3 cm from the beginning of the satellite's lifetime.

Validation

In the orbit determination for the GNSS satellites, the observations refer to the satellite antenna phase center. The SAO corrections together with satellite antenna phase center variations are needed to obtain the instantaneous location of the center of mass of the satellite. This is the point where the equation of motion and related parameters are referring to. If wrong SAO corrections are applied, the series of satellite positions will be deformed and cannot be represented by the equation of motion. That's why the correct usage of the SAO corrections is essential for a high quality orbit determination. Two series of orbits have been computed, one using the IGS-standard values for the SAO corrections (IGS14 antenna model, Schmid et al., 2016) and another one with the re-estimated SAO corrections.

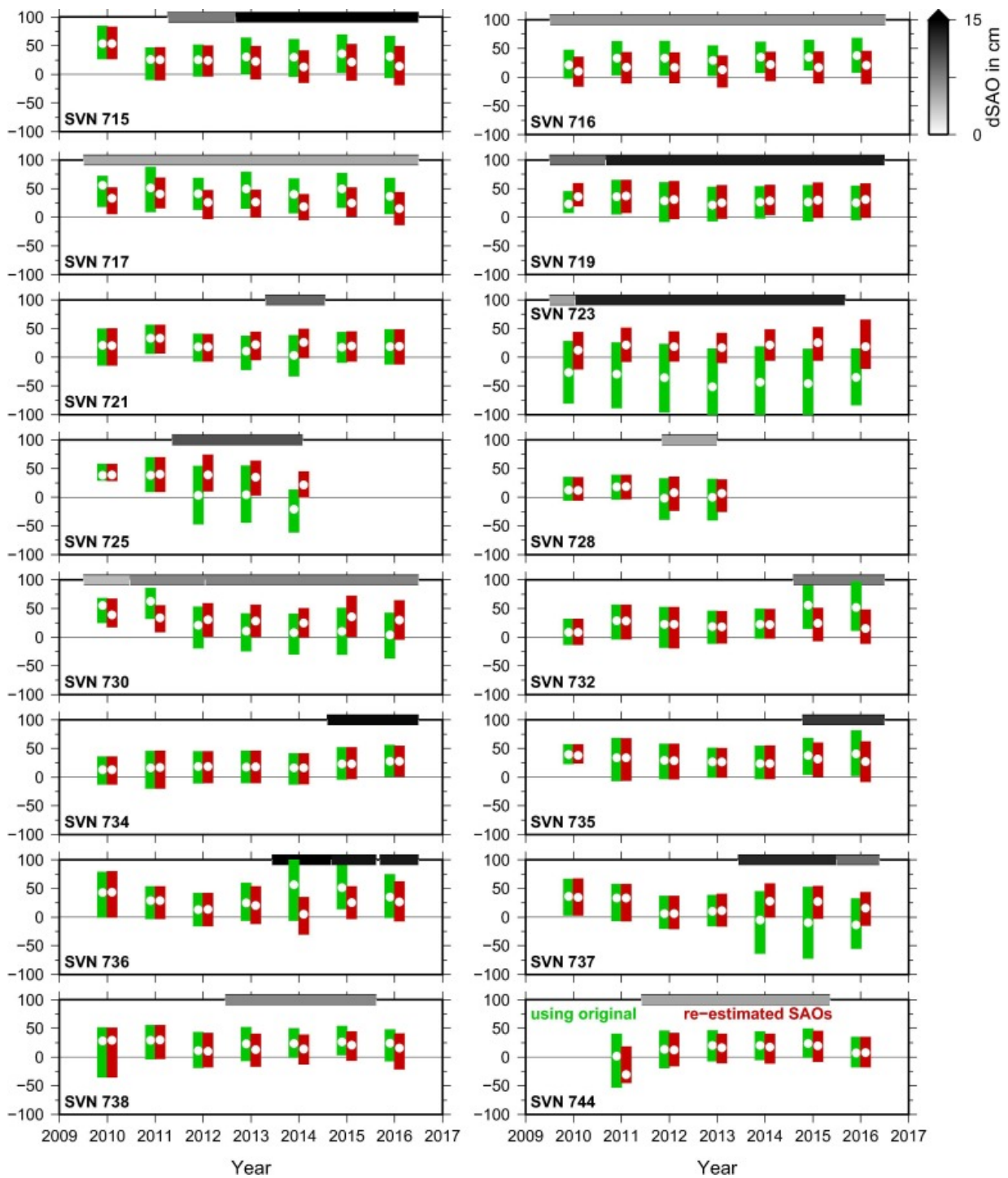


Figure 1. 24: Statistics on the SLR residuals to a certain satellite obtained within a year. The green and red bars cover the range from the quantile 25% to 75%. The white dot indicates the corresponding median value. All SLR residuals are given in mm. The gray lines on top of the plots indicate the magnitude of the difference between the original and re-estimated SAO corrections during a given interval.

SLR measurements were used to verify the orbits of GNSS satellites from the two solution series. An overview on the statistics of the SLR residuals is provided by Figure 1. 24. The green bars are obtained from the orbit solution using the original SAO values, whereas the red bars are related to the orbits using the re-estimated ones.

The bars cover the range from the 25% to the 75% quantile value of the SLR residuals. It means that the length of the bar is the interquartile range (IQR). The white dots represent the median (50% quantile) of the SLR residuals. The statistics is done for each year independently. It is clearly visible that the scatter of the SLR residuals (length of the bars) is reduced and becomes more consistent in time when using the re-estimated SAO.

For a better interpretation, the magnitude of the difference between the original and re-estimated SAO corrections in the X- and Y-component (with $dSAO = \sqrt{\Delta X^2 + \Delta Y^2}$) is provided by the bars on top of the individual plots. A darker gray (black for 15 cm or more) is related to a bigger deviation.

The plots in Figure 1. 24 confirm the improvement of the GLONASS orbits, in particular in the radial direction. There are examples (e.g., satellites 723, 725, or 732) for which the scatter of the SLR residuals is reduced by up to a factor of two. In other cases (e.g., satellite 730 or 736), an improvement of the long-term stability of the median (and quantile values) is achieved. For satellite 744 and the year 2011 there is only a very low number of SLR measurements available for this statistics (68 normal points compared to 1500...5000 typically available for the statistics per satellite and year – depending on the priority of the particular satellite in the SLR tracking network). This explains the apparent degradation of the orbit quality (median value at -4 cm whereas the other years show median values of +1...2 cm).

Summary

Unfortunately, it cannot be definitely concluded what is the reason for the observed deviation of the horizontal SAO corrections with respect to the nominal values. A reduced carrier-to-noise density reported in the observation RINEX files from different, globally distributed stations at least for some of the events suggests an issue with the satellite antenna or the related electronics. For a more detailed diagnostics more information from the system provider would be necessary. At least, applying the re-estimated SAO corrections instead of the original ones help to reduce the SLR residuals.

Advancing the orbit model for Galileo satellites during the eclipse seasons

D. Sidorov, R. Dach, L. Prange, A. Jäggi

Astronomical Institute, University of Bern

By the first quarter of 2019 the Galileo constellation can boast of 24 satellites that are considered in the CODE MGEX routine analysis (Prange et al. 2019). The products of this undertaking are submitted to the IGS on a regular basis. Although the switch of the MGEX analysis at CODE from the test to the operational environment has allowed to benefit from the use of the latest models and processing algorithms, modelling deficiencies are still observed in the Galileo products, in particular during the eclipse seasons. The results of these deficiencies are observed in the computed orbit overlaps at day boundaries (Sidorov et al., 2018), RMS of linear fits of the estimated satellite clocks (Prange et al., 2017) as well as in the satellite laser ranging (SLR) residuals (IGS MGEX Product Analysis, URL: <http://mgex.igs.org/analysis>). The analysis of the SLR residuals suggests that the other IGS analysis centers (AC) also suffer from Galileo orbit modelling complications during eclipse seasons – to a lower extent the shorter the arcs are. The necessity of actions in solving this issue is motivated by the fact that the resulting modelling errors may even propagate to other satellites and constellations via the common parameters in a multi-GNSS solution.

After gravitational attraction of the Earth, the Moon and the Sun, the solar radiation pressure (SRP) is the largest force that impacts the GNSS satellites. The Galileo satellites, by design having a large area-to-mass ratio, are more sensitive to this effect compared to other satellites due to their relatively low weight. While at periods with high Sun elevation above the orbital plane (β -angle) the SRP-induced forces do not undergo large variations, they vary significantly at low β -angles and reach extreme values during the satellite eclipse season. In addition to the SRP, thermal radiation (TR) is another non-negligible effect that should be considered, in particular, for Galileo satellites due to their design. Unlike the SRP, the TR-associated forces remain active both when the satellite is illuminated by the Sun and when it crosses the Earth's shadow. Thus, both effects cannot be taken into account by the same modelling strategy, in particular, by the use of the Empirical CODE Orbit Model (ECOM2; Arnold et al., 2015) employed at the CODE AC.

Thanks to the detailed Galileo satellite metadata packages (URL: <https://www.gsc-europa.eu/support-to-developers/galileo-satellite-metadata>) that were made publicly available by the European GNSS Agency (GSA), the satellite dimensions and surface properties of these satellites are known. According to these metadata, the Initial Orbit Validation (IOV) and Full Operational Capability (FOC) Galileo satellites are equipped with thermal radiators on the +X, +Y, -Y and -Z (FOC only) faces in a manufacturer-defined reference frame, Figure 1. 25. For the transformation from the manufacturer-defined reference frame to the IGS axis conventions, the reader is invited to consult Montenbruck et al. (2015). Taking into account only the radiator on the +X face (where the satellite clocks are installed) the associated TR-induced force at β -angles close to 0° creates accelerations that mostly act in the satellite along-track direction. Such a force cannot be fully captured by ECOM2 parameters, because they are switched off in the Earth's shadow. The introduction of a small constant acceleration (equivalent to an assumed power emission of 300W) in the satellite +X direction facilitates to mitigate this effect. Besides, the introduction of a once-per-revolution term in the direction satellite-Sun (D-component of the ECOM2) that is also kept active in the Earth's shadow in addition to the other ECOM2 parameters helps to account for the TR effect during eclipse seasons. Additionally, according to the provided metadata, thermal radiators installed on +Y and -Y faces of Galileo FOC satellites have different sizes, suggesting a constant TR-induced force in the satellite Y axis (also matches the ECOM2 Y axis). Activation of the constant term of ECOM2 in Y in the Earth's shadow compensates for this TR effect.

The findings of the investigation above were justified by processing the MGEX data during days 70-100 of the year 2018. This period is of particular interest as seven out of 15 Galileo satellites were passing the Earth's shadow during this time interval. The modifications to the orbit modelling positively influenced the computed solutions. In particular, significant improvements were observed in both, satellite orbit and clock modelling that was expressed by the reduction

of orbit misclosures at day boundaries and linear estimated clock fits, respectively, for the eclipsed Galileo satellites. The external SLR assessment of the refined orbits also showed improvements in solutions of the eclipsed satellites by reducing the RMS of the SLR residuals. As for the estimated empirical SRP coefficients, their previously highly uncertain behavior during eclipse seasons has become more regular and predictable.

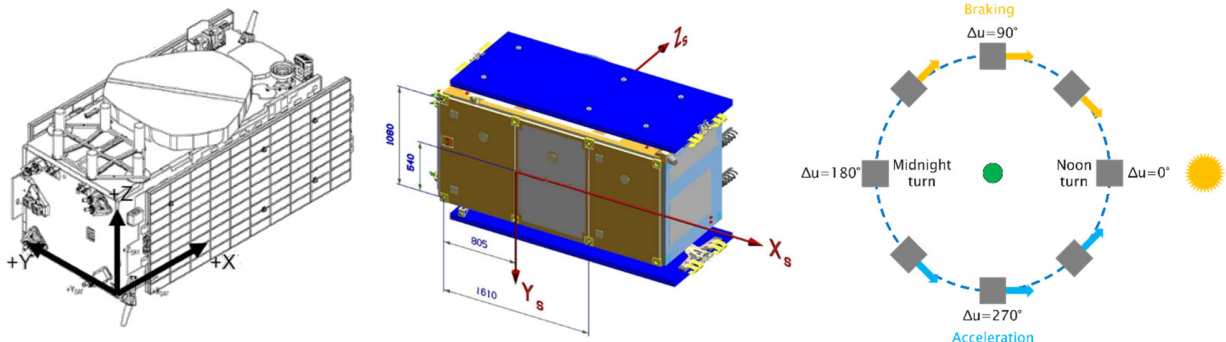


Figure 1. 25: IOV (left) and FOC (middle) Galileo satellites (Galileo Satellite Metadata, URL: <https://www.gsceuropa.eu>). Radiators are installed on +X, +Y, -Y faces and +X, +Y, -Y and -Z faces (in a manufacturer-defined reference frame) of IOV and FOC satellites, respectively. A sketch on the right shows a TR force impact from a +X radiator when $\beta=0^\circ$.

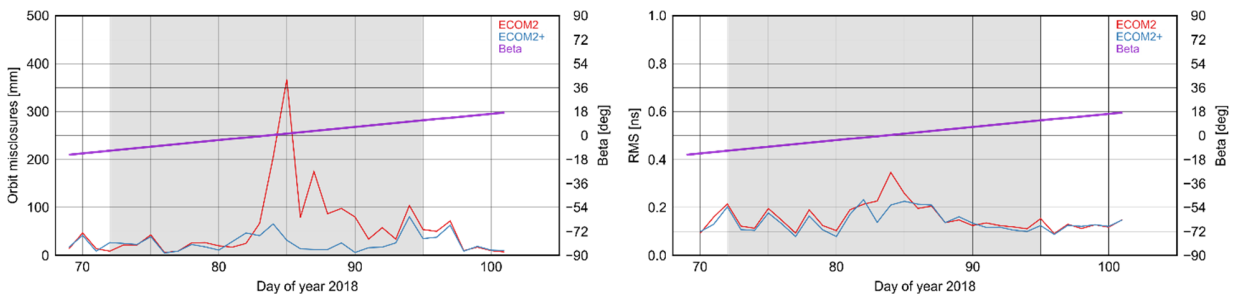


Figure 1. 26: Orbit misclosures at day boundaries (left) and RMS of linear clock fits (right) for Galileo E07 using ECOM2 (red) and adjusted ECOM2 (blue). The β -angle is shown in magenta, while the shaded area indicates the eclipse season.

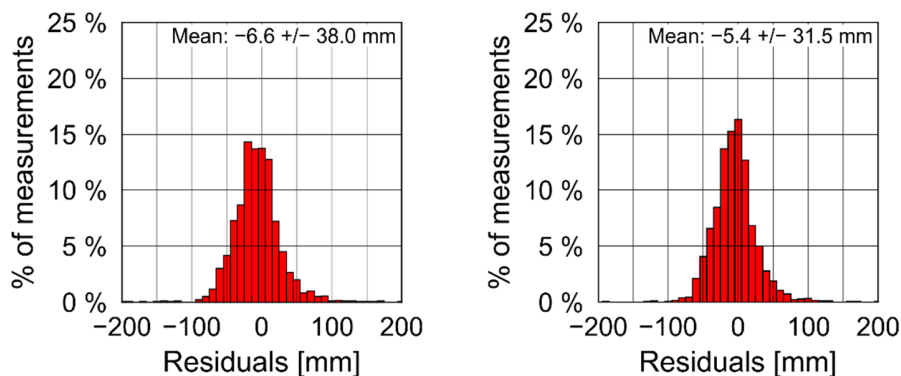


Figure 1. 27: Histograms of SLR residuals of Galileo orbits computed using ECOM2 (left) and adjusted ECOM2 (right) over days 70-101 of year 2018.

This study addressed the unaccounted TR-associated effects during orbit modelling of eclipsed Galileo satellites. If left unaccounted, these effects may significantly deteriorate the estimated orbits. The research outcomes have highlighted the importance of the satellite metadata in identifying the potential issues and refining the employed orbit models.

Validating the use of a Scalable Boxwing Model for GNSS satellites

L. McNair, A. Villiger, R. Dach, A. Jäggi

Astronomical Institute, University of Bern

A significant source of error in orbit modeling of Global Navigation Satellite System (GNSS) satellites is the effect of radiation pressure, both from the sun, and from the Earth. The new Empirical CODE Orbit Model (ECOM2) of the Center for Orbit Determination in Europe (CODE), introduced in 2014, attempts to empirically account for the Solar Radiation Pressure (SRP) effects (Arnold et al., 2015). This model has been shown to be particularly effective for GLONASS, Galileo and QZSS satellites outside of eclipse season, but is less effective during eclipse season and for other systems (Prange, L. et al, 2016). No a priori effect, e.g., from a boxwing model, is applied because any error, uncertainty, or significant simplification has a comparably large effect on the SRP corrections for the orbits if it cannot adequately be absorbed by empirical parameters.

The adjustable boxwing model is a semi-analytical model for radiation pressure which sees improved performance during eclipse season (Solano, 2014; Montenbruck et al., 2015; Montenbruck et al., 2017). In this model the optical properties of different surfaces are estimated as “adjustments” to the a priori boxwing model. The adjustable boxwing model is capable of achieving similar performance as the ECOM2, but worse performance during eclipse season, especially for GPS-IIA satellites. It is noted that in the adjustable boxwing model, optical properties of individual surfaces are estimated, but surface area is assumed to be perfectly known. Furthermore, for the surfaces of the “box” portion of the boxwing model, multiple quantities must be estimated.

AIUB has implemented a Scalable Boxwing Model in the development version of the Bernese GNSS Software (Dach et al., 2015), using scaling factors to validate and adapt the parameters of the boxwing models. In this model a maximum of one scale factor per surface is applied when computing SRP and PRP effects, and may account for errors in the a priori values of the optical properties and surface areas. Reliable satellite characteristics have only been released for Galileo and QZSS (see GSA 2016 and CAO 2017). They may serve as a reference (scaling factor of one is expected) when estimating the scaling factors. For the other GNSS satellites, the true satellite models remain unknown, so the scaling factors have a bigger impact on the orbits.

The quality of orbits produced by the Boxwing Model was shown by means of orbit misclosures at the day boundaries for all satellites. Figure 1. 28 shows the orbit misclosures obtained using only the ECOM2 solution, and Figure 1. 29 shows the orbit misclosures obtained using both the ECOM2 and a Boxwing model (according to Solano 2014 and GSA 2016). Despite the fact that there is a high correlation between the parameters estimated by the two different models, this approach is seen to improve the orbit misclosures, specifically during the period of time when eclipsing Galileo satellites impact the whole solution (Sidorov et al 2019). This effect is seen very clearly between Oct 2017 and Jan 2018 in Figure 1. 28. However, at earlier points in time the solution is not necessarily improved by the addition of the Boxwing Model, demonstrating the need for adjustments to the a priori models, which are implemented in the form of scale factors.

Scale factors were then computed for the one year period of time from 1 February 2017 through 31 January 2018. For this time period, the effect of different plate groupings was also studied. The plate groupings considered were Monoscale and Smartscale-2. The Monoscale plate grouping estimates a single scale factor for all plates on a given satellite, and is equivalent to estimating a satellite-wise scale factor. The Smartscale-2 plate grouping estimates one scale factor for all body or “box” plates, and a second scale factor for all solar panel or “wing” plates.

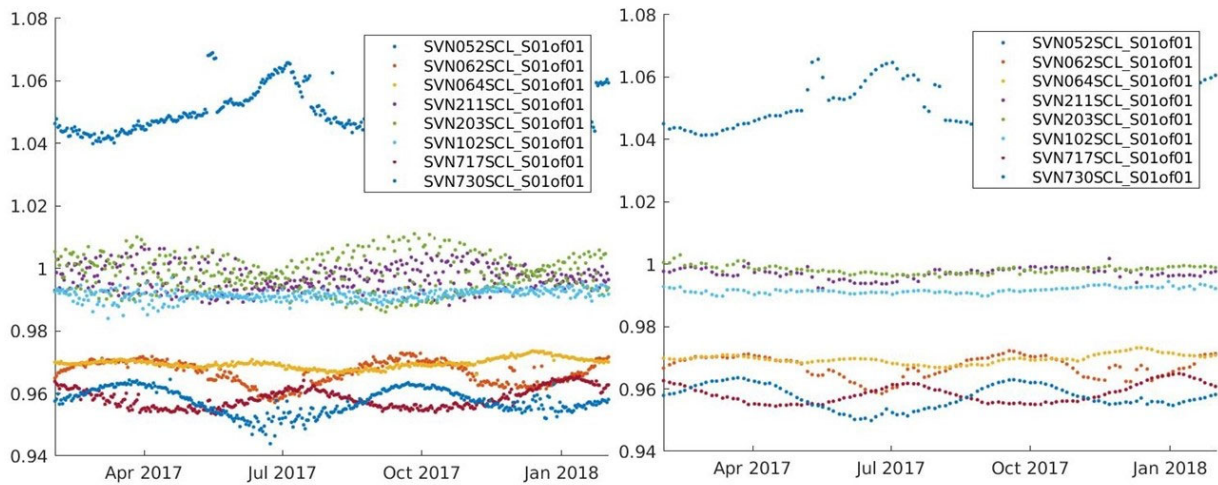


Figure 1. 30: Scale factors estimated for selected satellites, for one year, using the Monoscale model, daily solution (left) and weekly stack (right).

It was also possible to stack together the entire year worth of daily solutions to compute a weighted average scale factor for each satellite. These values are shown for all satellites in Figure 1. 31. In both Figure 1. 30 and Figure 1. 31 it can be seen that the computed scale factors for Galileo satellites, which are used as a reference, are very close to 1 (within about 2% for the daily solutions, and 1% for the weekly and yearly combinations), validating the approach. The scale factors for GPS and GLONASS are slightly farther away from 1 (up to about 8%), which is a further indication of imperfections in the corresponding boxwing models.

With the Smartscale-2 plate grouping, Galileo once again had the best performance, but GLONASS performed more similarly to Galileo. In both of these systems, there were correlations between the two estimated scale factors, and seasonal variations generally resulted in widening between the two (e.g. an increase in the estimated box scale factor simultaneous with a decrease in the wing scale factor). This was also true for GPS, but both scale factors for GLONASS and Galileo remained within about 80% of the nominal value, whereas for GPS they varied by up to 300%.

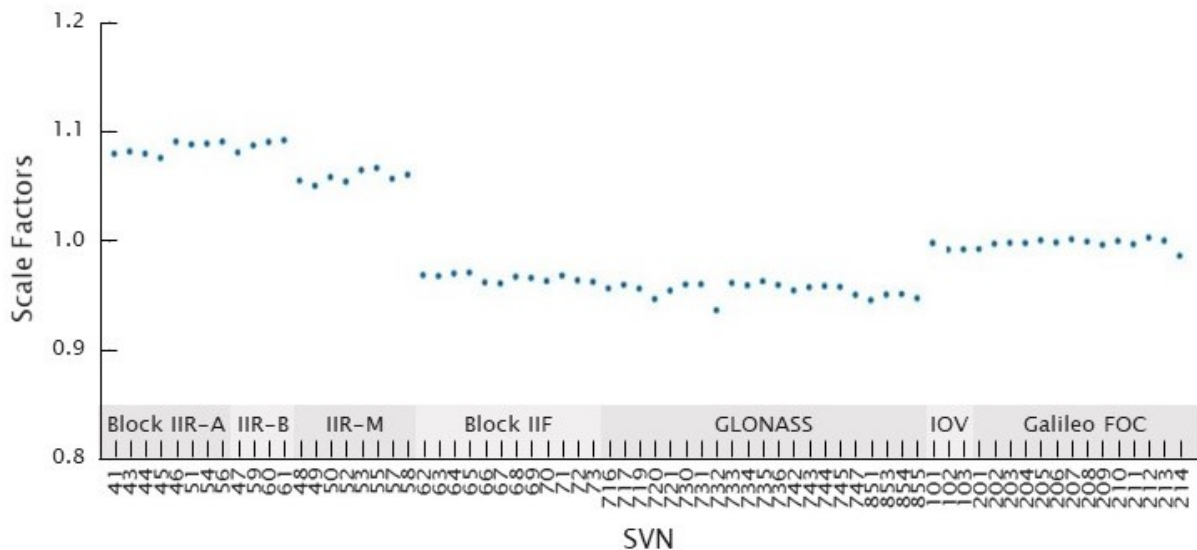


Figure 1. 31: Scale factors estimated for all satellites, using the Monoscale model, yearly stack, sorted by system and block.

There are many physical reasons for the correlations and covariances between scale factors of individual plates in the boxwing model, including similar optical properties, parallel plates, and attitude geometry. But the primary reason for the stronger correlation between the two scale factors in the Smartscale-2 plate grouping for GPS is related to the satellite body geometry. The body of GLONASS and Galileo satellites can be approximated by a rectangular prism, with the +/- X plates having a much smaller surface area than the +/- Z plates. Particularly during high-beta seasons, over the course of an orbit, the SRP force on the satellite body varies, being largest when only one of the +/-Z plates is illuminated, and smallest when only the +X plate is illuminated. Furthermore, when both the +X and one of the Z plates are illuminated, the resultant force is rarely parallel to the SRP force on the solar panels. Conversely, the bodies of GPS satellites more closely resemble cubes, so the SRP force on the satellite body remains relatively constant, and is usually nearly parallel to the SRP force on the solar panels.

Using the method described here of applying a Scalable Boxwing Model, it was possible to stack scale factors from an individual satellite and/or surface over many solutions for long periods of time in order to obtain a weighted average scale factor for that physical surface. The number of distinct scale factors per satellite which are possible to estimate in a meaningful way depends on characteristics of the satellite, specifically satellite body geometry and optical properties. Improvements can be seen at the daily solution level.

An empirical SRP model for the orbit normal attitude mode

L. Prange¹, G. Beutler¹, R. Dach¹, D. Arnold¹, S. Schaer^{1,2}, A. Villiger¹, A. Jäggi¹

¹ Astronomical Institute, University of Bern

² Federal Office of Topography swisstopo

The Center for Orbit Determination in Europe (CODE, Dach et al. 2018) is contributing to the Multi-GNSS Extension (MGEX, Montenbruck et al. 2013) of the International GNSS service (IGS, Johnston et al. 2017) since its start in 2012 with an orbit and clock solution currently including the observations from five systems, namely GPS, GLONASS, Galileo, BeiDou2 (BDS2), and QZSS. Data from the satellite systems BDS2 and QZSS contribute to CODE's MGEX (COM) solution since late 2013 and early 2014, respectively (see Prange et al. 2017 and Prange et al. 2019b). So far, only satellites with medium Earth orbits (MEO) and inclined geosynchronous orbits (IGSO) are considered for COM.

The COM solution series was started assuming yaw steering (YS) attitude for all satellites. The reduced Empirical Code Orbit Model (ECOM1, Springer et al. 1999) was applied as solar radiation pressure (SRP) model for all GNSS satellites all the time. Later, ECOM1 was replaced by ECOM2 (Arnold et al. 2015) for all satellites and dedicated attitude laws were applied for GPS, GLONASS, and Galileo satellites during their eclipses (see Prange et al. 2019b). Most BDS2 spacecraft as well as QZS-1 are, however, oriented according to the orbit normal (ON) attitude at times when the elevation of the Sun over the respective orbital plane (the so-called beta angle) is small. Since the ECOM decomposition was designed for the YS-mode, the established ECOM SRP models are not sufficient for properly modelling the SRP during the ON-mode periods (Prange et al. 2017). Therefore, some groups developed (semi-) analytical SRP models that perform well - at least for QZS-1 (e.g., Montenbruck et al. 2017, Darugna et al. 2018, and Zhao et al. 2018). However, most of these models cannot cover the SRP effect entirely. Hence, they still need to be supported by an empirical model.

We developed a family of empirical models able to absorb the SRP-forces in an efficient way for satellites flying in ON-mode attitude - including spacecraft in geostationary orbits (Prange et al. 2019a). These models (ECOM-TB) are using the terminator plane as the basis for the coordinate system in which the estimated SRP-parameters are defined (Figure 1. 32). In addition, a dependency of the estimated parameters from the beta-angle is considered. After intensive investigations and tests based on MGEX data the ECOM-TB was activated in the COM solution in summer 2018. Like older ECOM models, ECOM-TB can be used stand-alone or together with an a priori SRP model.

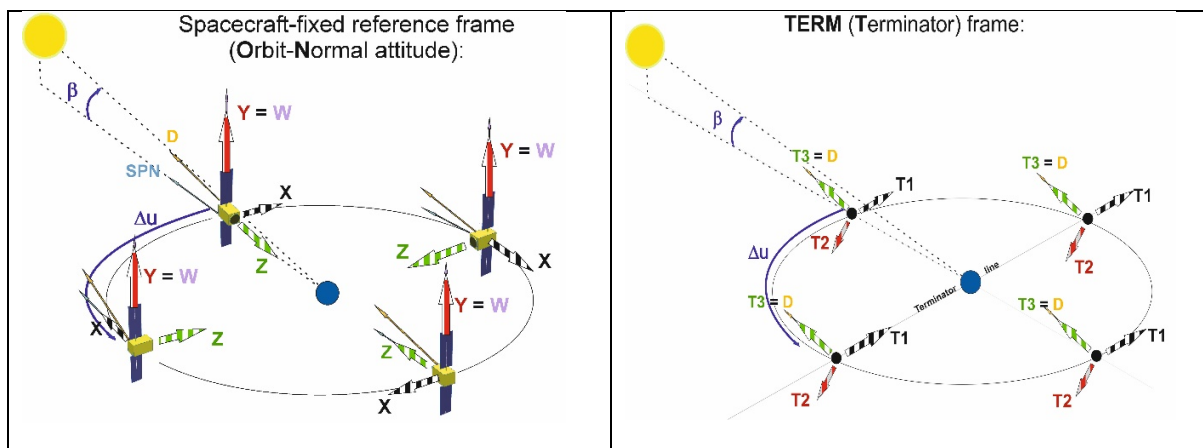


Figure 1. 32: Spacecraft-fixed reference frame under ON mode (left) and terminator reference frame (right).

Our validations (SLR residuals, orbit misclosures, long-arc orbit fits, linear fit of epoch-wise satellite clock corrections) show that the ECOM-TB is able to significantly improve the estimated orbits and clock corrections of QZS-1 during the ON mode (by about a factor of 4). This is confirmed by comparisons with external QZS-1 solutions in the frame of the IGS MGEX (Figure 1. 33).

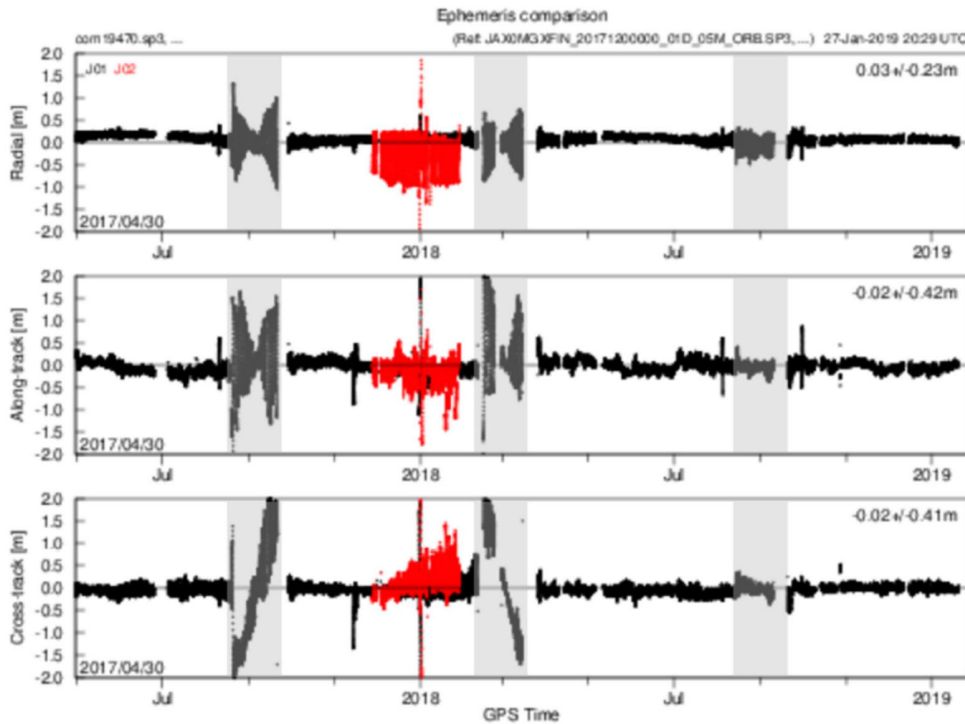


Figure 1. 33: Orbit comparison of QZS-1 orbits from the MGEX solutions “JAXA” and “COM”. Time windows with ON mode are shaded in gray (screenshot taken from <http://mgex.igs.org/analysis/>).

The benefits are less pronounced for BDS2. For this GNSS we encountered moderate (in the case of MEO satellites) or significant (in the case of IGSO satellites) difficulties to properly determine the SRP model coefficients in the case of using long arcs. We assume that various factors contribute to the limited model performance for BDS2: Heterogeneous density of the tracking network, unclear antenna offsets (the published estimates for the IGSO satellite offsets differ significantly from each other; see Huang et al. 2018), and unknown spacecraft properties. We addressed this issue by developing modified versions of the ECOM-TB for BDS2 spacecraft: For BDS2 MEO satellites stochastic pulses support the SRP model (ECOM-TBP). For BDS2 IGSO satellites we use a reduced version ECOM-TBMP (with 2 instead of 9 SRP parameters), also supported by pulses. With these modified versions of the SRP model we are able to improve the orbit and clock accuracy of BDS2 satellites in ON-mode by about a factor of 2 compared to ECOM2 (Prange et al. 2019a).

Satellite Laser Ranging to Low Earth Orbiters – Orbit and Network Validation

D. Arnold¹, O. Montenbruck², S. Hackel², K. Sośnica³

¹Astronomical Institute, University of Bern

²German Space Operations Center, Wessling, Germany

³Institute of Geodesy and Geoinformatics, Wrocław University, Wrocław, Poland

Satellite laser ranging (SLR, Combrinck 2010) to low Earth orbiters (LEOs) provides optical distance measurements with mm-to-cm-level precision. SLR residuals, i.e., differences between measured and modeled ranges, are commonly used for the quality assessment of orbits derived by radiometric tracking techniques, e.g., by means of Global Navigation Satellite Systems (GNSS).

While differences in the data handling strategies sometimes complicate the comparison of SLR validation results of different groups, in Arnold et al. (2018) we made the attempt to present consistently computed SLR validation results for a wide range of past and present LEO missions supported by the International Laser Ranging Service (ILRS, Pearlman 2002). We have pointed out the importance of line-of-sight-dependent range corrections for the various types of laser retroreflectors (see Figure 1. 34) and have demonstrated a 1-3 cm consistency (in terms of standard deviation) of SLR observations and GPS-derived precise orbits for these missions.

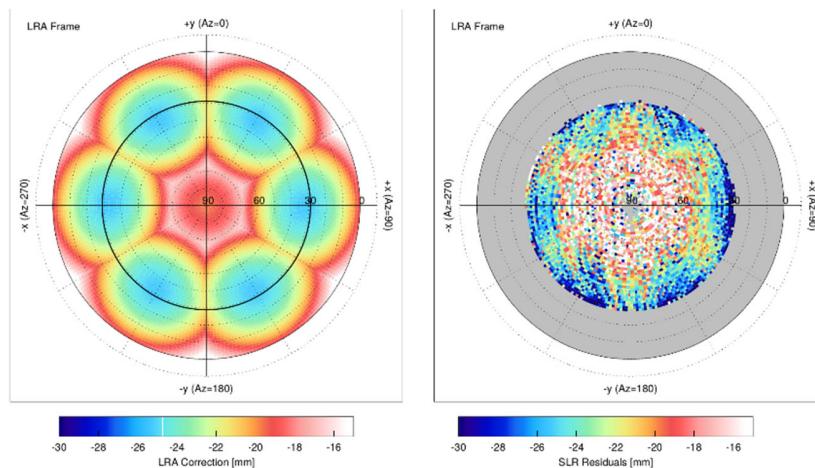


Figure 1. 34: Theoretically computed azimuth- and elevation-dependent range corrections for the SLR reflector mounted on the Sentinel-3 LEOs (left), as well as Sentinel-3A SLR residuals obtained in the absence of the range corrections (right), represented in a retroreflector reference system

Especially for LEOs, SLR observations are not only sensitive to radial orbit errors. We have presented an SLR residual-based parameter estimation approach to investigate systematic orbit errors and have demonstrated that it is well capable of detecting, e.g., cross-track orbit errors. As an example, Figure 1. 35 shows mean cross-track Sentinel-3A orbit differences w.r.t. a reference orbit for different iterations in the generation of empirical phase center variations (red), together with cross-track orbit offsets estimated from SLR residuals (green). It is obvious that the estimated orbit offsets clearly follow the true orbit differences. Therefore, SLR to LEOs is obviously capable of identifying orbit errors induced, e.g., by orbit parametrization issues or erroneous sensor offset information.

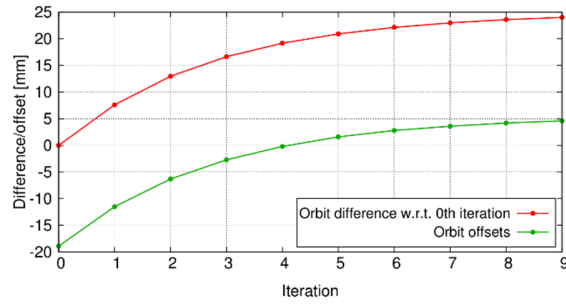


Figure 1. 35: Red: Mean differences in normal direction of orbit solutions obtained in iterations of a Sentinel-3A phase center variation map generation w.r.t. the orbit solution obtained without applying phase center variation corrections (iteration 0). Green: Orbit offset in normal direction estimated from SLR observations of high-quality stations over the period April to November 2016. SLRF2008 site coordinates were used

Making use of high-quality LEO orbit products, we have shown in Arnold et al., 2018 that SLR residual analysis is also capable of detecting and quantifying the SLR tracking network performance and individual station characteristics. Based on SLR residuals for the LEOs Swarm-C, TerraSAR-X, Sentinel-3A, and Jason-2 (covering an altitude range of about 500-1300 km) for the year 2016, we have estimated corrections to station coordinates, as well as range biases. Based on the reference frame SLR2008 (formally compatible with the IGB08 reference frame of the GPS-based LEO orbit products) we have found position and bias corrections well above the 1-cm level for the majority of stations, even reaching the decimeter range for a few sites. Depending on the coverage of individual stations, formal uncertainties of about 1–2 and 2–4mm are obtained for the horizontal and vertical components of the position corrections, respectively, when using a slightly conservative weight of 20mm per normal point. The same analysis in SLRF2014, even though formally “incompatible” with IGB08, yields much more consistent results, see Table 1. 3 which presents the SLR residual statistics for the four mentioned LEOs and for both reference frames, once without and once with applying the estimated coordinate and range bias corrections. Figure 1. 36 shows the station-wise standard deviations of SLR residuals for the four LEOs when using SLRF2014 before and after applying coordinate and range bias corrections. The majority of stations offer a ranging precision of better than 20mm, and a substantial fraction of stations achieves a standard deviation in the 5–10mm range. When restricting the statistics to 12 high-performing SLR stations (contributing 50-75% of all normal points), SLR residuals of 7mm standard deviation are obtained for the four LEOs in 2016.

Coordinates	Uncorrected [mm]	Corrected [mm]	Stations
SLRF2008	-1.4±24.2	0.0±11.7	32
SLRF2014	-1.9±16.5	0.0±11.7	32

Table 1. 3: SLR residuals (mean ± standard deviation) of Swarm-C, TerraSAR-X, Sentinel-3A, and Jason-2 orbits before and after adjustment of station coordinates and range biases. A common threshold of 20cm and an elevation cutoff of 10° were applied in all cases

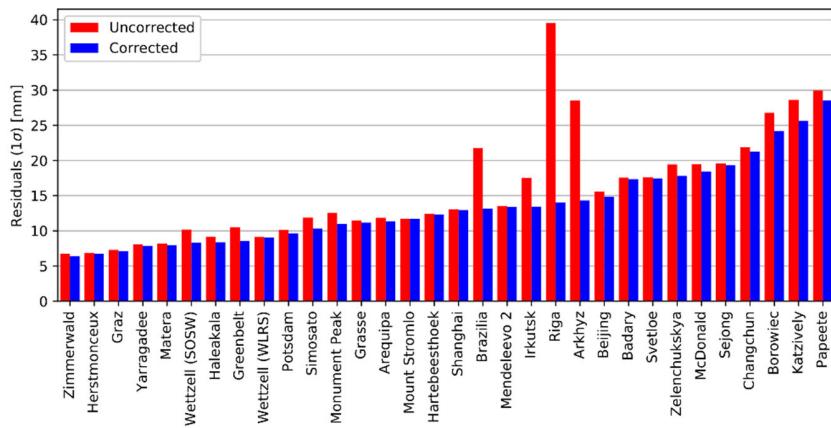


Figure 1. 36: SLR residuals of Swarm-C, TerraSAR-X, Sentinel-3A, and Jason-2 orbits for individual ILRS stations before and after correction of SLRF2014 site coordinates and station-specific range biases

Besides station coordinates and range biases, SLR residuals to LEOs have also been shown to be sensitive to timing errors at the SLR stations. As an example, timing biases for Papeete SLR station have been estimated from SLR residuals to Swarm-C, TerraSAR-X, and Jason-2 for January to February 2016 (-14.4 μ s) and March to June 2016 (-5.8 μ s). These values are consistent with independent timing bias estimations by Exertier et al. (2017) and Otsubo (2017).

As a summary, it can be stated that SLR residuals to LEOs are, beyond a means for simple orbit validation, on the one hand useful to identify systematic orbit errors that may result from deficiencies of the dynamical orbit model or improper information on the accommodation of sensors and antennas. Vice versa, high-quality LEO orbits may serve as reference for improving station positions and bias calibrations in the laser tracking network. Besides the use of local ties at suitably equipped fundamental sites, the SLR validation of GPS-based LEO orbits thus offers a complementary approach to integrate different space geodetic techniques in the construction of global reference frames.

The effect of SLR tracking scenarios to GNSS satellites in a combined

F. Andritsch, U. Meyer, R. Dach, T. Schildknecht, A. Jäggi

Astronomical Institute, University of Bern

The International Terrestrial Reference Frame (ITRF, Altamimi et. al 2016) combines microwave (MW) based observations to satellites of the Global Navigation Satellite Systems (GNSS) and Satellite Laser Ranging (SLR) observations to the pairs of LAGEOS and Etalon satellites among others using local ties at the stations. Experiments using SLR normal points (NP, binned full-rate data) to GNSS satellites that are equipped with retroreflectors (to allow for SLR measurements) as space ties instead of local ties for the combination were conducted in the past (e.g., Bruni et al, 2018, Thaller et al, 2008).

Such space-ties related experiments need a sufficient bases of NPs. At AIUB a simulation study has been conducted in order to identify the optimal tracking scenario at the SLR stations for such applications. The effect on the obtained geodynamical and geodetic parameters of such a combined solution was compared. The strategy to derive the combined GNSS+SLR solution is based on the normal equation (NEQs) derived from independent observations and is illustrated in *Figure 1. 37*, see Andritsch et al. (2018a). The simulation tool for realistic SLR observations was described in Andritsch et al. (2016).

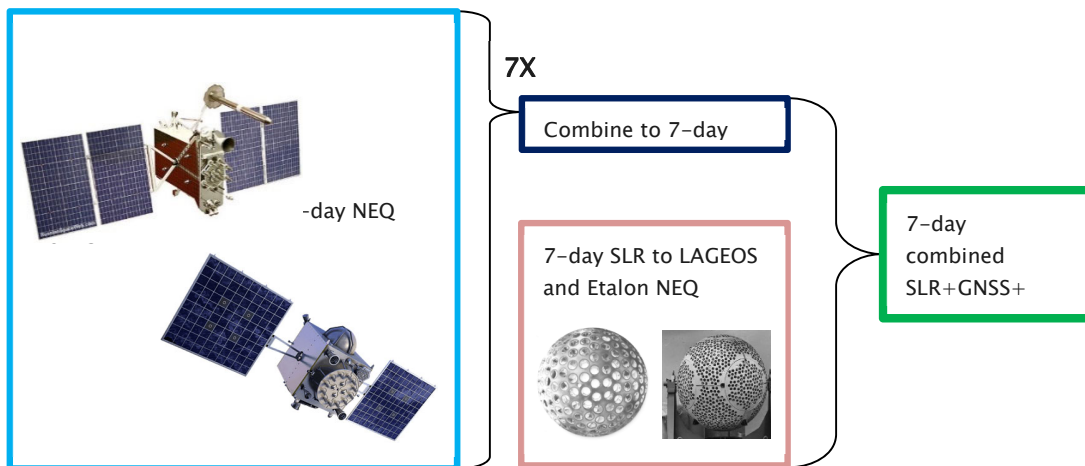


Figure 1. 37: Combined weekly solution of microwave (MW) observations to GPS and GLONASS, SLR observations to GLONASS and SLR observations to LAGEOS and Etalon.

The biggest problem of a rigorous combination of observations of these two techniques is the large difference in the density of the station network as well as the level of activity of the respective networks. SLR stations are only able to track one target at a time and they depend on sufficient weather conditions for taking measurements. On the other hand, the GNSS MW observations are generated by a much denser network with about 10 to 15 observations per measurement epoch (typically with a sampling of 5 minutes). This leads to a ratio of about 1:2000 of SLR w.r.t. MW measurements. To overcome this imbalance the weight of the SLR observations w.r.t. the GNSS ones is increased by 2000 in the combination process.

The following tracking scenarios were studied:

- All GLONASS with equal priority (allGLONASS)

- 2 GLONASS per orbital plane (2GLONASS)
 - GLONASS tracking to only those satellites
- Arranged tracking between European stations (EUROPE)
 - Six stations alternate tracking to the 6 prioritized satellites on a bi-weekly basis
- GPS and GLONASS equally (2SYSTEM)
 - Simulated retroreflectors on all GPS satellites
 - Number of targets increases to 60

It was shown in Andritsch et al. (2018b) that altering the priority of the GLONASS satellites for the ILRS stations has small impacts on some parameters of a combined weighted solution. Station coordinates and the geometry of the solution are not affected in a significant way by changing the SLR tracking strategies to the GLONASS satellites. This is the case because the station coordinates as well as the geocenter coordinates are mostly dominated by the larger number, by a factor of more than 4, of LAGEOS observations (see Figure 1. 38) and the huge number of MW-observations to the GNSS satellites. These observations remain unchanged between the scenarios.

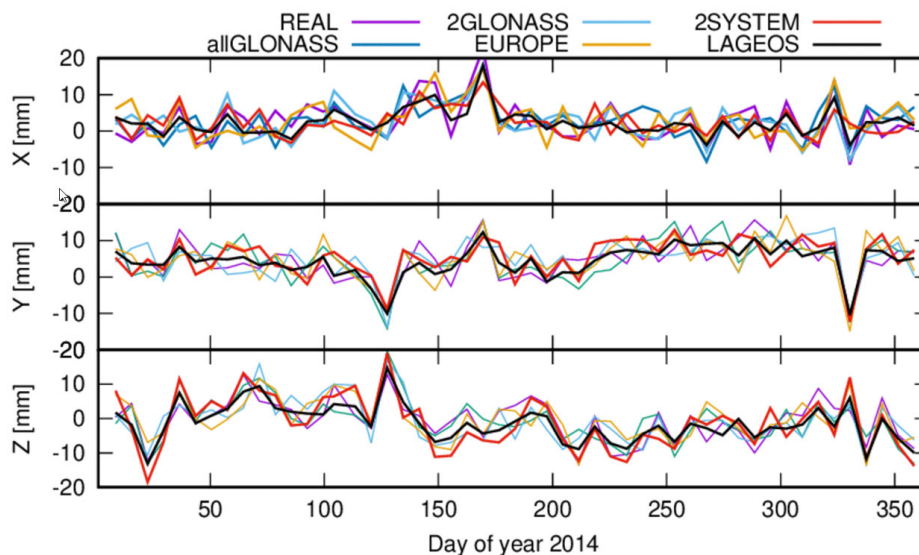


Figure 1. 38: Geocenter coordinates for the different scenarios. Variations between the different weeks dominate the change in tracking scenario.

The differences between the separate scenarios in a single weekly solution are small, as they only affect a comparatively small number of NPs each week. When for a few satellites only a small number of NPs is provided in a specific week by some stations the formal errors in this week are above average.

An advantage of the simulation is that the same set of SLR measurements can be reproduced with different noise functions. This allows to distinguish between the effect of the geometry of the station network and available observations and the noise of the observations. It turned out that the geometric effect is dominating the noise effect because the differences between the solutions obtained with various noise functions are smaller than the variations from week to week. The same holds for the different tracking scenarios. This means it is more important how many NPs a station is producing at a given day than which satellite exactly the station is observing.

Only for the ERPs in the combined solution it is beneficial to tend towards a uniform observation of all GLONASS satellites compared to focusing on a subset. The formal errors suggest that there might not be enough NPs currently to evenly observe two GNSS systems with the given tracking activities.

A Simulation Toolkit for Satellite Laser

M. Meindl, C. Lanegger, M. Rothacher

Institute of Geodesy and Photogrammetry, ETH Zürich, Switzerland

Satellite laser ranging (SLR) is nowadays widely used as complementary technique to validate satellite orbits determined by, e.g., global navigation satellite systems (GNSS). A SLR simulation toolkit was developed (Lanegger, 2017) in order to plan observation campaigns and generate ideal SLR measurements sequences.

The simulation toolkit takes the satellite's orbital parameters, its geometry of retroreflectors and data about active ground stations as input. As a first step, it calculates the satellite trajectory by solving Kepler's equation. Subsequently the footprint of the satellite laser retroreflectors is computed for every specific moment along the satellites orbit.

Once the footprint is known, the toolkit analyses at each time step, if the satellite is located in the visibility region of any of the active stations. If that is the case, the program calculates the mean number N_{pe} of returning photons using the radar link budget equation (Degnan, 1993):

$$N_{pe} = \eta_q \left(E_T \frac{\lambda}{hc} \right) \eta_t G_t \sigma \left(\frac{1}{4\pi R} \right)^2 A_r \eta_r T_a^2 T_c^2$$

where η_q is the quantum efficiency of the detector, E_T is the laser pulse energy, λ is the wave length, hc is Planck's constant multiplied by the speed of light, η_t and η_r are the transmitter and satellite optics efficiency, G_t is the transmitter gain, σ is the optical cross section of the retroreflectors, R is the slant range to the satellite, A_r is the effective telescope area, T_a is the one-way atmospheric transmission, and T_c is the one-way transmissivity of cirrus clouds. All station specific parameters are obtained from the site logs provided by the international laser ranging service ILRS (available at <https://ilrs.cddis.eosdis.nasa.gov>).

The output data obtained during the simulation is stored in several text files, which can be used for post-processing. Moreover, the toolkit provides various visualizations: a map showing all laser observatories, the ground track of the satellite and its current location; a detailed overview of the visibility of the satellite and the expected number of returned photons; sky plots for each station showing all satellite passes; access time and number of returned photons for each single laser observatory (Figure 1. 39 exemplary shows the statistics for station Zimmerwald).

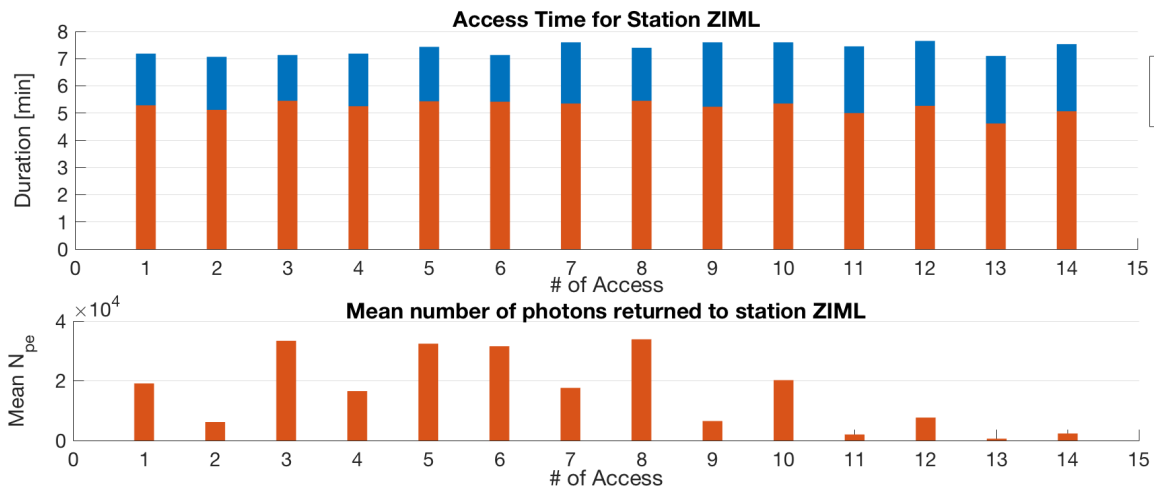


Figure 1. 39: Access time and mean number of returned photons for 14 passes for station Zimmerwald (blue: at least one photon returned, red: at least 100 photons returned).

So far, the simulation toolkit has been successfully tested by performing a simulation of the satellite Astrocast-01 over a period of 7 days. In the meantime, the Astrocast-01 satellite was launched (December 03, 2018). Once first SLR observations are available, the results of the simulation tool will be verified.

Analysis of the Short VLBI Baseline at the Wettzell Observatory

I. Herrera-Pinzón¹, M. Rothacher¹, J. Kodel², U. Schreiber²

¹ Chair of Mathematical and Physical Geodesy, Institute of Geodesy and Photogrammetry, ETH Zurich

² Geodetic Observatory Wettzell, Institute for Astronomical and Physical Geodesy, Technical University Munich

The analysis of short VLBI baselines, with lengths of less than a few hundred metres, contributes to identify local effects and instrument-specific biases, as many other error source relevant for long baselines (tropospheric delays, Earth rotation, quasar coordinates, station motion, etc.) are practically eliminated for such short baselines. The identification of technique-specific biases constitutes a pre-requisite to improve the realisation of the ITRF and to fulfil the GGOS goals in terms of accuracy and stability. In particular, these intra-technique experiments are expected to provide insights into systematic technique-related errors, leading eventually to a better agreement with the local ties at the fundamental sites. For this purpose, station coordinates, zenith tropospheric delays, clock offsets and Earth orientation parameters) were estimated from a global network and a subset of these parameters from the short VLBI baseline at the Fundamental station Wettzell in Germany, realised by the legacy 20 m dish Radio Telescope Wettzell (RTW) and the new 13.2 m diameter TWIN Telescope Wettzell (TTW1). The main task was to compare the derived parameters among the VLBI solutions and, for station coordinates, with the terrestrial survey results to study the performance of the VLBI solutions.

The VLBI data was processed in a tailored version of the Bernese GNSS Software v5.2. For the parametrisation, four different approaches have been designed, where the modelling of the dry atmosphere, the solid Earth tides and ocean loading, are common for all these solutions. The first approach (GLO) is a global solution, where all VLBI observations of a global network were used. The second processing approach (BAS) is a short baseline solution, where only the RTW – TTW1 (WETTZELL – WETTZ13N) baseline observations were used. The datum for the station coordinates is given by heavily constraining the coordinates of WETTZELL. Earth rotation parameters were not estimated, and receiver clock offsets were set up each 24 h for WETTZ13N, for each session. No troposphere zenith wet delays between the two stations were estimated. The third approach (BA2) is identical to the approach BAS except that here troposphere zenith wet delays were estimated as piece-wise linear functions with a time resolution of 2 h and mapped with the wet VMF model for WETTZELL. The fourth solution (BA3), using the baselines WETTZELL-NYAL and WETTZ13N-NYAL, because the short baseline in Wettzell could not be correlated directly, will not be discussed here. A set of surveyed local ties report a baseline length of 123.3070 ± 0.0007 m. Baseline length differences with respect to these values have been computed (see

Figure 1. 40). Moreover, the mean values and standard deviations over the time series have been calculated, resulting in average values and standard deviations of -0.8 ± 4.9 mm for the GLO solution, -0.3 ± 0.8 mm for the BAS solution, and -0.1 ± 1.3 mm for the BA2 solution. The comparison of the baseline length shows an excellent agreement with differences below 1 mm, albeit the large standard deviations for the global solutions.

In addition to the baseline length, the differences per component with respect to the local ties are analysed, in an ENU system.

Figure 1. 41 displays these differences where the up component shows a larger scatter, while the north component displays the best performance. This behaviour is attributed to the orientation of the baseline, since RTW is located at the north of TTW1. From the investigated solutions, the BAS approach shows the best performance, on account of its parametrisation, which is based on only data of the short baseline and estimates the smallest number of parameters (coordinates and clock offsets), which strengthens the calculation of the estimated parameters.

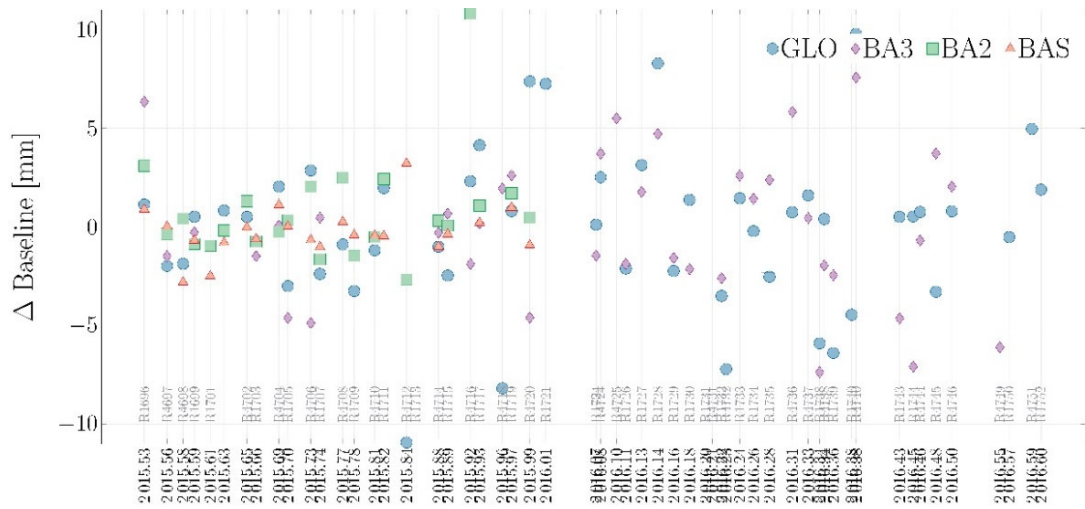


Figure 1. 40: Baseline length differences [mm], with respect to the local tie, for the baseline WETTCELL-WETTZ13N (Wetzell, Germany)

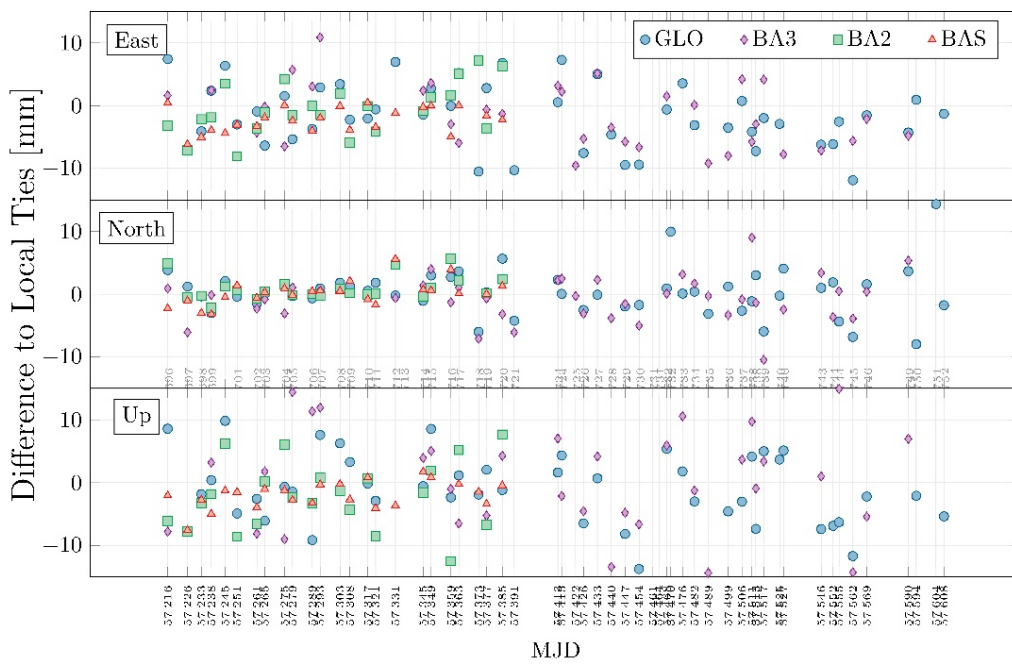


Figure 1. 41: ENU differences [mm], with respect to the local tie, for the baseline WETTCELL-WETTZ13N (Wetzell, Germany)

Investigations on time Dissemination for VLBI Observations at the Wettzell Observatory

I. Herrera-Pinzón¹, M. Rothacher¹, J. Kodel², U. Schreiber²

¹ Chair of Mathematical and Physical Geodesy, Institute of Geodesy and Photogrammetry, ETH Zurich

² Geodetic Observatory Wettzell, Institute for Astronomical and Physical Geodesy, Technical University Munich

As an independent source of information, the Two-Way Optical Time Transfer system (TWOTT) provides the difference between the clock corrections of the two hydrogen masers of the VLBI telescopes in Wettzell (Germany), with a higher temporal resolution and a much better RMS performance than the VLBI clock estimates. Moreover, the TWOTT residuals with respect to a linear fit show the same behaviour as the VLBI clock estimates. Figure 1. 42 shows the comparison of the residuals with respect to a linear fit for both, the TWOTT data (green) and VLBI (blue), where both share the same overall behaviour, but the higher resolution and smaller RMS of the TWOTT data is evident. Notice that for session R4712 (bottom), the TWOTT residuals follows the quadratic behaviour of the clock.

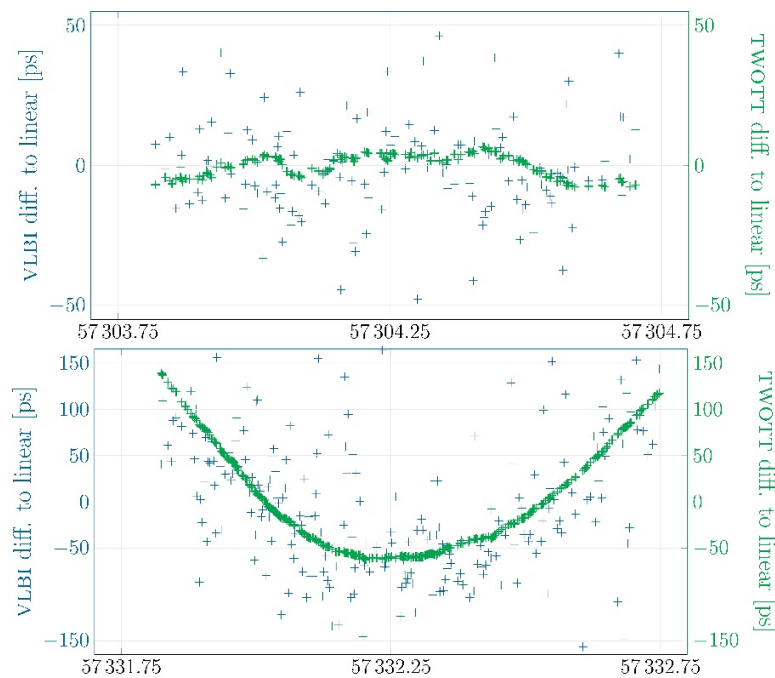


Figure 1. 42: TWOTT residuals with respect to a linear fit (green) and VLBI residuals with respect to a linear fit (blue), sessions R4708 (top) and R4712 (bottom).

The ultimate goal for the TWOTT is to make the estimation of clock corrections unnecessary, apart from one clock offset per session. To test whether the TWOTT data can replace the clock estimation, the TWOTT time series of clock corrections was introduced into the VLBI analysis. As TWOTT and VLBI clock corrections differ by a large offset. Therefore, a mean clock offset is removed for each session. The resulting values are used as clock corrections in a VLBI solution, where only coordinates are estimated. In this way, 13 sessions with TWOTT data were processed and compared with the BAS approach. Furthermore, the comparison of each coordinate solution with respect to the local tie is under investigation. This process yields similar results per component for both solutions, with sub-mm differences for the mean over time

Figure 1. 43 shows the time series of the local tie comparison, with and without TWOTT data. While most of the solutions are nearly identical, differences are evident in sessions R1707 (where less than 25% of TWOTT data was available) and R4712 (showing a quadratic behaviour of the clock). For the latter, the use of the TWOTT data improves the agreement of the solution with respect to the local tie. Thus, the TWOTT is able to account for this clock behaviour, without introducing new parameters in the estimation. Typically the quadratic behaviour could be solved by estimating the clock with shorter intervals, piece-wise linear, but this will increase the number of parameters required, thus weakening the solution. In this sense, there is a great potential in the use of the TWOTT data since it yields comparable results in terms of station coordinates (and their comparison with the local tie) to those obtained from the VLBI estimation. Furthermore, for sessions with atypical clock behaviour (quadratic rather than linear), the use of TWOTT improves the consistency of the solutions

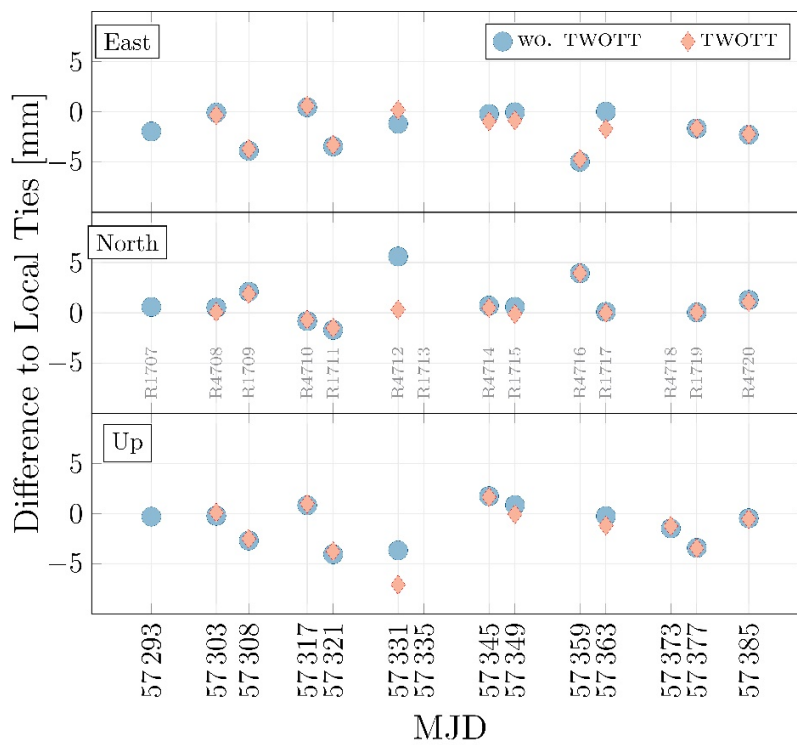


Figure 1. 43: Difference to local ties per component for solutions with and without the introduction of TWOTT data

Multi-Year Analysis of GNSS Short Baselines at Co-Location Sites

I. Herrera-Pinzón and M. Rothacher

Chair of Mathematical and Physical Geodesy, Institute of Geodesy and Photogrammetry, ETH Zürich

GNSS stations suffer from irregularities and discontinuities in the coordinate time series. While often associated with hardware/software changes and the influence of the local environment, these discrepancies constitute a major threat for ITRS realisations. Co-located GNSS receivers provide the opportunity to mitigate their influence while improving the accuracy of estimated positions by examining data breaks, local biases, deformations, time-dependent variations and the comparison of GNSS baselines with existing local tie measurements. With the use of co-located GNSS data from fundamental sites, we performed a global multi-year analysis with the aim of delivering homogeneous time series of coordinates to analyse system-specific error sources in the local baselines.

This analysis includes the generation of GNSS-based coordinate time series, the assessment of the corresponding discrepancies with the available local ties, and the determination of the time-dependent variations in the local GNSS baselines. All available observations were processed daily, in separate small cluster networks using the Bernese GNSS Software. First, a group of solutions including an L1-only, an L2-only and an ionosphere-free linear combination (called L3 in the following), were calculated without estimating any tropospheric parameters (NT). In a second stage, L1-, L2-, and L3-solutions were generated with the estimation of troposphere parameters (except for the reference station) as piece-wise linear functions (TR). Daily station coordinates for these six different types of solutions at eight fundamental sites were estimated. While the RMS of the residuals are better than 2mm for the horizontal component and 4mm for the vertical component, these time series suffer from the effect of jumps due to hardware changes and site-specific environmental factors. Figure 1. 44 shows the height component of these residuals for station WTZZ (Wetzell, Germany), for the six processing strategies.

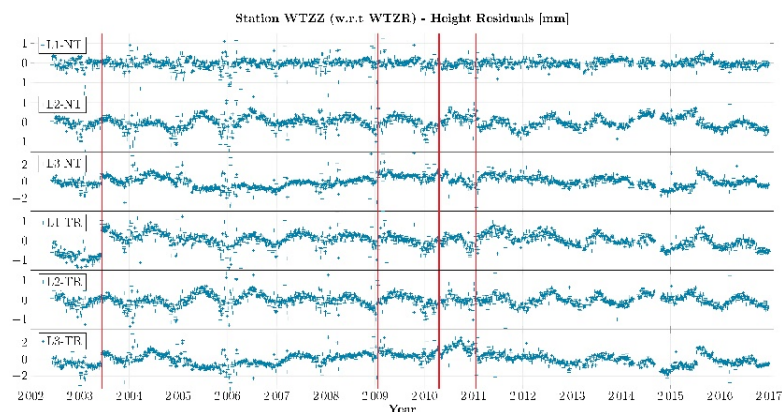


Figure 1. 44: Residuals of the height component of station WTZZ with respect to WTZR (Wetzell, Germany). Vertical solid lines indicate changes in hardware.

In general, the different processing approaches deliver clean time series with repeatabilities better than 1mm in 60% of the investigated solutions, and exceeding 2mm in only 16% of the cases. Single-frequency L1-NT and L2-NT solutions show comparably small results. In contrast, solutions with troposphere estimates are considerably worse, with the worst results for the L3-TR solution that corresponds to a global processing strategy. Few outliers (repeatabilities > 3mm) are detected, with two specific sites (Irkutsk and Obninsk) showing the worst values, especially for the height component. In particular, for station IRKJ (Irkutsk), Figure 1. 45 shows the coordinate residuals for the height component stacked over 11 years. The image on the left corresponds to the L1-NT solution, while the image on

the right to the L3-TR solution, with high variability with respect to each other. Time series in the two plots are driven by the presence of periodic signals. Large differences of up to 12mm for L1-NT and 20mm for L3-TR, with high levels of noise are observed between the months of November and March most certainly caused by snow on the antennas.

The local terrestrial measurements are used to examine the deviations of the GPS-based baselines from these local ties. As an example, at the first investigated site, Arequipa, the baseline is realised using the surveyed local tie of station AREG with respect to station AREQ, with a local system centred at station AREQ. Figure 1. 46 shows the difference of the GPS baseline with respect to the surveyed local tie. Solutions without troposphere estimation show smaller differences with respect to the local tie than the corresponding solutions with troposphere estimation. The largest discrepancies are obtained for the L3 solutions for the height component, while the single-frequency solutions show the best results. It is encouraging to see that L1-NT and L2-NT solutions deviate by less than 1mm from the local tie values. A bias above 2mm is observed in the height component for most of the solutions, and reaches a maximum of 4.5mm for L3-TR. Even with an agreement between the L1-NT and the L2-NT solutions and the terrestrial local ties at the sub-millimetre level, the L3 solutions deviate by up to 4mm.

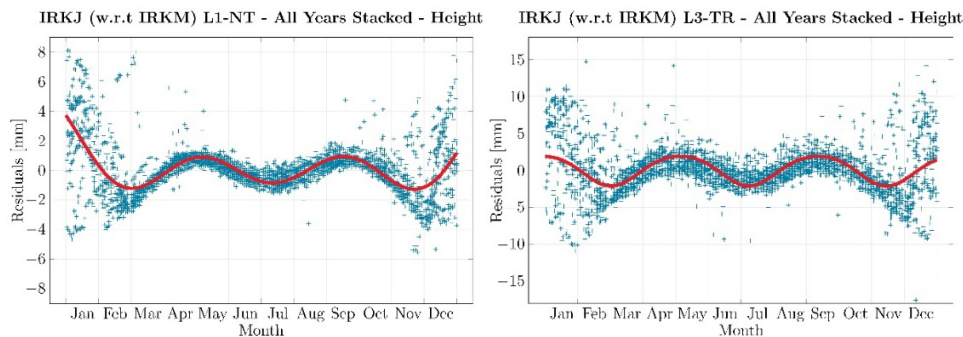


Figure 1. 45: Time series of height residuals for station IRKJ with respect to IRKM (Irkutsk - Russia). Daily values are stacked for 11 years. Left: L1-NT solution. Right: L3-TR solution. Solid curves represent the fitted Fourier series.

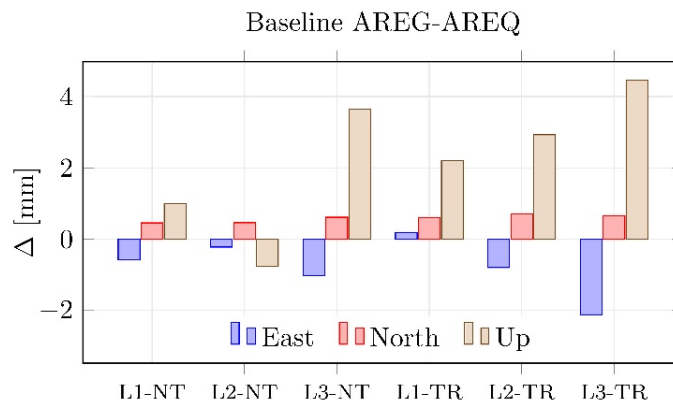


Figure 1. 46: Differences between GPS solutions and surveyed terrestrial measurements. Baseline AREG-AREQ, Arequipa, Peru

For the remaining sites, the comparison of the GNSS-based solutions with the local survey ties show discrepancies of up to 10 mm despite GNSS coordinate repeatabilities at the sub-mm level. The discrepancies are especially large for the solutions using the L3 linear combination and estimating tropospheric zenith delays, thus corresponding to the processing strategy used for global solutions. These demonstrate the need for a permanent high quality monitoring of the effects present in the short GNSS baselines at fundamental sites.

GNSS Antenna Phase Center Modeling and its impact on Precise Orbit Determination of the SWARM satellites

K. Chen, M. Rothacher

Mathematical and Physical Geodesy, Institute of Geodesy and Photogrammetry, ETH Zurich

Swarm is the Earth Explorer mission of the European Space Agency (ESA) to study dynamic processes in the Earth and its space environment. The mission consists of three identical satellites orbiting the Earth in near polar orbits initially at altitudes of about 460 km (Swarm-A and Swarm-C) and 530 km (Swarm-B), respectively. After the commissioning phase of three months, about 5 years of normal mission operations provide a wealth of data to investigate variations in Earth's interior, the atmosphere, the ocean, and in near-Earth space. The onboard GPS receivers, star cameras, accelerometers and laser retro-reflectors make the Swarm mission an interesting candidate to explore its contribution to geocenter, reference frame and precise orbit determination as well as gravity field monitoring in combination with other satellite missions or ground observations.

The precise orbit is very important for the science mission satellites. Especially the positions of the kinematic orbit are subsequently used as pseudo-observations for a gravity field recovery using the celestial mechanics method. Global Navigation Satellite System (GNSS) has been used as a key technology for satellite orbit determination since many years ago. Each Swarm satellite is equipped with an 8-channel, dual-frequency GPS space-borne receiver (van den IJssel et al. 2015). The reduced-dynamic (RD) and kinematic orbits of Swarm satellites were calculated and evaluated using Bernese GNSS Software 5.2. During the orbit determination process, we improved the dynamic model of RD orbit determination by using both, the JB2008 (Bowman et al. 2007) and the MSIS-86 model (Hedin 1987), to correct for air drag and we estimated empirical accelerations - in radial, along-track and cross track directions - to absorb remaining non-gravitational accelerations such as solar radiation pressure.

Precise knowledge of the absolute antenna Phase Center Variations (PCVs) for the GNSS antenna onboard the satellite is crucial for precise orbit determination. We used two different approaches to compute the PCV maps, the residual approach and the direct approach. In the residual approach an empirical PCV map is derived in an antenna-fixed coordinate system as bin-wise mean values of GPS carrier phase residuals from a Swarm RD orbit determination (Jäggi et al. 2009). In this approach, as the neglected PCVs are also absorbed by the estimated orbit parameters, the carrier phase ambiguities and the receiver clock corrections, the procedure was repeated several times to generate an incremental correction map with the same resolution to be added to the first correction map. In the direct approach, the PCVs of the receiver antenna are modeled as coefficients of piecewise linear functions in azimuth and elevation (polygon model) with a resolution of 5° , when processing the GPS carrier phase measurements. The daily normal equations are stored and accumulated into a combined system covering the entire time span of interest. This system can finally be inverted to solve for the PCV corrections. In order to select the optimal time span of GPS carrier phase measurements from the large dataset, we took into account the variations in solar radiation pressure, the changing of the ascending node with respect to the Sun and the intensity of the ionospheric activity.

Figure 1. 47 shows the estimated PCVs derived from the residual approach (left) and the direct approach (right), respectively. The patterns of the two approaches are similar. The magnitude of the estimated PCVs from the direct approach is superior to the residual approach since the neglected PCVs are not fully mapped into the residuals. Due to the inherent degrees of freedom in PCV parameters, the direct approach cannot be used without putting additional constraints. In order to prevent the system of normal equations to become singular, a zero-mean condition is imposed on all grid points for the piecewise linear PCV model. In addition, a priori constraints are required to prevent weakly determined PCV parameters, e.g. related to bins near the elevation cut-off angle, from shifting all other PCV parameters towards unrealistic values due to the zero-mean condition. The PCV maps derived from the direct approach are finally used to estimate final orbits.

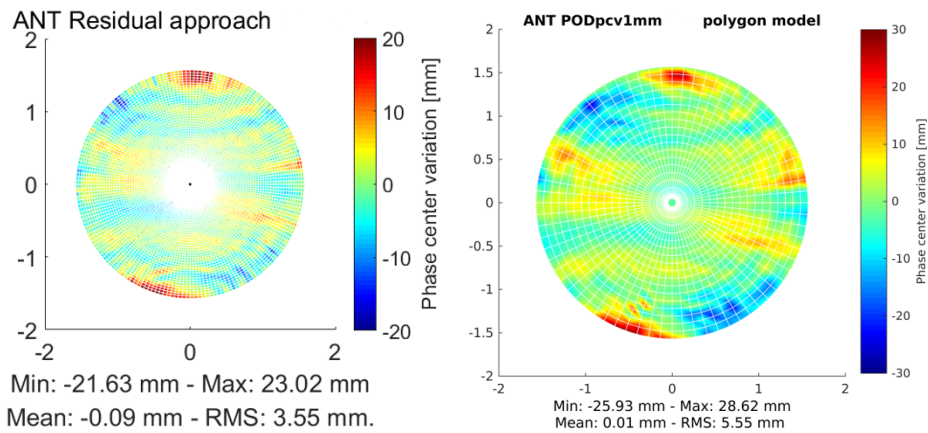


Figure 1.47: Estimated PCVs in millimeters for Swarm-A based on a long series of L3 carrier phase measurements in the year 2016 using the residual approach (left, $2^\circ \times 2^\circ$ resolution) and the direct approach (right, $5^\circ \times 5^\circ$ resolution), respectively. Note the different color scales.

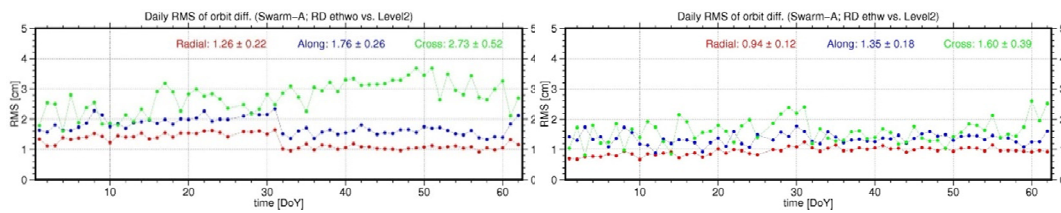


Figure 1.48: Daily RMS of orbit differences between calculated reduced-dynamic orbits (left: without PCV corrections, right: with PCV corrections) and ESA Level2 reduced-dynamic orbits

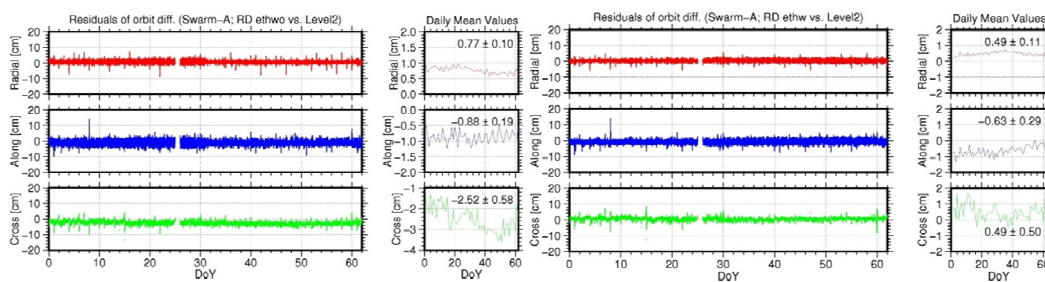


Figure 1.49: Orbit differences between calculated reduced-dynamic orbits (left: without PCV corrections, right: with PCV corrections) and ESA Level2 reduced-dynamic orbits

The improvement in the RD orbits after applying PCV corrections can clearly be seen in Figure 1.48 and Figure 1.49. The largest effect is visible in the cross-track direction. The numbers at the top of plots indicate the mean values and standard deviations of the series.

Kinematic solutions are particularly sensitive to a correct modeling of the antenna phase center location, as no constraints are imposed by dynamic models on the epoch-wise estimated positions. As shown in Figure 1. 50 and Figure 1. 51, the daily RMS and the mean values of the orbit differences are improved by about 2 cm, mainly in along-track direction, when using PCV corrections.

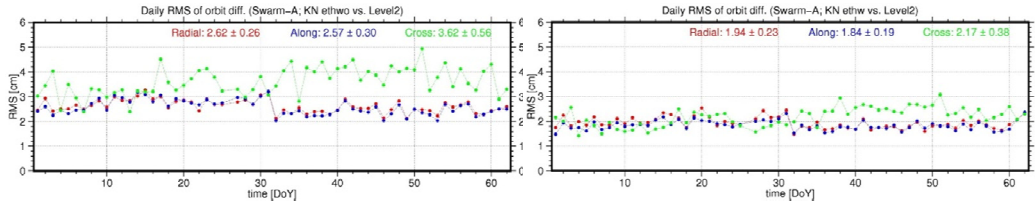


Figure 1. 50: Daily RMS of orbit differences between calculated kinematic orbits (left: without PCV corrections, right: with PCV corrections) and ESA Level2 kinematic orbits

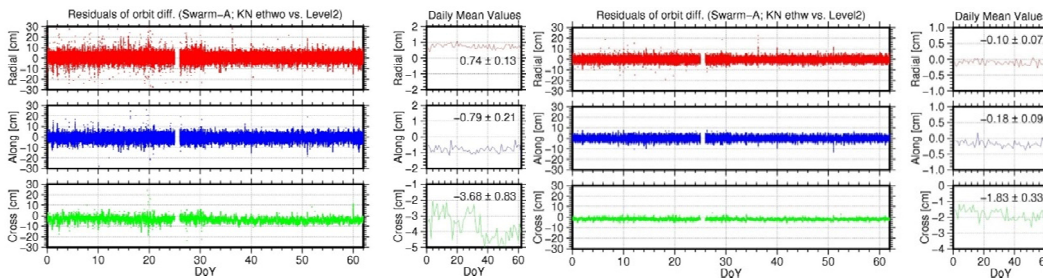


Figure 1. 51: Orbit differences between calculated kinematic orbits (left: without PCV corrections, right: with PCV corrections) and ESA Level2 kinematic orbits

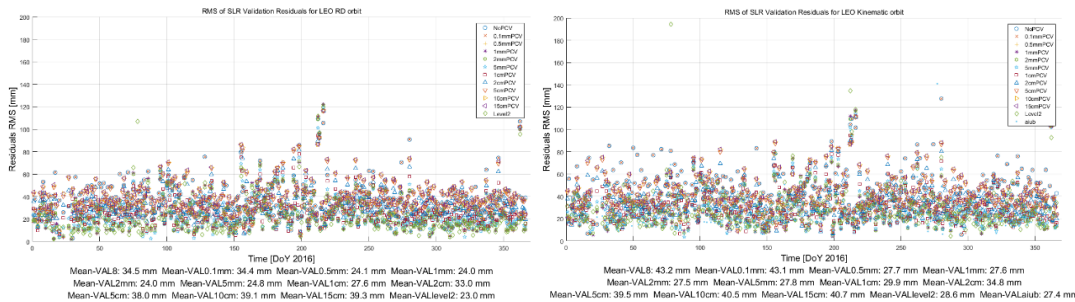


Figure 1. 52: Daily RMS of SLR residuals for reduced-dynamic (left) and kinematic (right) orbits of Swarm-A in the year 2016

The onboard laser retro-reflectors allow an independent validation of the computed orbits using satellite laser ranging (SLR) observations. Figure 1. 52 shows the daily RMS of SLR residuals for the RD (left) and the kinematic (right) orbit validation over the entire year 2016. We applied the estimated PCVs using different priori constraints for orbit determination, respectively. For the validation of all the results above, also the estimated orbits without PCV corrections, ESA Level2 orbits and AIUB kinematic orbits were used for comparison. The agreement with the independent SLR data was improved by about 1.0 cm for the RD orbits and 1.6 cm for kinematic orbits after applying the optimal PCV corrections, respectively.

Absolute field calibration system for multi-GNSS receiver antennas

D. Willi^{1,2}, D. Koch¹, M. Meindl¹, M. Rothacher¹

¹ Institute of Geodesy and Photogrammetry, ETH Zurich, Switzerland

² Federal Office of Topography swisstopo

GNSS receiver antennas are a key factor in GNSS positioning, as they are the interface between the free-air signals and the GNSS receivers. GNSS code and carrier-phase measurements are affected by direction dependent ranging errors due to the physical properties of GNSS antennas. The Institute of Geodesy and Photogrammetry at ETH Zurich developed an antenna calibration system, which is able to generate calibrations for GNSS carrier-phase measurements. The system is shown in Figure 1. 53. It consists of following elements:

- An industrial six-axis robot.
- The robot controller (including the power supply).
- A standard computer running a custom steering software.
- A reference antenna.
- Two GNSS receivers.



Figure 1. 53: Six-axis industrial robot KUKA KR 6 R900 sixx for GNSS receiver antenna calibration. The GNSS antenna in the back is the reference station.

A calibration consist of a sequence of roughly 2000 to 4000 different antenna orientations (lasting between 40 minutes and 4 hours). The antenna is rotated around the nominal Mean Phase Center (MPC) in order to keep the coordinates of the nominal MPC constant. The data is processed in an algorithm based on triple-differences (Willi et al. 2018). The

result is a Phase Center Correction which is independent from the reference antenna, thus the name “absolute field calibration”. The reference antenna is needed solely to eliminate errors as the satellite clock and satellite orbit errors, the receiver clock errors, the tropospheric and the ionospheric path delays.

The system is able to generate calibrations for all Code Division Multiple Access (CDMA) signals, namely for the GPS L1 and L2 signals and for the Galileo E1 and E5 signals. Figure 1. 54 shows an example of a calibration result for a geodetic grade antenna and the Galileo E5 signal.

The system is still under development and validation. Various comparisons undertaken with anechoic chamber calibrations generated by the University of Bonn and with absolute field calibrations generated by the German company Geo++® GmbH confirmed the plausibility of the results. The repeatability of the calibration was investigated as well. The quality of the results depends on the length of the calibration sequence and on the quality of the antenna to be calibrated. For a typical calibration sequence with a geodetic grade antenna, a repeatability of 0.5 mm is obtained, in terms of root-mean-square error over a 5 times 5 degrees grid spanning over the entire upper antenna hemisphere. The maximal error lies below a millimeter for elevations above 10 degrees but can reach up to 2 mm for elevations between 0 and 10 degrees (Willi 2019).

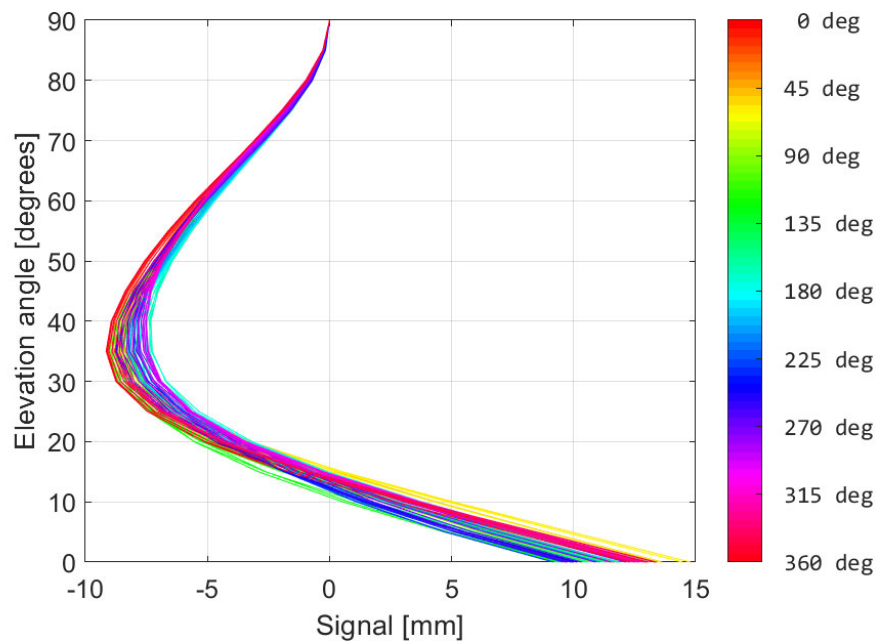


Figure 1. 54: Galileo E5 Phase Center Calibration for a Septentrio PolaNt Choke Ring B3/E6 antenna. Every colored line shows the Correction function for a certain azimuth.

Calibration of an industrial robot

D. Willi^{1,2}, S. Guillaume¹, T. Januth¹

¹ Institute of Geodesy and Photogrammetry, ETH Zurich, Switzerland

² Federal Office of Topography swisstopo

Industrial robots suffer from various errors that limit their accuracy. Errors arise because the actual robot geometry slightly differs from the nominal geometry. A current way to address these deficiencies is to estimate a geometrical model of the robot. The so-called Denavit-Hartenberg parameters allow describing every joint-link pair with only 4 parameters: 2 translations and 2 rotations. These parameters are estimated during the calibration procedure, using the nominal geometry to derive the initial values. The model fit is performed by minimizing the difference between the measured position of the robot and its position calculated from the angular readings of every axis. Typically, a very accurate laser-tracker is used to measure the robots position.

In the present study, the calibration of a six-axis industrial robot of type KUKA Agilus KR 6 R900 (see Figure 1. 55) was addressed. The robot is used for GNSS antenna calibration. This application requires a positioning accuracy of roughly 0.1 mm. During the GNSS antenna calibration, the phase center of the antenna is kept fixed in space, while the antenna is rotated around this point. During the robot calibration, the same sequence of orientations than during the GNSS antenna calibration is performed. The position of an illuminated sphere mounted on the robot flange is measured with the optical micro-triangulation system QDaedalus (see Figure 1. 56). QDaedalus consists of theodolites equipped with CCD cameras instead of eyepieces and specific software.

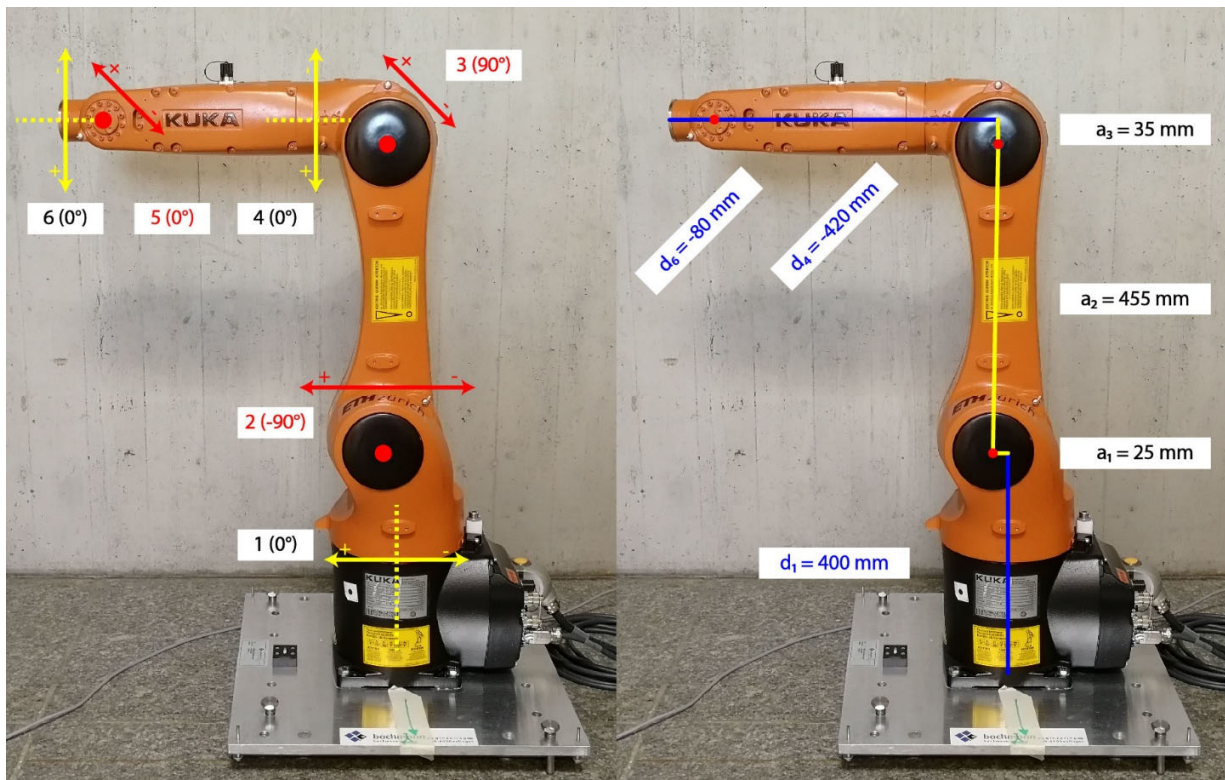


Figure 1. 55: The six-axis industrial robot KUKA KR 6 R900 sixx at IGP together with the angle conventions (left) and the non-zero length parameters (right) of the Denavit-Hartenberg representation of the KUKA robot.

For GNSS antenna calibration, the position and the attitude of the robot in the International Terrestrial Reference Frames is of interest as well. These additional parameters could be obtained thanks to a high accuracy network of benchmarks placed on the roof of the institute (Januth 2018). For these benchmarks, accurate global coordinates are available.

As a result, the accuracy of the robot could be reduced from over 0.5 mm to below 0.1 mm (Willi and Guillaume 2019) by using a Denavit-Hartenberg model. The calibrated robot fulfills the accuracy requirements for GNSS antenna calibration.

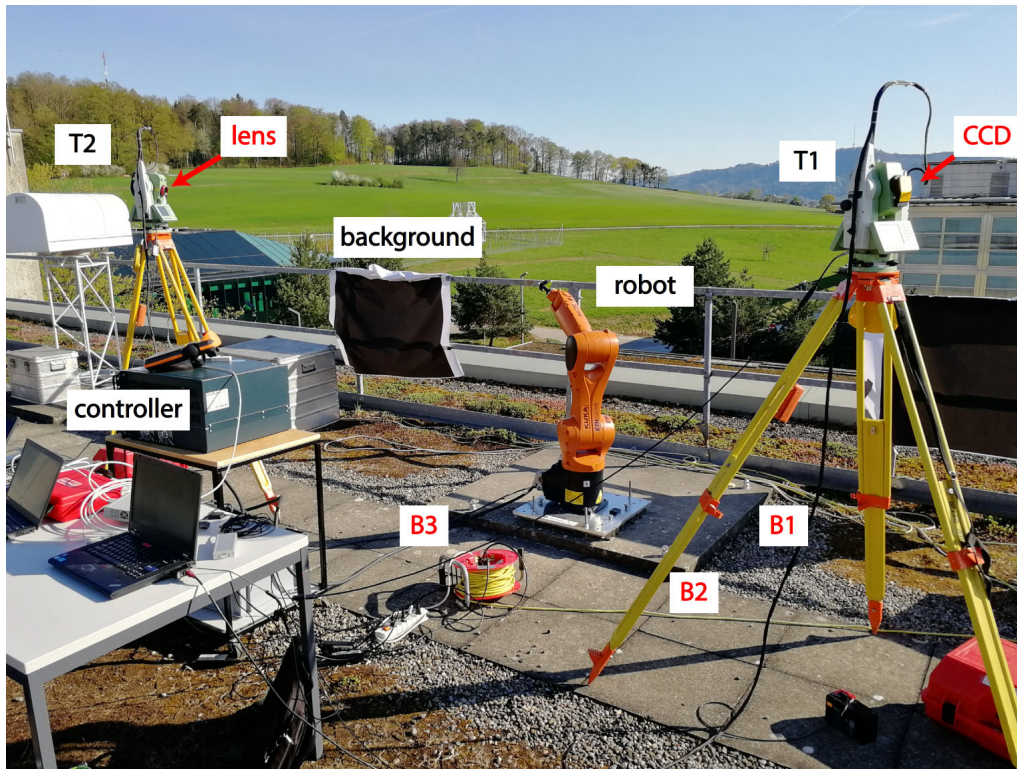


Figure 1. 56: Robot calibration set-up. The two theodolites are denoted by T1 and T2. The eyepieces of the theodolites were removed and replaced by a CCD camera (the so-called QDaedalus system). The black background serves to enhance the contrast to illuminated sphere mounted on the robot. The high-accuracy benchmarks used to determine the position and the attitude of the robot in the International Terrestrial Reference Frame are denoted B1 to B3. Source: Willi and Guillaume 2019.

Analysis of Permanent GNSS Networks at swisstopo (PNAC)

E. Brockmann, D. Ineichen, S. Lutz, S. Schaer

Federal Office of Topography swisstopo

The Automated GNSS Network of Switzerland (AGNES) is a multi-purpose reference network for national first order surveying, scientific research such as geodynamics and GNSS meteorology and serves as a base for the Swiss positioning service (swipos). AGNES was set up beginning in 1998 and reached its designated configuration of 29 stations by the end of 2001. After the enhancement of the network by GPS/GLONASS mid of 2007, totally 41 receivers are operating continuously to serve the various applications. Since the first quarter of 2015 the network is capable to support full Multi-GNSS functionality.

The characteristics of the permanent GNSS-networks analyzed at swisstopo are shown in Table 1. 4. The routine operation of the Permanent Network Analysis Center (PNAC) is divided into 3 sub-network solutions, which are generated on an hourly and daily basis. All analyses are done with the Bernese GNSS Software. The use of synergies with the global analyses of the permanent network of the International GNSS Service (IGS) performed at the Astronomical Institute of the University of Bern (AIUB) which operates the Center for Orbit Determination in Europe (CODE) could be realized by several software modules which are absolutely identical at AIUB and swisstopo. Furthermore, improvements of the BSW were developed and the software developments can be exchanged via the Concurrent Versions System (CVS).

Table 1. 4: Network analyses of permanent GNSS data at swisstopo.

Network solution	Stations (2014 -> 2019)	Processing interval	Delay
1: EUREF (EPN) sub-network	51 -> 61	daily	14-21 days
2: AGNES + sub-net EUREF	172 -> 204 (41 AGNES)	daily	14-21 days
3: AGNES + sub-net EUREF	176 -> 204 (41 AGNES)	hourly	1:45 hour

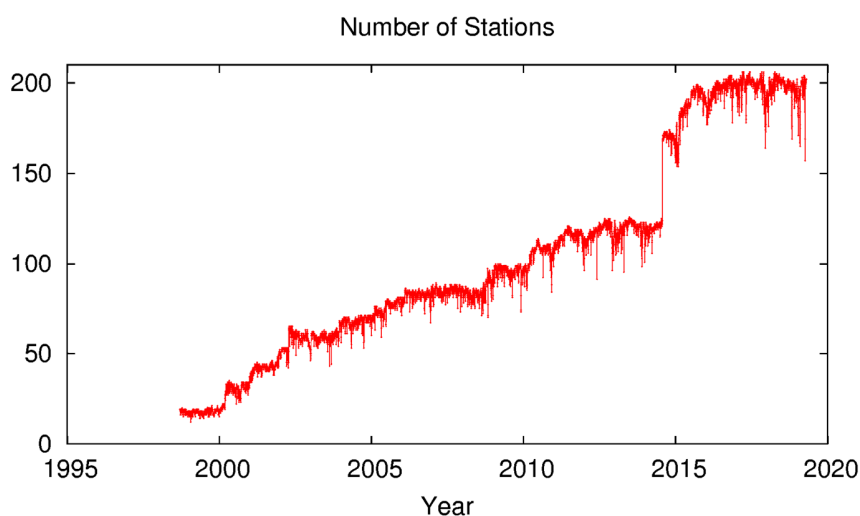


Figure 1. 57: Number of sites processed operationally on a daily basis.

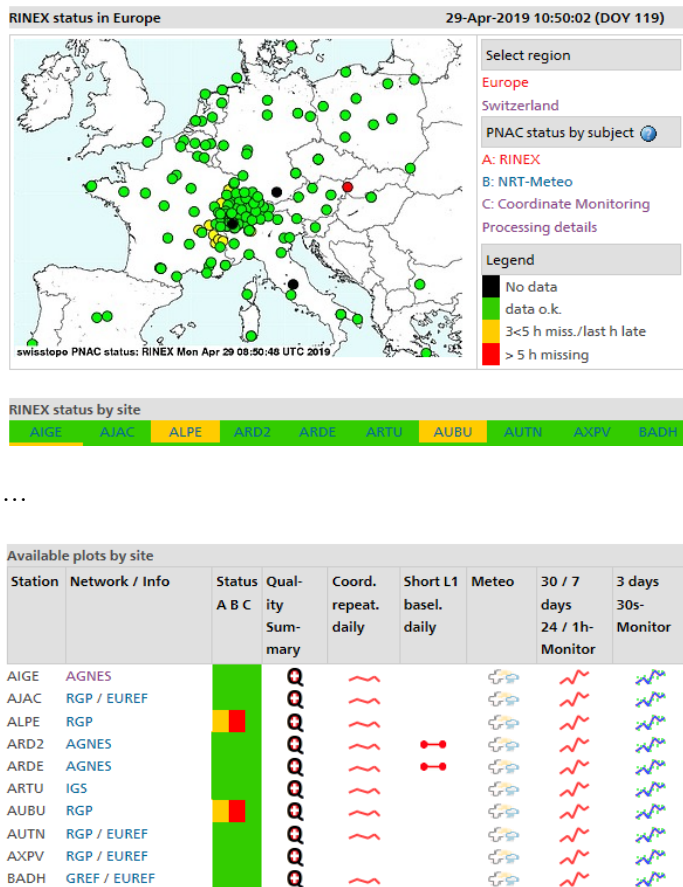


Figure 1. 59: Web-based monitoring of the permanent network analysis (<http://pnac.swisstopo.admin.ch/>).

The number of analyzed sites has continuously been increased (see Figure 1. 57) including foreign stations close to the Swiss national border (partly delivering also data in real-time for the positioning service), third-party stations, and new EPN stations. Especially, double stations are important, because the L1-only solutions (daily as well as kinematic every epoch) enable a reference station monitoring of even better performance as possible on longer distances using ionosphere-free data.

It is worth mentioning that the routine data processing is very similar (w.r.t. processing options as well as w.r.t. identical processing steps) to the performed re-processing where all data from 1996 until end of 2014 were reprocessed using GPS and GLONASS data. Figure 1. 58 shows the processed networks in Europe and Switzerland. In 2015, the complete Swiss permanent GNSS network AGNES was enhanced with GPS+GLO+GAL+BDS capable receivers. Already since mid 2016, most operational post-processing computations are based on Multi-GNSS. The complete data flow was switched from RINEX-2 to RINEX-3 and the analysis is performed with a multi-GNSS development version BSW5.3. The near real-time analysis remained a GPS and GLONASS processing due to missing high-quality ultra-rapid multi-GNSS orbit products. Since 2016, the focus has been on an increased number of used satellites and no longer an increased number of stations (see Figure 1. 57).

The main processing products are coordinates for reference frame maintenance and zenith total delay estimates for numerical weather prediction and climate monitoring. From solution 1 of Table 1. 4, swisstopo contributes, as one of several European processing centers of the European Permanent Network EPN, weekly (and daily) coordinate and

troposphere parameters and also rapid and ultra rapid products for EUREF coordinate monitoring purposes. Solution 2 and 3 of Table 1. 4 are used for monitoring the Swiss reference frame in near real-time and for generating products used in federal surveying and for scientific applications (Tectonics, GNSS meteorology). Beside contributing with NRT troposphere estimates to the EGVAP project (EUMETNET), swisstopo contributes since 2014 also to the COST project GNSS4SWEC. The time series and the performed re-processing activities enable a first analysis of the troposphere estimates over longer time periods.

Since several years, a public web platform is available and continuously extended showing the status of the processing (see Figure 1. 59). Roughly, 8000 plots are available for being checked. The web system is updated twice an hour. Since 2016, the system is hosted on aws (amazon web cloud). Additionally, the system releases e-mail and SMS messages in case of problems.

Maintenance of the CHTRF reference

E. Brockmann, D. Ineichen, S. Lutz

Federal Office of Topography swisstopo

The last validation of the stability of the LV95 reference points took place in summer 2016. About 200 points were observed for 48 hours using all currently available satellite systems. For the first time, data of the European Galileo and the Chinese BeiDou satellites were recorded in the field. All measurements were analysed together with the data of the permanent AGNES stations, which were enhanced to multi-GNSS already beginning 2015. The experiences, how to analyse multi-GNSS data with a development version BSW5.3, were gained with this data set. At the same time, the CODE analysis center started to provide regularly multi-GNSS orbits as input for densification solutions. Probably for the first time worldwide, multi-GNSS measurements were operationally used for campaign and permanent station analysis at a national mapping agency.

One result of multi-GNSS processing is the detection of a systematic difference between a GPS and a Galileo height estimate of about 12 mm due to missing Galileo antenna phase center corrections for the receiver antennas.

To validate the stability of the network, all available data back to 1989 was used. Permanent data as well as campaign data were partly reprocessed as shown in Figure 1. 60. Totally, 6 billion observations were used (1 million observation files) to determine coordinates and, where possible, velocities. Velocities are solved for if the data cover at least a time interval of two years (for campaigns at least two campaigns).

Coordinates were estimated at epoch 1.1.2018. Less than 3% (6 points) of all points exceed the horizontal difference to the officially adopted coordinates of 2 cm. For the height only a single point exceed the level of 3 cm. Coordinates are published in the Swiss National Reference System CH1903+. A special web platform enable an easy access to the results. Thanks to the in-house developed data viewer map.geo.admin.ch (see Figure 1. 61) various additional information may be displayed (e.g. geology and tectonic layer)

Figure 1. 62 shows the horizontal velocity field derived for all LV95 reference points and AGNES stations.

Additional 140 EPN and IGS sites are located outside the scope of the figure. The size of the error ellipses are empirically determined and are slightly different in the lower figure, where also a correlation of the velocities with tectonics and seismicity is shown.

The horizontal velocities in Switzerland are small. The assumption of a zero velocity field is correct with a standard deviation of about 0.2 mm/year. 95% of all points show a horizontal velocity component of below 0.6 mm/year.

Nevertheless, there are systematic velocities in the south of the rivers Rhone and Rhine which are slightly below the 1 mm/year level. In the Jura mountain close to France some smaller systematics are visible.

A test data set with vertical velocities is also available. Currently, differences to levelling and other information are studied. Nevertheless, the uplift of the Alps has a much stronger signal (up to 3 mm w.r.t. the stable European plate).

CH1903+ is the official reference frame for Switzerland. In order to guarantee a longer lifetime, swisstopo prepares the generation of a velocity model to be operationally used in Swiss federal surveying. A velocity model is already foreseen in the system definition, but currently a static reference system is assumed. Such a model can quite easily be implemented, e.g. in the positioning system swipos, but offline or web-based tools need to be developed and seriously tested before being introduced in praxis.

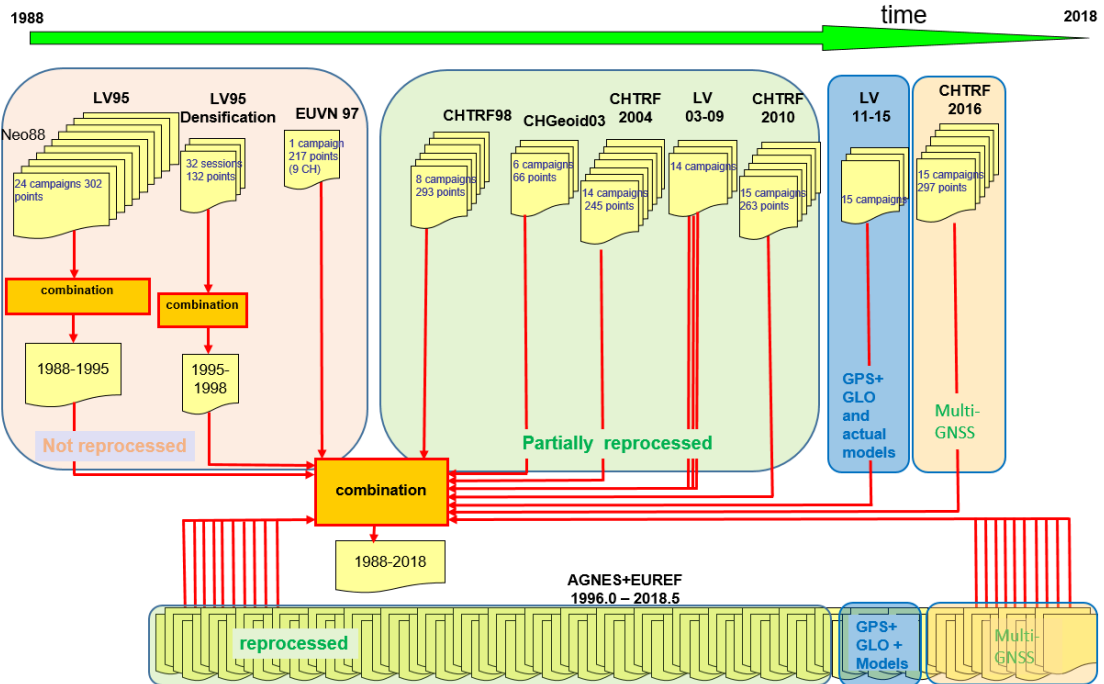


Figure 1. 60: Combination scheme using all available Swiss GNSS data.

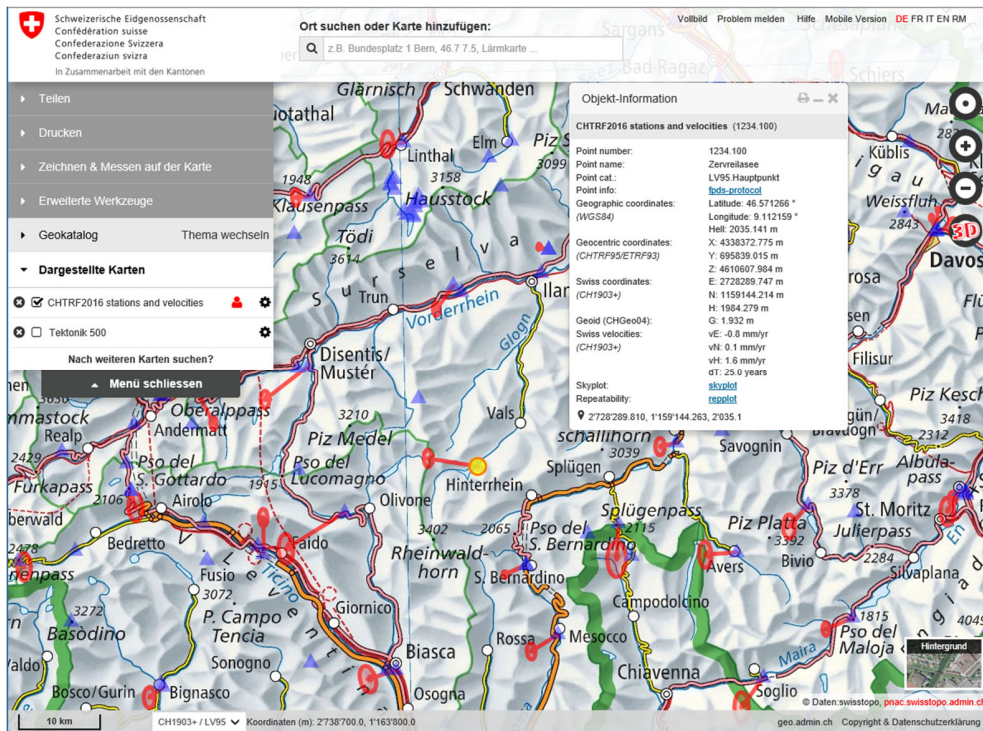


Figure 1. 61: Web-portal of the Permanent Network and Analysis Center PNAC for the publication of the results of the CHTRF2016 combination (<http://pnac.swisstopo.admin.ch/> → CHTRF2016). Various information is displayed for each individual point (coordinates in different reference systems, sky plots, repeatabilities, velocities).

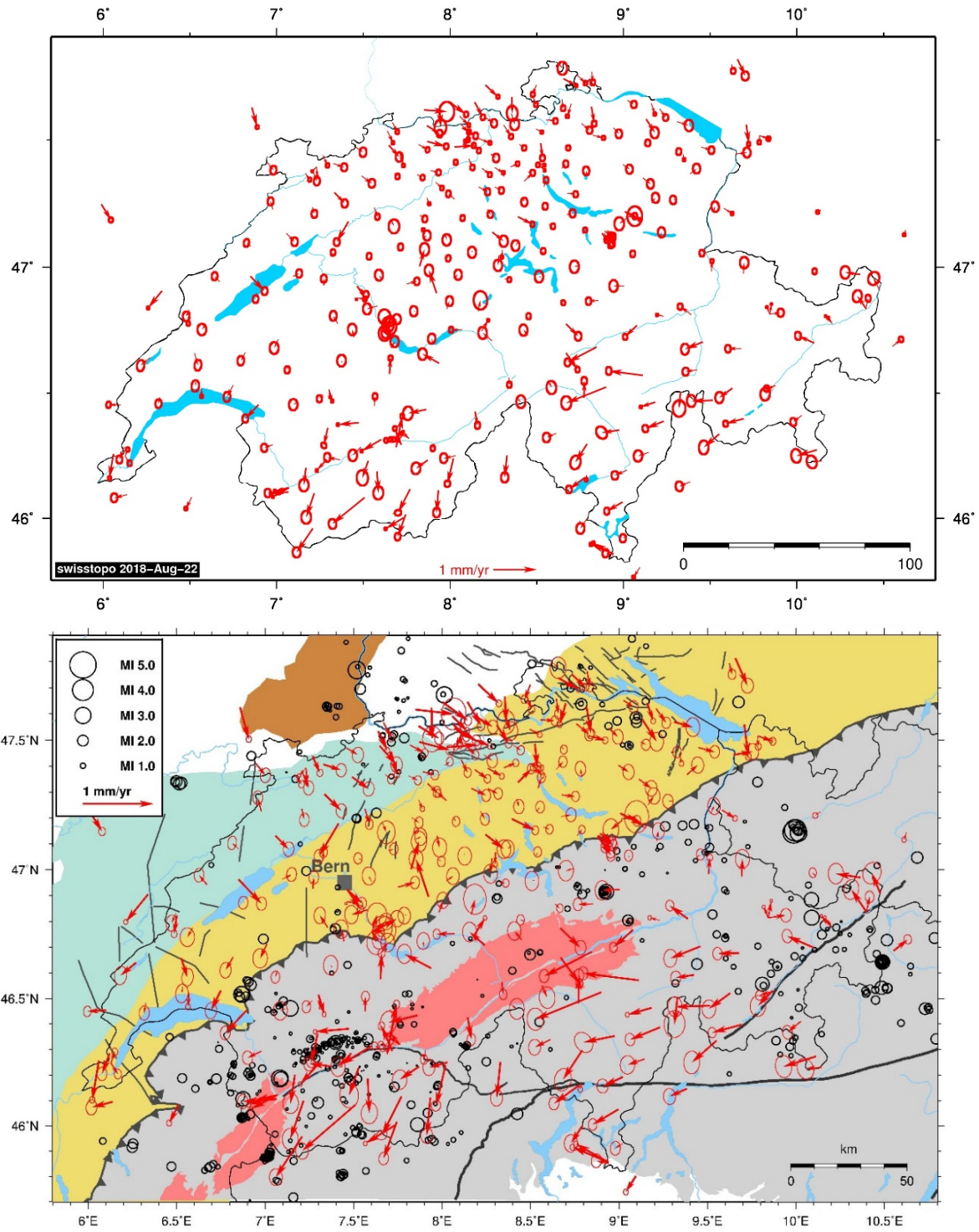


Figure 1. 62: Horizontal velocities CHTRF2016 (top figure; bottom figure together with geology and seismology).

EUREF Working Group on “European Dense Velocities”

E. Brockmann, S. Lutz

Federal Office of Topography swisstopo

The working group “European Dense Velocities” under the umbrella of EUREF (European Reference Frame in Europe) was established in May 2017 to enable the generation of an European-wide dense velocity field. The project follows the classical approach of densifying national and regional velocity fields. The goal is to derive a harmonised and comprehensive European dense velocity field from a distributed processing concept making use of the detailed knowledge of the partners and to conserve the inner geometry of the inputs to a large extent. The method is based on the contributions of individual velocity fields generated by the national mapping agencies and other analysis centers. Those institutions know their processed station well and are able to model possible jumps in the time series best possible. Beside velocity fields from permanent GNSS networks, also dense velocity fields stemming from campaigns are integrated. Examples of the Central East European Initiative and from Switzerland are shown. Velocity fields from levelling can be used to improve the vertical velocity information. As an example of the strength of the method, results from a very dense combined INSAR/GNSS analysis are integrated for the area at the borders of Germany, France and Switzerland. Finally, complete velocity grids can be used in the combination process. This is important in regions, such as Scandinavia, where users already use velocity fields in praxis and where the velocity fields were generated based on a combination of several methods.

More than 20 velocity fields in the common reference system ETRF2000 have been collected (see Table 1. 5).

Table 1. 5: Contributions to the EUREF working group “European Dense Velocities” (http://pnac.swisstopo.admin.ch/divers/dens_vel).

Num	Solution	Analysis Centre
001	alp08	AlpArray Initiative
002	alps17	BAdW/DGFI (https://doi.org/10.5194/essd-2018-19)
003	basc08	ARANZADI's Department of Applied Geodesy (ARA)
004	cat08	Institut Cartografic i Geologic de Catalunya (ICGC)
005	cgn08	Central European GPS Geodynamic Reference Network Consortium (CEGRN): 2016 campaign combination
006	cgn14	Central European GPS Geodynamic Reference Network Consortium (CEGRN): 2018 Multi-annual combination
007	ch08	swisstopo - Permanent stations
008	ch08l	swisstopo - Permanent stations - levelling
009	ch16	swisstopo - Permanent and campaign stations
010	epn14	EPN Reference Frame Coordinator
011	epnd14	EUREF WG on EPN Densification
012	esp08	Instituto Geografico Nacional (IGN Spain)
013	gr08	Aristotle University of Thessaloniki
014	gref08	Federal Agency for Cartography and Geodesy (BKG)
015	gsrm14	Global Strain Rate Map (V3 2016, Nevada Bureau of Mines and Geology)
016	gurn08	GNSS Upper Rhine Graben Network (GURN)
017	gurn08d	GNSS Upper Rhine Graben Network (GURN) - combined InSAR
018	gut14	Gdansk University of Technology
019	gut14x	Gdansk University of Technology, extended version
020	hepos	Hellenic Positioning System (HEPOS)
021	igs08	IGS Reference Frame Coordinator
022	it08	Universita di Padova
023	itrf14	ITRF Coordinator
024	nkg03	Nordic Geodetic Commission (NKG)
025	noqu08	Universite de Montpellier
026	rgp08	Institut national de l'information geographique et forestiere (IGN France)
027	svn14	Surveying and Mapping Authority of the Republic of Slovenia
028	walp08	Universite de Montpellier

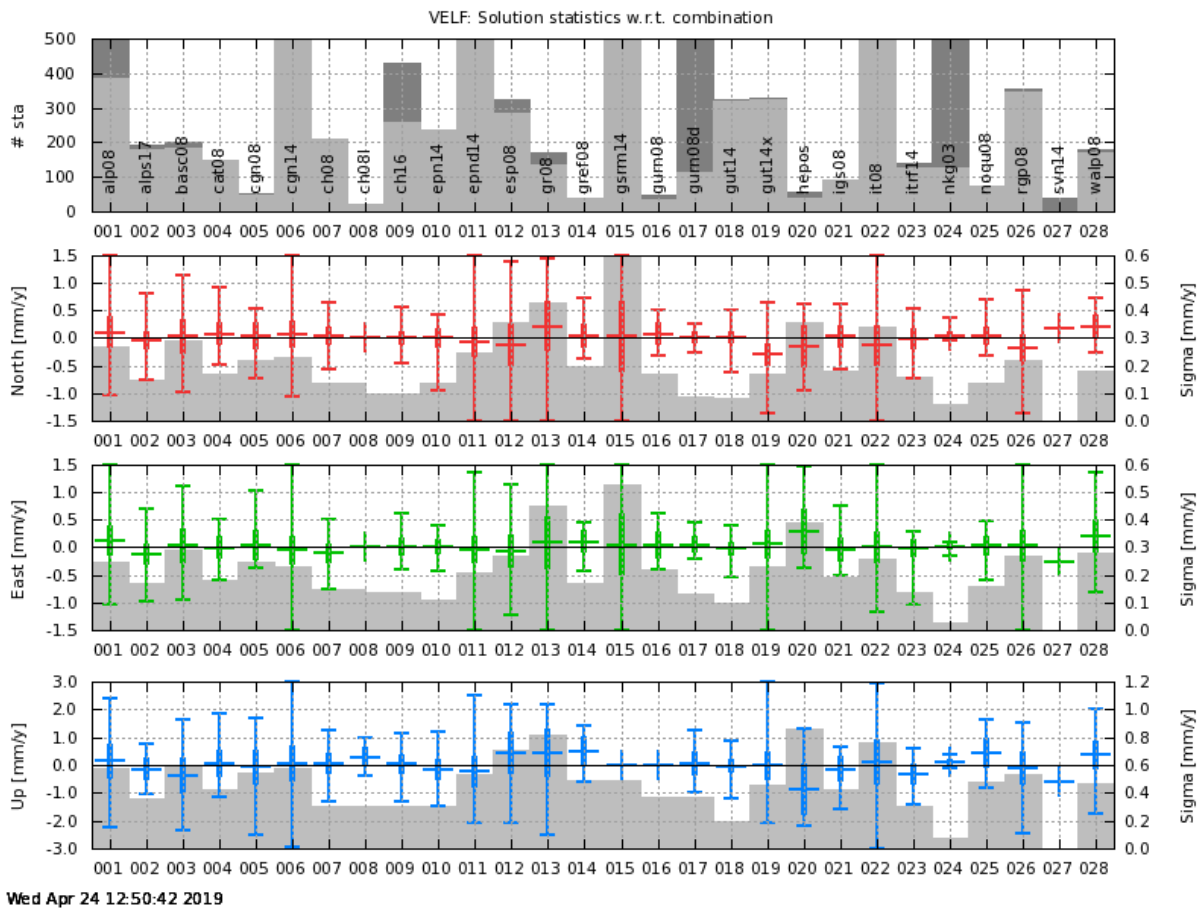


Figure 1. 63: Statistics of the agreement of each individual solution with respect to the combination.

Totally, about 5000 stations with velocity information are available. More than 2000 sites in Europe are available in two or more solutions. Some classical stations are present in many solutions (ZIMM: 18, GRAS: 16, GRAZ: 15, etc.). The velocities were analysed and successfully combined. The agreement of the solution is for the horizontal components on a level of 0.2 – 0.3 mm/yr (standard deviation; grey bars in Figure 1. 63), covering usually 50-200 common stations. Furthermore, almost no significant velocity biases w.r.t. ETRF2000 are visible.

Solutions in the “faster” (3-4 cm/yr) moving regions of southeastern Europe show slightly worse agreements. A web platform (http://pnac.swisstopo.admin.ch/divers/dens_vel) gives feedback to the contributors of the velocity fields so that possible discrepancies may be eliminated.

The European dense velocity field is the basis for a deformation model for Europe. It allows an interesting knowledge exchange with geologists, seismologists and geophysicists and it is an important part to enable the maintenance of the European reference frame, which currently assumes no deformations of the European plate. Due to the high precision of the current GNSS methods and due to the age of 30 years of ETRS89 and of many other European national reference systems, the small but significant movements within the European plate need to be modelled in order to ensure a horizontal reference frame realization of below 1-2 cm also for the next decades.

Figure 1. 64 and Figure 1. 65 show the horizontal velocity field in its current status (April 2019) for two different zoom levels. Whereas the horizontal velocities are on a level of clearly below 1 mm/yr for the stable part of the European

plate, the velocities reach 3–4 mm/yr in Italy and 3–4 cm/yr in Greece and Turkey. The polygon covering the Nordic countries Norway, Sweden, Finland and Denmark shows the NKG velocity grid.

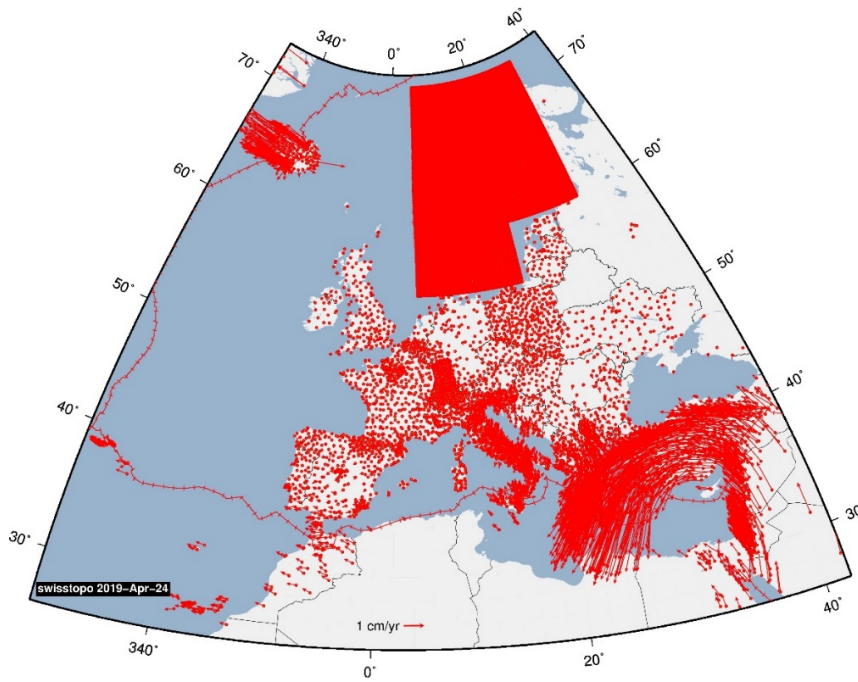


Figure 1. 64: Horizontal velocities derived by the “European Dense Velocities” working group.

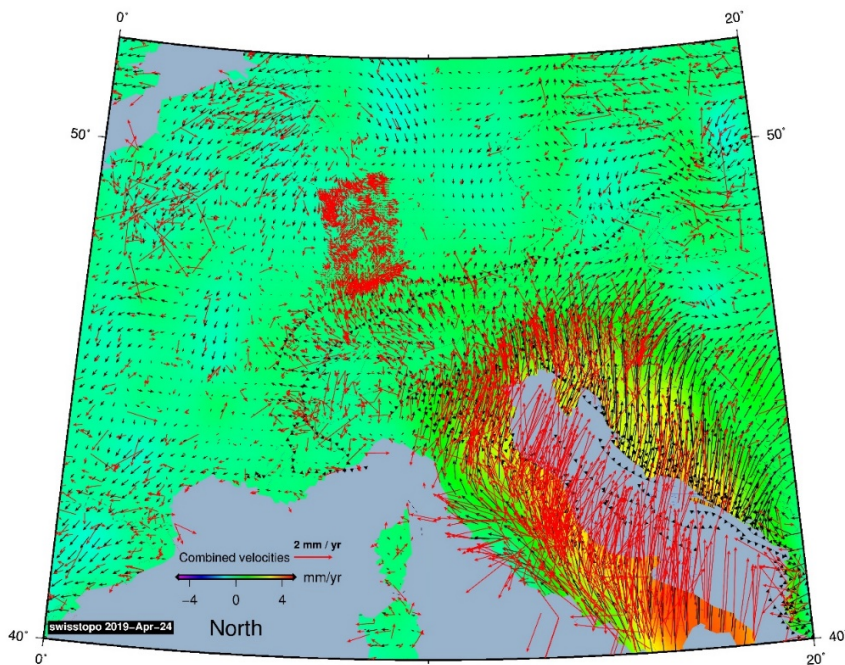


Figure 1. 65: Horizontal velocities model derived by the “European Dense Velocities” working group (zoom to central Europe; in red estimated velocities; in black a velocity model; background color is the velocity grid for the north component).

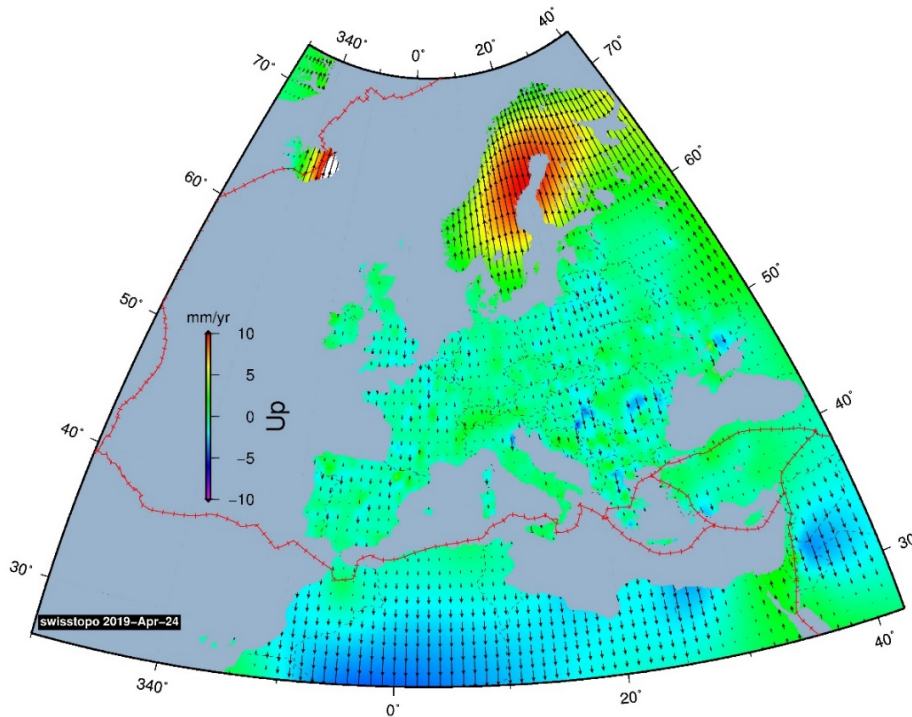


Figure 1. 66: Vertical velocities model derived by the “European Dense Velocity” Working Group.

A model can be fitted through the combined velocity field (Figure 1. 65 for horizontal velocities in central Europe). The vertical information from GNSS is much noisier than for the horizontal velocities. Figure 1. 66 shows a very smoothly fitted version for the vertical velocities showing mainly the postglacial uplift in Scandinavia as the dominant movement in Europe. At present, model calculations are mainly used to detect outliers in the data sets or to find locally unstable stations. In future, a data set for calculating a European velocity grid will be derived which may be used for reference frame maintenance (and harmonized with possible used national velocity models) and geophysical applications.

Multi-GNSS activities at swisstopo

S. Lutz, E. Brockmann, D. Ineichen, S. Schaer

Federal Office of Topography swisstopo

Global Navigation Satellite Systems (GNSS) are used for satellite-based positioning, navigation and time transfer services. Multi-GNSS covers the two established systems for high-accuracy, dual-frequency data analysis GPS and GLONASS as well as Galileo, BeiDou, QZSS, and IRNSS. This means more carrier frequencies and new and enhanced signals that are suitable for satellite geodesy.

In May 2015, the receivers of the Automated GNSS Network of Switzerland (AGNES) were replaced for multi-GNSS capability. At the beginning of 2016, the field equipment for the national (e.g. CHTRF2016) and local GNSS measurement campaigns of swisstopo was changed from GPS-only to multi-GNSS, too. Different manufacturers were examined beforehand. After an extensive evaluation of all available RINEX-2 and RINEX-3 observables from the AGNES and many other stations in Europe, the Permanent Network Analysis Center (PNAC) at swisstopo switched mid of 2016 from a two-system (GPS, GLONASS) to a fully-combined four-system (GPS, GLONASS, Galileo, BeiDou) data analysis processing scheme for the operational daily and the field campaign results. The comprehensive and ongoing automated RINEX file monitoring is an important source of information when, e.g., station operators updated their equipment, or new GNSS satellites are transmitting signals.

<http://pnac.swisstopo.admin.ch> → PNAC monitoring → swisstopo: Daily RINEX-2/3 monitor

A development version of the Bernese GNSS Software Version 5.2 from the Astronomical Institute of the University of Bern (AIUB) was installed and is continuously maintained in order to process the RINEX-3 data and to integrate the multi-GNSS orbit products from the Center for Orbit Determination in Europe (CODE) in a highly consistent way. This includes also ambiguity resolution for all involved systems. The impact of additional systems on the combined coordinate and troposphere estimates can be assessed and controlled on the basis of so-called inter-system translation parameters with respect to a virtual GPS-only solution (see Figure 1. 67).

swisstopo is involved in diverse international working groups and projects dealing with different aspects of multi-GNSS analysis: Chairing the EUREF Multi-GNSS and the IGS Bias and Calibration Working Groups, participation in the IGS RINEX and the IGS Precise Point Positioning with Ambiguity Resolution (PPP-AR) Working Groups. Critical aspects of the antenna phase center corrections for the new signals was recently investigated together with ETH Zurich.

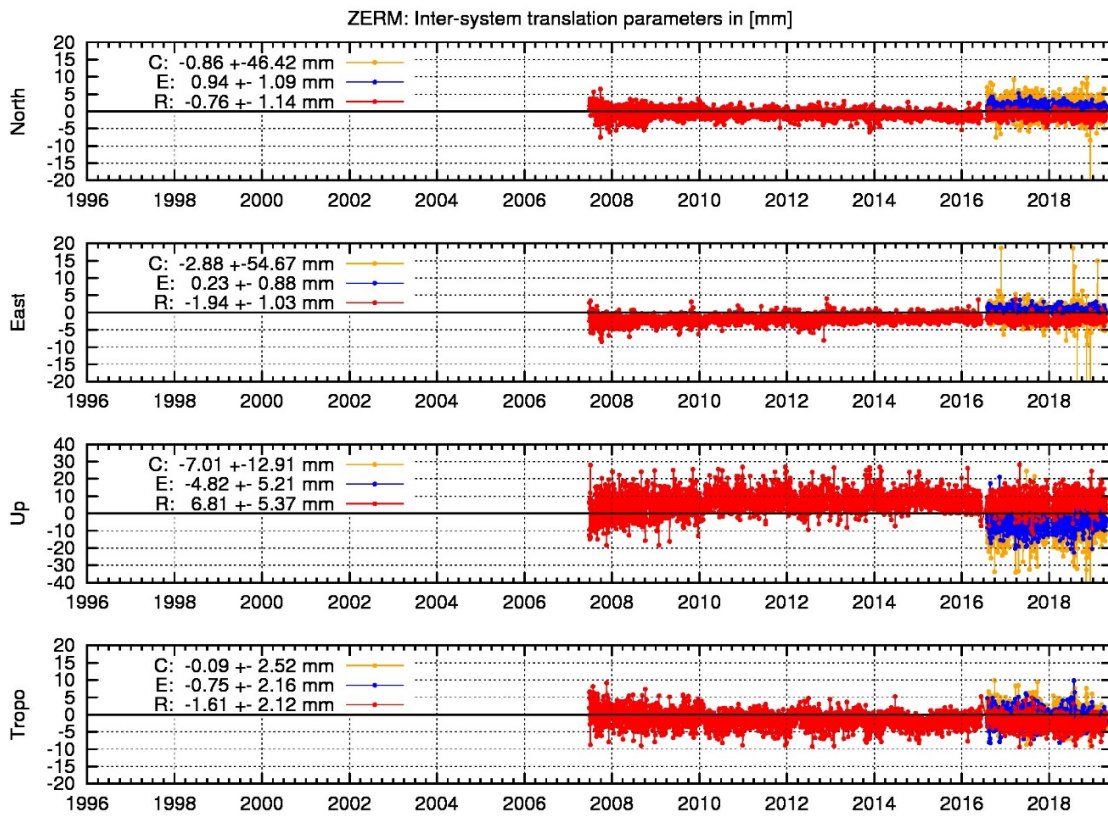


Figure 1. 67: Inter-system translation parameters of the AGNES station ZERM with the most limited sky-view of 76%. The impact of each individual (non-GPS) system is in the order of a few millimeters.

Extended Monitoring of the PNAC-Analysis Key Parameters

D. Ineichen, E. Brockmann, S. Lutz

Federal Office of Topography swisstopo

Until recently, the Permanent Network Analysis Center (PNAC) at swisstopo monitored the processing procedures mainly with the help of text-based program output files, partially condensed to session-wise summary files. The increasing amount of available information has made this type of control both cumbersome and time-consuming. Therefore, we have made some efforts to monitor the processing not only with text files, but also with the help of graphic files.

These plot files are compiled in an HTML file and are thus accessible via web browser. For the daily processing, not only the data of the current evaluations are displayed, but also those of the entire time series (starting in 1996). Thus, not only the values of the individual analysis key parameters themselves, but also their temporal changes become visible. Such changes can be caused intentionally, e.g. through adjustments of the corresponding processing procedures, but also unintentionally (input data problems, software bugs). The graphical monitoring helps in these cases to provide solutions of consistent quality.

Analysis parameters monitored in such a way are, for instance, the number of available RINEX files delivering GPS/GLONASS/Galileo/BeiDou data, the number of tracked and processed satellites, rejected observation files, RINEX header inconsistencies, RMS values of orbit fits, number of iterations for the residual screening and corresponding RMS values, number of resolved ambiguities for all applied resolution strategies, and the number of observations and the corresponding RMS of the final daily solution.

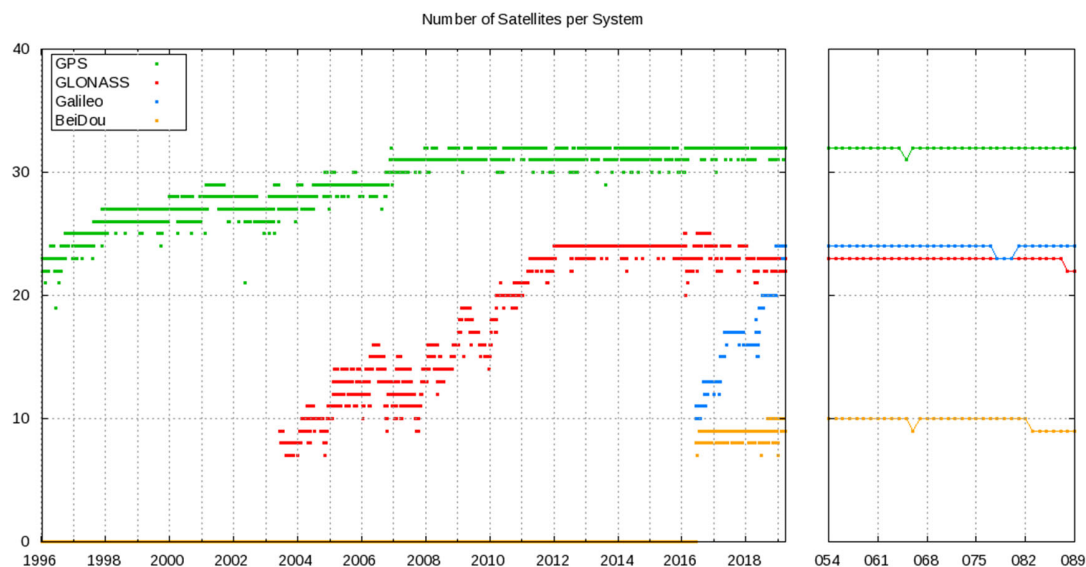


Figure 1. 68: Number of processed satellites per day: GPS (green), GLONASS (red), Galileo (blue), and BeiDou (orange, no BDS3 so far).

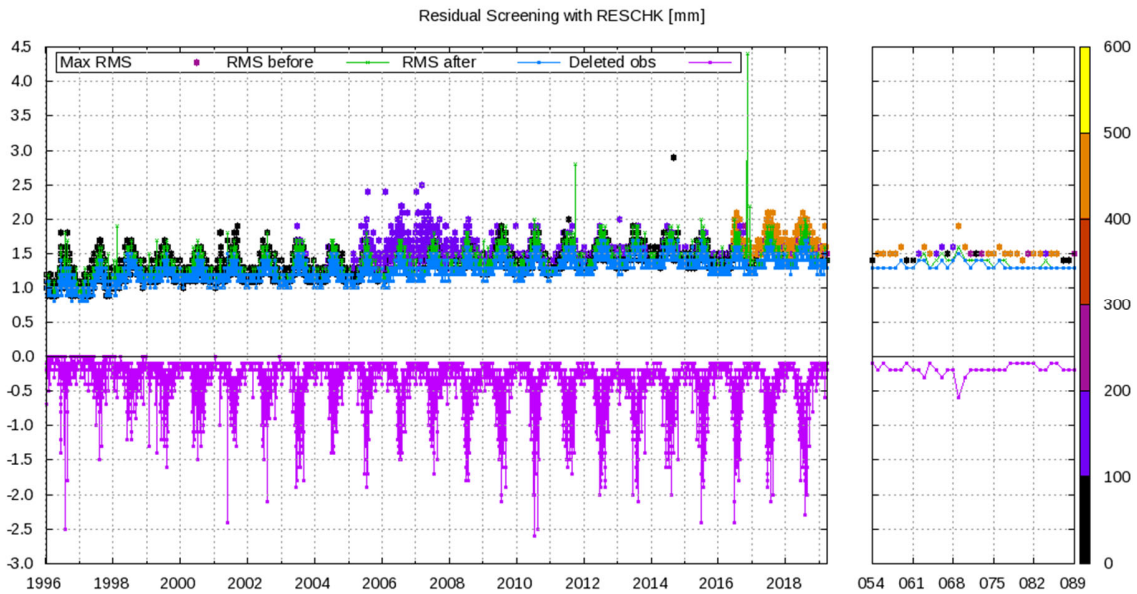


Figure 1. 69: Key values from daily observation residual screening: Maximum RMS per satellite (colored star according to the color bar on the right hand side; 0-99: GPS, 100-199: GLONASS, 200-299: Galileo, 300-399: SBAS, 400-499: BeiDou, 500-599: QZSS), total RMS before screening (green), total RMS after screening (blue), and percentage of deleted observations (violet).

The resulting plots are shown by means of two examples. Figure 1. 68 shows the number of processed satellites per satellite system of the final daily solutions. From the beginning of the series in 1996 until DOY 207, 2014, the results are stemming from reprocessing activities. GLONASS observation data are included since 2003 and the daily solutions are based on additional Galileo and BeiDou data starting on DOY 164, 2016. In the left part of the figure, a zoom into the last five analysis weeks is shown, which makes it easier to detect data or analysis problems of the current solution.

Figure 1. 69 shows a summary of the results of the daily observation residual screening. Plotted are the maximum RMS of one satellite (star, the color is indicating the concerned internal satellite number), the total RMS of all baselines before data screening, the total RMS of all baselines after data screening, and the total percentage of deleted observations.

The constantly updated plots of all monitored parameters are available on the following website: http://pnac.swisstopo.admin.ch/pages/en/agnes_statistics.html.

Two similar web sites allow the monitoring of swisstopo's contribution to the European Permanent Network ("euref_statistics.html") and the monitoring of the hourly near real-time solutions for troposphere parameters and coordinates ("amet_statistics.html").

Transition of reference frames LV03 → LV95 («Bezugsrahmenwechsel», «Changement de cadre de référence MN03 - MN95»)

A. Wiget

Federal Office of Topography swisstopo

The Federal Act on Geoinformation (SR 510.62) rules in Art. 5 that the Federal Council shall define the official geodata under federal legislation and that it shall issue regulations on the qualitative and technical requirements for official geodata under federal legislation, in particular on the geodetic origin and projection framework (etc.). The Ordinance on Geoinformation (SR 510.620) then defines the geodetic reference systems and frames to be applied in Switzerland (Art. 4). In Art. 53 it determines that the transition of the reference frame from the old frame “LV03” to the newly by swisstopo defined “LV95” has to be completed for all reference data (including cadastral survey data) until December 31, 2016.

swisstopo (Division of Geodesy) has initiated and directed this transition of the reference frames and was strongly involved in its implementation. Of course first by defining, installing and establishing the necessary infrastructure like reference points and permanent GNSS stations (see article by Wiget et al. on CHTRF2016 in this report; or Schneider, Gubler and Wiget, 2015). But further more there was a lot of work to be done by defining the mathematical method of the transition (finite element transformation FINELTRA), by densifying the LV95 network down to the regional and even local level and by identifying the reference points for the transformation (Transformationsstützpunkte TSP) and the dataset of the national triangular transformation network (CHENyx06) (see article by Wiget and Kistler in this report). The process and the different parts of the “Landesvermessung 1995” (LV95) are well documented in the “swisstopo DOKU” series (former “Berichte aus der L+T”).

This work was done in close cooperation with the cantonal surveying institutions. And finally, to optimally support all institutions and users in the transformation process, a package of software tools had to be developed, e.g. the main software REFRAME. Together with the definition and establishment of the new LV95 reference system, the creation of this transformation dataset represents the biggest geodetic control survey project since the original “official” federal surveys of Switzerland at the end of the 19th century (“Landestriangulation LV03”). Further details and data for download are published on the website of swisstopo (<https://www.swisstopo.admin.ch/en/knowledge-facts/surveying-geodesy/new-coordinates/transition.html>).

The illustration on the next page (Figure 1. 70) shows the changes in coordinates between the old and the new Swiss reference frame, namely for the main survey points in the form of shift vectors (from LV03 to LV95) and the density of vectors with the aid of colour-coding (from map.geo.admin.ch; see Wiget and Kistler in this report).

With great satisfaction it can be stated that this transition of reference frames could be realized by swisstopo together and in close cooperation with the institutions of all 26 cantons in time and without major problems by the end of 2016.

Major parts and non-negligible aspects of the transition process were information and communication, first from swisstopo to the cantons and the professionals in surveying; but then – and even more difficult – to all users of coordinates and geodata and finally to the general public. The strategy and the basic documents for this communication were developed by swisstopo. The cantons, the surveyors and other producers of geodata as well as of geo-software were informed and trained directly, at an early stage and in a competent way by swisstopo (Division of Geodesy). Special attention was given to special users like the army and “blue light organizations” (e.g. police or REGA).

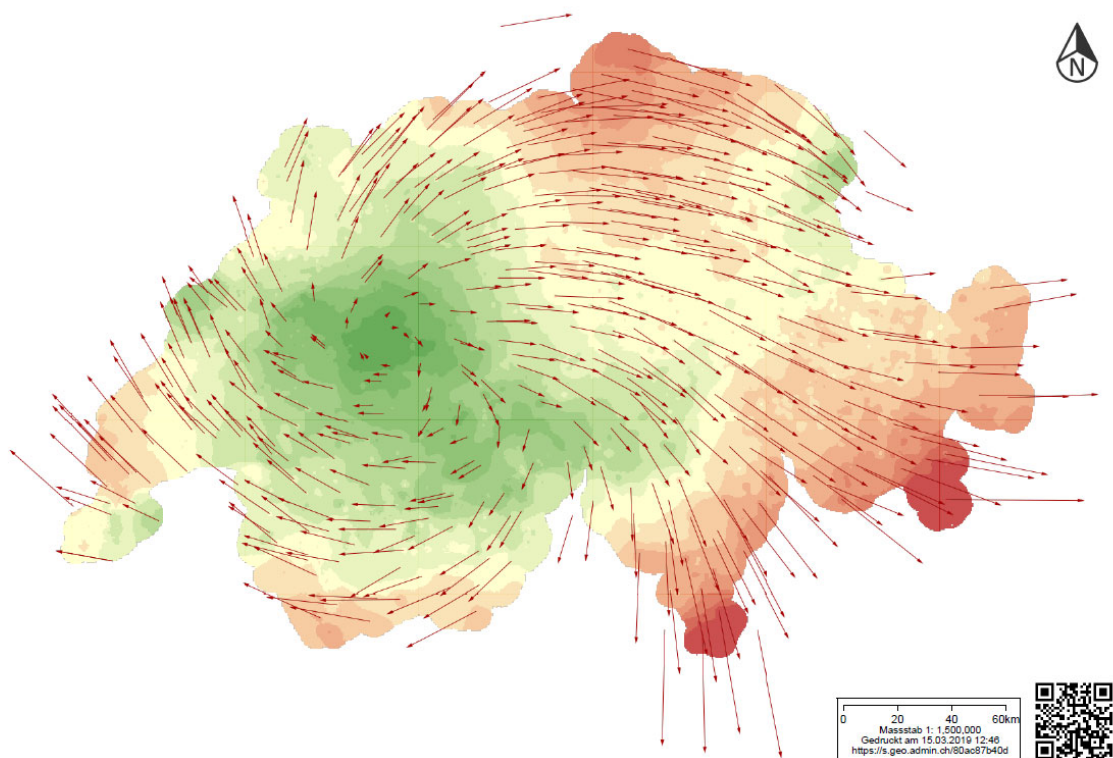


Figure 1. 70: Displacement vectors or coordinate changes of the pass points (TSP1) from the old frame LV03 to the new one LV95 (direction and absolute value of the local rectification) showing the deformations of LV03, represented in relation to Zimmerwald (BE). The greatest coordinate changes of about 1.5 m appear in the south Ticino and in Poschiavo valley (GR).

But since the practical part and the realization of the transition in the different cantons followed their specific schedule (mainly in the years from 2010 to 2016), the public was informed by the cantonal institutions. Nevertheless, in order to be able to do this in an efficient way, swisstopo produced and made available the necessary publications, flyers, text modules, videos, etc. For all this it was important that these products were done in a professional way, with correct and complete contents but still generally understandable. So they had to be tailored to suit the market needs. As an example for such a publication we refer to the article in the GeoPanorama 4/2015 published by the Platform Geosciences of the SCNAT (Wiget, 2015).

At the end of the process it can be said, again with great satisfaction, that the information and communication for the professionals and users were competent and comprehensive, effective and on time. And also the general public was informed on due time and with the desired level of detail. At least, there were no complaints nor (and even more important) any accidents or major harms connected to the whole process of coordinate changes.

It might be worth to be mentioned that for the media and the public the most interesting and noted effect of the transition of reference frames were the changes in the surfaces / areas, e.g. of the different cantons.

Flächenänderung in der Schweiz durch die Umstellung von LV03 auf LV95

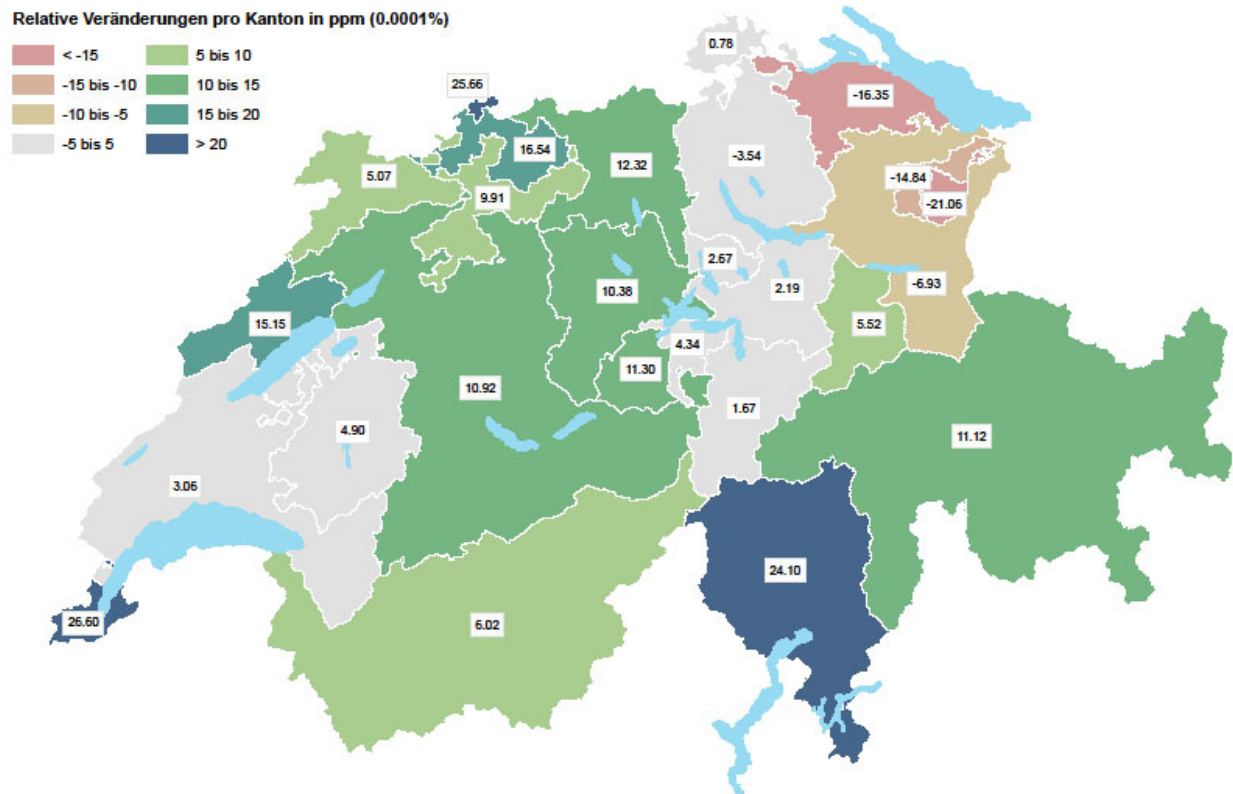


Figure 1. 71: Relative changes of the areas of the cantons due to the transition of reference frames LV03 → LV95 (not to be interpreted as real surface changes).

Geodetic Reference Datasets and GIS Data of the Swiss Geodetic Survey (swisstopo) available on the Federal Geoportal and the Map Viewer map.geo.admin.ch

A. Wiget and M. Kistler

Federal Office of Topography swisstopo

Following the aim of the Federal Act on Geoinformation (SR 510.62) the geodetic reference datasets of swisstopo are made publicly available on the national portal for geodata „map.geo.admin.ch“. Since 2017, for easy finding and fast access, all geodetic datasets are grouped in the topic «Geodesy».

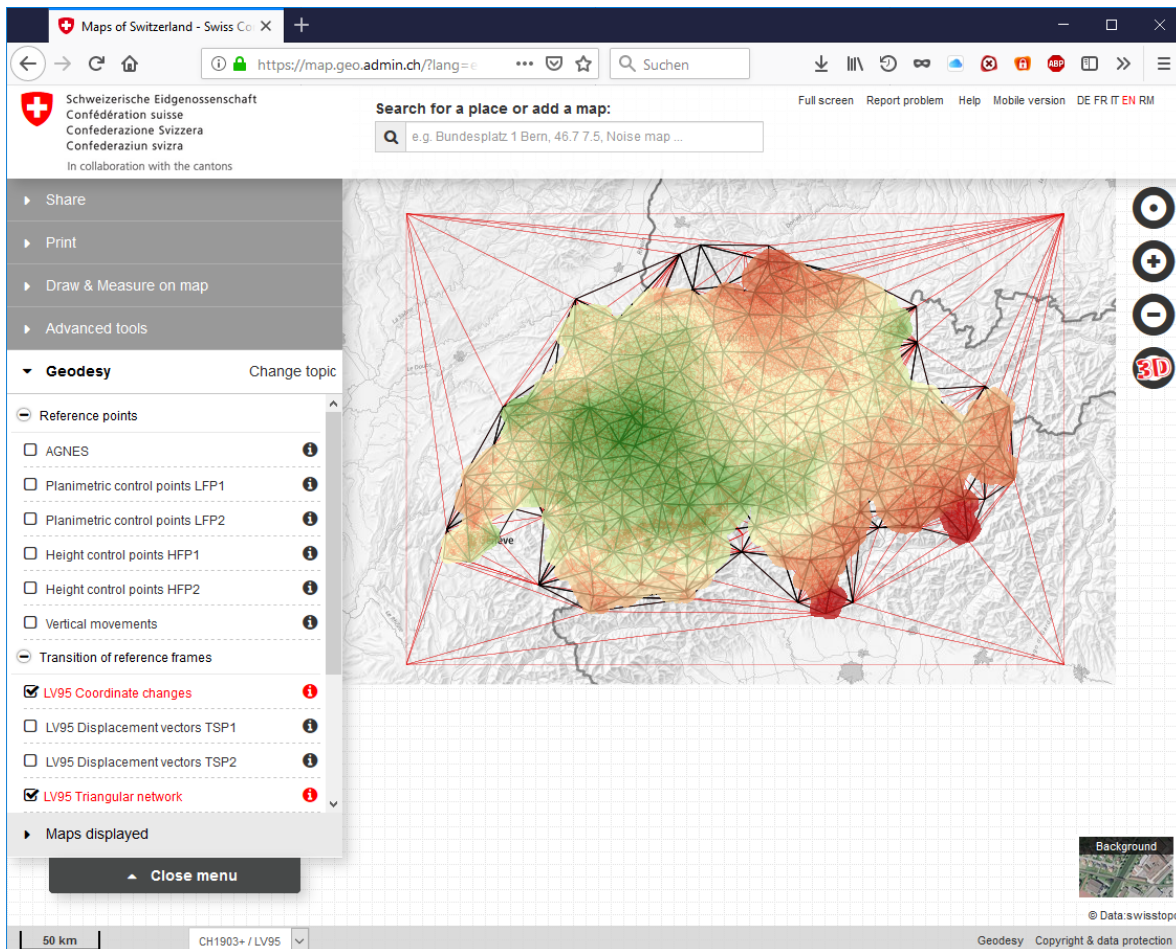


Figure 1. 72: topic «Geodesy» on map.geo.admin.ch

The following datasets are available on the topic «Geodesy»:

1. Reference points (Referenzpunkte, Points de référence, Punti di riferimento)

- AGNES GNSS permanent stations
- Planimetric control points (Lagefixpunkte) LFP1
- Planimetric control points (Lagefixpunkte) LFP2
- Height control points (Höhenfixpunkte) HFP1
- Height control points (Höhenfixpunkte) HFP2
- Vertical movements (Vertikalbewegungen)

2. Transition of reference frames (Bezugsrahmenwechsel, Changement de cadre de référence, Cambiamento di quadro di riferimento)

- LV95 Coordinate changes LV03 → LV95 (Koordinatenänderungen)
- LV95 Displacement vectors (Verschiebungsvektoren / Transformationsstützpunkte) TSP1
- LV95 Displacement vectors (Verschiebungsvektoren / Transformationsstützpunkte) TSP2
- LV95 Triangular network for the transition of reference frames (Dreiecksvermaschung)
- LV95 Transformation accuracy (Transformationsgenauigkeit)
- Areas with low distortions (Spannungsarme Gebiete)
- Height Transformation (HTRANS) LHN95 - LN02

3. Gravity field (Schwerefeld, Champ de pesanteur, Campo di gravitazione)

- Gravimetric base network (Landesschwerenetz)
- Deviations off the vertical (Lotabweichungen)
- Swiss Geoidmodel in CH1903
- Swiss Geoidmodel in ETRS89
- Gravimetric measuring points (Gravimetrische Messpunkte) 1:100'000
- Bouguer anomalies (Bouguer-Anomalien) 1:500'000
- Gravimetric Atlas (Gravimetrischer Atlas) 1:100'000

4. Background data (Hintergrunddaten, Données de fond, Dati di fondo)

- Coordinate grid (Koordinatennetz) CH1903+ / LV95
- Coordinate grid (Koordinatennetz) CH1903 / LV03
- Coordinate grid (Koordinatennetz) WGS84
- Tectonics / Tectonic Map of Switzerland (Tektonik) 1:500'000
- Geology / Geological Map of Switzerland (Geologie) 1:500'000
- Geological Atlas / Geological Map of Switzerland (Geologischer Atlas GA25) 1:25'000

CHTRF2016: 4th re-observation of the national GNSS network LV95

A. Wiget, St. Beckel, E. Brockmann, J. Carrel, M. Kistler, U. Marti, A. Schlatter and U. Wild

Federal Office of Topography swisstopo

Stable and accurate geodetic reference frames are part of a modern national infrastructure. They are the basis for precise national (official) as well as for private practical surveying and positioning, for geodynamic applications, for geographic information systems (GIS) and for cartography. The importance and need of a new, GPS based three-dimensional reference frame in Switzerland was recognized by swisstopo in the 1980ies (D. Schneider, E. Gubler and A. Wiget, 2015).

The Swiss national three-dimensional geodetic reference frame (Swiss Terrestrial Reference Frame CHTRF) is represented by more than 200 stable points of the LV95-network and 31 permanent stations of the automatic GNSS network AGNES. The concept and the realization of the “Landesvermessung 1995 (LV95)” is documented in the “swisstopo DOKU” series (former “Berichte aus der L+T”); the final report is planned to be published in 2019 (swisstopo-DOKU, 2019).

The LV95-network was established and first observed between 1989 and 1994. The three-dimensional coordinates (CHTRF95- and LV95-coordinates) of the LV95-points were published in 1995 (therefore the name “Landesvermessung 1995”). The network is periodically re-observed following a six year turn since 1998 (CHTRF98, CHTRF2004, CHTRF2010; see Wiget et al., 2010a). Therefore, a new re-observation campaign of the complete network was due and conducted in 2016 (CHTRF2016). The concept and organization of the 2016-campaign is described in (Carrel and Beckel, 2017).

The maintenance concept guarantees the quality of the three-dimensional reference frame CHTRF / LV95 regarding

- the control of the stability of the points,
- the check of the 3D-coordinates and their uncertainty,
- the proof of the reliability and consistency of the points and their coordinates,

and it provides a meaningful density of data for the long-term determination of the velocity field of these points and stations, respectively, eventually allowing to estimate the recent kinematics of the upper crust within Switzerland and relative to its surrounding countries in Europe (Brockmann, 2018; see also publication of Brockmann et al. in this national report). Furthermore, we refer to the description and monitoring of the quality standards of the national geodetic survey (Wiget et al., 2010b; Wiget et al., 2015, 2016, 2017).

The following main goals of the CHTRF2016 campaign can be mentioned:

- **Control of the official reference frame LV95:** The re-observation allows the proof of the quality (see above) of LV95 and the application of coordinate changes or station exchanges if necessary. The criteria for this are published in the maintenance concept of the national geodetic survey (swisstopo Report 09-14) and in its quality standards (swisstopo Report 10-11).
- **Determination of the reference frame CHTRF2016:** New re-observation of the network for the long-term monitoring of tectonic movements in Switzerland. With this 4th re-observation the time span since the first observation is growing to approx. 22 – 28 years.
- **NEOTEK2016:** Re-observation of a densified network of reference points in northern Switzerland which were specially established for Nagra (National Cooperative for the Disposal of Radioactive Waste) in 1988 and are since regularly re-observed together with the LV95-network.

The number of observed points / stations in the CHTRF2016-campaign was as follows:

31	AGNES permanent stations
104	Main points (H) of LV95
105	Densification points (V) of LV95
7	additional points in NEOTEK 2016
<u>7</u>	CHGeoid2003 points for the combination with the geoid determination
223	Total number of (passive) reference points

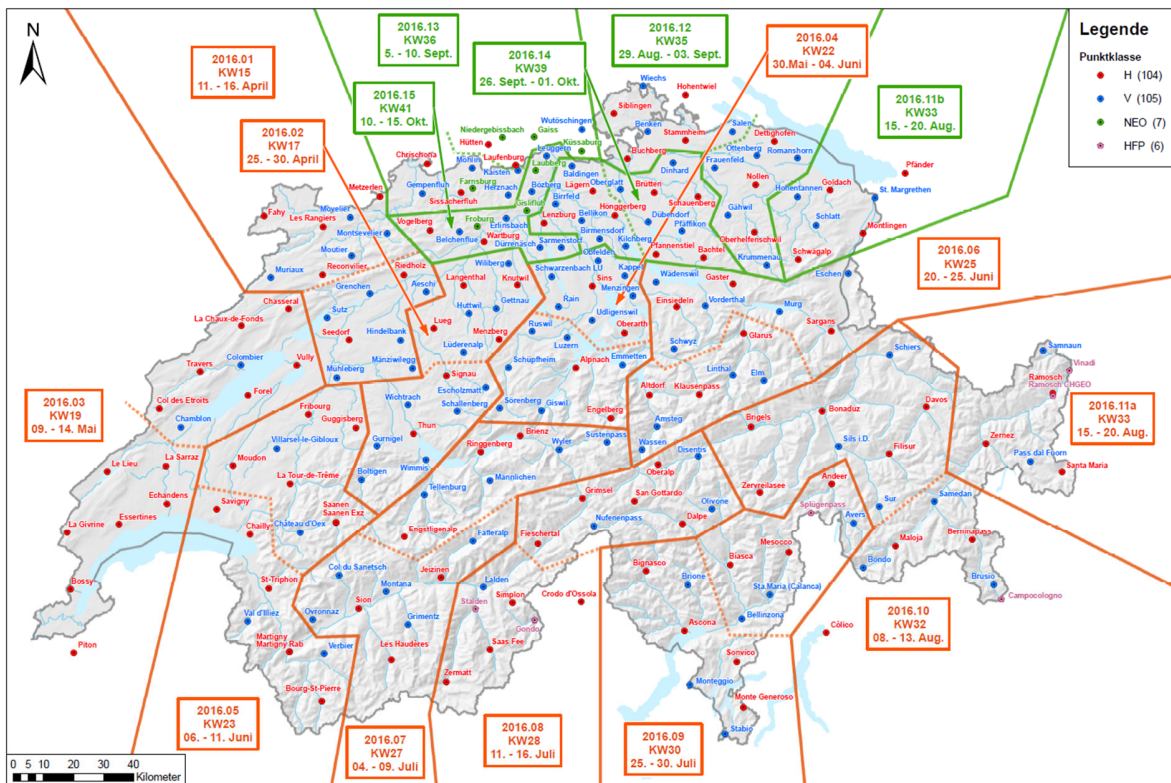


Figure 1. 73: Network of reference points observed in CHTRF2016 and their subdivision in weekly campaign areas.

The GNSS measurements were done using 8 swisstopo-owned Trimble NetR9 GNSS receivers with calibrated Trimble Zephyr Geodetic model 2 antennas. Each observer (2 per week) had operated 4 receivers. Further statistical details and their comparison with the former campaign CHTRF2010 are given in the following table (from Carrel and Beckel, 2017, swisstopo Report 16-08):

Indicators	CHTRF2016	CHTRF2010	Difference
Number of GNSS-operators	10	16	- 6
Number of campaign weeks	15	15	0
Number of GNSS receivers per week	8	8	0
Number of field-days per campaign	90	90	0
Number of person-field-days	188	195	- 7
Number of observed points (without AGNES stations)	223	221	+ 2
Total number of point observations	225	224	+2
Total amount of GNSS observation time [h]	9852	9618	+ 234
Mean observation time per point [h]	44.18	42.94	+ 3%
Max. / Min. observation time per point [h]	87.4 / 31.8	75.5 / 19.2	+ 11.9 / 12.6
Total kilometers driven by car [km]	31'139	36'937	- 16%

Table 1. 6: Statistics of the CHTRF2016 campaign, compared with the CHTRF2010-campaign.

Measurements for the National Height System

A. Schlatter, A. Wiget, U. Marti, B. Mattli

Federal Office of Topography swisstopo

Between 2015 and 2018 a total of 380 km (around 95 km per year) of leveling observations have been performed within the National Height Network LHN95 (see red lines in Figure 1. 74). This is 40 km/year less than the average as between 2007 and 2014. The main reason is a reduction of staff in the team responsible for the maintenance of the national height frame. Usually, these measurements were carried out on lines that were leveled 40 to 50 years ago for the last time.

The main part leveled in this epoch were third observations of 1st order levelling lines:

- Chur – Ilanz – Disentis (2015)
- Gletsch (VS) – Fiesch – Brig (2015/16)
- Aarburg – Burgdorf – Bern – Zimmerwald (2016)
- Kaiserstuhl – Laufenburg – Basel (2017/18)
- Koblenz – Brugg (2018)

In 2016, the third precision levelling from Bern to the fundamental station in Zimmerwald was measured (after the connections in 1995 and 2005). These special control measurements related to the national height frame showed no significant height changes of the geodetic fundamental point of Switzerland.

In the reporting period, two precise levellings through larger tunnels are worth to mention.

After 4 years of renovation work in the more than 100 years old and 20 km long Simplon tunnel, the third precise levelling was carried out in 2016. The two older measurements date back to 1906 und 1979. With the latest measurement, the recent crustal movements along the tunnel profile between Brig (VS) and Italy could be confirmed in an impressive way.

After the Gotthard and the Lötschberg railway base tunnels (57, respectively 36 km) the 16 km long Ceneri tunnel between Bellinzona and Lugano is the third main project of the New Rail Link through the Alps. After the successful breakthrough in 2015, a precise levelling line was installed and the measurements were carried out in 2017. This part is now integrated in the national height network LHN95 (in the same manner as the Gotthard and Lötschberg base tunnels).

Besides these line measurements, which principally serve for the realization of the two national vertical reference frames (LN02 and LHN95), geoid determination and the investigation of recent crustal movements, regular local maintenance works were performed in the observing period. The national height network contains today around 4'500 km of leveling lines with approximately 8'500 benchmarks.

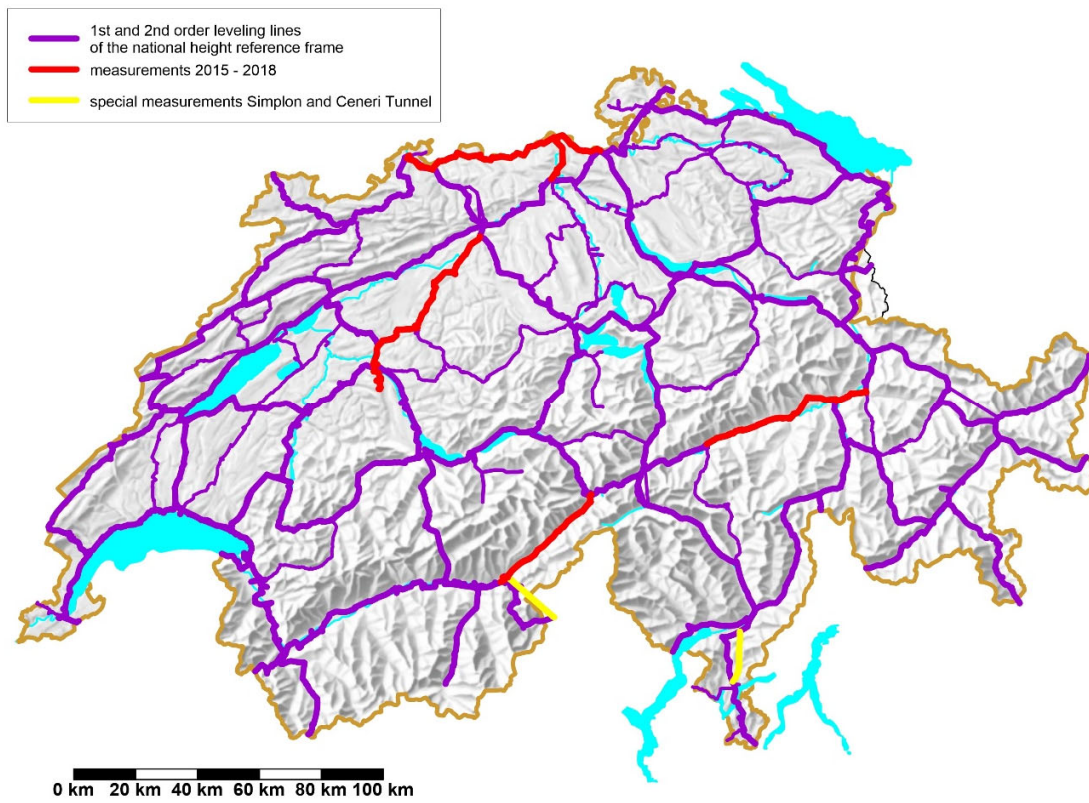


Figure 1. 74: Measurements 2015 – 2018 for the National Height System LHN95

Impact of the modeling of station clocks on geodetic parameters

K. Wang^{1,2}, M. Rothacher¹

¹ Chair of Mathematical and Physical Geodesy, Institute of Geodesy and Photogrammetry, ETH Zurich

² now at Curtin University

In current GNSS applications, receiver clock corrections are typically determined independently for every measurement epoch to reach a high positioning precision. The fact that the clocks, especially very good clocks, do not jump by arbitrary values from one epoch to the next is hardly used at present. Making optimal use of the quality of the receiver clocks should, therefore, stabilize the solutions significantly and improve the positioning results.

Weinbach et al. (2011) have shown that modelling the clock behaviour using a low-order polynomial for a very stable frequency standard can significantly improve the vertical component of kinematic Precise Point Positioning (PPP) solutions. A loose relative constraint may improve the stability of kinematic heights on the code positioning level by up to 70%-80%. In our study, a stochastic model using relative constraints between subsequent and near-subsequent clock parameters has been applied for receivers equipped with high-stability Hydrogen Masers (HM). The relationship between the weight of the relative constraints and the impact on the kinematic solutions have carefully been studied using GPS phase observation. Experiments using real data and simulated data confirmed that the short-term as well as the long-term stabilities of the kinematic solutions are significantly improved by up to a factor of three, especially in the less accurate vertical direction, through constraining subsequent and near-subsequent stochastic clock parameters appropriately (see Figure 1. 75).

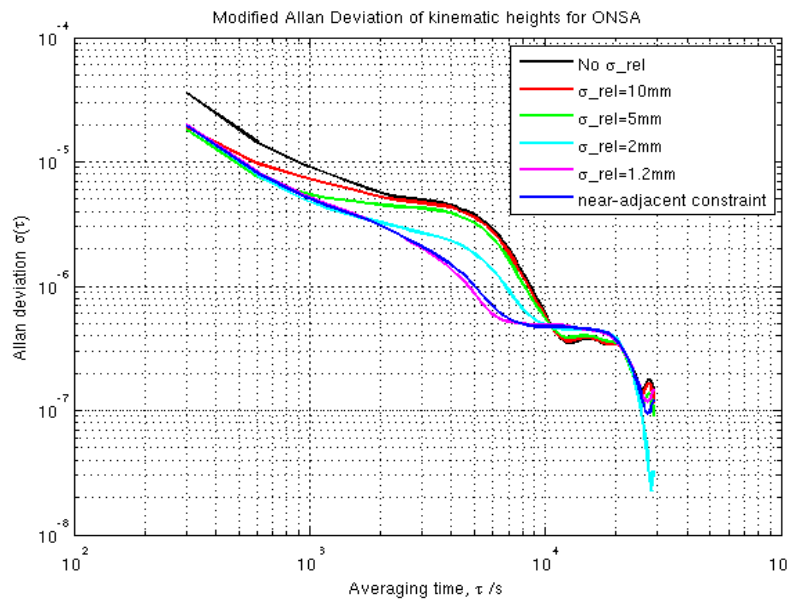


Figure 1. 75: Modified Allan deviations of kinematic height estimates for station ONSA using PPP and applying different relative constraints on the receiver clock estimates

Further investigations have also been performed concerning the correlation between troposphere parameters and the positioning results using relative constraints on clock parameters. Experiments have shown that the kinematic positioning results can further be improved by appropriately increasing the time resolution of the estimated troposphere parameters (e.g. up to 15 minutes, see Figure 1. 76). In addition, when comparing the wet zenith troposphere estimates from PPP solutions with water vapour values from water vapour radiometers, it could be shown that the wet troposphere zenith delays resulting with applying clock modelling were in better agreement than those derived without clock modelling (see Table 1. 7), especially for high temporal resolutions of the GPS-derived zenith wet delays.

The improved performance of the kinematic PPP solutions has been evaluated in detail in (Wang and Rothacher, 2013) and (Wang and Rothacher, 2017). A considerable benefit is to be expected for the (near) real-time monitoring of deformations, earthquakes and water vapor.

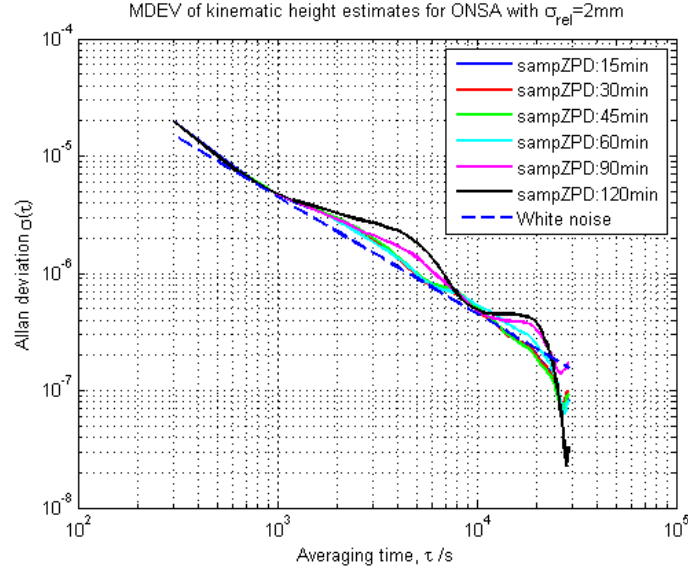


Figure 1.76: Modified Allan deviations of kinematic height estimates for station ONSA using PPP with relative constraints on the receiver clock estimates and applying different time resolutions for the zenith path delay (ZPD) estimation.

Table 1.7: RMS of differences between zenith wet delays (ZWD) at Onsala from WVR data and from GPS using different time resolutions for the ZWD estimation and applying or not applying relative clock constraints.

Date	RMS of ΔZWD [m]					
	2 h	1 h 30 min	1 h	45 min	30 min	15 min
Without clock model						
August 20, 2014	0.0068	0.0060	0.0065	0.0070	0.0066	0.0084
August 21, 2014	0.0223	0.0227	0.0344	0.0405	0.0327	0.0383
August 22, 2014	0.0093	0.0075	0.0092	0.0091	0.0106	0.0107
August 23, 2014	0.0155	0.0137	0.0155	0.0166	0.0169	0.0167
August 24, 2014	0.0125	0.0125	0.0138	0.0134	0.0153	0.0150
With clock model						
August 20, 2014	0.0060	0.0057	0.0061	0.0064	0.0064	0.0071
August 21, 2014	0.0062	0.0089	0.0074	0.0093	0.0096	0.0105
August 22, 2014	0.0086	0.0075	0.0087	0.0084	0.0085	0.0083
August 23, 2014	0.0126	0.0129	0.0136	0.0136	0.0145	0.0152
August 24, 2014	0.0101	0.0092	0.0113	0.0097	0.0111	0.0100

This study has been financed by the ESA project “Satellite and Station Clock Modelling for GNSS” (AO/1-6231/09/D/SR).

Geocenter variations derived from a combined processing of LEO and ground-based GPS observations

B. Männel^{1,2}, M. Rothacher¹

¹ Chair of Mathematical and Physical Geodesy, Institute of Geodesy and Photogrammetry, ETH Zurich

² now at Deutsches GeoForschungsZentrum (GFZ) Potsdam

The GPS observations provided by the global IGS (International GNSS Service) tracking network play an important role for the realization of a unique terrestrial reference frame that is accurate enough to allow the monitoring of the Earth's system. Combining these ground-based data with GPS observations tracked by high-quality dual-frequency receivers on-board Low Earth Orbiters (LEO) might help to further improve the realization of the terrestrial reference frame and the estimation of the geocenter coordinates, GPS satellite orbits and Earth rotation parameters (ERP).

To assess the scope of improvement, we processed a network of 50 globally distributed and stable IGS-stations together with four LEOs (GRACE-A, GRACE-B, OSTM/Jason-2 and GOCE) over a time interval of three years (2010-2012). To ensure fully consistent solutions the zero-difference phase observations of the ground stations and LEOs were processed in a common least-square adjustment, estimating GPS orbits, LEO orbits, station coordinates, ERPs, site-specific tropospheric delays, satellite and receiver clocks and ambiguities.

The results of such a combination showed that there is a significant impact of the individual LEO and a combination of all four LEOs on the geocenter coordinates. The formal errors are reduced by around 20% due to the inclusion of one LEO into the ground-only solution, while in a solution with four LEOs the reduction is even larger and, in addition, LEO-specific characteristics are significantly reduced.

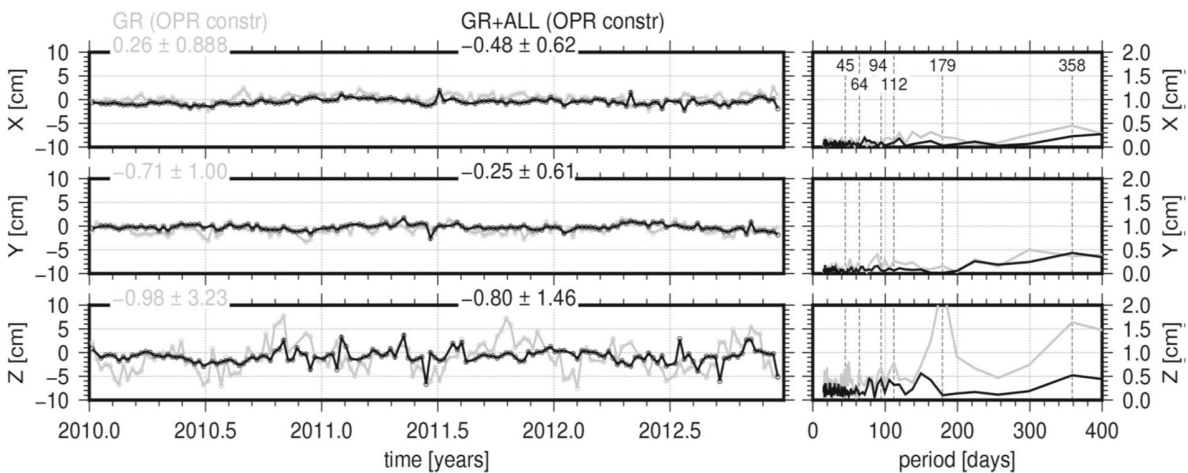


Figure 4. 1: Geocenter results from a ground-only (GR, gray) and a ground network plus four LEO combination (GR+ALL, black) solution; left: time series; right: amplitude spectra; the periods of the major peaks are indicated.

The derived geocenter coordinates were also compared to LAGEOS results and external solutions based on GPS and SLR data. All details are given in (Männel and Rothacher, 2017).

Kinematic determination of GNSS orbits including clock modeling

D. Koch¹, M. Rothacher¹, M. Meindl¹, K. Wang^{1,2}

1 Institute of Geodesy and Photogrammetry, ETH Zurich, Zurich, Switzerland

2 now at Department of Spatial Sciences, Curtin University, Australia

The availability of high-precision GNSS orbits is an essential prerequisite for highly accurate positioning applications. The present orbit products of the IGS analysis centers are based on dynamic orbit models including a variety of perturbations. Solar radiation pressure acceleration, being dependent on the shape, materials and attitude of the satellite is expected to be the major error source in orbit modeling. It is well-known that the errors caused by these modeling deficiencies are propagating into further products like satellite clock corrections, station coordinates, Earth rotation parameters and troposphere zenith delays, producing artefacts in the time series at the draconitic period of about 352 days.

In contrast to the orbit determination strategy used by the IGS analysis centers, we performed a purely kinematic estimation of the satellite position. The positions are determined independently from epoch to epoch and are free of any assumptions on the dynamic orbit models. Due to the extremely high correlation between the radial orbit component and the satellite clock correction, the radial orbit component is, however, poorly determined.

The latest generation of GNSS satellites are equipped with advanced, extremely stable clocks (e.g., the Passive Hydrogen Masers (PHM) on Galileo and the Rubidium Atomic Frequency Standards (RAFS) on GPS Block IIF), allowing a modeling of the satellite clock behavior by using a low-degree polynomial instead of an epoch-wise estimation. With this approach, the radial orbit component and the satellite clock corrections can be de-correlated to a degree, leading to significant improvements in the radial component of the kinematic orbit determination. The assessment of the benefits resulting from the modeling of the satellite clocks was the primary goal of this work.

The satellite clock corrections have been modeled by two components. The deterministic part consists of a linear polynomial representing the behavior of the clock over one day. The stochastic model is making use of relative constraints between subsequent epochs to account for short-time variations of the clock. The clock modeling has been implemented into a least-squares adjustment and is estimated together with the kinematic positions of the satellites. The precise orbits from CODE-MGEX (COM) have been taken as a priori values for the kinematic orbit estimation and served as reference orbits for comparisons.

The initial results are based on GNSS data of GPS week 1886 and a network of 73 ground stations distributed around the world. The GNSS data sampling interval was 5 minutes. This analysis focuses on 11 Galileo satellites (2 in orbit validation (IOV) and 6 full operational capability (FOC) satellites with active PHM, 1 IOV on RAFS and the 2 FOC with active PHM placed on an elliptical orbit) and the 12 Block IIF GPS satellites (10 operating on RAFS and 2 working on Digital Cesium Beam Frequency Standards (DCBFS)). By varying the relative constraints σ_r applied to the clock estimates, a distinct behavior of the radial component residual is observed (see Figure 1.77): For the Galileo PHM and GPS Block IIF RAFS, radial orbit errors are decreasing with increasing constraints, showing the positive effect of the decorrelation mentioned above.

A minimum plateau is reached, when the relative constraints are decreased to below 1 mm. This plateau corresponds to a standard deviation of the radial component of 2 to 8 cm depending on the satellite. This is the consequence of 1) systematic errors in the CODE orbits used as reference, 2) possible deviations of the clock from a linear behaviour as well as 3) the noise inherent to the kinematic estimation. On the other hand, satellites with less stable clocks show an improvement for medium constraints (around 3 cm), but clearly degrade for very tight clock constraining.

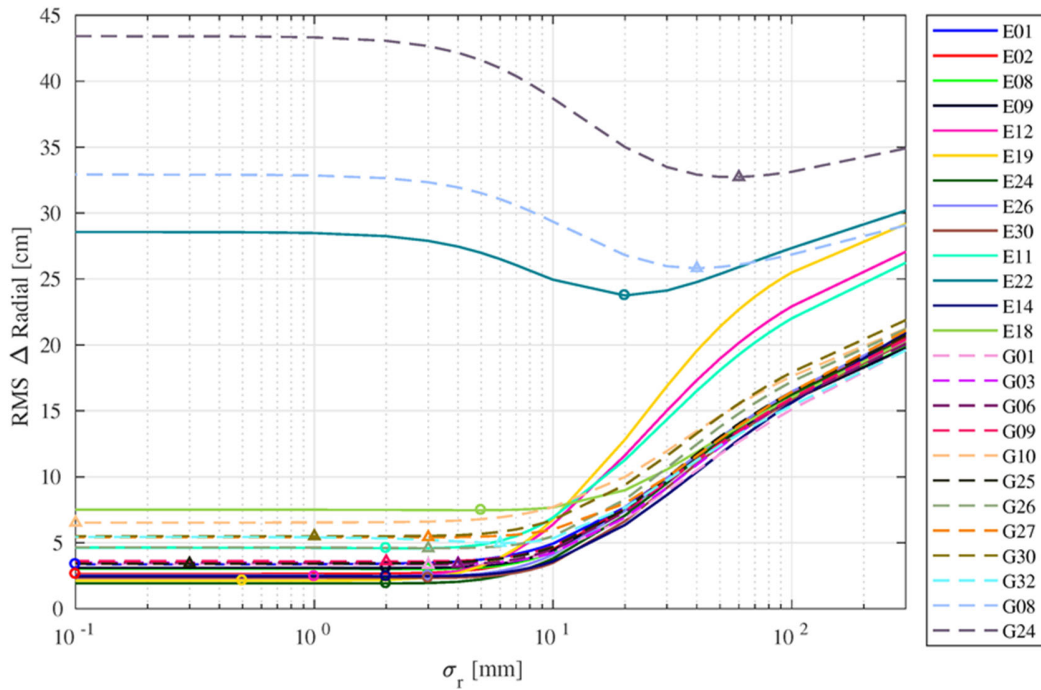


Figure 1.77: RMS of the difference in the radial component between kinematic orbit and ESOC dynamic orbit for different relative constraints σ_r . The circles and triangles represent the minimum RMS for each satellite, for Galileo and GPS, respectively.

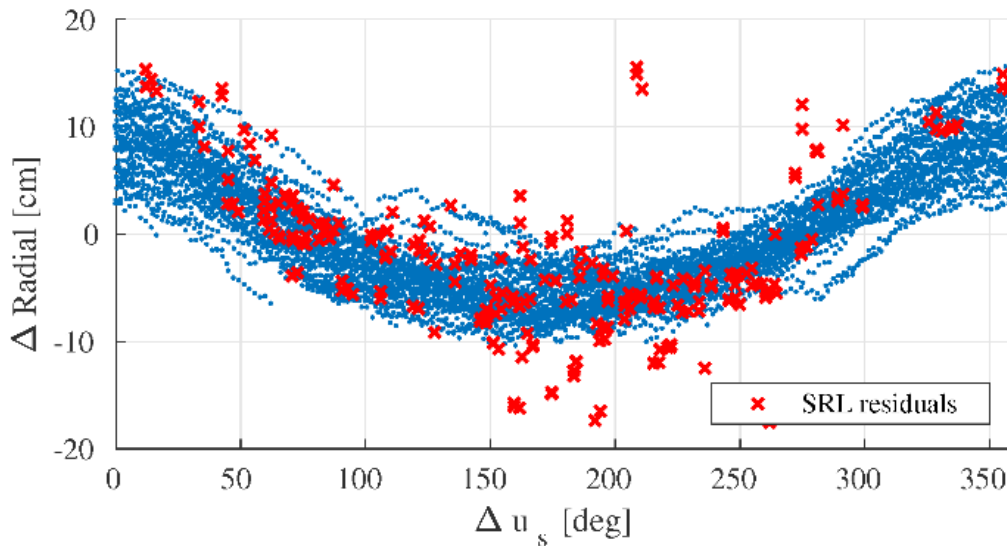


Figure 1.78: Kinematic orbit differences (blue dots) plotted together with the SLR residuals (red crosses) w.r.t. the ESOC dynamic orbit for Galileo satellite E01 as a function of the argument of latitude w.r.t. the Sun.

Finally, the kinematic orbits have been used to assess the deficiencies in the dynamic orbit models based on the analysis of the differences between the kinematic and different dynamic orbits and of the residuals obtained from satellite laser ranging (SLR) data (see Figure 1.78). In addition, because the kinematic positions refer to the antenna phase center and not to the center of mass, the satellite attitude behavior of the different satellite systems can be monitored and validated. The results are documented in (Koch et al., 2017).

Bibliography Commission 1

- Altamimi, Z., Rebischung, P., Métivier, L., Xavier, C. (2016): ITRF2014: A new release of the International Terrestrial Reference Frame modeling nonlinear station motions. *J. Geophys. Res. Solid Earth*, 121, doi: 10.1002/2016JB013098.
- Altamimi Z., E. Brockmann, C. Bruyninx, A. Caporali, R. Dach, J. Dousa, R. Fernandes, A. Kenyeres, J. Legrand, M. Lidberg, T. Liwosz, R. Pacione, M. Sacher, W. Söhne, G. Stangl, J. Torres, C. Völksen (2019): "Present and future of European reference frames", 16th European Geosciences Union – General Assembly, Vienna, Austria, 04/08 - 04/12/2019.
- Andritsch, F., Maier, A., Dach, R., Jäggi, A., (10 October 2016). Simulation of realistic SLR observations to optimize tracking scenarios. In: 20th International Workshop on Laser Ranging. Potsdam, Germany. 10.10.2016.
- Andritsch, F., Dach, R., Meyer, U., Schildknecht, T., Jäggi, A., (2018a). Combined SLR and GNSS solution using co-locations in space. In: 21st International Workshop on Laser Ranging. Canberra, Australia. 05. November, 2018.
- Andritsch, F., Dach, R., Meyer, U., Schildknecht, T., Jäggi, A., (2018b). The effect of SLR tracking scenarios to GNSS satellites in a combined GNSS/SLR solution. In: EGU General Assembly 2018. Vienna, Austria. 08.-13. April, 2018.
- Angermann D, Baustert G, Galas R, Zhu SY (1997). EPOS.P.V3 (Earth Parameter & Orbit System): software user manual for GPS data processing; version September 1997, Scientific Technical Report 97/14
- Arnold, D., Meindl, M., Beutler, G., Dach, R., Schaer, S., Lutz, S., Prange, L., Sośnica, K., Mervart, L., Jäggi, A. (2015): CODE's new solar radiation pressure model for GNSS orbit determination. *J Geod*, 89(8): 775-791. doi: 10.1007/s00190-015-0814-4.
- Arnold, D., S. Lutz, R. Dach, A. Jäggi, J. Steinborn; 2016: Near Real-Time Coordinate Estimation from Double-Difference GNSS Data - A Case Study for the National Multi-Hazard Early Warning System in the Sultanate of Oman. In IAG 150 years, edited by C. Rizos and P. Willis, pp. 691-697, DOI: 10.1007/1345_2015_173
- Beutler G., M. Meindl, S. Lutz, R. Dach, S. Scaramuzza, A. Sušnik, D. Arnold, A. Jäggi; 2016: Estimation of polar motion, polar motion rates, and GNSS orbits in the IGS. IGS Workshop 2016, Sydney, Australia, 8-12 February, 2016
- Bowman, B.R., W. K. Tobiska, F.A. Marcos, C. Valladares (2007) The JB2006 empirical thermospheric density model. *Journal of Atmospheric and Solar-Terrestrial Physics*, doi:10.1016/j.jastp.2007.10.002.
- Brockmann E., et al. (2015): "Multi-GNSS activities at EPN and at swisstopo", EUREF-TWG in Warsaw, March 23-24, 2015.
- Brockmann E. et al. (2015): "National Report of Switzerland", EUREF-Symposium in Leipzig, June 3-5, 2015.
- Brockmann E. (2015): "Reprocessed GNSS tropospheric products at swisstopo", GNSS4SWEC workshop, Thessaloniki, May 11-14, 2015.
- Brockmann E. et al. (2015): "Multi-GNSS activities at EPN and at swisstopo", EUREF-Symposium in Leipzig, June 3-5, 2015.
- Brockmann E. (2015): "Impact of GLONASS on reprocessed Zenith Total Delay Estimates", GNSS4SWEC workshop, Wroclaw, September 29 – 30, 2015.
- Brockmann E. (2015): "swisstopo Report for EGVAP 2015", EGVAP expert meeting, Wroclaw, October 1, 2015.
- Brockmann E., et al. (2015): "Multi-GNSS activities at EPN and at swisstopo", EUREF-TWG in Bern, October 13, 2015.
- Brockmann E., D. Andrey, D. Ineichen, L. Kislig, J. Liechti, S. Lutz, C. Misslin, S. Schaer and U. Wild (2016): "Automated GPS Network in Switzerland (AGNES)", International Foundation HFSJG, Activity Report 2016, University of Bern, 2016.

- Brockmann E. et al. (2016): “National Report of Switzerland”, EUREF-Symposium in SanSebastian, Spain, 25-27 May, 2016
- Brockmann E. et al. (2016): “Densifying Velocity Fields in Europe: Advantages of the classical approach”, EUREF-Symposium in SanSebastian, Spain, 25-27 May, 2016
- Brockmann E. (2016): “swisstopo Report for EGVAP 2016”, EGVAP expert meeting, Copenhagen Dec 6-7, 2016.
- Brockmann E., D. Andrey, D. Ineichen, L. Kislig, J. Liechti, S. Lutz, S. Schaer and U. Wild (2017): "Automated GPS Network in Switzerland (AGNES)", International Foundation HFSJG, Activity Report 2017, University of Bern, 2017.
- Brockmann E. et al. (2017): “National Report of Switzerland”, EUREF-Symposium in Wroclaw, Poland, May 17-19, 2017
- Brockmann E., S. Lutz, D. Ineichen, S. Schaer (2017): “Multi-GNSS developments for the EPN and for the Swiss networks”, EUREF-Symposium in Wroclaw, Poland, May 17-19, 2017
- Brockmann E. et al. (2017): “Charter of the EUREF Working Group on European Dense Velocities”, EUREF-Symposium in Wroclaw, Poland, May 17-19, 2017
- Brockmann E. et al. (2017): “Towards an European Dense Velocities Field”, EUREF-Symposium in Wroclaw, Poland, May 17-19, 2017
- Brockmann E., S. Lutz, D. Ineichen, S. Schaer (2017): “Impact of Multi-GNSS analysis on precise geodetic applications”, IAG-IASPEI scientific Assembly in Kobe, Japan, July 30 – August 4, 2017
- Brockmann E. (2017): “swisstopo Report for EGVAP 2017”, EGVAP expert meeting, DeBilt Nov. 28-29, 2017.
- Brockmann E., D. Andrey, D. Ineichen, L. Kislig, J. Liechti, S. Lutz, and U. Wild (2018): "Automated GPS Network in Switzerland (AGNES)", International Foundation HFSJG, Activity Report 2018, University of Bern, 2018.
- Brockmann E. (2018), LV95 / CHTRF2016 (Swiss Terrestrial Reference Frame 2016): Teil 2: Auswertung der GNSS-Messungen 2016 und Resultate der Gesamtausgleichung, Report 16-19, Wabern, 2018.
- Brockmann E., S. Lutz, D. Ineichen, S. Schaer (2018), Maintaining the Swiss Terrestrial Reference Frame CHTRF using Multi-GNSS, EUREF-Symposium in Amsterdam, The Netherlands, May 30 – June 1, 2018.
- Brockmann E. et al. (2018): “National Report of Switzerland”, EUREF-Symposium in Amsterdam, The Netherlands, May 30 – June 1, 2018.
- Beutler G., Brockmann, E., Gurtner, W., Hugentobler, U., Mervart, L., Rothacher, M., Verdun, A. (1994): Extended orbit modeling techniques at the CODE processing center of the International GPS Service for Geodynamics (IGS): theory and initial results. *Manuscr Geod* 19:367-384.
- Bock, H., Dach, R., Jäggi, A., Beutler, G. (2009): High-rate GPS clock corrections from CODE: support of 1 Hz applications. *J Geod*, 83(11):1083–1094. doi: 10.1007/s00190-009-0326-1. Bruyninx C., 2004, "The EUREF Permanent Network: a multi-disciplinary network serving surveyors as well as scientists", *GeoInformatics*, Vol 7, pp. 32-35
- Bruni, S. Rebeschung, P., Zerbini, S., Altamimi, Z., Errico, M., Santi, E.; (2018): Assessment of the possible contribution of space ties on-board GNSS satellites to the terrestrial reference frame, *J Geod*, vol. 92(4) 383-399, DOI: 10.1007/s00190-017-1069-z.
- Bruyninx C., H. Habrich, W. Söhne, A. Kenyeres, G. Stangl, C. Völksen, 2012, Enhancement of the EUREF Permanent Network Services and Products, "Geodesy for Planet Earth", IAG Symposia Series, Vol 136, pp. 27-35, DOI 10.1007/978-3-642-20338-1_4
- Cabinet Office (CAO), Government of Japan (2017). QZSS Satellite Information. URL: <http://qzss.go.jp/en/technical/qzssinfo>
- Caissy, M., Agrotis, L., Weber, G., Hernandez-Pajares, M., Hugentobler, U. (2012): The International GNSS real-time Service. *GPS World*, pages 52–58.

- Carrel, J., Beckel St. (2017): LV95 / CHTRF2016 (Swiss Terrestrial Reference Frame 2016) Teil 1: Messkonzept und Messkampagnen vom April bis Oktober 2016 im Landesnetz LV95. swisstopo Report 16-08. Bundesamt für Landestopografie swisstopo, Wabern.
- Combrinck L (2010) Satellite laser ranging. In: Xu S (ed) Sciences of Geodesy, vol 1. Springer, Berlin, pp 301–338. https://doi.org/10.1007/978-3-642-11741-1_9
- Cordelli, E., Schlatter, P., Schildknecht, T. (2018). Simultaneous multi-filter photometric characterization of space debris at the Swiss Optical Ground Station and Geodynamics Observatory Zimmerwald. Advanced Maui Optical and Space Surveillance Technologies Conference (AMOS) 2018, Wailea, Hawaii, USA, September 11-14.
- Cordelli, E., Schlatter, P., Lauber, P., Schildknecht, T. (2018). Use of a night-tracking camera for real time correction of the pointing of the SLR system. 21st International Workshop on Laser Ranging 2018, Canberra, Australia, november 5-9.
- Cordelli, E., Rodriguez, J., Schlatter, P., Lauber, P., Schildknecht, T. (2018). Real time improvement of orbits of space debris by using SLR and astrometric data acquired by a night-tracking camera. 21st International Workshop on Laser Ranging 2018, Canberra, Australia, november 5-9.
- Cordelli, E., Lauber, P., Prohaska, M., Rodriguez, J., Schlatter, P., Schildknecht, T. (2019). Recent Developments at the Swiss Optical Ground Station and Geodynamics Observatory Zimmerwald. 1st ESA NEO and Debris Detection Conference 2019, ESA/ESOC, Darmstadt, Germany, January 22-24.
- Cordelli, E., Schlatter, P., Lauber, P., Schildknecht, T. (2019). Use of a night-tracking camera for characterization and orbit improvement of defunct spacecraft. 1st ESA NEO and Debris Detection Conference 2019, ESA/ESOC, Darmstadt, Germany, January 22-24.
- Dach, R., S. Lutz, P. Walsler, P. Fridez (Eds); 2015: Bernese GNSS Software Version 5.2. User manual, Astronomical Institute, University of Bern, Bern Open Publishing. DOI: 10.7892/boris.72297; ISBN: 978-3-906813-05-9.
- Dach, R., S. Schaer, S. Lutz, D. Arnold, H. Bock, E. Orliac, L. Prange, A. Villiger, L. Mervart, A. Jäggi, G. Beutler, E. Brockmann, D. Ineichen, A. Wiget, D. Thaller, H. Habrich, W. Söhne, J. Ihde, P. Steigenberger, and U. Hugentobler; 2015: Center for Orbit Determination In Europe: IGS Technical Report 2014. International GNSS Service: Technical Report 2014; edited by Y. Jean and R. Dach (AIUB), IGS Central Bureau and University of Bern, Bern Open Publishing, pp. 21-34, May 2015.
- Dach, R., S. Schaer, D. Arnold, E. Orliac, L. Prange, A. Sušnik, A. Villiger, A. Maier, L. Mervart, A. Jäggi, G. Beutler, E. Brockmann, D. Ineichen, S. Lutz, A. Wiget, A. Rülke, D. Thaller, H. Habrich, W. Söhne, J. Ihde, U. Hugentobler; 2016: Center for Orbit Determination In Europe: IGS Technical Report 2015. International GNSS Service: Technical Report 2015; edited by Y. Jean and R. Dach (AIUB), IGS Central Bureau and University of Bern, Bern Open Publishing, pp. 25-44, June 2016. DOI: 10.7892/boris.80307
- Dach, R., S. Schaer, D. Arnold, E. Orliac, L. Prange, A. Sušnik, A. Villiger, A. Maier, L. Mervart, A. Jäggi, G. Beutler, E. Brockmann, D. Ineichen, S. Lutz, A. Wiget, A. Rülke, D. Thaller, H. Habrich, W. Söhne, J. Ihde, U. Hugentobler; 2017: Center of Orbit Determination in Europe: IGS Technical Report 2016. International GNSS Service: Technical Report 2016; edited by A. Villiger and R. Dach (AIUB), IGS Central Bureau and University of Bern, Bern Open Publishing, pp 25-44, May 2017. DOI: 10.7892/boris.99278
- Dach, R., S. Schaer, D. Arnold, E. Orliac, L. Prange, A. Sušnik, A. Villiger, A. Jäggi, G. Beutler, E. Brockmann, D. Ineichen, S. Lutz, A. Wiget, J. Dostal, D. Thaller, W. Söhne, J. Bouman, I. Selmke, U. Hugentobler; 2018: Center of Orbit Determination in Europe: IGS Technical Report 2017. International GNSS Service: Technical Report 2017; edited by A. Villiger and R. Dach (AIUB), IGS Central Bureau and University of Bern, Bern Open Publishing, pp 32-44, June 2018. DOI: 10.7892/boris.116377
- Dach, R., Sušnik, A., Grahsl, A., Villiger, A., Schaer, S., Arnold, D., Prange, L., Jäggi, A. (2019): Improving GLONASS Orbit Quality by Re-estimating Satellite Antenna Offsets. Adv. Space Res., in press. doi: 10.1016/j.asr.2019.02.031
- Darugna F, Steigenberger P, Montenbruck O, Casotto S (2018). Ray-tracing solar radiation pressure modeling for QZS-1. Adv Space Res62, 935–943. doi:10.1016/j.asr.2018.05.036

- Degnan, J. (1993): Millimeter accuracy satellite laser ranging: a review. In Contributions of space geodesy to geodynamics: technology. Pages 133-162.
- Diehl T., Kissling E., Nibourel L., Herwegh M., Brockmann E., Schmid S.: "Structure and Deformation of the Central-Eastern Aar Massif", 16th European Geosciences Union – General Assembly, Vienna, Austria, 04/08 - 04/12/2019.
- Dilssner F, Springer T, Gienger G, Dow J (2011). The GLONASS M satellite yaw-attitude model. *Adv Space Res* 47(1):160–171. doi:10.1016/j.asr.2010.09.007
- European Global Navigation Satellite Systems Agency (GSA) (2016). Galileo Satellite Metadata. URL: <https://www.gsc-europa.eu/support-to-developers/galileo-satellite-metadata>
- Exertier P, Belli A, Lemoine JM (2017) Time biases in laser ranging observations: a concerning issue of space geodesy. *Adv Space Res* 60:948–968. <https://doi.org/10.1016/j.asr.2017.05.016>
- Fritsche, M., Sośnica, K., Rodriguez-Solano, C., Steigenberger, P., Wang, K., Dietrich, R., Dach, R., Hugentobler, U., Rothacher, M. (2014): Homogeneous reprocessing of GPS, GLONASS and SLR observations. *J Geod*, 88(7):625–642. doi:10.1007/s00190-014-0710-3.
- Grahl, A., Sušnik, A., Prange, L., Arnold, D., Dach, R., Jäggi, A. (2016): GNSS orbit validation activities at the Astronomical Institute in Bern. In: Proceedings of the 20th International Workshop on Laser Ranging, October 10–14, 2016, Potsdam, Germany.
- Hedin, A. E. (1987) MSIS-86 Thermospheric Model. *Journal of Geophysical Research*, 92(A5), 4649–4662. <https://doi.org/10.1029/JA092iA05p04649>
- Herrera-Pinzón, I., and M. Rothacher. Multi-Year Analysis of GNSS Local Ties at Fundamental Sites. Joint Scientific Assembly of the IAG and IASPEI 2017. Kobe, Japan. July 30 - August 4, 2017.
- Herrera-Pinzón, Iván and Rothacher, Markus. Assessment of GNSS and VLBI Local Baselines at Fundamental Sites. *Geodätische Woche 2017 – Geodätische Referenzsysteme und Erdrotation*. Berlin, Germany. September 26-28, 2017
- Herrera-Pinzón, Iván; Rothacher, Markus; Kodet, Jan and Schreiber, Ulrich. VLBI Estimation of Short Baselines at the Fundamental Site Wettzell. *EGU General Assembly 2018*. Vienna, Austria. April 7-12, 2018
- Herrera-Pinzón, Iván; Rothacher, Markus; Kodet, Jan and Schreiber, Ulrich. Analysis of the Short VLBI Baseline at the Wettzell Observatory. *Proceedings of the Tenth IVS General Meeting*. Longyearbyen, Norway. June 3-8, 2018
- Herrera-Pinzón, Iván; Rothacher, Markus; Kodet, Jan and Schreiber, Ulrich. Analysis of the Short VLBI Baseline at the Wettzell Observatory. *Tenth IVS General Meeting*. Longyearbyen, Norway. June 3-8, 2018
- Herrera-Pinzón, I., and M. Rothacher. Assessment of Local GNSS Baselines at Co-Location Sites. *Journal of Geodesy* (92). Springer, Berlin. Pages 1079 – 1095. ISSN: 0949-7714. DOI: 10.1007/s00190-017-1108-9.
- Huang G, Yan X, Zhang Q, (2018). Estimation of antenna phase center offset for BDS IGSO and MEO satellites. Presentation, IGS Workshop 2018, Wuhan, China
- Ineichen D., E. Brockmann, S. Lutz, S. Schaer (2015): "Reprocessing activities at swisstopo (LPT)", EUREF-LAC Workshop in Bern, October 14-15, 2015.
- Jäggi, A: (2007): Pseudo-stochastic orbit modeling of low Earth satellites using the Global Positioning System. In *Geodätisch-geophysikalische Arbeiten in der Schweiz*, volume 73. Schweizerische Geodätische Kommission, Institut für Geodäsie und Photogrammetrie, Eidg. Technische Hochschule Zürich, Zürich.
- Jäggi A, Dach R, Montenbruck O, Hugentobler U, Bock H, Beutler G (2009) Phase center modeling for LEO GPS receiver antennas and its impact on precise orbit determination. *J Geod* 83(12):1145-1162. doi:10.1007/s00190-009-0333-2
- Jäggi, A., Weigelt, M., Flechtner, F. Güntner, A., Mayer-Gürr, T. Martinis, S., Bruinsma, S., Flury, J., Bourgoigne, S. (2019): European Gravity Field Service for Improved Emergency Management (EGSIEM); this volume.
- Januth, T. (2017) Robot validation with the QDaedalus system: Integration of a robot in a global reference frame». Master Thesis, HES-SO, Yverdon, Switzerland.

- Johnston, G., Riddell, A., Hausler, G. (2017). The International GNSS Service. In Teunissen, Peter J.G., & Montenbruck, O. (Eds.), Springer Handbook of Global Navigation Satellite Systems (1st ed., pp. 967-982). Cham, Switzerland: Springer International Publishing, DOI: 10.1007/978-3-319-42928-1
- Kenyeres A., Horvath T., Völksen C., Pacione R., Szafranek K., Araszkievicz A., Dousa J., – Ineichen D., Brockmann E., Valdes M. (2016): “ITRF2014 Densification with EPN REPRO-2: First Experiences”. Presented at the EUREF2016 Symposium, San Sebastian, Spain, 25-27 May, 2016.
- Koch, D., M. Rothacher, M. Meindl, K. Wang, E. Schoenemann, W. Enderle (2017): Kinematic Determination of GNSS Orbits Including Clock Modeling, Proceedings of the 6th International Colloquium on Scientific and Fundamental Aspects of GNSS / Galileo, Technical University of Valencia, Valencia, Spain, October 25-27, 2017.
- Kouba J (2009). A simplified yaw-attitude model for eclipsing GPS satellites. GPS Solut 13(1):1–12. doi:10.1007/s10291-008-0092-1
- Lanegger, C. (2017): Simulation Toolkit for Laser Ranging to Satellites. Master theses, Institute of Geodesy and Photogrammetry, ETH Zürich.
- Lutz, S., M. Meindl, P. Steigenberger, G. Beutler, K. Sośnica, S. Schaer, R. Dach, D. Arnold, D. Thaller, A. Jäggi; 2016: Impact of the arc length on GNSS analysis results. Journal of Geodesy, vol. 90(4), pp. 365-378. DOI 10.1007/s00190-015-0878-1
- Lutz S., S. Schaer, D. Ineichen, E. Brockmann (2015): “Multi-GNSS analysis at swisstopo: Developments and first results”, EUREF-LAC Workshop in Bern, October 14-15, 2015.
- Lutz S., E. Brockmann (2018), Status Report on the Working Group on “European Dense Velocities”, EUREF-Symposium in Amsterdam, The Netherlands, May 30 – June 1, 2018.
- Lutz S., Brockmann E. (2019): “Status report of the Working Group European Dense Velocities”, 16th European Geosciences Union – General Assembly, Vienna, Austria, 04/08 - 04/12/2019.
- Männel, B., M. Rothacher (2017): Geocenter Coordinates from a Combined Processing of LEO and Ground-based GPS Observations, Journal of Geodesy, Vol. 91, Issue 8, p. 933-944, 2017
- Meindl, M, Beutler, G, Thaller, D, Dach, R, Jäggi, A (2013): Geocenter coordinates estimated from GNSS data as viewed by perturbation theory. Adv Space Res 51(7):1047–1064. doi: 10.1016/j.asr.2012.10.026
- MacLeod K, Agrotis L (2013). IGS RINEX Working Group Report 2011. International GNSS Service. Technical Report 2012, edited by Dach R and Jean Y (AIUB), IGS Central Bureau, pp. 191–194, 2013
- Montenbruck O, Rizos C, Weber, R, Weber G, Neilan RE, Hugentobler U (2013). Getting a Grip on Multi-GNSS: The International GNSS Service MGEX Campaign, GPS World, 24(7), pp. 44–49, 2013
- Montenbruck, O, Schmid, R, Mercier, F, Steigenberger, P, Noll, C, Fatkulin, R, Kogure, S, Ganeshan, AS, (2015). GNSS satellite geometry and attitude models. Adv Space Res 56, 1015–1029. doi:10.1016/j.asr.2015.06.019
- Montenbruck, O., P. Steigenberger, U. Hugentobler (2015): Enhanced solar radiation pressure modeling for Galileo satellites. J. Geod 89:283-297. Doi: 10.1007/s00190-014-0774-0
- Montenbruck, O., P. Steigenberger, F. Darugna (2017): Semi-analytical solar radiation pressure modeling for QZS-1 orbit-normal and yaw-steering attitude. Adv. Space Res. 59:2088-2100. Doi: 10.1016/j.asr.2017.01.036
- Otsubo T (2017) Multi-satellite bias analysis report v2 for worldwide satellite laser ranging stations. <http://geo.science.hit-u.ac.jp/slr/bias/>. Accessed 9 Apr 2018
- Pacione, R.; Araszkievicz, A.; Brockmann, E.; Douša, J. (2017) EPN-Repro2: A reference GNSS tropospheric data set over Europe, Atmos. Meas. Tech., 10, 1689-1705. doi:10.5194/amt-10-1689-2017.
- Pearlman MR, Degnan JJ, Bosworth J (2002) The International Laser Ranging Service. Adv Space Res 30(2):135-143. [https://doi.org/10.1016/S0273-1177\(02\)00277-6](https://doi.org/10.1016/S0273-1177(02)00277-6)
- Prange, L., Arnold, D., Dach, R., Schaer, S., Sidorov, D., Stebler, P., Sušnik, A., Villiger, A. Jäggi, A. (2019): CODE five system solution for the IGS MGEX; this volume.

- Prange L, Dach R, Lutz S, Schaer S, Jäggi A (2016). The CODE MGEX Orbit and Clock Solution. In: Rizos C, Willis P (eds). IAG 150 years, International Association of Geodesy Symposia. Springer, New York, pp 767–773. doi: 10.1007/1345_2015_161
- Prange L, Orliac E, Dach R, Arnold D, Beutler G, Schaer S, Jäggi A (2017a). CODE's five-system orbit and clock solution—the challenges of multi-GNSS data analysis. *Journal of Geodesy* 91, 345–360. doi:10.1007/s00190-016-0968-8
- Prange L, Villiger A, Sidorov D, Dach R, Schaer S, Beutler G, Sušnik A, Jäggi A (2017b). Impact of new background models on GNSS orbit determination. 6th International Colloquium - Scientific and Fundamental Aspects of GNSS / Galileo, Valencia, Spain, 25-27 October 2017
- Prange L, Beutler G, Dach R, Arnold D, Schaer S, Jäggi A (2019a). An empirical solar radiation pressure model for satellites moving in the orbit-normal mode. Submitted to *Advances in Space Research*
- Prange, L., Arnold, D., Dach, R., Schaer, S., Sidorov, D., Stebler, P., Sušnik, A., Villiger, A. Jäggi, A. (2019): CODE five system solution for the IGS MGEX; this volume.
- Prange L, Beutler G, Dach R, Arnold D, Schaer S, Villiger A, Jäggi A (2019b). An empirical SRP model for the orbit normal attitude mode. This volume
- Rachman, A., Schildknecht, T., Vananti, A. (2018). Analysis of temporal evolution of debris objects rotation rates inside AIUB light curve database. 69th International Astronautical Congress (IAC) 2018, Bremen, Germany, October 1-5.
- Ray, J, Altamimi, Z, Collilieux, X, van Dam, T (2008): Anomalous harmonics in the spectra of GPS position estimates. *GPS Solut* 12(1):55–64. doi: 10.1007/s10291-007-0067-7
- Schaer S, Villiger A, Dach R, Prange L, Jäggi A (2018). New ambiguity-fixed IGS clock analysis products at CODE. Presentation. IGS Workshop 2018, Wuhan, China, 29. Oct-02-Nov. 2018
- Schaer S, Villiger A, Arnold D, Prange L, Dach R, Jäggi A (2019): Ambiguity Resolution in Zero-Difference Solutions and for PPP; this volume.
- Schmid, R., Rothacher, M. (2003): Estimation of elevation-dependent satellite antenna phase center variations of GPS satellites. *J. Geod*, 77 (7–8): 440-446. doi: 10.1007/s00190-003-0339-0.
- Schmid, R., Dach, R., Collilieux, X., Jäggi, A., Schmitz, M., Dilssner, F. (2016): Absolute IGS antenna phase center model igs08.atx: status and potential improvements. *J. Geod*, 90 (4): 343-364. doi: 10.1007/s00190-015-0876-3.
- Schneider D., Gubler, E., Wiget, A. (2015): Meilensteine der Geschichte und Entwicklung der Schweizerischen Landesvermessung. *Geomatik Schweiz* 11/2015, p. 462 – 483.
- Seitz, M., Bloßfeld, M., Angermann, D., Schmid, R., Gerstl, M., Seitz, F. (2016): The new DGFI-TUM realization of the ITRS: DTRF2014. doi:10.1594/PANGAEA.864046.
- Sidorov D, Dach R, Prange L, Jäggi A (2018). Improved orbit modelling of Galileo satellites during eclipse seasons. Poster. IGS Workshop 2018, Wuhan, China, Oct. 29 - Nov. 02, 2018
- Sidorov D, Dach R, Prange L, Jäggi A (2019). Advancing the orbit model for Galileo satellites during the eclipse seasons. This volume
- Solano, C. J. R. (2014): Impact of non-conservative force modeling on GNSS satellite orbits and global solutions. PhD Thesis. urn:nbn:de:bvb:91-diss-20140822-1188612-0-8
- Sonka, A. B., Gornea, A. I., Anghel, S., Birlan, M. (2017). Photometric Observations of Near Earth Asteroid 2012 TC4. *Romanian Astronomical Journal*, vol. 27, no. 3, pp. 223-231, December 2017.
- Sošnica, K., Thaller, D., Dach, R., Steigenberger, P., Beutler, G., Arnold, D., Jäggi, A. (2015): Satellite laser ranging to GPS and GLONASS. *J Geod*, 89(7):. 725-743. DOI 10.1007/s00190-015-0810-8.
- Springer TA, Beutler G, Rothacher M (1999). A new solar radiation pressure model for GPS satellites. *GPS Sol*. 3(2), 50—62
- Springer T (2010). URL: <http://www.positim.com/napeos.html>

- Sušnik, A., Grahsl, A., Arnold, D., Villiger, A., Dach, R., Jäggi, A., Beutler, G. (2019): GNSS reprocessing results in the framework of the EGSIM project, this volume.
- Steffen, R., Legrand J., Steffen H., Lidberg M., Kenyeres A., Brockmann, E., Lutz, S. (2019): “Deformation model for Europe: Application of the least-square collocation”, 16th European Geosciences Union – General Assembly, Vienna, Austria, 04/08 - 04/12/2019.
- Steigenberger, P., Lutz, S., Dach, R., Schaer, S., Jäggi, A. (2014): CODE repro2 product series for the IGS. Published by Astronomical Institute, University of Bern. URL: http://www.aiub.unibe.ch/download/REPRO_2013; DOI: 10.7892/boris.75680.
- Steigenberger P, Fritsche M, Dach R, Schmid R, Montenbruck O, Uhlemann M, Prange L (2016). Estimation of satellite antenna phase center offsets for Galileo. *J Geod* 90(8):773–785. doi:10.1007/s00190-016-0909-6
- Steigenberger P, Thoenert S, Montenbruck O (2018). GNSS Satellite Transmit Power and its Impact on Orbit Determination. *Journal of Geodesy*, 92 (6), pp. 609-624. Springer. DOI:10.1007/s00190-017-1082-2
- Sušnik, A., Grahsl, A., Arnold, D., Villiger, A., Dach, R., Jäggi, A., Beutler, G. (2019): GNSS reprocessing results in the framework of the EGSIM project, this volume.
- swisstopo (2017): Topic «Geodesy» with reference datasets and GIS data of the Swiss Geodetic Survey on the federal geoportal and the map viewer map.geo.admin.ch.
- swisstopo-DOKU Reihe [bzw. „Berichte aus der L+T“] (1995-2019): Teile 1 – 15 zum Aufbau der neuen Landesvermessung der Schweiz 'LV95'. Bundesamt für Landestopografie swisstopo, Wabern.
- Thaller, D., Dach, R., Seitz, M. Beutler, G., Mareyen, M., Richter, B. (2011): Combination of GNSS and SLR observations using satellite co-locations. *J Geod*, vol. 85(5) 257-272, DOI:10.1007/s00190-010-0433-z.
- van den IJssel, J., J. Encarnação, E. Doornbos, and P. Visser (2015), Precise science orbits for the Swarm satellite constellation, *Adv. Space Res.*, 56(6), 1042–1055, doi:10.1016/j.asr.2015.06.002
- Villiger A., A. Geiger, P. Limpach, E. Brockmann (2015): “The Geodetic Three Dimensional Strain-Rate Field in Switzerland: New Methods and Results”, IUGG Prague, June 22 - July 2, 2015.
- Villiger, A., S. Lutz, A. Sušnik, L. Prange, S. Schaer, R. Dach, A. Jäggi; 2017: CODE's update of the Clock Products. International GNSS Service (IGS) Workshop 2017, Paris, France, July 3-7, 2017
- Villiger A, Schaer S, Dach R, Prange L, Susnik A, Jäggi A (2019a). Determination of GNSS pseudo-absolute code biases and their long-term combination. Submitted to *Journal of Geodesy*
- Villiger A, Schaer S, Dach R, Prange L, Sušnik A, Jäggi A (2019b). Determination of GNSS pseudo-absolute code biases and classification of receiver tracking technology. This volume
- Villiger A, Prange L, Dach R, Zimmermann F, Kuhlmann H, Jäggi A (2019c). Consistency of antenna products in the MGEX environment. This volume
- Wang, K., M. Rothacher (2013): Stochastic modeling of high-stability ground clocks in GPS analysis, *Journal of Geodesy*, Volume 87, Issue 5, pp.427-437, doi 10.1007/s00190-013-0616-5, 2013
- Wang, K., M. Rothacher, M. Meindl, E. Schoenemann, W. Enderle (2017): Improvement in the estimation of troposphere zenith delays using high-accuracy clocks, presented at the Workshop 2017 of the International GNSS Service (IGS) in Paris, France, 2017
- Weinbach, U., S. Schön (2011): GNSS receiver clock modeling when using high-precision oscillators and its impact on PPP, *Advances in Space Research*, vol. 47 (2), p. 229-238, 2011
- Willi, D., Koch, D., Meindl, M., Rothacher, M. (2018): Absolute GNSS Antenna Phase Center Calibration with a Robot. In: Proceedings of the 31st International Technical Meeting of The Satellite Division of the Institute of Navigation (ION GNSS+ 2018), Miami, FL, USA, pp. 3909-3926.
- Willi, D, Guillaume S. (2019): Calibration of a six-axis robot for GNSS antenna phase center estimation. *Journal of Surveying engineering*. Accepted for publication.
- Willi, D (2019): GNSS receiver synchronisation and antenna calibration. Doctoral Thesis, ETH Zurich, Zurich, Switzerland, <https://doi.org/10.3929/ethz-b-000308750>.

- Wiget, A., Brockmann, E., Kistler, M., Marti, U., Schlatter, A., Vogel, B., Wild, U. (2010a): Nachführungskonzept für die geodätische Landesvermessung. swisstopo Report 09-14, Bundesamt für Landestopografie, Wabern.
- Wiget, A., Andrey, D., Brockmann, E., Ineichen, D., Kistler, D., Marti, U., Schlatter, A., Vogel, B., Wild, U. (2010b): Qualitätsstandards der Landesvermessung. Indikatoren, Standards und Messgrößen für die Produkte der geodätischen Landesvermessung. swisstopo Report 10-11 (also available in french), Bundesamt für Landestopografie, Wabern.
- Wiget A., Andrey, D., Brockmann, E., Kistler, M., Marti, U., Schlatter, A., Wild, U. (2015, 2016, 2017): Qualitätsstandards der Landesvermessung: Erhebung und Auswertung der Messgrößen zur Beurteilung der Zielerreichung im Jahr 2015, 2016, 2017. swisstopo Reports 15-16, 16-16 und 17-02. Bundesamt für Landestopografie swisstopo, Wabern.
- Wiget A. (2015): Neue Koordinaten für die Schweiz – auf den Zentimeter genau / Nouvelles coordonnées pour la Suisse – au centimètre près. GeoPanorama 4/2015.
- Wu, X., Abbondanza, C., Altamimi, Z., Chin, T., Collilieux, X., Gross, R., Heflin, M., Jiang, Y., Parker, J., Wu, X. (2015): KALREF - A Kalman Filter and Time Series Approach to the International Terrestrial Reference Frame Realization. *J. Geophys. Res.*, 120, B03775, doi: 10.1002/2014JB011622.
- Zhao Q, Chen G, Guo J, Liu J, Liu X (2018). An a priori solar radiation pressure model for the QZSS Michibiki satellite. *J Geod* 92, 109–121. doi:10.1007/s00190-017-1048-4

2 Gravity Field

Absolute and Relative Gravity Measurements

U. Marti¹, H. Baumann² and S. Guillaume³

¹ Federal Office of Topography, swisstopo

² Federal Institute of Metrology METAS

³ Mathematical and Physical Geodesy, Institute of Geodesy and Photogrammetry, ETH Zurich

The LSN2004 (Landesschwerenetz 2004) is the gravimetric reference network of Switzerland. It is based on the stations of the former network SG95 (Schweregrundnetz 1995), which was extended by some new absolute and relative stations. Around 10 absolute stations form the backbone of LSN2004. The absolute measurements are repeated in an interval of 10 years - usually with the FG5-X #209 owned by METAS. Only at the ECGN station in Zimmerwald the absolute measurements are repeated every year whenever possible. On all absolute stations the vertical gravity gradient is measured.

Since 1999, the Federal Institute of Metrology (METAS) owns the only absolute gravimeter in Switzerland. This FG5 free fall instrument was upgraded to a FG5-X in 2012. It participates regularly at the international key comparison campaigns of the metrology institutes. Besides of the measurements in Zimmerwald and in the laboratories of METAS, between 2015 and 2018 absolute measurements in Switzerland have been performed in Interlaken, Brig, Alpiglen and Zerne. The results of these measurements are all published in the AGRAV database of BGI and BKG and are freely accessible.

The absolute measurements 2015 in Interlaken and Alpiglen are part of the calibration line Interlaken – Jungfrauoch, which was re-measured with relative instruments in 2016 and in 2017. The calibration campaign of August 2017 could be performed with four Scintrex CG-5 (owned by swisstopo/ETHZ, University of Lausanne, University of Neuchâtel and the private company RBR/geo2x) and one ZLS Burris instrument (by the Bavarian Academy of Sciences).

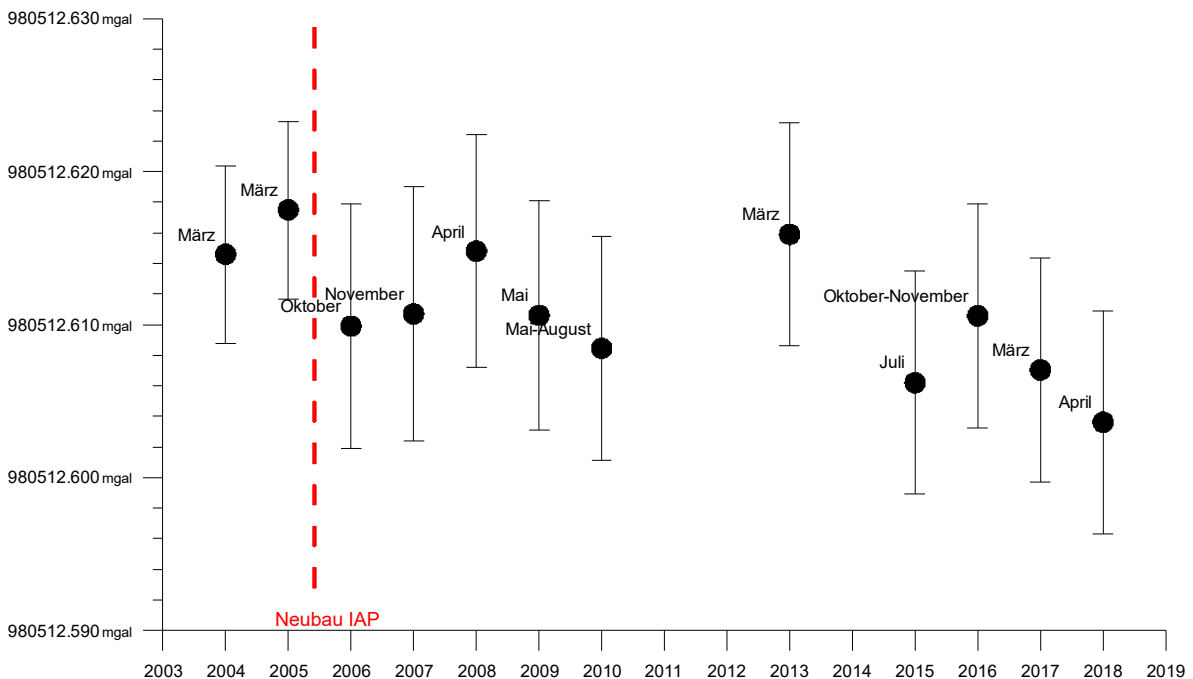


Figure 2. 1: Repeatability of absolute gravity measurements in Zimmerwald 2003-2018

The relative measurements for LSN2004 usually are performed with a Scintrex CG-5 owned jointly by swisstopo and ETH Zurich in order to improve the density, accuracy and stability of the network. The absolute gravity network (0 order network) is densified by relative measurements (1st and 2nd order network). These stations are usually identical to levelling or GNSS markers and are observed regularly since 2005. Per year, around 10 days of field measurements are carried out. Since 2015, a special effort is made to further densify this network by a 3rd order network, which is mainly formed by old reference stations from the 1950ies to 70ies which still exist. All absolute and relative observations since 1992 are treated in one common adjustment of around 400 points (as of end of 2018). The resulting accuracy is usually better than 0.008 mGal.

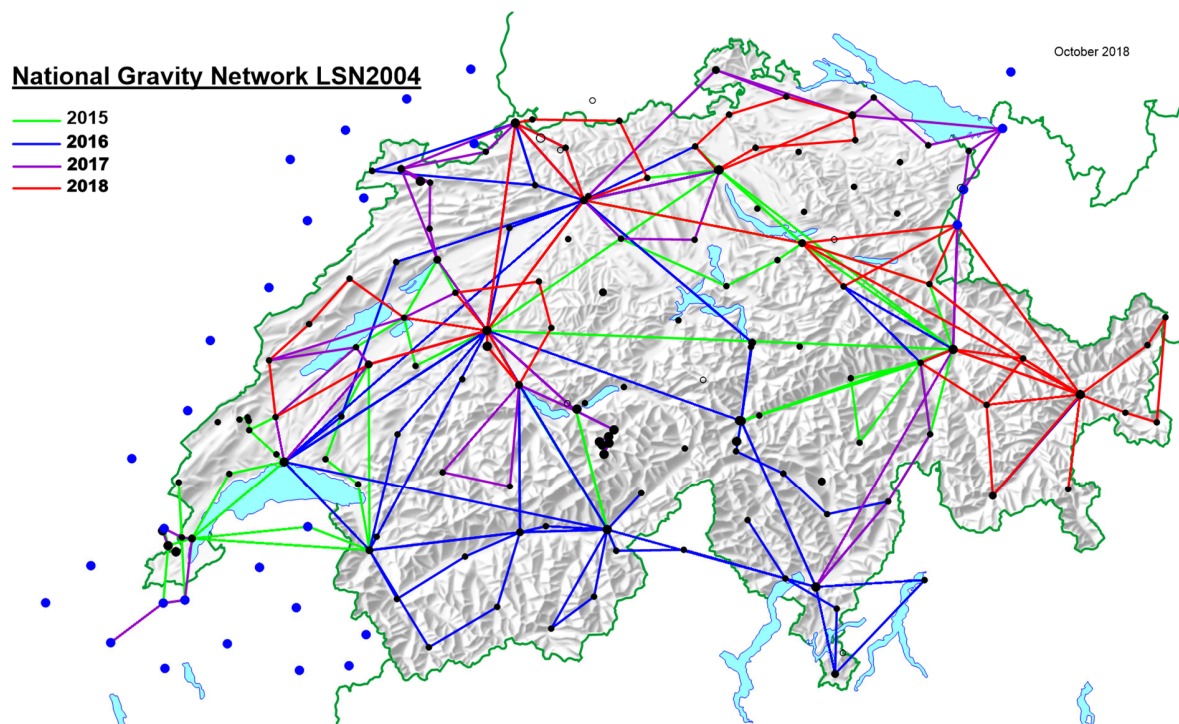


Figure 2. 2: Relative Measurements for LSN2004 (order 0-2) between 2015 and 2018

Gravity Measurements for the Vertical Network

U. Marti and A. Schlatter

Federal Office of Topography, swisstopo

The gravity measurements for the vertical network along the first and second order leveling lines are usually performed in the same year as the leveling measurements. They are used for the computation of geopotential numbers and orthometric heights and are only carried out on a representative selection of all existing leveling points. The criteria for the measurements since 1989 are the following: In flatter areas, a measurement is made every kilometer; in the mountains, the gravity difference between two neighboring points should not exceed 10 mGal (around 30 m height difference). For leveling benchmarks without measured gravity, the values are interpolated from the neighboring data on the line and from the gravity data set of the Swiss Geophysical Commission, as well as from mass models with an accuracy of better than 1 mGal, which is enough for the correction of the leveling data.

Until 2007, a Lacoste&Romberg type G gravimeter was used for these observations. Since 2011, a Scintrex CG-5 is used and more than 1400 points have been measured between 2011 and 2018. With the measurements of 2018, gravity data is now available on all the first and second order leveling lines of Switzerland. All these measurements are documented in the national database of the reference benchmarks (FPDS). It is foreseen to continue the measurements along the leveling lines in the future and to slowly replace the older measurements.

A specialty in 2017 was that it was possible to measure in the new railway tunnel of Monte Ceneri between Bellinzona and Lugano. The measurements have been performed roughly in 1 day on e-bikes. The distance between the points was 900 meters inside the tunnel and 300 meters near the portals. However, due to the still ongoing work at the epoch, it was not possible to get good results in every part of the tunnel. Another work to mention is the measurement of some third order (cantonal) lines in northern Switzerland in 2018. Their purpose is mainly for geodynamic investigations. It is not foreseen to make gravity measurements systematically on all third order lines.

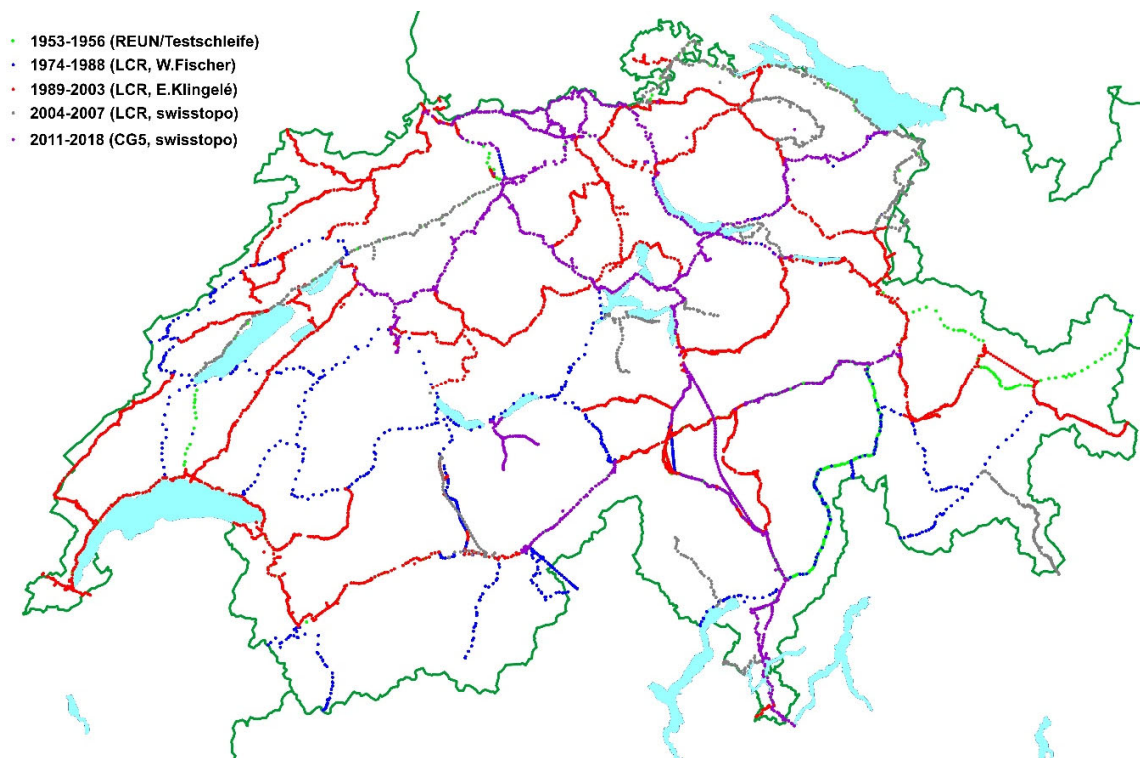


Figure 2. 3: Available gravity measurements along the Swiss leveling lines. Green dots: Measured 1953-1956 (Worden gravimeter); blue: measured 1974-1988 with a Lacoste&Romberg (LCR) gravimeter; red dots: measured 1989-2003 (LCR); grey: measured 2004-2007 (LCR); violet: measured 2011-2018 with Scintrex CG-5 gravimeter

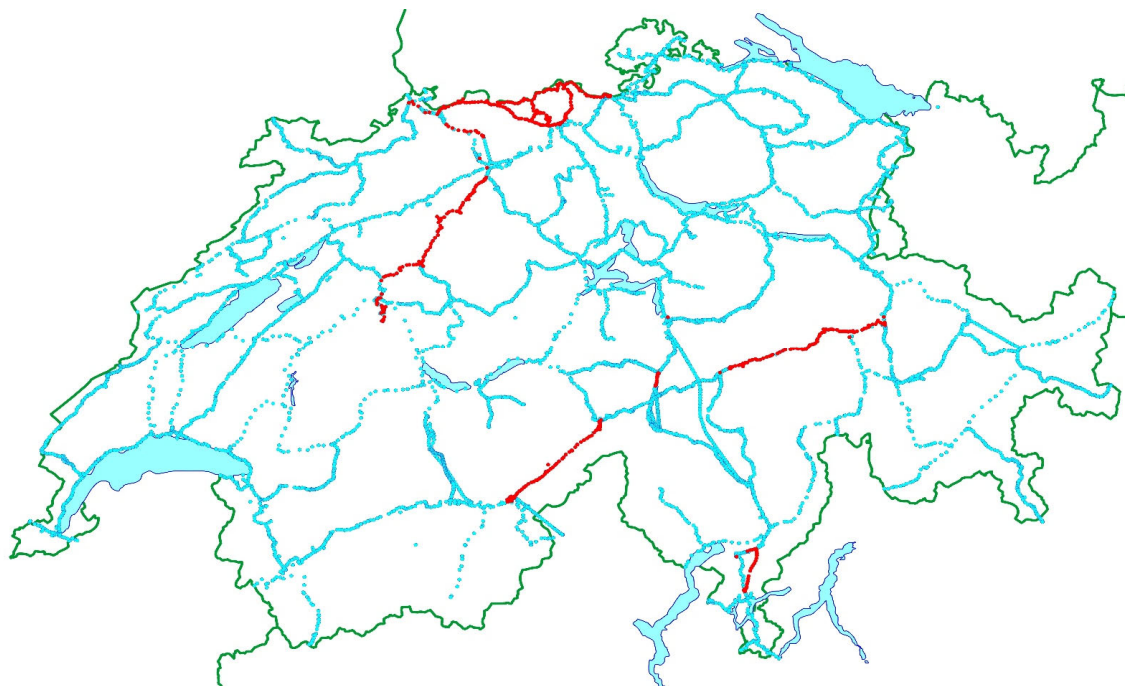


Figure 2. 4: Gravity measurements along the levelling lines 2015-2018 (red dots)

Geoid Determination

U. Marti

Federal Office of Topography, swisstopo

In 2016, a common project of swisstopo, BKG (Bundesamt für Kartografie und Geodäsie, Frankfurt/Leipzig) and BEV (Bundesamt für Eich- und Vermessungswesen, Vienna) was initiated, with the goal to compute a common geoid model for Switzerland, Germany and Austria (DACH-Geoid). The contract has been signed in October 2017 by the directors/presidents of the institutions mentioned above and the directors of the two further project partners LGL (Landesamt für Geoinformation und Landentwicklung; state of Baden-Württemberg) and LDBV (Landesamt für Digitalisierung, Breitband und Vermessung; state of Bavaria). Further technical partners include the technical universities of Munich and Graz.

First, all the necessary data sets have been prepared and exchanged between the project partners. This includes existing geoid and quasigeoid models, gravity data, deflections of the vertical and GNSS/leveling stations. As further information, a digital terrain model is necessary. It was decided to use EuroDEM as a common base for all computations, in order to avoid restrictions in data availability. Where available, also bathymetric data of lakes will be used.

In a first phase, the geoid should be calculated by all institutions in a test area. This area of about 300x200 km is located around Lake Constance. Except of the comparison of methodologies and software, this allows as well to check the data harmonization and investigations about the national height systems.

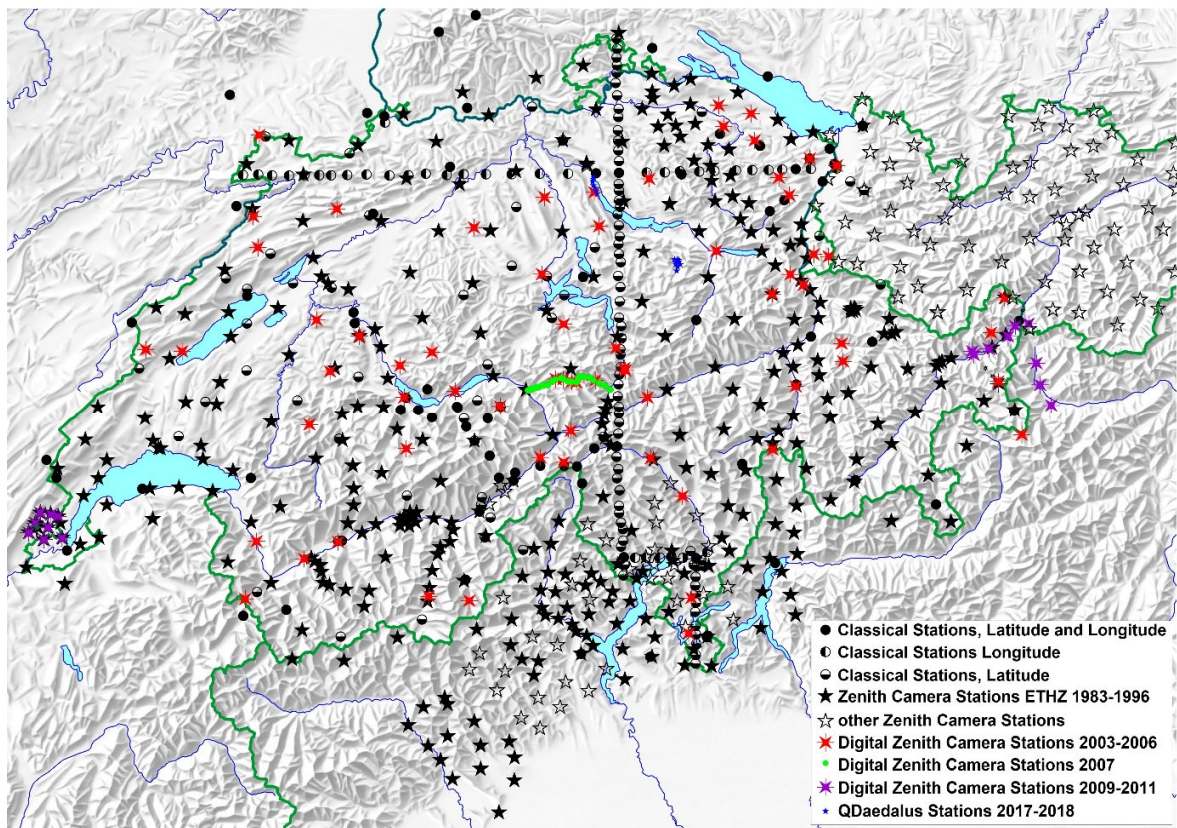


Figure 2. 5: Astro-geodetic data available in and around Switzerland

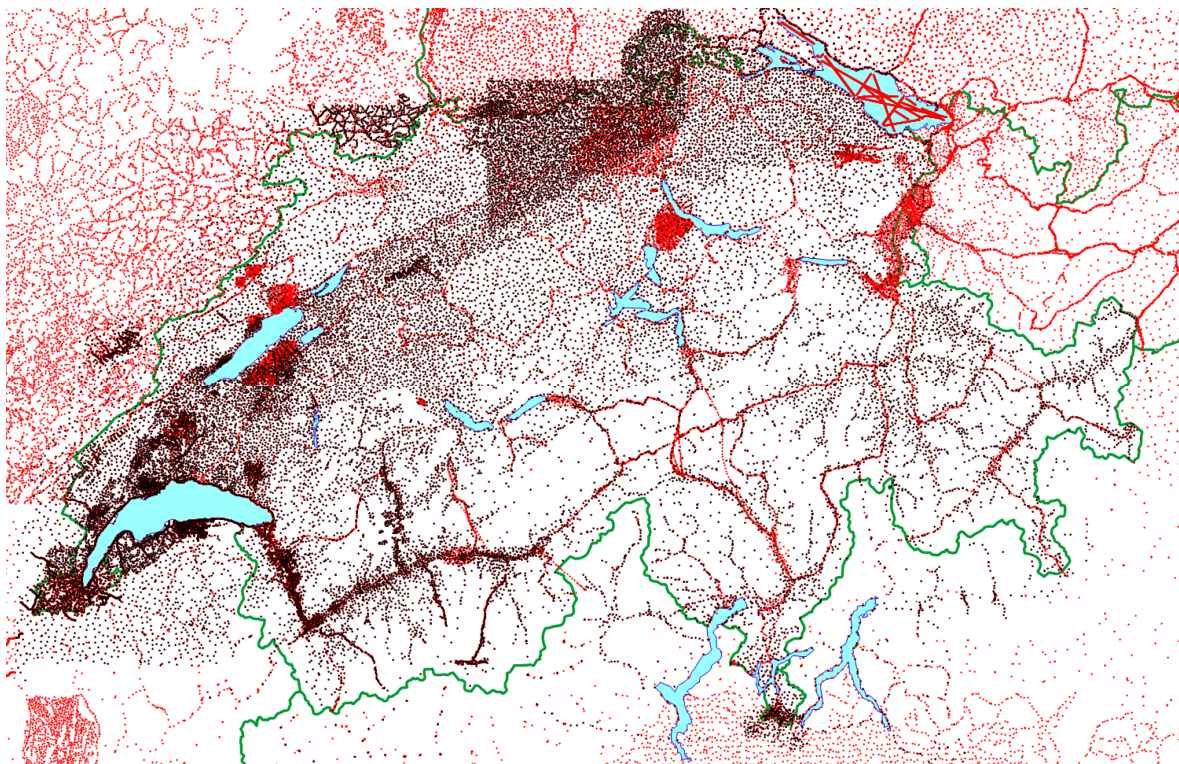


Figure 2. 6: available Gravity data in and around Switzerland. Black dots have been used for the gravimetric atlas of the Swiss Geophysical Commission



Figure 2. 7: GPS-Leveling stations of Switzerland

European Gravity Field Service for Improved Emergency Management (EGSIEM)

A. Jäggi¹, M. Weigel², F. Flechtner³, A. Güntner³, T. Mayer-Gürr⁴, S. Martinis⁵, S. Bruinsma⁶, J. Flury², S. Bourgogne⁷

¹ Universität Bern

² Gottfried Wilhelm Leibniz Universität Hannover

³ Helmholtz-Zentrum Potsdam Deutsches GeoForschungsZentrum

⁴ Technische Universität Graz

⁵ Deutsches Zentrum für Luft- und Raumfahrt e.V.

⁶ Centre National d'Études Spatiales

⁷ Géode & Cie

Earth observation satellites yield a wealth of data for scientific, operational and commercial exploitation. However, the redistribution of environmental mass is not yet part of the standard Earth observation data products. Monthly estimates of the global mass distribution, derived between 2002 and 2017 from the Gravity Recovery and Climate Experiment (GRACE) and from 2018 onwards by GRACE-FO (Follow-on), deliver fundamental insights into the global water cycle. Changes in continental water storage control the regional water budget and can, in extreme cases, result in floods and droughts that often claim a high toll on infrastructure, economy and human lives. The aim of the European Gravity Service for Improved Emergency Management (EGSIEM) was to provide consolidated mass redistribution products and to demonstrate that gravity products open the door for innovative approaches to flood and drought monitoring and forecast.

The timeliness and reliability of information is the primary concern for any early-warning system. EGSIEM increased the temporal resolution from one month, typical for GRACE products, to one day and provided gravity field information within 5 days (near real-time). Early warning indicators derived from these products were demonstrated to have the potential to improve the timely awareness of potentially evolving hydrological extremes and may help in the scheduling of high-resolution follow-up observations as performed at centers like the Center for Satellite Based Crisis Information (ZKI, operated by the German Aerospace Center). EGSIEM unified the combined knowledge of the entire European GRACE community and established a total of three prototype services: 1) a scientific combination service, 2) a near real-time service and 3) a hydrological/early warning service (see Figure 2. 8).

Starting in January 2015 EGSIEM has received funding from the European Commission (EC) for three years until the end of 2017. EGSIEM unified the knowledge of the entire European GRACE community to pave the way for a long awaited standardisation of gravity-derived products. Combining the results obtained from different analysis centers of the EGSIEM consortium, each of which performing independent analysis methods but employing consistent processing standards, has significantly increased the quality, robustness and reliability of these data. The successful work of the scientific combination service is continued after the EC-funded prototype phase as the International Combination Service for Time-variable Gravity Field Solutions (COST-G) under the umbrella of the International Association of Geodesy (IAG). Specifically COST-G is the Product Center for time-variable gravity fields of IAG's International Gravity Field Service (IGFS). The near real-time and hydrological services will be continued on a best effort basis as soon as GRACE-FO data will become publicly available.

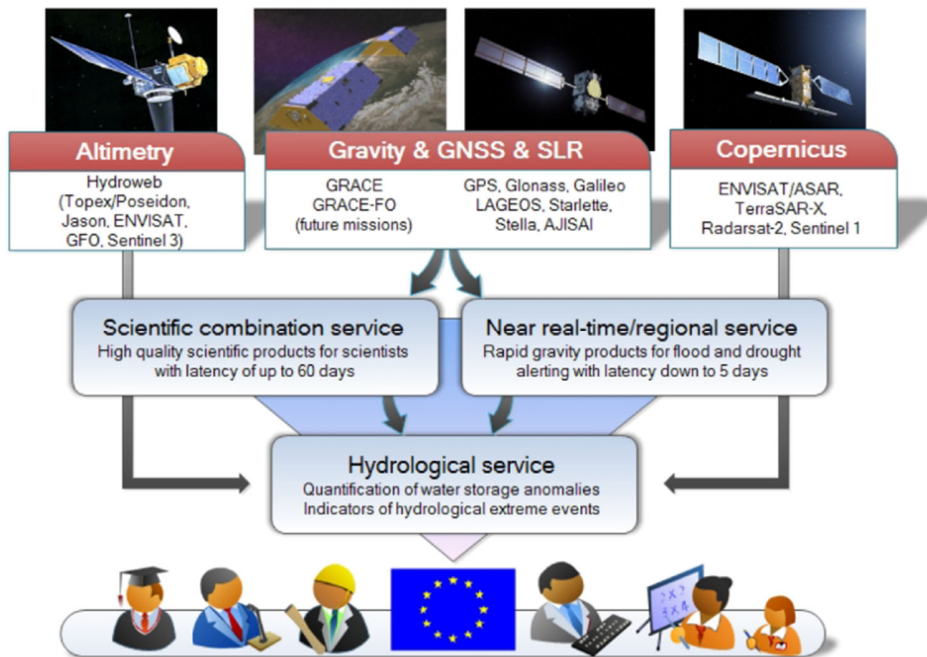


Figure 2. 8: General concept of the EGSiEM: Satellite data from Altimetry, Gravity, GNSS, SLR and Copernicus missions were used to create three services.

Acknowledgments:

EGSiEM was supported by the European Union's Horizon 2020 research and innovation program under the grant agreement No. 637010 and the Swiss State Secretariat for Education, Research and Innovation. All views expressed are those of the authors and not of the Agency.

Combination Service for Time-Variable Gravity Fields (COST-G)

U. Meyer, B. Jenny, Y. Jean, A. Jäggi

Astronomical Institute, University of Bern

Within the frame of the Horizon 2020 project European Gravity Service for Improved Emergency Management (EGSIEM; Jäggi et al, 2019) a prototype service for the combination of monthly GRACE gravity fields was developed (Meyer et al, 2018a). This service is continued as COST-G (Jäggi et al, 2018a; Meyer et al, 2018b), a product center of the International Gravity Field Service (IGFS) under the umbrella of the International Association of Geodesy (IAG).

The main goal of COST-G, as defined by the Terms of Reference, is to realize the long-awaited standardization of gravity-derived mass transport products and to improve their quality, robustness, and reliability by combining solutions from individual analysis centers (ACs). The ACs adopt different analysis methods but apply agreed-upon consistent processing standards to deliver time-variable gravity field models, e.g., from GRACE/GRACE-FO low-low satellite-to-satellite tracking (ll-SST), high-low satellite-to-satellite tracking (hl-SST), and Satellite Laser Ranging (SLR).

The final COST-G combination will be performed on the normal equation level (Meyer et al, 2019). Unless normal equations of all associated ACs become available, quality control of the most recent time-series and combinations on the solution level are performed (Jäggi et al, 2018b). The individual monthly models are combined by Variance Component Estimation (VCE) on the solution level (Jean et al, 2018). The VCE-derived relative weights are a quality indicator based on the noise levels of the individual solutions (Figure 2. 9).

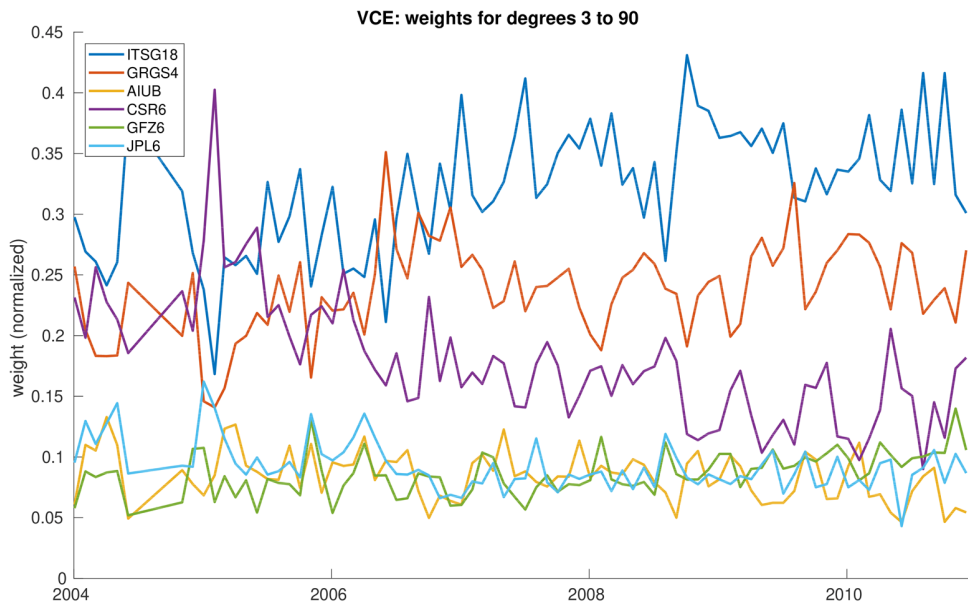


Figure 2. 9: VCE derived weights of the three GRACE-SDS RL06 gravity fields and the most recent alternative time-series ITSG2018, GRGS-RL04 and AIUB-RL02.

The combined gravity fields are validated in terms of their signal content and by their noise levels, assessed by so-called anomalies in regions where little short-term variability is expected, e.g., over the oceans (Figure 2. 10). The anomalies are defined as the differences to a deterministic signal model, derived from monthly means of all available time-series. In Figure 2. 10 the COST-G combination outperforms all individual time-series in terms of noise, with the exception of GRGS-RL04 that is regularized by a truncated Eigenvalue decomposition. In the final combination on the normal equation level this type of regularization will be avoided.

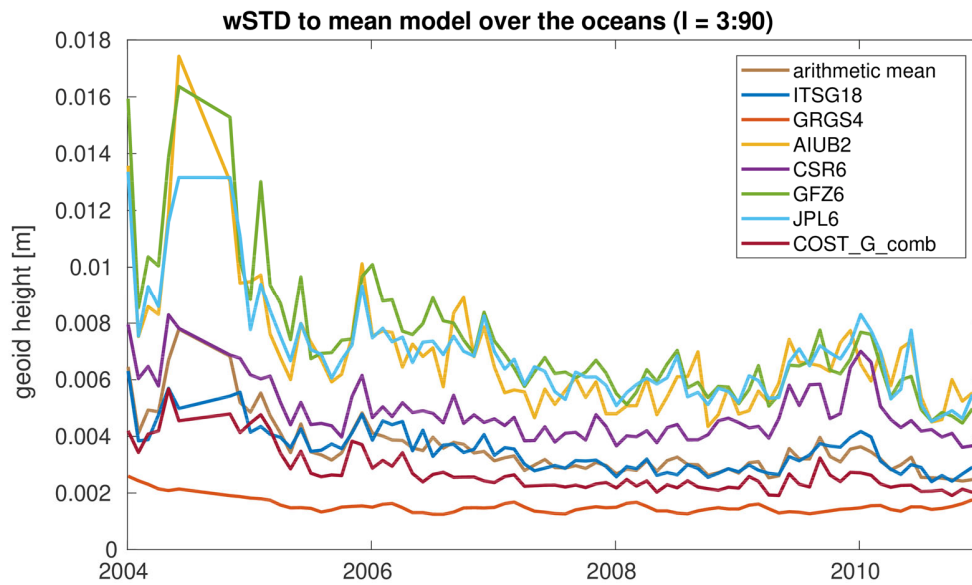


Figure 2. 10: Noise assessment of the individual and combined time-series in terms of the RMS of anomalies over the oceans.

Figure 2. 11 provides a spatial assessment of the noise levels of an individual time-series (GFZ-RL06 is chosen as an example) and the COST-G combination on the solution level. While on the continents non-seasonal signal that is not captured by the signal model is visible, the ocean areas are dominated by noise (with the exception of the Zapiola gyre near the coast of South America). The noise reduction by the combination is clearly visible, while the signal amplitudes over the continents are preserved.

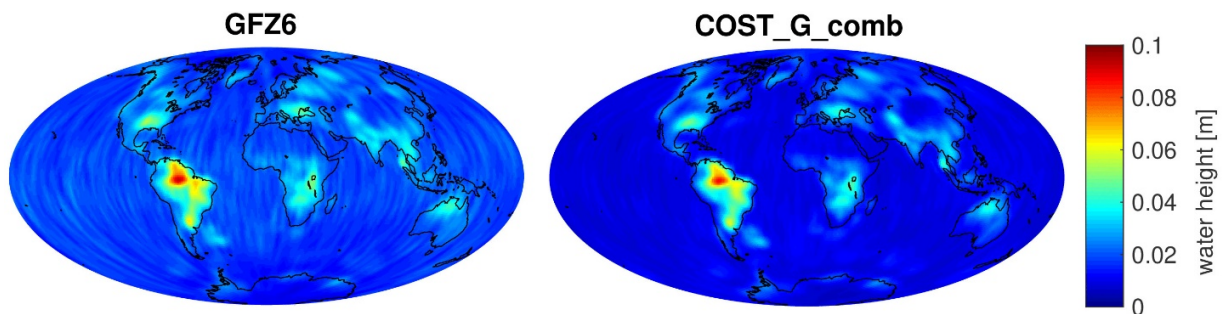


Figure 2. 11: RMS of monthly anomalies 2004-2010 per grid cell of 1° global grids; left: GFZ-RL06 time-series; right: COST-G combination on the solution level.

Combination of monthly Swarm gravity field solutions

U. Meyer¹, D. Arnold¹, L. Schreiter¹, C. Dahle², A. Jäggi¹

¹ Astronomical Institute, University of Bern

² GeoForschungsZentrum Potsdam

AIUB participates in the Swarm Data, Innovation, and Science Cluster (DISC), an international consortium to enhance the scientific return of the Swarm satellite mission. The tasks of AIUB include the determination of kinematic orbits of the three Swarm satellites, the estimation of monthly gravity field models from the GPS high-low tracking data (Jäggi et al, 2015, 2016), and the combination of the gravity field solutions of the Swarm DISC Analysis Centers (ACs) to finally provide optimally combined monthly gravity fields (Arnold et al, 2017; Jäggi et al, 2018).

The combination follows the procedures developed in the frame of the EGSIM project (Jäggi et al, 2019). All ACs provide unconstrained monthly gravity field solutions (Teixeira da Encarnação et al, 2016) in the gfc-format of the International Centre for Global Earth Models (ICGEM) and corresponding normal equations in the SINEX format¹ maintained by the International Earth Rotation and Reference Systems Service (IERS).

The steps necessary for the combination include:

1. the derivation of relative weights by Variance Component Estimation (VCE) on the solution level that are representative for the individual noise levels of the monthly gravity field contributions of the different ACs,
2. the determination of empirical factors to balance the impact of the individual ACs normal equations on pairwise combinations, and
3. the weighted combination on either solution or normal equation level.

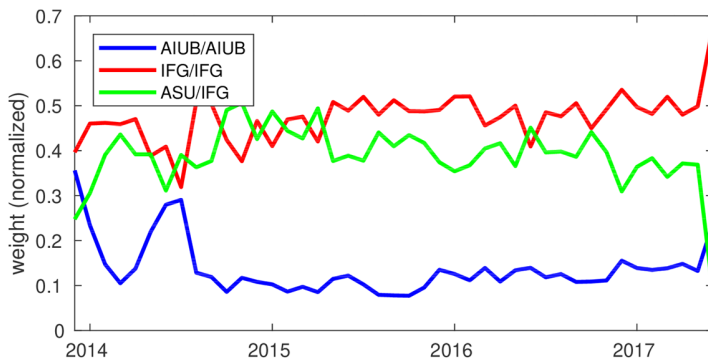


Figure 2. 12: VCE-derived relative weights in the case, where only three time-series were available, two of which were based on IFG kinematic orbits, one on AIUB kinematic orbits.

At the end of the project phase of the Swarm DISC project, only three different time-series of monthly gravity fields were available, because the first release of the School of Earth Science of the Ohio State University (OSU) was affected by regularization (Teixeira da Encarnação et al, 2018a,b). Moreover, only two of four ACs, namely AIUB and the Institute of Geodesy of the Graz University of Technology (IFG), provide kinematic orbits of the SWARM satellites.

Consequently, only three time-series, based on two sets of kinematic orbits, could be considered in the combination and the VCE-derived weights were biased (Figure 2. 12) towards the kinematic orbits used by IFG and by the Astronomical Institute of the Czech Academy of Sciences (ASU).

This situation changed during the extended project phase and by the end of the project a combination of all four ACs' time-series, two of which were based on the AIUB kinematic orbits, the other two on the IFG kinematic orbits, could

¹ <https://www.iers.org/IERS/EN/Organization/AnalysisCoordinator/SinexFormat/sinex.html>

be presented. The VCE-derive relative weights (Figure 2. 13) now testify the high quality of the AIUB contribution, especially during time periods with high ionosphere activity and non-optimal receiver settings (Dahle et al, 2017).

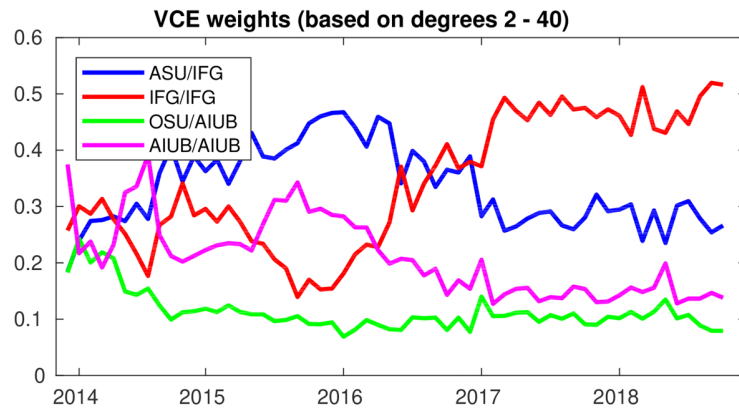


Figure 2. 13: VCE-derived weights of the final time-series, based on coefficients up to degree/order 40.

The SWARM gravity fields provide information, e.g., on ice mass variations in polar regions. This information is of special interest during the gap between the dedicated GRACE and GRACE-FO satellite missions. The monthly mass variations over Greenland (Figure 2. 14) nicely show the consistency in trend and phase between GRACE and SWARM results (both truncated at degree/order 6, C20 removed). At the corresponding spherical harmonic resolution SWARM slightly over-estimates the seasonal mass variation compared to GRACE (under investigation) and exhibits a significantly larger scatter. Compared to the individual AIUB time-series the scatter of the combined SWARM time-series is slightly reduced.

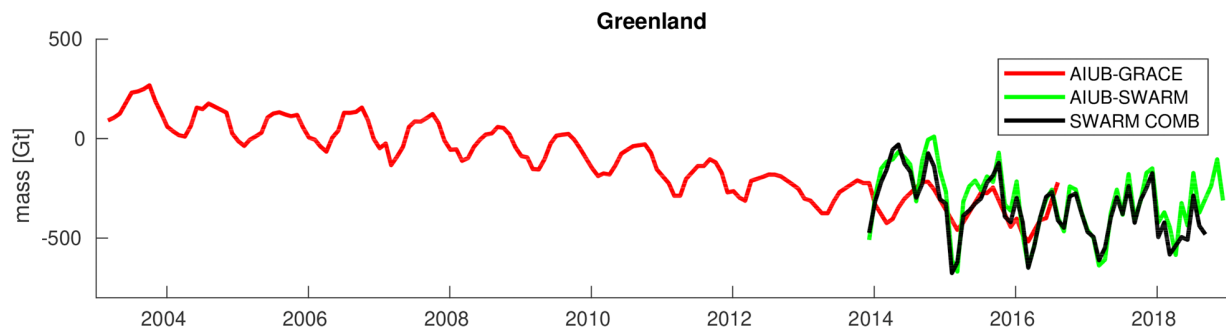


Figure 2. 14: Ice mass change in Greenland as observed by GRACE (red) or the SWARM satellites (green). By combination of different ACs the scatter is reduced (black).

Mitigating artifacts in Swarm GPS data for improved reconstruction of the topside ionosphere and plasmasphere

L. Schreiter, D. Arnold, A. Jäggi

Astronomical Institute, University of Bern

ESA's Swarm mission consists of three identical low earth orbit (LEO) satellites (usually identified as A, B, and C) to study the Earth magnetic field. The Swarm precise orbit determination (POD) GPS receiver is known to be affected by fast changing slant total electron content (TEC). This became clear during Swarm GPS only gravity field studies, where systematic biases, in the orbit, as well as in the derived gravity field solutions, could be observed near the geomagnetic equator. These biases are not caused by the so called higher order ionospheric terms in GPS positioning, but most likely by corrupted GPS data. To account for these corrupted data, weighting and screening methods have been developed to mitigate their impact on orbit and gravity field level.

The Swarm GPS receiver may not exclusively be used for orbit and gravity studies, but also for ionospheric studies. The dual frequency GPS receiver allows to perform slant TEC measurements and the high velocity of a LEO satellite is highly beneficial to obtain a good spatial sampling in a short period of time. Also having up to eight GPS satellite links available at a 1 Hz sampling gives rise to the idea to use Swarm for ionospheric tomography. Swarm is located in a near polar orbit at 445 km (the lower pair: Swarm A and Swarm C) and 510 km (Swarm B) initial altitude, so most of the topside ionosphere and plasmasphere is contained between Swarm altitude and GPS altitude.

Our approach is straightforward. We divide our research area in grid cells, compute the length of the line of sight in each grid cell as weight, and assume the electron density in each grid cell as a constant. All lines of sight are mapped into the plane vertically above the flight path of the Swarm satellite. Because we assume a higher variability in the lower regions the height of the grid cells is exponentially rising with altitude. The size of the grid cells in latitudinal direction is 0.5 degree. Constraints have to be applied, such that neighboring grid cells do not differ too much in electron density. In our case we use a Tikhonov regularization with a condition, that may be described, such that the weighted mean of the neighboring grid cells should be close to the electron density in the specific grid cell. Boundary conditions are given by the in situ plasma density measurements from the Swarm Langmuir probes. The Langmuir probes are known to underestimate the electron density and correction factors are applied (see Lomidze et. al., 2018). We use a single equatorial pass, which takes about 25 min., as basis for the reconstruction.

Tomography is usually an ill-posed problem. This motivates the regularization. It also should be mentioned, that the geometry of the line of sight is weak, because in high altitudes they tend to become close to parallel, see Figure 2. 15. Even if regularization is applied, it might happen, that data affected by receiver artifacts has an impact on the reconstruction. For this purpose we have focused on Swarm GPS data known to be affected by large ionospheric disturbances. Strategies to downweight such data in the POD have been developed (see Schreiter et al., 2019). We have employed the downweighting strategy based on the second time derivative of the geometry-free linear combination of phase observations on both GPS frequencies.

Our results show that GPS data problematic for orbit and gravity field determination are also problematic for the reconstruction of the ionosphere and plasmasphere. In Figure 2. 16 residuals from the ionosphere-free linear combination of the phase measurements as obtained from a kinematic positioning of the Swarm-A satellite are shown. The residuals of a satellite heavily affected by receiver artifacts (GPS satellite PRN 27) are highlighted in red. In Figure 2. 17 the result of the reconstruction is shown. The figures show the topside electron density reconstructed with (left) or without (right) applying GPS data downweighting. Figure 2. 18 shows the differences of the electron densities, as well as the line of sight to G27 at the epoch, where the ionosphere-free phase residuals reached maximum. This clearly shows the impact of G27 on the electron density reconstruction.

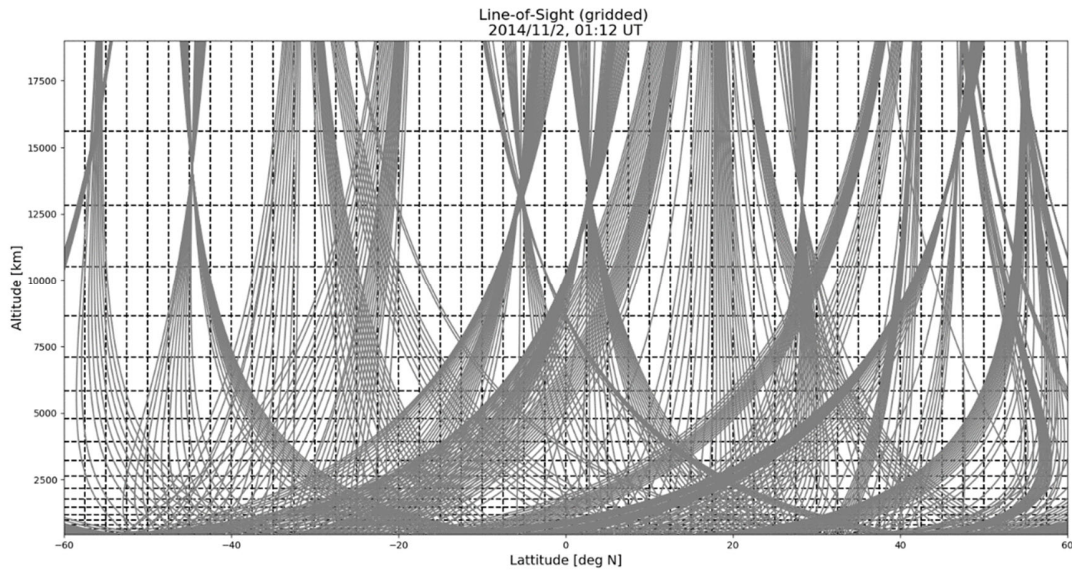


Figure 2. 15: Ray geometry for an equatorial pass with grid cells

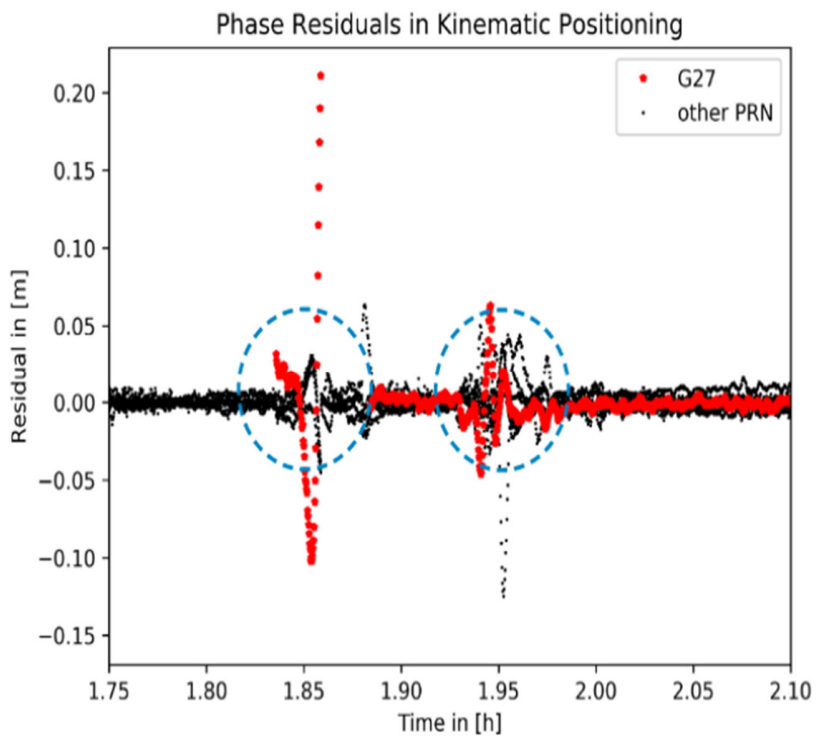


Figure 2. 16: Residuals from the ionosphere-free linear combination of the phase measurements as obtained from a kinematic positioning of the Swarm-A satellite for 2014, doy 305. The disturbed epochs are marked with the circles. G27, showing the largest phase residuals, is shown in red.

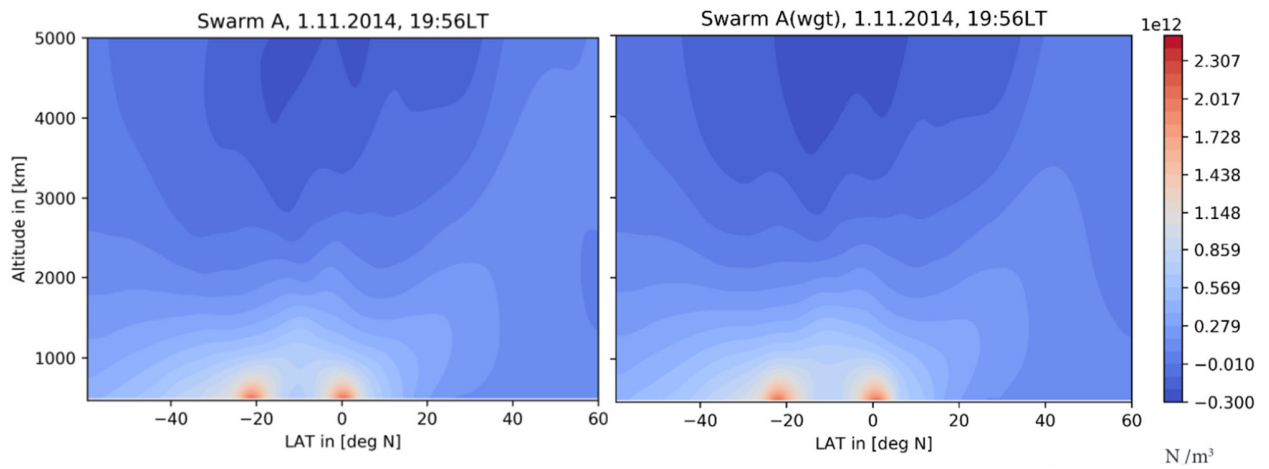


Figure 2. 17: Reconstructions of the topside electron density with (left) and without (right) GPS data downweighting

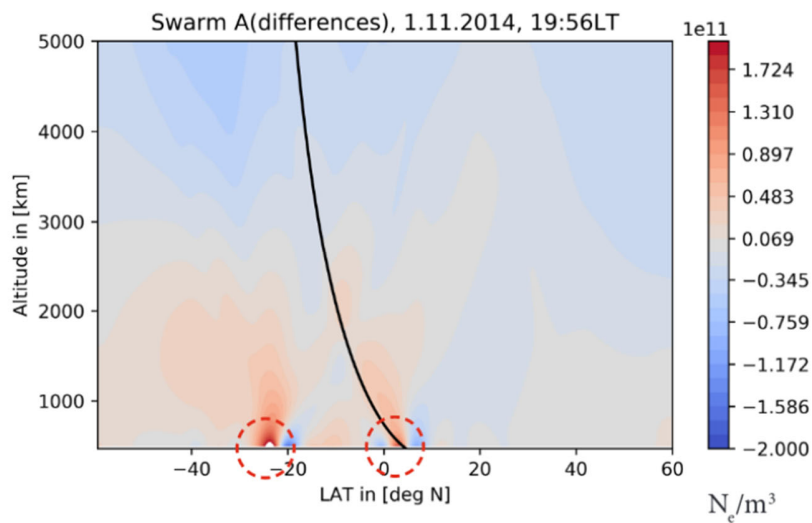


Figure 2. 18: Differences of the reconstructions shown in Figure 2. 17. The circles mark the disturbed epochs from Figure 2. 16, the black line corresponds to the line of sight of G27 at the epoch, where the ionosphere-free phase residuals reached maximum.

Lunar gravity field solutions computed at AIUB

S. Bertone, D. Arnold, V. Girardin, A. Jäggi

Astronomical Institute, University of Bern

The NASA mission GRAIL (Gravity Recovery And Interior Laboratory Zuber et al., 2013) inherits its concept from the GRACE (Gravity Recovery And Climate Experiment) mission to determine the gravity field of the Moon. The Ka-Band Range Rate (KBRR) inter-satellite data allows for a highly accurate estimation of the lunar gravity field on both sides of the Moon (Asmar et al., 2013), which is crucial to improve the understanding of its internal structure and thermal evolution.

In this report we discuss our latest GRAIL-based lunar gravity fields generated with the Celestial Mechanics Approach (Beutler, 2010; Arnold, 2015) using the Bernese GNSS Software (BSW, Dach et al., 2015). We provide independent solutions based on a combination of all available datasets, i.e., one- and two-way Doppler and KBRR data, iterated from both the pre-GRAIL SGM150J (Matsumoto et al, 2010) and the GRAIL GRGM900C (Lemoine et al, 2014) gravity field.

Orbit: data, modeling and parametrization

Based on one-way X-band and two-way S-band Doppler data, we perform orbit determination by solving six initial orbital elements, dynamical parameters, and stochastic parameters in daily arcs using a least-squares adjustment. We also implemented an accurate modeling of non-gravitational forces, including accelerations due to solar and planetary (albedo and IR) radiation pressure (Floberghagen et al., 1999), based on the 28-plate macromodel developed by Fahnestock et al. (2012) to represent the GRAIL satellites. Empirical and pseudo-stochastic parameters are estimated on top of our dynamical modeling to absorb its deficiencies. We analyze the impact of different parametrizations using either pulses (i.e., instantaneous velocity changes) or piecewise-constant accelerations (PCA) on our orbits.

Root Mean Square (RMS) values of KBRR residuals are shown in Figure 2. 19 over the lunar surface. They are based on a weighted combination of two-way Doppler and KBRR data, GRGM900C background field and a modeling of non-gravitational forces (solar and lunar radiation pressure) acting on GRAIL satellites. Residuals on most areas are close to the nominal KBRR accuracy of $0.03 \mu\text{m/s}$, while correlations with topography, and hence residual signal to improve the gravity solution, are still visible. On the other hand, the systematic signal at mid-latitudes was already identified by Lemoine et al. (2014) as due to an inaccurate evaluation of light/shadow transitions when using a simple cone-model. We later applied a more accurate definition of light-shadow transitions using time-series of the electrical current measured by the on-board solar panels.

Based on these improved orbits, one- and two-way Doppler and KBRR data are then used together with an appropriate weighting for a combined orbit and gravity field determination process.

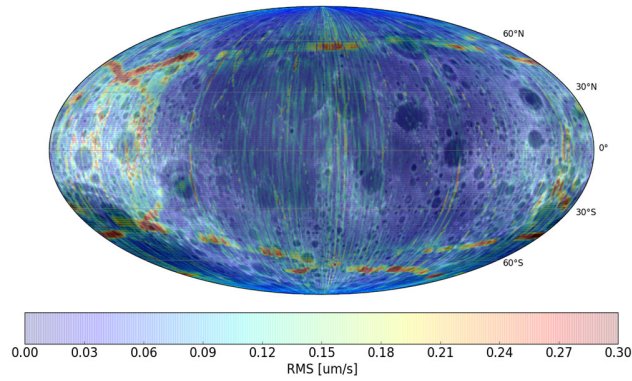


Figure 2. 19: Root Mean Square (RMS) values of KBRR residuals using a weighted combination of two-way Doppler and KBRR data.

Gravity field and tidal coefficients solutions

We present our latest independent solutions of the lunar gravity field, where KBRR data and Doppler one-way and two-way observations from the primary mission phase (PM, March-May 2012) are used. We combine all data types on Normal Equations (NEQ) level, using an appropriate weighting based on their relative accuracy.

First, we show gravity solutions based on the recent GRAIL GRGM900C gravity field, in order to validate our modeling and parametrization and show the potential quality of the fields resulting from our approach.

Figure 2. 20 shows the difference degree amplitudes of our degree and order (d/o) 350 solution w.r.t. its a priori field GRGM900C compared to the GL420 solution developed by the same group (Zuber et al., 2013). The three solutions are quite close at lower degrees and only start differing around degree 70, where features due to the parametrization, as already seen in Arnold et al. (2015), show up. Also, in Figure 2. 21 we show how combining one- and two-way Doppler data (here, a 1:10 weighting is applied in favor of two-way) can lead to improvements in the gravity field solution.

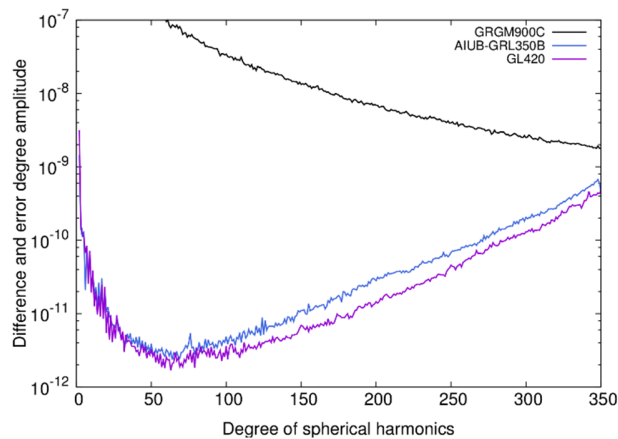


Figure 2. 20: A solution based on GRGM900C up to d/o 600

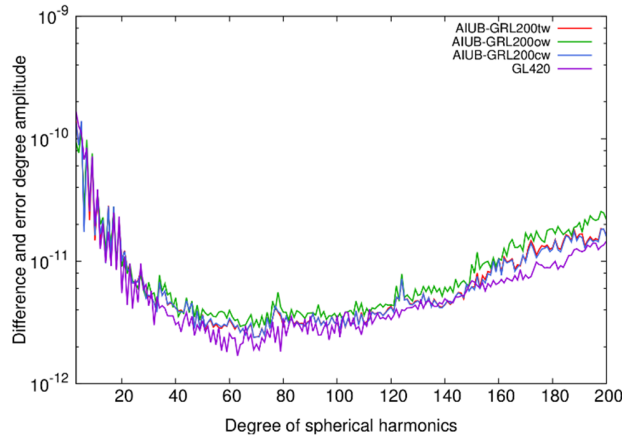


Figure 2. 21: Combined one- and two-way Doppler- and KBRR-based solutions (a priori GRGM900C up to d/o 600, 0.1:1:10⁸ relative weighting)

After validating our procedures, we proceed to our independent gravity field solution based on an iterative procedure starting from the SGM150J gravity field. Figure 2. 22 sketches our procedure to gradually enlarge the parameter space while adding new data to our gravity field solution. As an example, the first iteration shown in Figure 2. 22 (red line), is only based on data from the month of April 2012, when the GRAIL probes were flying on a higher orbit with very low eccentricity, as the rather low resolution SGM150J field could not sustain orbits of an appropriate quality at lower altitudes. Adding the whole PM data then allows for improved solutions, while the increasing quality of orbits and fields allows for an increased weighting of the highly accurate KBRR data. Beside difference degree amplitudes, we use both correlations with topography and post-fit KBRR residuals as quality measures of our iterated gravity field solutions.

It is worth noticing that these solutions require an extensive computational and storage load, which is achievable thanks to the parallel processing pipeline (based on Intel BLAS/MKL) implemented within the BSW and with the computational power available on the UBELIX cluster at the University of Bern.

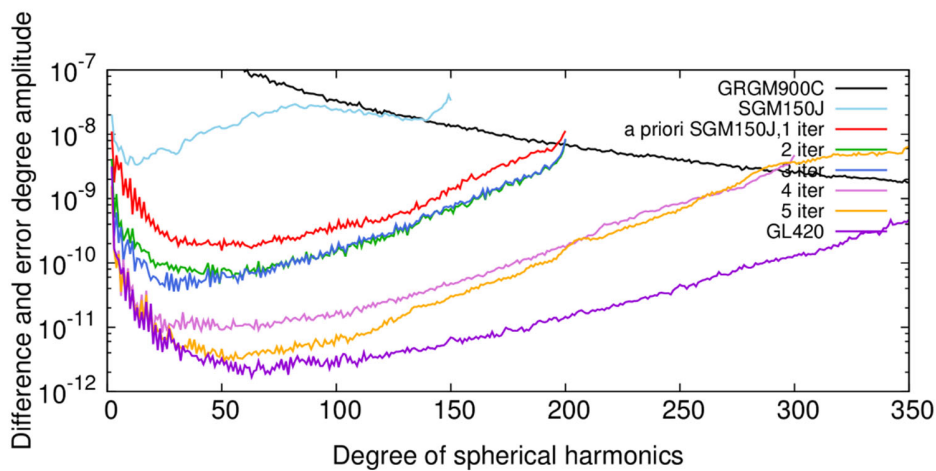


Figure 2. 22: Difference degree amplitudes w.r.t. GRGM900C of solutions iterated from SGM150J with progressively enlarged parameter space

AIUB-RL02: an improved time-series of monthly gravity fields from GRACE data

U. Meyer, A. Jäggi

Astronomical Institute, University of Bern

Gravity field determination at AIUB is treated as an extended orbit determination problem. The unknown coefficients of the gravity field are co-estimated with orbit and instrument parameters. Deficiencies in the force model are absorbed by constrained pseudo-stochastic accelerations at 15 minute intervals. A first AIUB time-series of monthly GRACE gravity fields was presented by Meyer et al. (2012).

With the availability of re-processed GRACE Level-1B data (Release 02), a re-processing of the time-series of monthly gravity field models became necessary. This opportunity was taken to also update the background force model, i.e., switch to the more recent atmosphere and ocean de-aliasing products AOD1B-RL05 (Flechtner and Dobsław, 2013) and the ocean tide model EOT11a (Savcenko and Bosch, 2011), to include shallow tides (admittances) in the tide-modelling, and to revisit the accelerometer parametrization (Meyer et al, 2015). The latter had become necessary due to a distinctive sensitivity to temperature variations of the accelerometer, aggravated by the reduction of the temperature stabilization onboard of the GRACE satellites in 2011 that became necessary due to battery failures.

The accelerometer artifacts could be absorbed, at least partially, by daily scale factors in all three axis of the co-rotating orbital frame. The reduction of the noise level achieved by the re-processing enabled the extension of the spherical harmonic resolution of the monthly gravity fields beyond degree 60 and order 45 to better exploit the sensitivity of the monthly gravity fields to temporal variations, as indicated by significance tests of secular and annual variations (Figure 2. 23). Two time-series were released: AIUB-RL02 (60) up to degree/order 60 of the spherical harmonic expansion, and AIUB-RL02 (90) up to degree/order 90. Both time-series originate from independent solutions with different parameter spaces (Meyer et al, 2016).

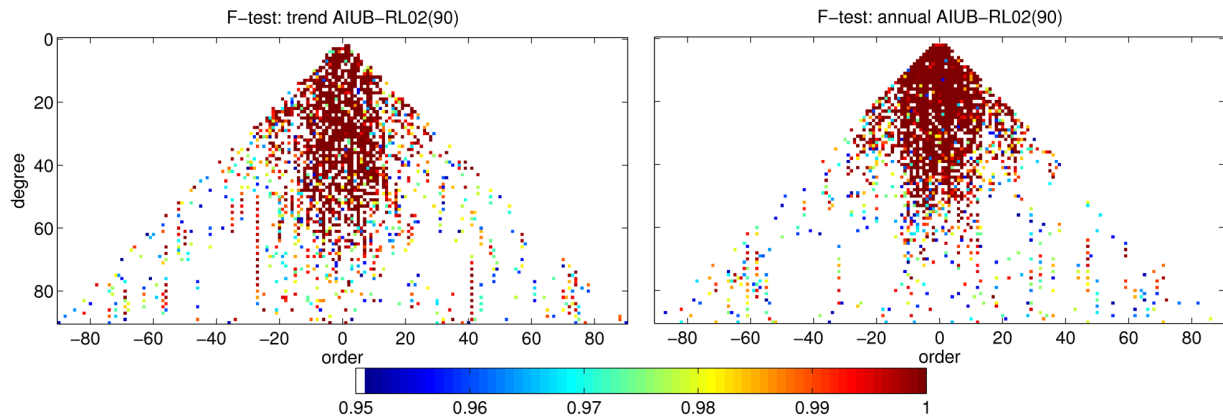


Figure 2. 23: Cumulative distribution function indicating significance of secular (left) or annual (right) variations per spherical harmonic coefficient of the monthly gravity fields.

The time-series of monthly gravity fields enables the study of mass transport processes in the system Earth, related mainly to the hydrological cycle or to ice melt caused by climate change, and to geophysical phenomena like glacial isostatic adjustment (GIA) or Earth quakes that cause mass re-distribution in the crust. Secular mass variations as derived from the AIUB-RL02 (60) time-series are shown in Figure 2. 24. To avoid signal attenuation no smoothing was applied and therefore the GRACE-typical noisy stripes in North-South direction are visible. Major mass loss is indicated at the coast of Greenland, the Bay of Alaska, the West Coast of Antarctica and the ice fields of Patagonia, but also, due to groundwater irrigation, in Central India. The large Sumatra earthquake in December 2004 is also visible as an apparent mass trend.

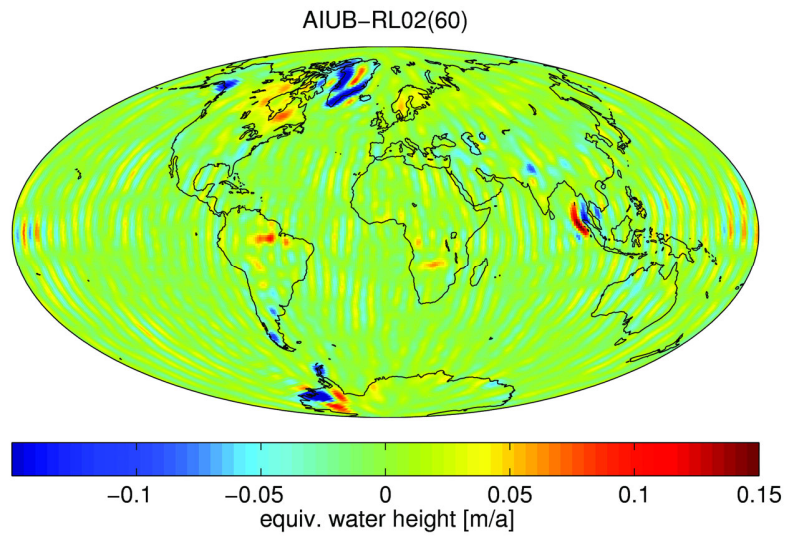


Figure 2. 24: Annual mass trends in equivalent water height as derived from the monthly AIUB-RL02 (60) gravity fields 2003-2014 without smoothing.

Figure 2. 25 provides a zoom on the polar regions where most of the climate relevant ice melt is happening. As opposed to radar altimetry, GRACE mass estimates are independent from assumptions on ice density, but suffer from a reduced spatial resolution and signal attenuation due to leakage. To eventually derive ice mass change a GIA model has to be applied (Meyer et al, 2017).

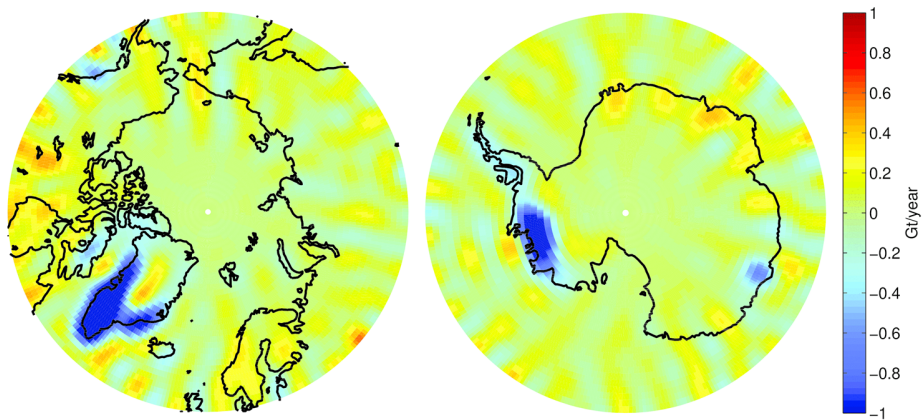


Figure 2. 25 Annual mass change in polar regions (left: Arctic, right: Antarctic) per 1° grid cell for the time period 2010-2014 as derived from unsmoothed AIUB-RL02 (60).

Low-degree time-variable gravity fields from satellite laser ranging

U. Meyer, A. Grahl, R. Dach, A. Jäggi

Astronomical Institute, University of Bern

At AIUB the orbits of the classical satellite laser ranging (SLR) cannonball satellites are determined either routinely (Otsubo et al, 2019), as is the case for the two LAGEOS and ETALON satellites, or at least regularly on a best effort basis. The latter is true for the geodetic satellites in low Earth orbits, the so-called SLR-LEOs: Starlette, Stella, Larets, LARES, AJISAI and the old Earth observation satellite Beacon-C. For the SLR satellites LAGEOS and ETALON orbiting the Earth at high altitudes 7- or 10-day arcs are determined, while the SLR-LEOs are processed in daily arcs and stacked to 10-day batches. The geometric or geophysical parameters estimated in the frame of a generalized orbit determination process of the SLR satellites are coordinates of the SLR stations, range biases for selected stations, Earth orientation parameters, geocenter coordinates, and the low degree spherical harmonic coefficients of the Earth's gravity field (Grahl et al, 2017).

The SLR satellites are sensitive to the mass distribution and to large scale mass variations in the system Earth (Meyer et al, 2015; Sošnica et al, 2015). They therefore can be used to derive, e.g., ice mass loss in polar regions (Meyer et al, 2018). Due to the sparse observation coverage, depending on the inhomogeneous spatial distribution of the SLR tracking station network, monthly SLR gravity field solutions can only be determined from a combined processing of SLR satellites orbiting the Earth at different inclinations. The spatial distribution of mass change in polar regions as determined for 5-year time periods from SLR observations is shown in Figure 2. 26. Clearly visible is the mass loss (blue) in southern Greenland and at the West Coast of Antarctica that has already been indicated by GRACE results (Meyer et al, 2016).

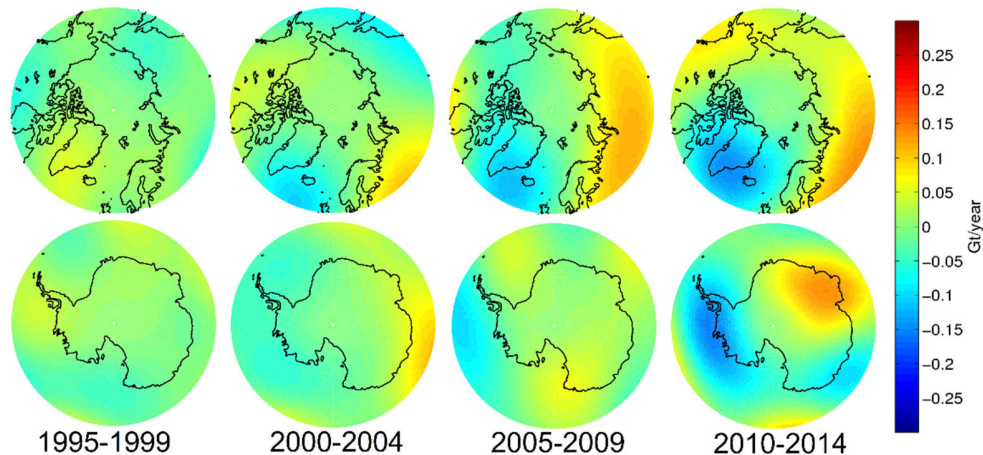


Figure 2. 26: Mass trend per 1° grid cell in polar regions (top: Arctic, bottom: Antarctic) as determined from monthly gravity field solutions derived from SLR observations.

Of special interest in the context of climate change is the history of ice mass change prior to the start of the GRACE satellites (launched in March 2002) and in the time-period between the end of the GRACE mission (the latest available GRACE K-band observations were collected in June 2017) and the start of GRACE-FO (launched in May 2018, but suffering from an outage of the instrument processing unit at one of the satellites between July and October 2018). From a combined processing of all available SLR satellites meaningful mass change signals can be determined since the availability of LAGEOS-2 (launched in 1992) and Stella (launched in 1993) normal points. Monthly mass variations from either a combined SLR processing (blue) or from the GRACE AIUB-RL02 time-series of monthly gravity fields (red) are shown in Figure 2. 27 (Meyer et al, 2019). For comparison the GRACE gravity fields were truncated at the max. degree/order 6 of the SLR solutions and the effect of C_{20} , which is suffering from systematic errors in case of GRACE, has been removed.

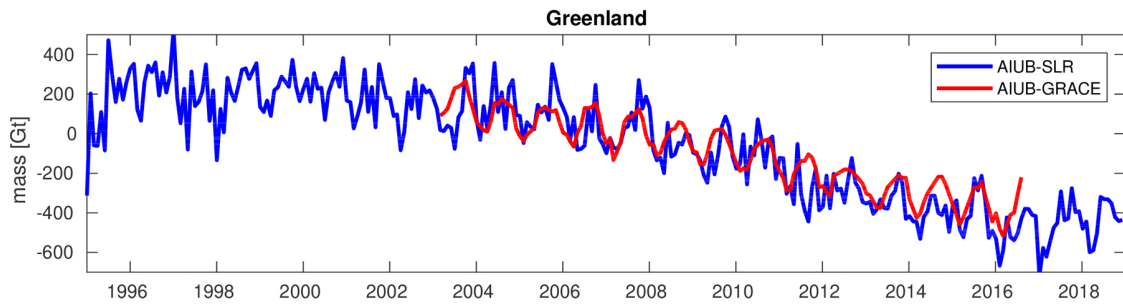


Figure 2. 27: Monthly mass variations within Greenland as observed by SLR and GRACE at common spherical harmonic resolution of degree/order 6 (effect of C_{20} removed).

The truncation of the gravity field solutions at low spherical harmonic resolution causes signal leakage and therefore leads to a drastic underestimation of mass change signal. This effect is exemplified for ice mass loss observed by either GRACE or SLR at the West Coast of Antarctica (Figure 2. 28). At the same spherical harmonic resolution results for GRACE and SLR are very much comparable. As it is also observed for Greenland, the major ice melt indicated by GRACE sets in around 2003. GRACE was launched just in time to observe it.

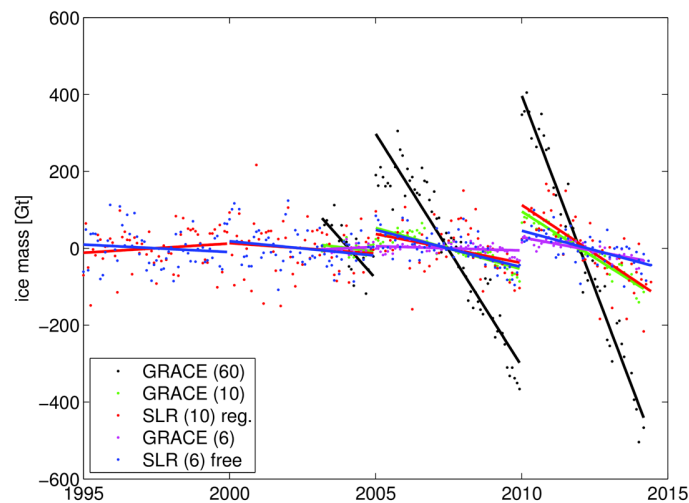


Figure 2. 28: Mass trends within 5-year periods at the West Coast of Antarctica, as derived from GRACE or SLR data at various spherical harmonic resolutions.

Deflections of the Vertical Measurement through Rocky Mountains for the NGS with the CODIAC ETH Zurich System

S. Guillaume, A. Wolf, B. Bürki

Mathematical and Physical Geodesy Lab, Institute of Geodesy and Photogrammetry, ETH Zurich

In the context of the Geoid Slope Validation Survey of NGS, the astrogeodetic system CODIAC of the ETH Zurich was successfully deployed.

CODIAC ETH Zurich System

The Compact Digital Astrometric Camera CODIAC is a zenith camera system entirely designed, developed and manufactured at the Institute of Geodesy and Photogrammetry of ETH Zurich (Guillaume, 2015). It is designed in order to facilitate the use by non astrogeodetic experts (Figure 2. 29).

Geoid Slope Validation Surveys GSVS

The US National Geodetic Survey (NGS) wants to determine a new geoid at centimeter level accuracy based on different gravity observables. In this context a series of Geoid Slope Validation Surveys (GSVS) has been performed in 2011 (Smith et al., 2013), 2014 (Wang et al., 2017) and 2017 in order to validate the observation, the processing strategies and the precision of the proposed method. The third GSVS survey took place in the summer of 2017, across the high, rugged terrain of southern Colorado in the Rocky Mountains from Durango to Walsenburg (Figure 2. 30). Leveling, long session GNSS, absolute gravity, and deflections of the vertical (DoV) were observed on over 223 benchmarks with a spacing of about 1.5 km.

First Determination of the Deflection of the Vertical with two CODIAC System in parallel

For this last campaign, two identical CODIAC systems were deployed. In the beginning of the campaign, during the training session, both systems could determine the DoVs at very close locations (approximately 5 meters apart) and at the same time. The results are very promising and show differences below 0.05 arcsec.

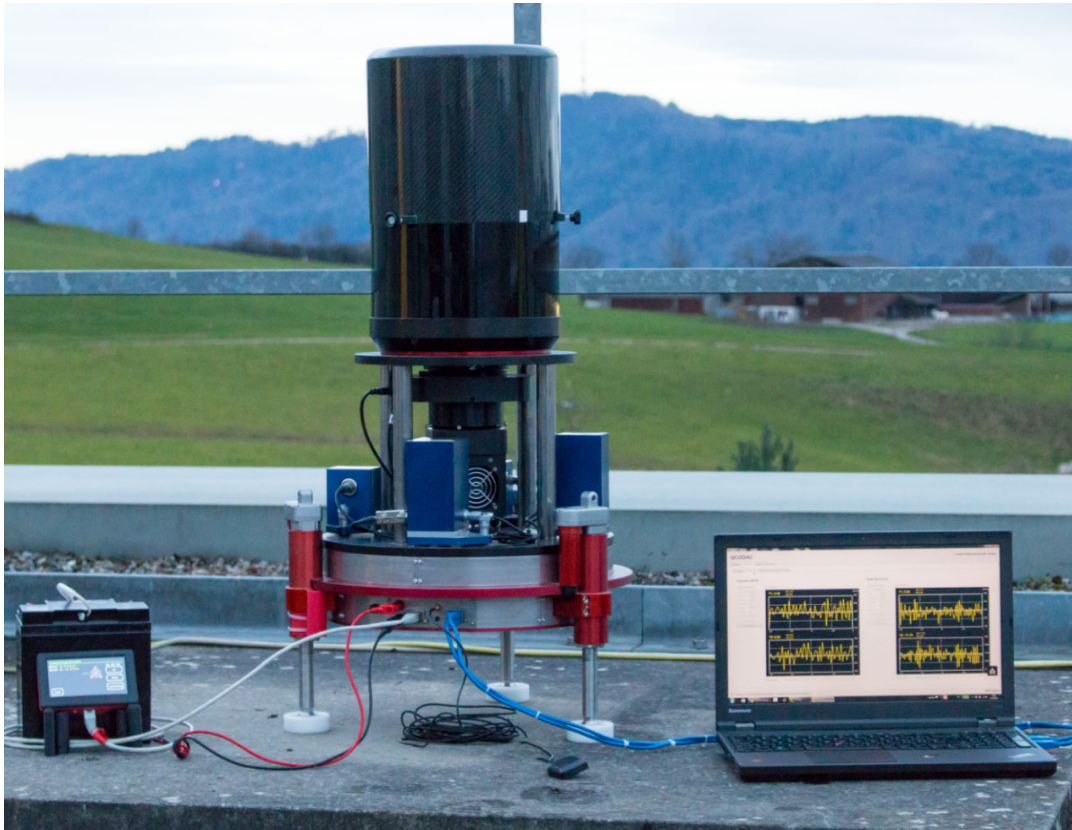


Figure 2. 29: CODIAC deployed on the roof of the Institute of Geodesy and Photogrammetry at ETH Zurich.

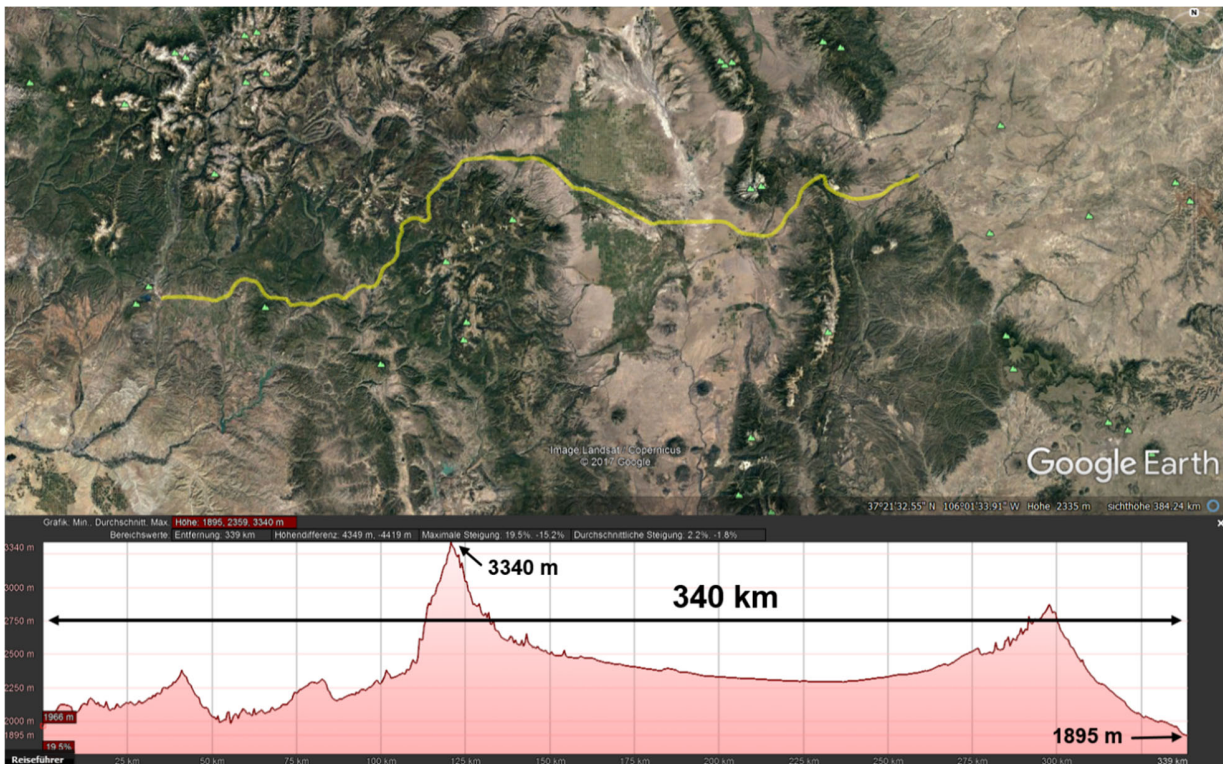


Figure 2. 30: Profile of the Geoid Slope Validation Survey 2017.

Deflections of the Vertical Measurements in Perth by TU Munich with the ETH Zurich QDaedalus System

S. Guillaume

Mathematical and Physical Geodesy Lab, Institute of Geodesy and Photogrammetry, ETH Zurich

QDaedalus ETH Zurich System

QDaedalus is a measurement system developed at the Institute of Geodesy and Photogrammetry at ETH Zurich (Bürki, 2010) and (Guillaume, 2012). It is composed of both, hardware and software components. The basic idea is to replace the eye-piece of an existing total station by a CCD camera in a non-destructive way in order to measure fully automatically very accurate spatial directions to visible. In addition to the CCD camera and the total station, a small electronic interface, including a low-cost GNSS receiver which permits the precise timing of the images. This allows efficient and low-cost determination of deflections of the vertical (DoVs) in a very portable way.

Measurement Campaign in Perth by TU Munich

The QDaedalus system was deployed by our colleagues of the Institute of Astronomical and Physical Geodesy of the TU Munich for a measurement Campaign in Perth in Australia (Schack, 2017). They observed 39 benchmarks with a 1 km spacing (Figure 2. 31). The DoVs measurements could be observed with a precision of ~ 0.2 arcsec (Hauk, 2014) and permit to determine a quasigeoid profile at a centimeter level accuracy. The astronomical quasigeoid heights are in 20–30 mm (RMS) agreement with three independent gravimetric quasigeoid models (Figure 2. 33), and the astrogeodetic DoVs agree to 0.2–0.3 arcsec (north–south) and 0.6–0.9 arcsec (east–west) RMS (Figure 2. 32). Tilt-like biases of ~ 1 mm over ~ 1 km are present for all quasigeoid models within ~ 20 km of the coastline, suggesting inconsistencies in the coastal zone gravity data. The DoV campaign in Perth proved that such profiles can be measured with a limited effort and could improve geoid models where data are particularly scarce.

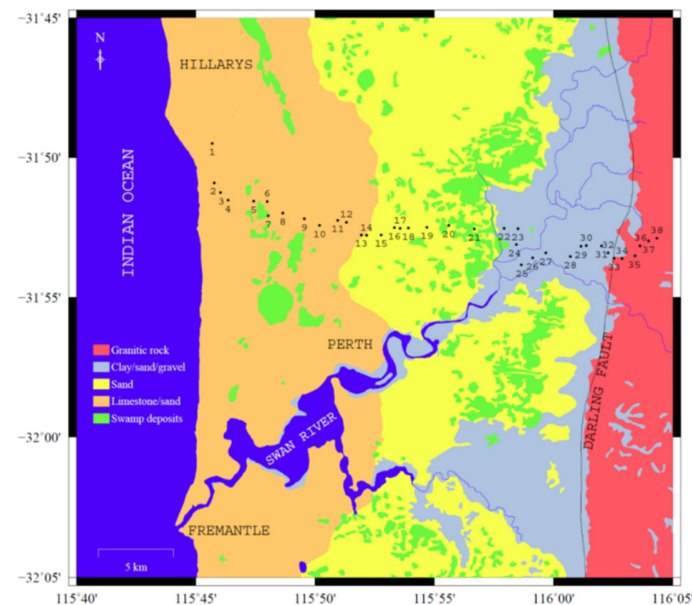


Figure 2. 31: The DoV profile in Perth, Australia (Schack, 2017).

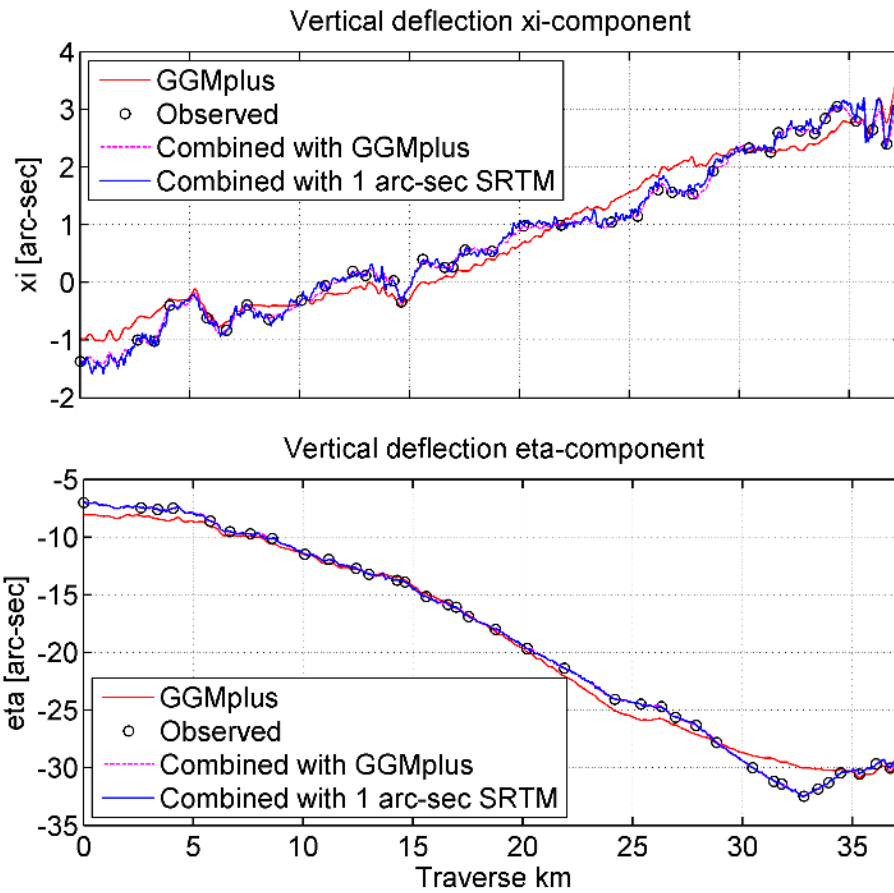


Figure 2. 32: Comparison of between the QDaedalus astro-geodetic DoVs and the DoVs from various models (Schack, 2017).

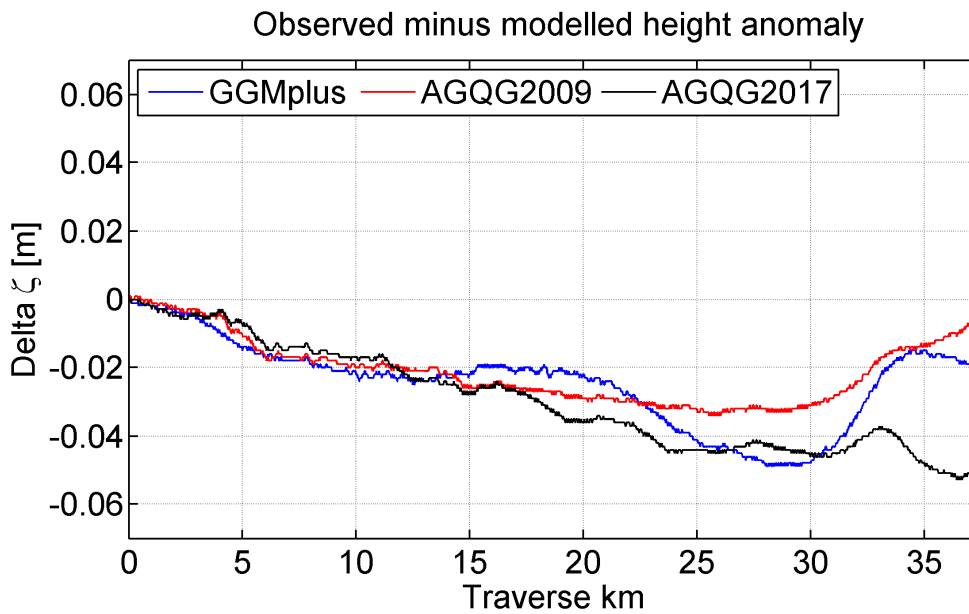


Figure 2. 33: Comparison between various quasigeoid models (Schack, 2017).

Bibliography Commission 2

- Arnold, D., Meyer, U., Dahle, C., Jäggi, A. (2017): Combined Swarm/Sentinel Gravity Fields. Presented at Fourth Swarm Science Meeting, Banff, Alberta, Canada, March 20 - 24, 2017.
- Arnold, D.; Bertone, S.; Jäggi, A.; Beutler, G., Mervart, L. (2015). GRAIL gravity field determination using the Celestial Mechanics Approach. *Icarus*. 261. 182-192, doi: 10.1016/j.icarus.2015.08.015.
- Asmar, S. W.; Konopliv, A. S.; Watkins, M. M.; Williams, J. G.; Park, R. S.; Kruizinga, G.; Paik, M.; Yuan, D.-N.; Fahnestock, E.; Strelakov, D.; Harvey, N.; Lu, W.; Kahan, D.; Oudrhiri, K.; Smith, D. E., Zuber, M. T. (2013) The Scientific Measurement System of the Gravity Recovery and Interior Laboratory (GRAIL) Mission. *Space Science Reviews*, 2013, 178, 25-55, doi: 10.1007/s11214-013-9962-0.
- Beutler, G.; Jäggi, A.; Mervart, L., Meyer, U. (2010): The celestial mechanics approach: theoretical foundations. *Journal of Geodesy*, 2010, 84(10), 605-624, doi: 10.1007/s00190-010-0401-7.
- Bürki, B., Guillaume, S., Sorber, P., Oesch, H.-P. (2010): DAEDALUS: A versatile usable digital clip-on measuring system for Total Stations. International Conference on Indoor Positioning and Indoor Navigation (IPIN), Zürich, IEEE. DOI: 10.1109/IPIN.2010.5646270.
- Condamine, S. (2016): Validierung von Schweregradienten auf LSN2004-Punkten. Master-Thesis 2016/Nr.7. Fachhochschule Nordwestschweiz. Muttenz.
- Condamine, S., Marti, U. (2017): Analyse von Schweregradienten im LSN2004. Swisstopo-Report 17-06.
- Dach, R., Lutz, S., Walser, P., Fridez, P., editors (2015): Bernese GNSS Software, Version 5.2. Astronomical Institute, University of Bern, Bern, Switzerland, ISBN 978-3-906813-05-9. doi: 10.7892/boris.72297. User manual.
- Dahle, C., Arnold, D., Jäggi, A. (2017): Impact of tracking loop settings of the Swarm GPS receiver on gravity field recovery. *Adv Space Res*, vol. 59(12), pp. 2843-2854; doi: 10.1016/j.asr.2017.03.003
- Fahnestock, E.; Park, R.; Yuan, D.-N., Konopliv, A. (2012). Spacecraft Thermal and Optical Modeling Impacts on Estimation Of the GRAIL Lunar Gravity Field. AIAA/AAS Astrodynamics Specialist Conference 2012. 10.2514/6.2012-4428.
- Flechtner, F., Dobslaw, H. (2013): AOD1B Product Description Document for Product Release 05. GRACE Project Document JPL 327-750, Version 4.0, <http://isdc.gfz-potsdam.de/grace>
- Floberhagen, R., Visser, P., Weischede, F. (1999). Lunar albedo force modeling and its effect on low lunar orbit and gravity field determination. *Adv Space Res*. 23. 733-738. doi: 10.1016/S0273-1177(99)00155-6.
- Grahl, A., Dach, R., Jäggi, A., Sošnika, K., Thaller, D. (2017): Impact of estimating geodetic parameters on gravity field coefficients. Presented at European Geosciences Union (EGU) General Assembly 2017, Vienna, Austria, April 24 - 28, 2017.
- Guillaume, S. (2015): Determination of a Precise Gravity Field for the CLIC Feasibility Studies. Geodätisch-geophysikalische Arbeiten in der Schweiz. Band 94.
- Guillaume, S., Bürki, B., Griffet, S., Mainaud-Durand, H. (2012): QDaedalus: Augmentation of Total Stations by CCD Sensor for Automated Contactless High-Precision Metrology. Proceedings of FIG Working Week 2012, Rome, Italy, 6-10 May 2012.
- Hauk, M., Hirt, Ch., Ackermann, Ch. (2014): Erprobung des astrogeodätischen Messsystems QDaedalus zur Bestimmung von genauen Lotabweichungen. Technische Universität München, Master Thesis D253.
- Ihde, J., Barzaghi, R., Marti, U., Sánchez, L., Sideris, M., Drewes, H., Foerste, Ch., Gruber, T., Liebsch, G., Pail, R. (2015): Report of the Ad-hoc Group on an International Height Reference System (IHRG); In: IAG Reports 2011-2015 (Travaux de l'AIG Vol. 39)
- Ihde, J., Sánchez, L., Barzaghi, R., Drewes, H., Foerste, Ch., Gruber, T., Liebsch, G., Marti, U., Pail, R., Sideris, M. (2017): Definition and Proposed Realization of the International Height Reference System (IHRG). *Surv Geophys* (2017) 38:549–570. DOI 10.1007/s10712-017-9409-3.
- Jäggi A., Jenny, B., Meyer, U., Flechtner, F., Bettadpur, S., Boening, C., Mayer-Gürr, T., Lemoine J.-M. (2018b): Combination Service for Time-variable Gravity Field Models (COST-G) – current status. Presented at AGU Fall Meeting 2018, Washington, DC, USA, Dec. 10 - 14, 2018.

- Jäggi, A., Dahle, C., Arnold, D., Bock, H., Meyer, U., Beutler, G., van den Ijssel, J. (2016): Swarm kinematic orbits and gravity fields from 18 months of GPS data. *Adv Space Res*, vol. 57 (1), pp. 218-233; doi: 10.1016/j.asr.2015.10.035.
- Jäggi, A., Dahle, C., Arnold, D., Meyer, U., van den Ijssel, J. (2015): Orbit and Gravity Field Solutions from Swarm GPS Observations. Presented at IUGG 2015 Prague, Czech Republic, June 22 - July 2, 2015.
- Jäggi, A., Meyer, U., Jean, Y., Flechtner, F., Mayer-Gürr, T., Lemoine, J.-M. (2018a): Combination Service for Time-Varying Gravity Field Solutions (COST-G): Transition from an EGSIM prototype service into a product center of the IGFS. 42. Presented at COSPAR Scientific Assembly, Pasadena, CA, USA, July 14 - 22, 2018.
- Jäggi, A., Meyer, U., Schreiter, L., Sterken, V., Dahle, C., Arnold, D., Teixeira da Encarnação, J., Visser, P., Doornbos, E., van den Ijssel, J., Mao, X., Iorfida, E., Bezděk, A., Sebera, J., Klokočník, J., Mayer-Gürr, T., Zehentner, N., Shum, C.K., Zhang, Y., Lück, C., Rietbroek, R., Kusche, J. (2018): Assessment of individual and combined gravity field solutions from Swarm GPS data and mitigation of systematic errors. Presented at EGU General Assembly, Session ST3.5/EMRP4.33/G4.4, Vienna, Austria, April 8 - 13, 2018.
- Jäggi, A., Weigelt, M., Flechtner, F., Güntner, A., Mayer-Gürr, T., Martinis, S., Bruinsma, S., Flury, J., Bourgogne, S., Steffen, H., Meyer, U., Jean, Y., Sušnik, A., Grahl, A., Cann-Guthäuser, K., Dach, R., Li, Z., Chen, Q., van Dam, T., Gruber, C., Poropat, L., Gouwleeuw, B., Kvas, A., Klinger, B., Lemoine, J.-M., Biancale, R., Zwenzner, H., Bandikova, T., Shabanloui, A. (2019): European Gravity Service for Improved Emergency Management (EGSIEM) - from concept to implementation. Submitted to *Geophysical Journal International*.
- Jean, Y., Meyer, U., Jäggi, A. (2018): Combination of GRACE monthly gravity field solutions from different processing strategies. *J Geod*, 92(11), pp 1313–1328; doi: 10.1007/s00190-018-1123-5;
- Lemoine, F. G.; Goossens, S.; Sabaka, T. J.; Nicholas, J. B.; Mazarico, E.; Rowlands, D. D.; Loomis, B. D.; Chinn, D. S.; Neumann, G. A.; Smith, D. E., Zuber, M. T. (2014): GRGM900C: A degree 900 lunar gravity model from GRAIL primary and extended mission data. *Geophys Res Lett*, 2014, 41, 3382-3389, doi: 10.1002/2014GL060027.
- Lomidze, L., Knudsen, D. J., Burchill, J., Kouznetsov, A., Buchert, S. C. (2018): Calibration and validation of Swarm plasma densities and electron temperatures using ground based radars and satellite radio occultation measurements. *Radio Science*, 53, 15,A S.36. <https://doi.org/10.1002/2017RS006415>
- Marti, U. (2017): Aufbau der neuen Landesvermessung der Schweiz 'LV95' (Teil 14): Das Geoid der Schweiz 2004 „CHGeo2004“. Swisstopo-Doku Nr. 22d.
- Marti, U. (2017): Définition de la nouvelle mensuration nationale de la Suisse 'MN95' (14ème partie): Le géoïde de la Suisse 2004 «CHGeo2004». Swisstopo-Doku Nr. 22f.
- Marti, U. (2017): Gravimeter-Eichstrecke Interlaken-Jungfrauoch. Arbeiten in den Jahren 2010-2016. Swisstopo-Report 17-04.
- Marti, U., Baumann, H., Bürki, B., Gerlach, C. (2016): A First Traceable Gravimetric Calibration Line in the Swiss Alps. In: IGFS 2014 (Jin and Barzaghi, eds.). Proceedings of the 3rd International Gravity Field Service (IGFS), Shanghai, China, June 30 - July 6, 2014. IAG Symposia Series Nr. 144. DOI 10.1007/1345_2015_52, Springer Verlag, 2016.
- Marti, U., Vitushkin, L., Wziontek, H. (2016): The role of a new Global Absolute Gravity Reference System in relation to the Global Geodetic Reference Frame. Proceedings of the 4th IAG Symposium "Terrestrial Gravimetry. Static and Mobile Measurements (TG-SMM 2016)At: St Petersburg, Russia Volume: pp 124-127
- Matsumoto, K., Goossens, S., Ishihara, Y., Liu, Q., Kikuchi, F., Iwata, T., Namiki, N., Noda, H., Hanada, H., Kawano, N., Lemoine, F.G., Rowlands, D.D. (2010): An improved lunar gravity field model from SELENE and historical tracking data: Revealing the farside gravity features. *J. Geophys. Res.-Planets*, 115: E06007, doi: 10.1029/2009JE003499.
- Mauri G., Marguet, L., Jansen, G., Marti, U., Baumberger, R., Allenbach, R., Kuhn, P., Altwegg, P., Miller, S. (2017): Combined Use of Land Gravity Data and 3D Geological Model to image deep geological Basin. Case of Region of La Broye. Switzerland. Proceedings of 46th IASTEM International Conference, Seoul, South Korea.

- Meyer, U., Arnold, D., Bentel, K., Jean, Y., Jäggi, A. (2017): GRACE satellite gravimetry to assess global hydrology and ice melt. Presented at 15th Swiss Geoscience Meeting, Davos 2017, Davos, Switzerland, Nov. 17 – 18, 2017.
- Meyer, U., Jäggi, A., Beutler, G. (2012): Monthly gravity field solutions based on GRACE observations generated with the Celestial Mechanics Approach. *Earth and Planetary Science Letters*, vol. 345-348, pp. 72-80.
- Meyer, U., Jäggi, A., Jean, Y., Arnold, D. (2015): Improving the noise model for AIUB monthly gravity field solutions. Presented at IUGG 2015, Prague, Czech Republic, June 22 - July 2, 2015.
- Meyer, U., Jäggi, A., Jean, Y., Beutler, G. (2016): AIUB-RL02: an improved time-series of monthly gravity fields from GRACE data. *Geophysical Journal International*, vol. 205, pp. 1196-1207; doi: 10.1093/gji/ggw081.
- Meyer, U., Jean, Y., Arnold, D., Kvas, A., Mayer-Gürr, T., Lemoine, J.-M., Bourgoigne, S., Dahle, C., Flechtner, F., Jäggi, A. (2018a): The EGSIM combination service: final results and further plans. Presented at EGU General Assembly 2018, Vienna, Austria, April 8 - 13, 2018.
- Meyer, U., Jean, Y., Kvas, A., Dahle, C., Lemoine, J.-M., Jäggi, A. (2019): Combination of GRACE monthly gravity fields on the normal equation level. Submitted to *J Geod*.
- Meyer, U., Jenny, B., Dahle, C., Flechtner, F., Save, H., Bettadpur, S., Landerer, F., Boening, C., Kvas, A., Mayer-Gürr, T., Lemoine, J.-M., Bruinsma, S., Jäggi, A. (2018b): COST-G: The new International Combination Service for Time-variable Gravity Field Solutions of the IAG/IGFS. Presented at GSTM 2018, Potsdam, Germany, Oct. 9 - 11, 2018.
- Meyer, U., Sośnica, K., Arnold, D., Dahle, C., Thaller, D., Dach, R., Jäggi, A. (2019). SLR, GRACE and SWARM gravity field determination and combination. Submitted to *Remote Sensing*.
- Meyer, U., Sośnica, K., Maier, A., Jäggi, A. (2015): Combined GRACE / SLR monthly gravity field solutions. Presented at EGU General Assembly 2015, Vienna, Austria, April 12 - 17, 2015.
- Meyer, U., Sośnica, K., Thaller, D., Dach, R., Jäggi, A. (2018): Mass change in Greenland and Antarctica derived from SLR and GRACE. Presented at POLAR2018 Open Science Conference, Davos, Switzerland, June 19 - 23, 2018.
- Otsubo, T., Müller, H., Pavlis, E.C., Torrence, M.H., Thaller, D., Glogotov, V., Wang, X., Sośnica K., Meyer, U., Wilkinson, M.J. (2018): Rapid response quality control service for the laser ranging tracking network. *J Geod*; doi: 10.1007/s00190-018-1197-0; in print.
- Sánchez, L., Marti, U., Ihde, J. (2017) : Le chemin vers un système de référence altimétrique global et unifié. *Revue XYZ • N° 150. 1/2017*.
- Savcenko, R., Bosch, W. (2011): EOT11a - a new tide model from Multi-Mission Altimetry, in OSTST Meeting, San Diego, 19–21 October.
- Schack P., Hirt C., Hauk M., Featherstone W.E., Lyon T. J., Guillaume S. (2018): A high-precision digital astrogeodetic traverse in an area of steep geoid gradients close to the coast of Perth, Western Australia. *Journal of Geodesy* 92 (10), p. 1143-1153, 2018.
- Schlatter, A., U. Marti, A. Wiget (2016): AlpTransit Gotthard base tunnel: Aspects of gravity field, heights and geodynamics. AVN 2016.
- Schreiter, L., Arnold, D., Sterken, V., Jäggi, A. (2019): Mitigation of ionospheric signatures in Swarm GPS gravity field estimation using weighting strategies. *Ann. Geophys.*, 37, 111-127, <https://doi.org/10.5194/angeo-37-111-2019>, 2019
- Smith D., Holmes, S., Li, X., Guillaume, S., Wang, Y., Bürki, B., Roman, D., Damiani, T. (2013): Confirming regional 1 cm differential geoid accuracy from airborne gravimetry: The Geoid Slope Validation Survey of 2011. *Journal of Geodesy*, 87 (10-12), p.885-907. 2013.
- Sośnica, K., Jäggi, A., Meyer, U., Thaller, D., Beutler, G., Arnold, D., Dach, R. (2015): Time variable Earth's gravity field from SLR satellites. *J Geod*, vol. 89(10), pp. 945-960; doi: 10.1007/s00190-015-0825-1.
- Teixeira da Encarnação, J., Arnold, D., Bezdek, A., Dahle, C., Doornbos, E., van den Ijssel, J., Jäggi, A., Mayer-Gürr, T., Sebera, J., Visser, P., Zehentner, N. (2016): Gravity field models derived from Swarm GPS data. *Earth, Planets and Space*, vol. 68:127; doi: 10.1186/s40623-016-0499-9.

- Teixeira da Encarnação, J., Visser, P., Doornbos, E., van den Ijssel, J., Mao, X., Iorfida, E., Arnold, D., Jäggi, A., Meyer, U., Bezdek, A., Sebera, J., Klokočník, J., Ellmer, M., Mayer-Gürr, T., Zehentner, N., Guo, J.-Y., LLuk, P., Shum, C.K., Zhang, Y. (2018a): Signal contents of combined monthly gravity field models derived from Swarm GPS data. Presented at EGU General Assembly 2018, Vienna, Austria, April 8 - 13, 2018.
- Teixeira da Encarnação, J., Visser, P., Doornbos, E., van den Ijssel, J., Mao, X., Iorfida, E., Arnold, D., Jäggi, A., Meyer, U., Bezdek, A., Sebera, J., Klokočník, J., Ellmer, M., Mayer-Gürr, T., Zehentner, N., Guo, J.-Y., LLuk, P., Shum, C.K., Zhang, Y. (2018b): Observing Earth's mass transport processes with the SWARM satellites. Presented at GGHS-2018, Copenhagen, Denmark, September 17 - 21, 2018.
- Wang, Y., Becker, C., Mader, G., Martin, D., Li, X., Jiang, T., Breidenbach, S., Geoghegan, C., Winester, D., Guillaume, S., Bürki, B. (2017): The Geoid Slope Validation Survey 2014 and GRAV-D airborne gravity enhanced geoid comparison results in Iowa. *Journal of Geodesy*, 91 (10), p. 1261-1276, 2017.
- Zuber, M. T.; Smith, D. E.; Watkins, M. M.; Asmar, S. W.; Konopliv, A. S.; Lemoine, F. G.; Melosh, H. J.; Neumann, G. A.; Phillips, R. J.; Solomon, S. C.; Wieczorek, M. A.; Williams, J. G.; Goossens, S. J.; Kruizinga, G.; Mazarico, E.; Park, R. S., Yuan, D.-N. (2013) Gravity Field of the Moon from the Gravity Recovery and Interior Laboratory (GRAIL) Mission. *Science*, 2013, 339, 668-671, doi: 10.1126/science.1231507.

3 Earth Rotation and Geodynamics

CODE Contributions to Earth Rotation Monitoring

S. Schaer², R. Dach¹, A. Villiger¹, A. Jäggi¹

¹*Astronomical Institute, University of Bern, Switzerland*

²*Swiss Federal Office of Topography (swisstopo), Wabern, Switzerland*

The CODE stands for Center of Orbit Determination in Europe - a joint venture of Astronomical Institute, University of Bern, Switzerland, Bundesamt für Landestopografie (swisstopo), Wabern, Switzerland, Bundesamt für Kartographie und Geodäsie, Frankfurt a. Main, Germany, and Ingenieurinstitut für Astronomische und Physikalische Geodäsie, Technische Universität München, Germany. CODE is one of the global Analysis Centers (AC) of the International GNSS Service (IGS). The activities of CODE as an IGS AC are described in Dach et al. (2009) or Schaer et al. (2019).

The satellite orbits of Global Navigation Satellite Systems (GNSS) realize a quasi-inertial reference system, so that the analysis of tracking data from the global network of the IGS allows it to estimate Earth rotation parameters (ERPs). As a result x and y positions of the Earth's rotation axis in an Earth-fixed frame (polar motion) and rates thereof as well as excess length of day (LOD) are obtained.

Since April 1994 also daily values for drifts in nutation in longitude and obliquity are estimated at CODE. Since GPS week 1486 (June 29, 2008) CODE is internally using a 1-hour resolution for polar motion and LOD parameters. The ERPs are represented as a piece-wise linear polygon, so that continuity at the interval boundaries is automatically guaranteed. For the delivery to external sources (e.g., to the IGS via SINEX files) the representation of the parameters is transformed to offset and drift per 1-day interval applying some continuity conditions at the day boundaries. Separate time series are provided directly to the International Earth Rotation and Reference Systems Service (IERS) for further analysis.

In 2015, software and (final) processing was further developed and prepared for the capability to set up EOPs satellite wise. The same, by the way, applies also to the geocenter coordinate (GCC) parameters. By this expanded parameter setup, studies on the basis of NEQ results become feasible in assessing EOP (and GCC) differences specific to individual satellite systems, satellite planes, satellite groups (or blocks), etc. It is obvious that no (significant) differences (e.g. between GPS-derived and GLONASS-derived EOPs) should be present in the ideal case. A related analysis is reported in Scaramuzza et al., 2017.

Today a time series of more than 25 years is available from CODE. Figure 3. 1 shows the Chandler wander of the Earth's rotation axis starting with July 1993. The accuracy of the daily values as compared to other techniques is a few 0.1 mas. Figure 3. 2 shows the variations of excess length of day for the time period of more than 25 years.

In the frame work of the 2nd reprocessing campaign of the IGS, a time series of ERP based on homogeneous and most up-to-date models has been generated (see Lutz et al. 2015).

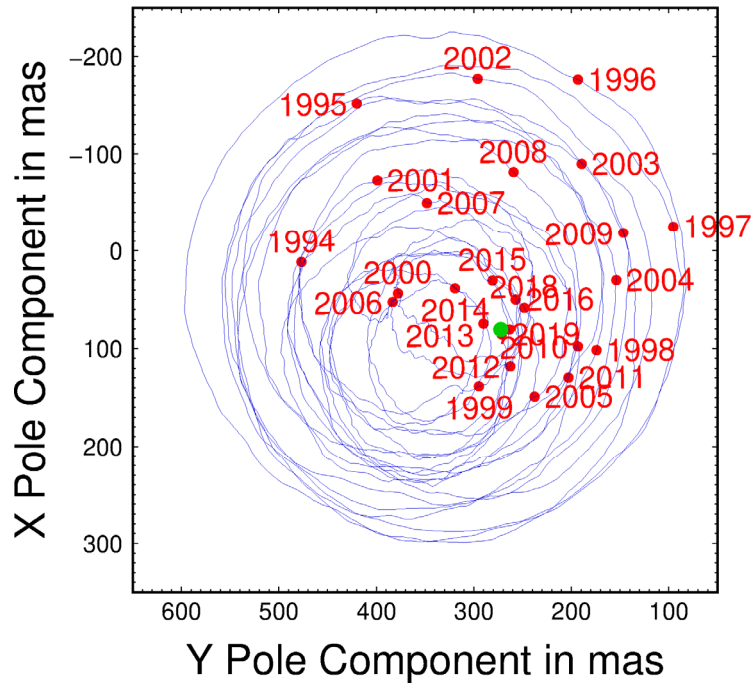


Figure 3. 1: Polar motion derived from GNSS observations from July 1993 until March 2019.

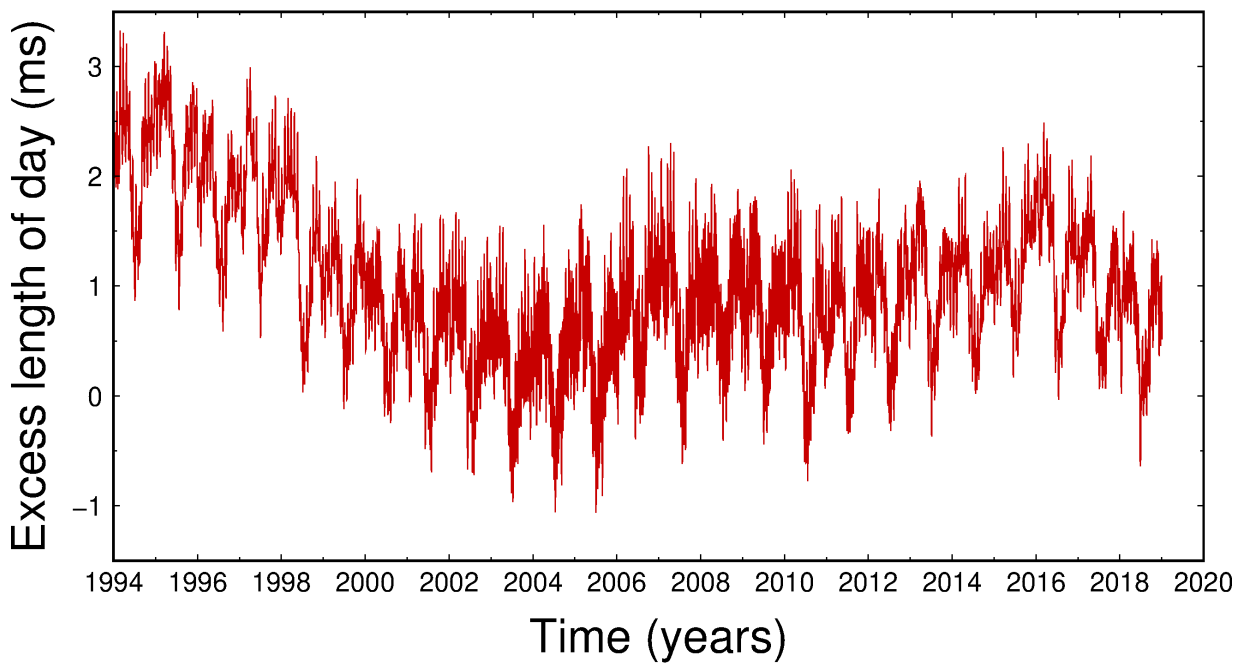


Figure 3. 2: Excess length of day derived from GNSS observations from July 1993 until March 2019.

Dependency of geodynamic parameters on the GNSS constellation

S. Scaramuzza^{1,2}, R. Dach¹, G. Beutler¹, D. Arnold¹, A. Sušnik^{1,3}, A. Jäggi¹

¹ Astronomical Institute, University of Bern

² Now with: University Basel

³ Now with: School of Civil Engineering and Geosciences, Newcastle University, Newcastle NE1 7RU, UK

Earth rotation parameters and geocenter coordinates are some of the most important results for geodynamic interpretation from global solutions of GNSS (Global Navigation Satellite System) data. Various authors have reported about spurious effects in such time series, e.g., related to deficiencies in the orbit modelling and/or effects from the constellation geometry (for instance, Meindl, 2011; Meindl et al. 2013, Ray et al. 2008, 2013).

In a dedicated study, the effect was investigated based on a global GNSS network solution for the years 2012 to 2016, where already a full GLONASS constellation was in space. The following solutions were consistently generated:

- So-called **GPS-only** and **GLONASS-only** solutions, where the relevant parameters were computed independently. The station coordinates and receiver clock corrections were identical between the two systems. The solution was based on the capability of the Bernese GNSS Software (Dach et al, 2015), where system-wise Earth-rotation parameters and geocenter coordinates can be estimated. This approach guarantees the full consistency between the series.
- A **combined GPS/GLONASS solution (CMB)**, corresponding to a typical rigorous combined solution of GPS and GLONASS measurements.
- To study in greater detail the effect of the number of planes in a GNSS, an additional series of solutions was generated, where the geodynamic parameters were derived separately for **two artificial GPS sub-systems (GPS_o and GPS_e)** and for GLONASS. The two GPS sub-systems were derived by splitting the GPS constellation into two groups of three orbital planes each (GPS_o for the odd-numbered planes and GPS_e for the even-numbered planes), where the planes within each group are separated by 120° in the equator as for the three-plane constellations. The two sub-systems are consequently rotated by about 60° relative to each other. The number of the orbital planes and their relation to each other is comparable to the GLONASS constellation. During the time period analysed, the number of active satellites per sub-system varied between 13 and 18; about 16 on average. There have been between 3 and 8 satellites per plane, in average 5 to 6. The differences in the ascending nodes of the orbital planes between GLONASS and GPS_o were ~15° and between GLOANSS and GPS_e ~75°.

Geocenter coordinates

The estimates of the geocenter z-coordinates for the combined and GPS-only solutions are very similar. The amplitudes for the GPS_o and GPS_e series are slightly larger compared to the GPS-only solution. The absolute values for these series are below 7–8 cm. There is no larger excursion for solutions containing GPS whereas the GLONASS-only series shows values up to 20 cm.

The GPS-only series are close to the combined solution. This means that the combined solution is dominated by GPS, which is also clearly visible in the related formal errors. For GLONASS, the local extrema in the geocenter time series are related to the maximum elevation of the Sun above the orbital plane (β angle). This correlation results in a 3 cycles per year (cpy) periodicity, as already discussed by Meindl et al. (2013). For the two GPS sub-systems, this relation is less pronounced, which indicates that the higher inclination of the GLONASS orbits is more critical than the number of orbit planes.

Figure 3. 3 shows the amplitude spectra of the estimated geocenter z-coordinates from GPS-only, GLONASS-only, the combined solution and the two GPS sub-system series. Compared to GPS-only, GPS_e has slightly larger amplitudes at 1 cpy and 2 cpy and a smaller one at 3 cpy, while GPS_o has slightly larger amplitudes at 1, 2 and 3 cpy. The

differences between all spectra for series containing GPS are very small, whereas the amplitudes for the GLONASS-only series are much bigger.

Summary

A reduction of the number of orbital planes in a GNSS from 6 to 3 has only a minor effect on the geocenter estimates. Apart from the correlation of the geocenter z-coordinate with the empirical solar radiation pressure parameters, the generally larger formal errors for GLONASS orbits may also have a negative impact on the geocenter z-coordinate estimate. Better orbit models, in particular for GLONASS, might improve the estimates.

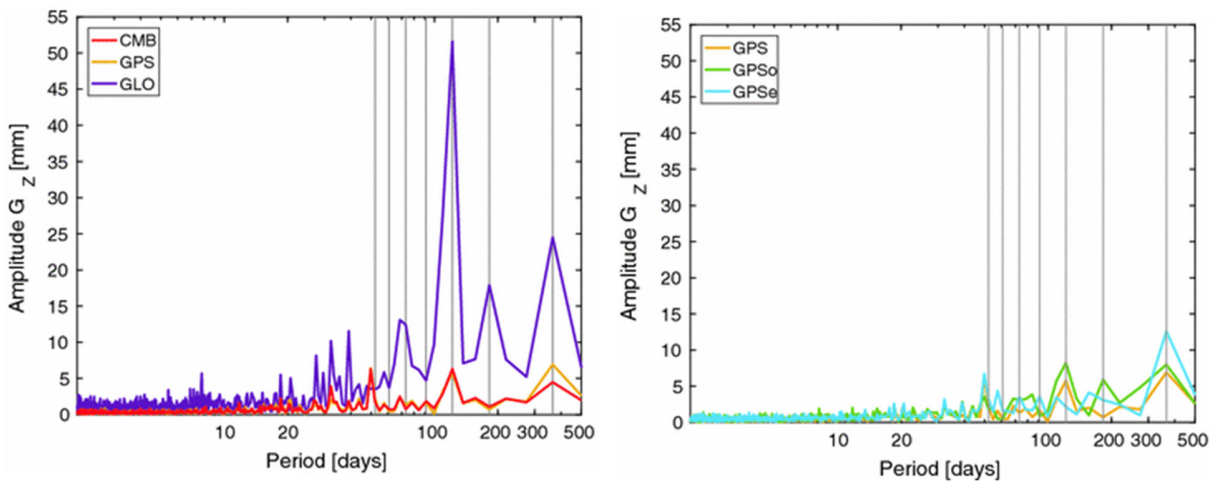


Figure 3.3: Amplitude spectra of the geocenter z-coordinate from GPS, GLONASS and the combined solution (left) and from GPS, GPSo and GPSe (right)

Earth Rotation Parameters

The difference of the polar motion estimates with respect to the corresponding IERS 08 C04 values is analyzed subsequently. The spectra of the time series of these differences are shown in Figure 3.4. GLONASS, GPSo and GPSe, (i.e., all the systems with 3 orbital planes) have a pronounced signal at 3 cpy. This signal is particularly large for GLONASS and GPSe in the y-coordinate. The series based on the combined and the full GPS solutions show a much smaller amplitude at this period in both components. The difference between the spectra of sub-systems GPSo and GPSe are related to the different ascending nodes of their orbital planes, which are oriented in a different way relative to the heterogeneously distributed global station network.

As the pole coordinates derived from 3-plane series have systematic differences w.r.t. the IERS 08 C04 series in particular at the 3cpy period, we ask the question how pole coordinates based on a combination of 2 systems with 3 planes each behave. Such a scenario might occur by combining GLONASS and Galileo. For that purpose, we introduce an additional solution named RGo consisting of a combination of GPSo and GLONASS. It was realized by combining the geodynamic parameters for these two sub-solutions to derive this additional series next to GPS, GLONASS and the GPS sub-systems. The ascending nodes of the orbital planes of GPSo and GLONASS differ only by $\sim 15^\circ$ during the considered time interval. This small difference in the ascending nodes was chosen to study how a combination of two 3-planes systems behaves under rather unfavorable constellation geometries.

Figure 3.4 contains also the amplitude spectra of RGo. It has also a larger amplitude than the full GPS at 3 cpy in the x-component. However, it is by a factor two smaller than the one for GLONASS or the GPS sub-systems. On the other hand, the amplitude of RGo is even the smallest one for the y-component. A combination of these two 3-plane systems therefore reduces the signal at this period – disregarding the relatively small difference in the ascending nodes. The additional number of satellites due to the larger number of planes, as constructed in the RGo solution, leads to a more

stable constellation geometry of RGo for obtaining polar motion series than individual three-plane constellations. This may be explained by the findings of Dach et al. (2009), showing that a combination of two systems with different orbit properties can reduce geometric effects of the single systems.

Summary

The pole coordinates estimated with a 3-plane GNSS may result in systematic differences with a 3 cpy signature. The formal errors of the estimates show a similar pattern. We also showed that the combination of two 3-plane systems reduces the initially observed differences, even when the two systems have similar ascending nodes. This underlines the positive effect of combining observations to satellites with different orbit characteristics. Future combinations of 3-plane systems as, e.g., GLONASS and Galileo, should therefore improve the ERP quality. Estimating the pole coordinates based on a GNSS with more than 3 orbital planes or on a combination of different GNSS in general reduces ERP inconsistencies.

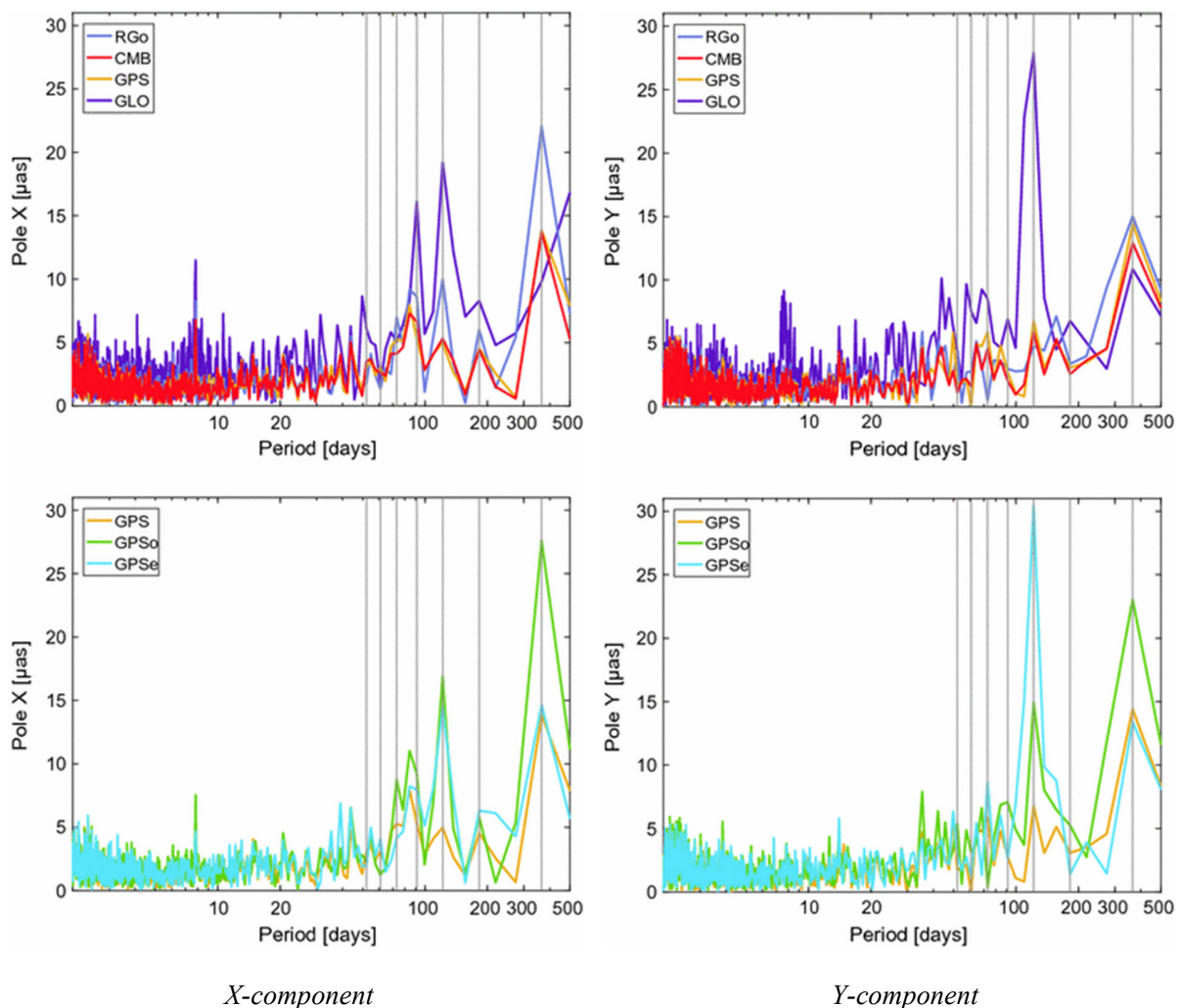


Figure 3. 4: Amplitude spectra of the differences of the polar motion to the corresponding IERS 08 C04 series from GPS, GLONASS, the combined solution and RGo (top) and from GPS, GPS0 and GPSe (bottom).

Acknowledgements

The study was funded by the Swiss National Science Foundation in the frame of the Project “Advanced Satellite Orbit Modelling for GPS, GLONASS and Galileo” (200021_153429).

The Future of National GNSS-Geomonitoring Infrastructures in Switzerland

J. Clinton¹, A. Geiger², S. Häberling², F. Haslinger¹, M. Rothacher², A. Wiget³ and U. Wild³

¹ Swiss Seismological Services (SED)

² Institute of Geodesy and Photogrammetry, ETH Zurich

³ Federal Office of Topography, swisstopo

Experts of the Swiss Federal Office of Topography swisstopo (Division of Geodesy), the Swiss Seismological Services (SED) and the Institute of Geodesy and Photogrammetry (IGP; Mathematical and Physical Geodesy MPG) at ETH Zurich came together to discuss actual and future questions and needs of optimal national GNSS infrastructures and of the data exchange when combining GNSS receivers and seismometers in monitoring networks. The results of these discussions and the conclusions are published in a White Paper in the publication series of the Geodetic Commission *Geodätisch-geophysikalische Arbeiten in der Schweiz* (Clinton et al., 2017).

The document outlines a vision for the future of national GNSS-geomonitoring infrastructures in Switzerland, developed by three named key institutions, and endorsed by the Swiss Geodetic Commission and the Swiss Geophysical Commission. While permanent GNSS networks provide key services for society and have a clear economic and commercial value, the paper primarily addresses scientific aspects of GNSS monitoring. Reflecting on global standards and recent scientific insights and trends, a main focus is set on outlining advances in network design, network density, encompassing hardware and multi-sensor co-location, data management and exchange, and data products. The current GNSS network for Switzerland, AGNES, is a high quality, multi-purpose, automated network that today covers applications such as national geodetic survey, positioning services, geodynamics, and meteorology. While it is on par with many advanced networks regarding overall station spacing and instrumentation quality, improvements in data management organization and distribution seem feasible, especially with regards to real-time and short-term applications, and when coordinating with other stakeholders. One particular finding is that further enhancements of the existing applications and expansion to the field of seismology and local seismic monitoring would have the potential to contribute significantly to the overall seismic hazard assessment in Switzerland.

The White Paper concludes with nine key recommendations proposed as actions. Following these recommendations will also contribute to a better understanding of the ongoing tectonic and seismic processes, and may support applications in future earthquake early warning and rapid event characterization systems, providing new insight, redundancy and higher reliability.

Applications	Requirements
Seismology	High spatial density of the multi-GNSS network and co-location with seismic instruments, inter-station distance of 10-20 km, 1 sps (ring buffer 20 sps for 14 days), real-time access, real-time PPP processing and more accurate near real-time processing (2 min)
Task force	High point density of campaign points, available equipment, well-defined procedures of task force measurements (over 3 months), high sampling rate up to 20 sps, no real-time access, post-processing
Geodynamics	Densification, long-term measurements and stability of the monumentation, post-processing
Local monitoring	Densification (ionosphere), reference stations linked to AGNES, real-time access, reference station with real-time processing possibility
Meteorology	Densification especially in Alpine regions and at different heights, real-time access, near real-time processing

National Survey	Selective densification (to improve positioning services), monument monitoring, real-time capabilities, post-processing
-----------------	---

Table 3. 1: Summary of the requirements for new and enhanced existing applications using permanent GNSS networks in Switzerland.

Applications	Requirements				
	Spatial densification	Co-location	High-rate data	Real-time processing	Central data management
Seismology	x	x	x	x	x
Task force	x	(x)	x		x
Geodynamics	x				x
Local monitoring	x	(x)	(x)	(x)	x
Meteorology	x	x	(x)	(x)	x
National Survey	x		(x)	(x)	x

Table 3. 2: Matrix showing the importance of some requirements for different applications. The brackets denote a requirement of not highest priority for the corresponding application.

Instantaneous Detection of Hazardous Ground Movements with GNSS

R. Hohensinn, A. Geiger, M. Meindl and D. Willi

Institute of Geodesy and Photogrammetry, ETH Zurich

A focus of the Institute for Geodesy and Photogrammetry (IGP) of ETH Zurich lies on the GNSS data processing for the monitoring of slope movements in high Alpine regions in the Swiss Alps. The slope movements under investigation are especially related to the thawing of permafrost areas (e.g. rock glaciers), as these can cause threats for humans and infrastructure. The project series X-Sense2, which is funded by the SNF (Swiss National Science Foundation), focuses on the development of wireless Geo-sensor networks and related technologies for the monitoring of such environmental changes in high-alpine regions in the Swiss alps. It is a joint collaboration of several institutes of ETH Zurich and the University of Zurich, led by the Computer Engineering and Networks Laboratory (TIK) of ETH. Figure 3. 5 shows an autonomous GNSS monitoring station which is deployed by the X-Sense project partners. The IGP computes both static and RTK solutions, utilizing the measurements from nearby reference stations installed on bedrock.



Figure 3. 5: Example of a self-sufficient GNSS monitoring station of ETH Zurich, located in the Swiss Alps.

In order to bridge the gap from monitoring to early warning in real-time, the IGP is developing and testing algorithms for the instant detection of hazardous slope movements by means of estimates of the instantaneous GNSS station velocity, based on observations of receiver-to-satellite line-of-sight velocity (range-rates). These velocities are obtained from time derivatives of GNSS phase measurements. The estimates of the instantaneous station velocity are then tested epoch-wise for significance. In order to reduce false alarms, a cumulative criterion includes the movement information over several epochs to reach a decision. Experimental tests reveal that -- depending on the sampling interval -- velocities down to the mm/s-level can be resolved (Hohensinn et al., 2018a). Based on an experiment with a robotic arm it was shown that it can even be possible to detect movements at the sub-mm/s level (Hohensinn et al., 2019). Figure 3. 6 shows some results for the tests with the robot for a 1D sinusoidal movement, with GNSS measurements (GPS and Galileo) collected at a sampling rate of 1 Hertz. Plot (a) illustrates the magnitude of the estimated instantaneous velocity, together with the movements that were detected epoch-wise. The sinusoid can clearly be resolved, and the minimum detectable velocity lies at around 0.95 mm/s. Plot (b) shows the detected movements after applying a cumulative decision criterion extending over several epochs, with the goal to reduce the number of false alarms.

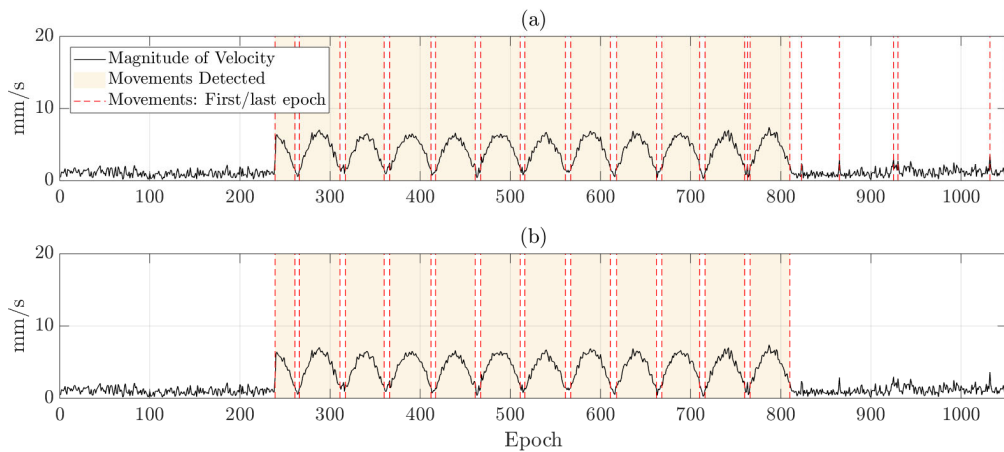


Figure 3. 6: Results for the tests with the robot arm for a sinusoidal movement. Plot (a) shows the magnitude of the estimated GNSS receiver velocity, and the movements that were detected epoch-wise. Plot (b) shows the detected movements after applying the cumulative decision criterium.

It can be concluded that the developed algorithm has the potential to resolve ground movements at the millimeter-per-second level, and even below. Movement information can be provided within seconds, and it thus can give an important contribution to natural hazard early warning systems. The algorithm was also successfully tested to detect and localize a strong earthquake in Central Italy. In order to enhance the reliability of the velocity estimates, ongoing research focusses on the further development of the integrity monitoring of the observations. Additionally, aspects on the quality of the velocity observations are further investigated in terms of multi-GNSS and multi-frequency processing, and the development of additional statistical testing criteria is envisaged.

furthest station, and around 5 dm/s for the station closest to the earthquake. The time-of-first arrival of the seismic waves was then used for a GNSS-only hypocenter determination of the earthquake. Based on a simple seismic velocity model, the hypocenter coordinates of the earthquake (together with the origin time) are estimated sequentially: It was started with the arrival times of an initial set of 7 stations, and then with each new detected arrival of a station, the hypocenter estimate was updated. Figure 3. 8 shows the results for a comparison with a precise (official) reference solution, both for the East and North component, as well as for the focal depth of the earthquake (red lines) and the origin time. The blue band indicates the standard deviation of the estimates.

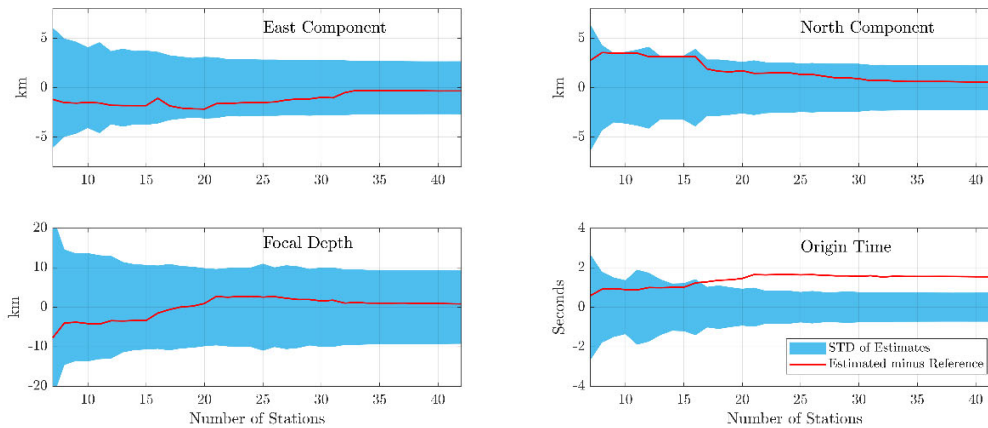


Figure 3. 8: Results from the GNSS-only earthquake hypocenter estimation. The red lines indicate the difference w.r.t. a reference solution. The blue band indicates the standard deviation of the estimates.

The GNSS-only hypocenter localization comes as close as 1 kilometer to the reference solution. It can be concluded that GNSS with densely deployed stations can give an independent contribution to an earthquake early warning system for strong earthquakes. Ongoing research focuses on the GNSS minimum detectable velocities depending on earthquake magnitude and station distance, and on a fully automatic characterization of the detected seismic phases.

Consistency of PPP GPS and strong-motion records: case study of Mw9.0 Tohoku-Oki 2011 earthquake

P. Psimoulis^{1,2}, N. Houlié^{2,3}, M. Meindl², and M. Rothacher²

¹*Nottingham Geospatial Institute, The University of Nottingham, Nottingham NG7 2TU, UK*

²*Geodesy and Geodynamics Lab., Geodesy and Photogrammetry Institute, ETH Zurich, Zurich 8093, Switzerland*

³*Seismology and Geodynamics, Institute of Geophysics, ETH Zurich, Zurich 8092, Switzerland*

GPS and strong-motion sensors are broadly used for the monitoring of structural health and Earth surface motions, focusing on response of structures, earthquake characterization and rupture modeling. Several studies have shown the consistency of the two datasets within at certain frequency (e.g., $0.03 < f < 0.2$ Hz). We assess the compatibility of Precise Point Positioning (PPP) GPS and strong-motion data by comparing their respective displacement waveforms for several frequency bands ($f < 0.3$ Hz). For this purpose, we use GPS and strong-motion records of the Mw9.0 Tohoku 2011 earthquake at 23 very closely spaced sites and conclude that the agreement between the two datasets depends on the frequency of the excitation, the direction of the excitation signal and the distance from the excitation source.

The displacement waveform analysis was applied for each one of the frequency bands and for each component of the 23 collocated GPS and strong-motion sites. Initially, the time lags between -2 and 3 seconds. The plot of the time lags of the three components of all frequency bands versus the distance from the epicenter shows that the time lags are independent of the distance from the epicenter and less dispersion appears at the time lags of the vertical component relatively to that of the horizontal components. The larger time lag for each collocated site appears generally at the highest frequency band for the horizontal components, while for the upward component this appears at the lowest frequency band. Furthermore, the time lags seem to be independent of the distance between the collocated sensors, indicating that the latter did not affect the collocation conditions of the two sensors.

Based on the computed time lags of the collocated sites, the corresponding displacement time series were shifted for the "synchronization" and the corresponding residuals were computed. The first impression of the GPS and strong-motion displacement time series (see Figure 3. 9) reveal rather small relative amplitude difference (i.e. ~6-7cm for the GPS550 and K-NET MYG011), which finally proved to be significantly larger according to the corresponding computed residuals. The amplitude of the residuals decreases with the increase of the frequency band and the distance from the epicenter. This is made clearer by computing the standard deviation and the maximum value of the residuals. The standard deviations range mainly between a few sub-millimeters up to 10cm, while the maximum estimated residuals range between 1mm and 30cm. By excluding the collocated sites very close to the epicenter (< 100 km), the computed standard deviation and maximum residuals ranges are limited up to 4-5 cm.

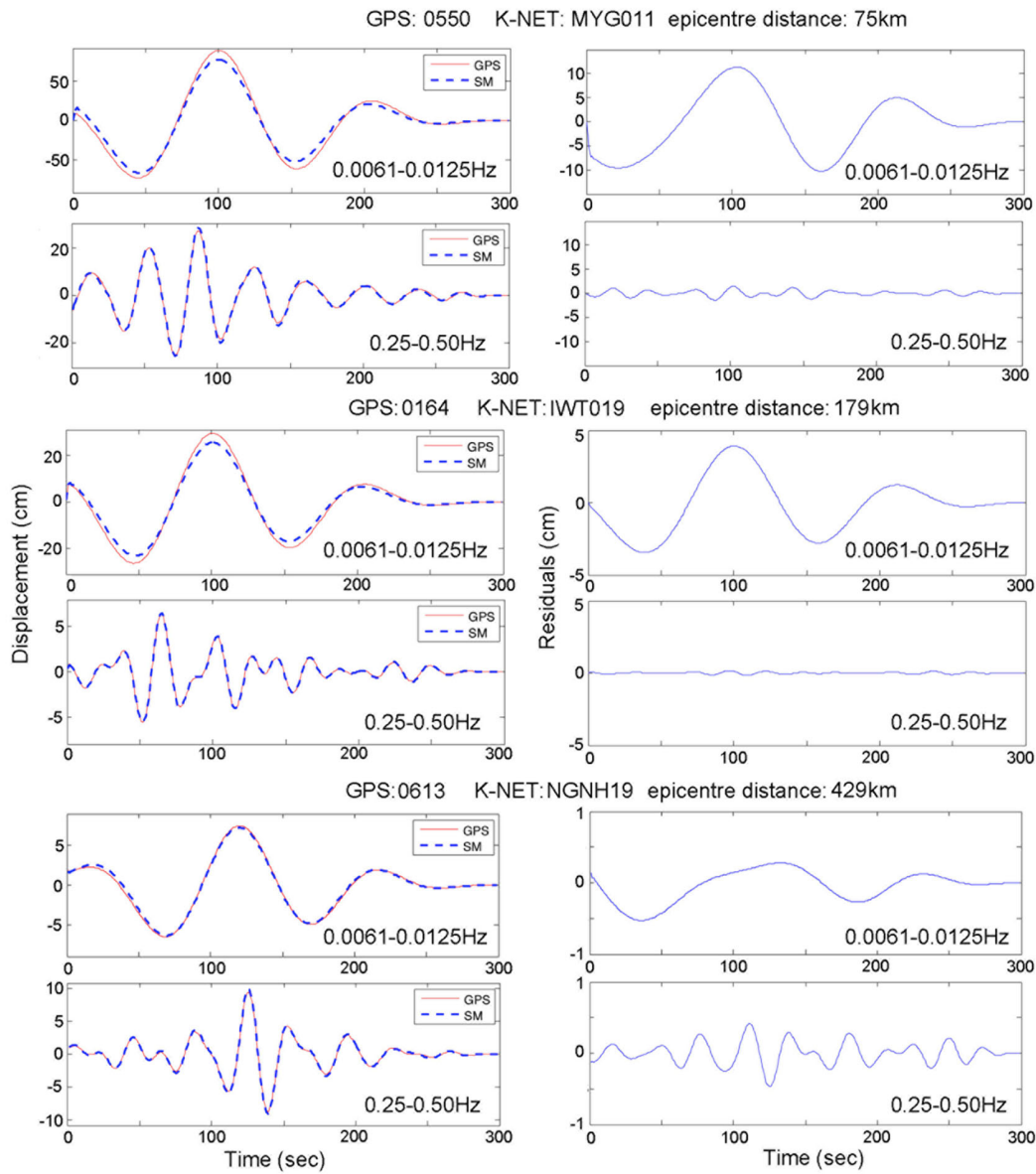


Figure 3. 9: Displacement of three collocated GPS and strong-motion sites for two frequency bands (0.0061-0.0125Hz and 0.25-0.50Hz) for three distances from the epicentre and the corresponding computed residuals.

Performance of high-rate GPS waveforms at long periods: Moment tensor inversion of the 2003 Mw8.3 Tokachi-oki earthquake

K. Kelevitz^{1,2}, N. Houlié^{1,2}, D. Giardini¹ and M. Rothacher²

¹ *Institute of Geophysics (SEG), ETH Zurich, Switzerland*

² *Mathematical Physical Geodesy (MPG), ETH Zurich, Switzerland*

We present the comparison of long period ($40 < T < 500$ s) 1Hz Global Positioning Systems (GPS) recorded in Japan during the 2003 Tokachi-Oki megathrust event ($M_w = 8.3$, 2003 Sept 25) with both very broadband seismograms and synthetic waveforms. We show that GPS can provide valuable data between periods of 40 s and 160 s, especially in the near-field of the earthquake where seismograms are clipped. In the light of the comparison with synthetic seismic displacement waveforms, the performance of GPS does not vary from 0 km to 1300 km. We conclude GPS waveforms recorded in the near-field of a large event can be used for seismological applications, such as characterising of earthquake moment tensors, imaging earthquake source, and investigate the structure of lithosphere and upper mantle. In this paper we recover the focal mechanism of the Tokachi-Oki event inverting the GPS data recorded within 300 km of the epicenter.

We suggest GPS records have the potential to supplement networks of broadband seismometers and to enhance the imaging of earthquake sources. Better characterization of finite seismic sources will then improve the imaging of large-scale structures in the upper- and mid-mantle. Next generation of velocity models can include these long-period data recorded by the high-rate GPS receivers. In the future we plan to use these GPS waveforms, not only on an ad-hoc basis after the largest events, but on a regular basis for earthquakes with magnitude $M_w > 6$, or even smaller as technology evolves further, and coverage of GPS stations increase. We will also be able to benefit from the Galileo satellites once they are fully operational, to reach even more accuracy with more satellites in the sky.

Use of a GPS-derived troposphere model to improve InSAR deformation estimates in the San Gabriel Valley, California

Nicolas Houlié^{1,2}, Gareth J. Funning³, and Roland Bürgmann⁴

¹MPG, Institute of Geodesy and Photogrammetry, ETH, Zurich, Switzerland

²SEG, Institute of Seismology and Geodynamics, ETH, Zurich, Switzerland

³Department of Earth Sciences, University of California, Riverside, CA, USA

⁴Berkeley Seismological Laboratory, University of California, Berkeley, CA, USA

We evaluate the potential of troposphere models derived from ground meteorological data (pressure, temperature and relative humidity) and GPS data to improve InSAR measurements and models derived from them. We test this approach on a ERS-2/ENVISAT dataset collected during a transient surface deformation episode that occurred from January to July 2005 in the San Gabriel Valley, southern California, USA. We find that the interferometric phase change observed over the corresponding period cannot be solely attributed to hydrological uplift associated with rising groundwater levels, but also includes a significant contribution from differential tropospheric delay due to differing quantities of water vapour in the troposphere on the two SAR observation dates. We show that if the tropospheric phase contribution is mistakenly interpreted as range change associated with changes in groundwater storage, both the surface displacement and the groundwater storage coefficient may be overestimated by up to 30%. This method could be applied in real-time where meteorological measurements are available near one or more GPS permanent site(s).

The correction proposed here is a first order correction that may improve the processing of InSAR data by correcting the troposphere contribution in quasi-realtime. Obviously, this approach is only possible in areas served by dense networks of continuous GPS sites (e.g. California and Japan), although through initiatives such as the Plate Boundary Observatory (PBO) under the EarthScope project, density of telemetered continuous GPS stations is ever-improving – indeed,

Figure 3. 10 shows how the network in the study area has been densified by the addition of PBO stations since 2005. Where the coverage is sufficient, it is not a great computational challenge to implement this type of analysis. A large data volume is not required (a 30-second sampling for GPS data is sufficient), and the analysis can be run episodically (in this case, every two hours), rather than continuously. In addition, the observation times of the major SAR satellites are known in advance, and thus additional models can be scheduled automatically to cover those times. Another feature of our strategy is that if a dense network is not available, the troposphere delay mapping and interpolation parameters can be adjusted to the current network density. Since most of the networks dedicated to the measuring of continental deformation have an inter-site distance of ~ 30–50 km, in such configuration our strategy would still be able to provide continuous static troposphere delay corrections at a given location, albeit at degraded resolution. Given the impact of troposphere corrections to GPS coordinate time series that results from the inclusion of meteorological data from a single site, an open question is whether further improvements across the network may be possible if additional such data were available at other sites.

One could envisage the widespread installation of meteorological sensors at continuous GPS stations as already seen for seismic instruments installed in insulated vaults. Campaign GPS measurements may also potentially benefit from temporary deployments of portable sensors during observation epochs. At the time of writing, meteorological data are increasingly, like some types of GPS data, available in real-time (from seconds to minutes after observations). The methodology presented in the study allows for the computation of troposphere delay maps in real-time at a sampling interval of less than 2 hours.

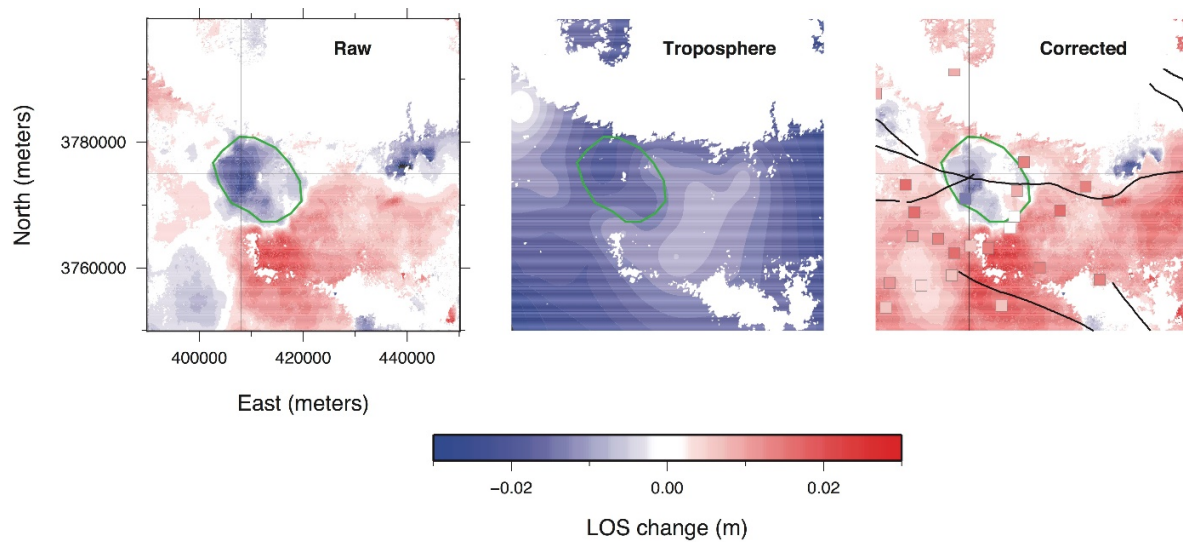


Figure 3. 10: Example of SAR troposphere correction. a) InSAR observables (unwrapped phase, converted to displacement) of the area between 2005, January 26th and 2005, July 20th. b) Interpolated troposphere model estimated from the GPS zenithal troposphere delay measurements after reprojection into the InSAR line-of-sight.

Vertical tectonics at an active continental margin

N. Houlié^{1,2} and T.A. Stern³

¹ *Institute of Geophysics (SEG), Earth Sciences Department (ERDW), ETH-Zurich*

² *Mathematical Physical Geodesy (MPG), Institut für Geodäsie und Photogrammetrie, ETH-Zurich*

³ *Victoria University, Wellington, New Zealand*

Direct observations of vertical movements of the earth's surface are now possible with space-based GPS networks, and have applications to resources, hazards and tectonics. Here we present data on vertical movements of the Earth's surface in New Zealand, computed from the processing of GPS data collected between 2000 and 2015 by 189 permanent GPS stations (Figure 3. 11). We map the geographical variation in vertical rates and show how these variations are explicable within a tectonic framework of subduction, volcanic activity and slow slip earthquakes. Subsidence of > 3 mm/yr is observed along southeastern North Island and is interpreted to be due to the locked segment of the Hikurangi subduction zone. Uplift of 1-3 mm/yr further north along the margin of the eastern North Island is interpreted as being due to the plate interface being unlocked and underplating of sediment on the subduction thrust. The Volcanic Plateau of the central North Island is being uplifted at about 1 mm/y, which can be explained by basaltic melts being injected in the active mantle-wedge at a rate of ~ 6 mm/y. Within the Central Volcanic Region there is a 250 km² area that subsided between 2005 and 2012 at a rate of up to 14 mm/y. Time series from the stations located within and near the zone of subsidence show a strong link between subsidence, adjacent uplift and local earthquake swarms.

The intent of this study is to assess the quality of the vertical GPS velocity field after a decade of GPS deployment within a plate boundary, while attempting to isolate regional trends of either subsidence or uplift. A first attempt at making a vertical uplift rate map from cGPS in New Zealand was made from data collected by just 27 stations of the LINZ array over 8 years (Houlié and Stern, 2012). At that time data points were too sparse to map local anomaly patterns with accuracy. In this study, the vertical rates of the 157 stations spanning up to 12 years allow the detection of a more diverse, and accurate patterns of uplift. We show that the vertical cGPS field is consistent with our knowledge of geological vertical movements, on both short and long term time scales, and with regional tectonics. The absolute level of vertical movement may still have > 2 mm/yr uncertainty, due to base line issues, but the uncertainty on relative movement for different parts of the country are now in the 1-2 mm/yr range. This pattern will consolidate and improve with another ~ 10 years of data.

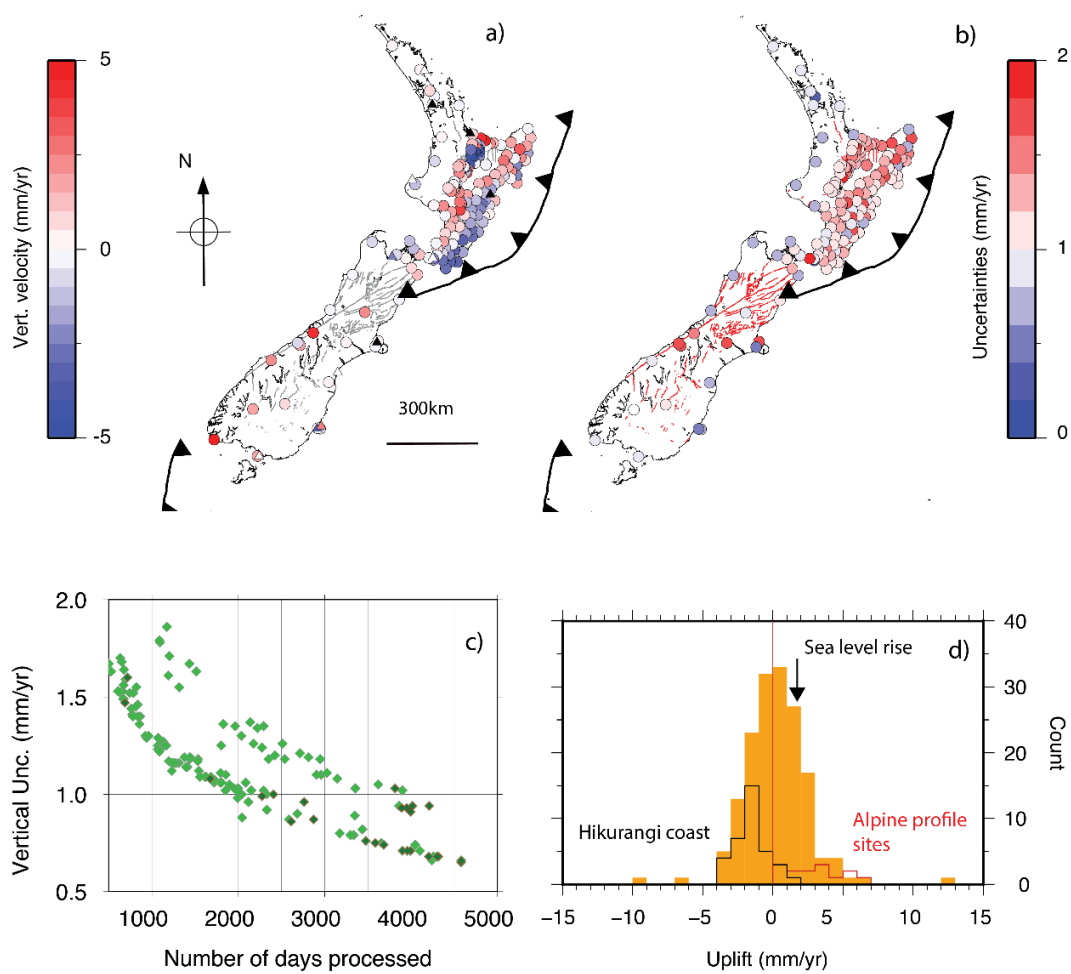


Figure 3. 11: Uplift rates (a) and associated uncertainties (b) for New Zealand adjusted as described in the text. (c) Uncertainties for cGPS stations plotted against number of days processed (green diamonds, in days). In supplementary materials, same plots are available for each subnetwork. Deep green diamonds are stations of the "LINZ" back bone array. (d) Distribution of uplift rates showing the approximate normal distribution with a mean of -0.4 mm/yr (standard deviation of 3.6 mm/yr , average uncertainty = 1.2 mm/yr). If the Rotorua stations are excluded, the mean is 0.1 mm/yr , std deviation = 2.9 mm/yr and the average uncertainty = 1.2 mm/yr . Rates for other station groups are presented in Table 1. We group as "Hikurangi" the sites located in eastern North Island along the Pacific coast. There is a spatial coincidence of the subsidence in this area with the area for which the subduction is thought to be locked. All rates are presented in the supplementary materials. For reference, campaign vertical rates constrained across Alpine fault by Beavan et al. (2010) are shown in red. Faults lines are from the GNS fault data base (<https://data.gns.cri.nz/af/>) (GNS New Zealand, 2015).

The potential of high-rate GPS for strong ground motion assessment

C. Michel¹, K. Kelevitz², N. Houlié², B. Edwards³, P. Psimoulis⁴, Z. Su⁵, and D. Giardini²

¹ Swiss Seismological Service (SED), ETH Zurich, Switzerland

² Institute of Geophysics (SEG), ETH Zurich, Switzerland

³ Department of Earth, Ocean and Ecological Sciences, University of Liverpool, UK

⁴ Nottingham Geospatial Institute, University of Nottingham, UK

⁵ Mathematical Physical Geodesy (MPG), ETH Zurich, Switzerland

We show that high-rate GPS can have a vital role to play in near real-time monitoring of potentially destructive earthquakes. We do this by investigating the potential of GPS in recording strong ground motions from earthquakes in Switzerland and Japan. The study uses finite-fault stochastic ground motion simulation based on Fourier amplitude spectra and duration models previously developed for both countries, allowing comparisons in terms of both Fourier and time domain characteristics (here the Peak Ground Velocity, PGV).

We find that earthquakes of magnitude $M_w > 5.8$ can be expected to be recorded by GPS in real-time at 10 km distance, i.e. their Fourier spectrum exceeds the noise of the instruments enough to be used in strong motion seismology. Post-processing of GPS time series lowers the noise and can improve the minimum observable magnitude by 0.1-0.2. As GPS receivers can record at higher rates (> 10 sps), we investigate which sampling rate is sufficient to optimally record earthquake signals and conclude that a minimum sampling rate of 5 sps is recommended. This is driven by recording events at short distances (below 10 km for magnitude 6 events and below 30 km for magnitude 7 events).

Furthermore, the Maximum Ground Velocity derived from GPS is compared to the actual PGV for synthetic signals from the stochastic simulations and the 2008 $M_w=6.9$ Iwate earthquake. The proposed model, confirmed by synthetic and empirical data, shows that a reliable estimate of PGV for events of about magnitude 7 and greater can be basically retrieved by GPS in real-time and could be included for instance in ShakeMaps for aiding post-event disaster management (see Figure 3. 12).

We showed that GPS is able to provide critical data at intermediate to long periods ($T > 0.5$ s) for hazard assessment although the current standard sample rate for GPS is only 1 sps (Nyquist period of 2s). A useful estimate of PGV can even be retrieved for large earthquakes ($M_w > 7$). Given current processing techniques, the standard GPS sampling rate of 1 sps is sufficient for far field recordings of earthquakes. Higher sampling rates (5 sps or more) would however be required in order to record all possible on-scale energy for near field records (ie for stations located within a 10 km epicentral distance for magnitude 6 events and within 30 km for magnitude 7) and for megathrust earthquakes at larger distances. This higher sampling rate is particularly crucial in order to retrieve more accurate estimates of PGV in the near field. We find that using sampling rates above 5 sps does not provide any additional information for earthquake ground motion recordings except at very short distances (below 5 km). This is true even using more accurate post-processed methods. PGV values (especially those extracted using post-processed data) can complement PGV datasets from seismological stations when developing ground motion models, especially for large events where GPS data is available at short distances. Moreover, real-time GPS processing methods such as PPP would allow integration of high rate GPS data in near-real-time seismological products such as ShakeMap.

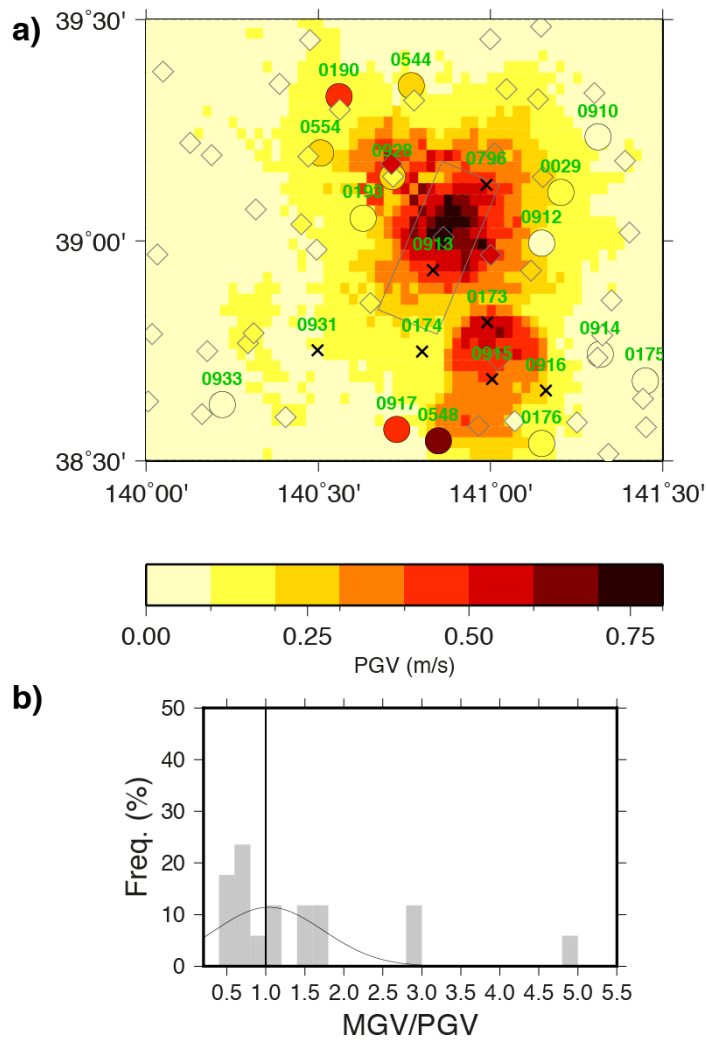


Figure 3. 12: a) USGS Shakemap of the Iwate-Miyagi Nairiku $M_w=6.9$ event and PGV from strong-motion stations (diamonds) compared to MGV derived from GPS (circles, station numbers provided). Crosses represent GPS stations that failed recording the event. The source extent is from Yokota et al. (2009). The good agreement between the ShakeMap and the GPS dataset suggests that the GPS data could have been integrated in a post-processed version.

b) Distribution of the MGV/PGV ratio for the available GPS stations. The fitted distribution uses the median and the LI norm.

Real-time magnitude characterization of large earthquakes using the predominant period derived from 1Hz GPS data

P. Psimoulis¹, N. Houlié^{2,3}, and Y. Behr⁴

¹ Nottingham Geospatial Institute, The University of Nottingham, Nottingham, NG7 2TU, UK

² Mathematical Physical Geodesy, Institute of Geodesy and Photogrammetry, ETH Zurich, Zurich 8093, Switzerland.

³ Seismology and Geodynamics, Institute of Geophysics, ETH Zurich, Zurich 8092, Switzerland

⁴ Swiss Seismological Service, ETH Zurich, Zurich 8092, Switzerland

Earthquake Early Warning (EEW) systems' performance is driven by the trade-off between the need for a rapid alert and the accuracy of each solution. A challenge for many EEW systems has been the magnitude saturation for large events ($M_w > 7$) and the resulting underestimation of seismic moment magnitude. In this study, we test the performance of high-rate (1Hz) GPS, based on seven seismic events, to evaluate whether long-period ground motions can be measured well enough to infer reliably earthquake predominant periods. We show that high-rate GPS data allow the computation of a GPS-based predominant period (τ_g) to estimate lower bounds for the magnitude of earthquakes and distinguish between large ($M_w > 7$) and great ($M_w > 8$) events and thus extend the capability of EEW systems for larger events. It is also identified the impact of the smoothing factors on the τ_g results and how the sampling rate and the computation process differentiates τ_g from the well-known τ_p .

We have shown that GPS can be used to constrain seismic moment M_w of large earthquakes ($M_w > 7.0$), by computing the predominant seismic period from GPS data (τ_g). The capability of GPS in recovering the period more accurately than the amplitude of the recorded motion (Psimoulis et al., 2008; Moschas & Stiros, 2014; Häberling et al., 2015) and the limited required filtering during the processing of GPS data (i.e. only differentiation) leads to robust and reliable estimation of τ_g without the problems of magnitude saturation known due to the processing procedure of the seismic data. The GPS τ_g estimation was computed by using two smoothing factors α (0.99 and 0.36), corresponding to low-pass filters with long- and short-period impulse responses (see Figure 3. 13). We further established τ_g - M_w laws, which can be used to complement τ_p - M_w relationships from seismic data to reliably constrain magnitude of earthquakes $> M_w 7.0$.

In conclusion, GPS-based EEW systems could be implemented and support existing seismic data-based EEW systems. τ_g time-series analyses would be routinely conducted estimating the τ_g^{max} values for the short- and long-period smoothing factors and by calculating the corresponding statistical characteristics (e.g. mean, spread, etc.) could provide the existing seismic warning systems with additional information to constrain the size of an earthquake of magnitude $M_w > 7$. The potential collocation of GPS and strong-motion sensors would lead potentially to even more accurate computation of the velocity through Kalman filtering (Bock et al., 2011) or other existing EEW algorithms (Benedetti, 2014) and enhance the performance of τ_g .

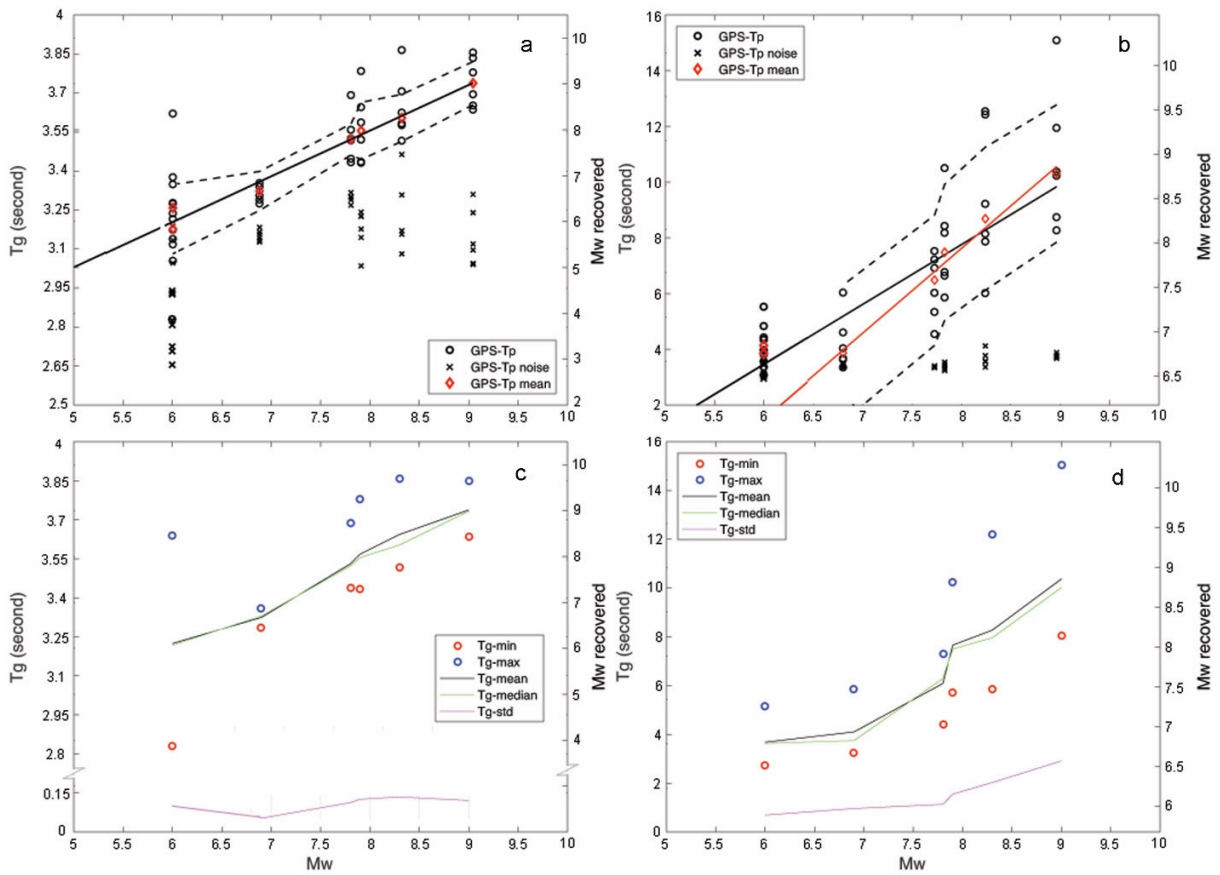


Figure 3. 13: (top panel) Semi-empirical relationship between magnitude and τ_g for the post-processed datasets (Tohoku-oki $M_W 9+$ 2011 and $M_W 7.9$ aftershock, Tokachi-Oki, 2003, Iwate 2008, Napa 2014 and Parkfield 2004) for (a) $\alpha=0.99$ (b) and $\alpha=0.36$. The median of each τ_g is indicated using a red diamond. The red solid line for $\alpha=0.36$ corresponds to the linear regression by excluding the earthquakes of $M_W 6.0$. The dotted lines express the uncertainty level of the M_W estimates. (bottom panel) Standard deviations, mean average, median, and maximum and minimum values for (c) $\alpha=0.99$ (d) and $\alpha=0.36$ for all τ_g measurements computed in this study. Three groups of events can be defined ($M_W < 7.0$, $M_W \geq 7.9-8.3$ and $M_W > 8.5$).

Detection of ground motions using high-rate GPS time-series

P. A. Psimoulis¹, N. Houlié^{2,3,4}, M. Habboub¹, C. Michel⁴, M. Rothacher²

¹ Nottingham Geospatial Institute, University of Nottingham, Nottingham, UK

² Mathematical and Physical Geodesy (MPG), Institute of Geodesy and Photogrammetry, ETH Zurich, Switzerland

³ Seismology and Geodynamics (SEG), Institute of Geophysics, ETH Zurich, Switzerland

⁴ Swiss Seismological Service (SED), Institute of Geophysics, ETH Zurich, Switzerland

Monitoring surface deformation in real-time help at planning and protecting infrastructures and populations, manage sensitive production (i.e. SEVESO-type) and mitigate long-term consequences of modifications implemented. We present RT-SHAKE, an algorithm developed to detect ground motions associated with landslides, sub-surface collapses, subsidences, earthquakes or rock falls. RT-SHAKE detects first transient changes in individual GPS time series before investigating for spatial correlation(s) of observations made at neighbouring GPS sites and eventually issue a motion warning. In order to assess our algorithm on fast (seconds to minute), large (from 1cm to meters) and spatially consistent surface motions (see Figure 3. 14), we use the 1Hz GEONET GNSS network data of the Tohoku-Oki M_w 9.0 2011 as a test scenario. We show the delay of detection of seismic wave arrival by GPS records is of ~ 10 seconds with respect to an identical analysis based on strong-motion data and this time delay depends on the level of the time-variable noise. Nevertheless, based on the analysis of the GPS network noise level and ground motion stochastic model, we show that RT-SHAKE can narrow the range of earthquake magnitude, by setting a lower threshold of detected earthquakes to M_w 6.5-7, if associated with a real-time automatic earthquake location system.

We successfully present RT-SHAKE, an algorithm designed to detect surface motions using GNSS real-time data streams. The testing and calibration of RT-SHAKE using Tohoku M_w 9.0 2011 earthquake dataset revealed that the GPS network data can be used to detect ground motion larger than 1-2cm with great robustness; the displacements of the ground motion may correspond to a wide range of geohazards (e.g. large earthquakes, landslides, cliff collapses). RT-SHAKE based on GPS data proved to be consistent with results derived by the KiK-net and K-NET strong motion networks and due to the exceptional dimensions of the Tohoku-oki 2011 earthquake, the GPS network detected displacements corresponding to P-waves. The delay of ~ 5 -10s in the detection of the ground motion relatively to the strong motion networks due to the higher noise level of the GPS time series.

The two-stage checks of the RT-SHAKE algorithm aim to eliminate the false alarms by resolving problems of outliers or GPS site-specific effect. The checks of the RT-SHAKE algorithm manage to limit the false alarms to nine for the period prior to the earthquake, corresponding to GPS time series of ~ 15000 samples. The false alarms still occur, due to triggering by GPS-sites, which are affected by poor satellite constellation or problematic satellite(s) (Msaewe et al., 2017). However, this weakness can be resolved by using additional parameters, such as the DOP values or the SNR of the satellite signals, to evaluate whether a potential detected motion is real or an artefact of the GPS solution due to the satellite constellation, the satellite signal and/or local interference (Msaewe et al., 2017, Peppas et al., 2018). Additional techniques for the long-term analysis of the GPS time series, such as neural networks, may be used to enhance the modelling of the GPS time series and limit number of false alarms (Kaloop and Hu, 2015). Since the algorithm is developed to be able for application also in other sensors (i.e. seismic sensors, tiltmeters, etc.), potential triggered GPS sites could be spatially checked with additional sensors of other monitoring networks, to limit even further the false alarms.

The developed algorithm can be used not only for the detection of the ground deformation due to earthquakes, but also for the direct monitoring of other types of geohazards related to motion (e.g. landslides, tsunamis, volcanoes), through the detection of the propagated motion. The GPS detection may be delayed with respect other sensors (i.e. seismic sensors, accelerometers, etc.), but still provide prompt information about the severity and the spatial characteristics of a given event. Following appropriate modifications the same code may be applied to real-time data from seismic data and/or other sensors to monitor geohazards.

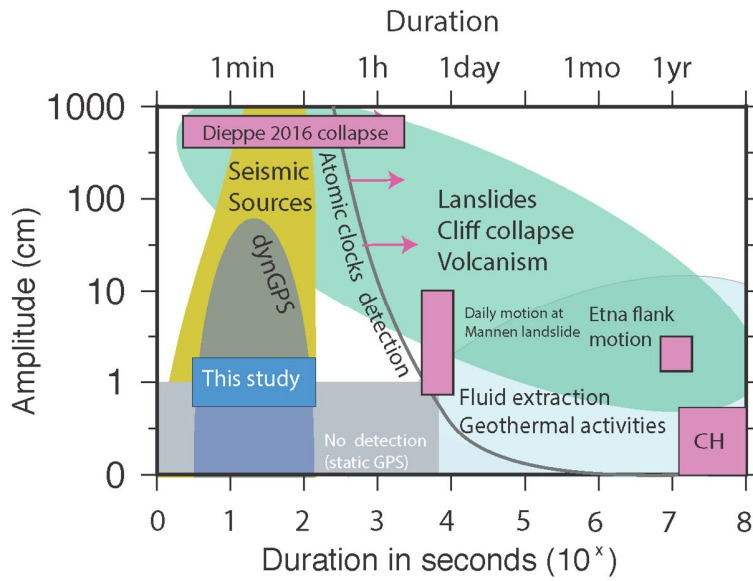


Figure 3. 14: Amplitude vs duration diagram for various geological catastrophic processes. We show detection limits for GPS, dynamic GPS and micro-gravimetry. In this study, as in any real-time algorithm, we focus on detecting small amplitudes as fast as possible. dynGPS curves are from analyses of dynamic GPS time-series recorded during seismic wave propagations (Houlié et al., 2014; Houlié et al., 2011; Kelevitz et al., 2017). Sensitivity curve for atomic clock are from (Bondarescu et al., 2012; Bondarescu et al., 2015). Slower deformation cases are from Houlié et al., 2006 for Etna and Houlié et al., 2018 for deformation in Switzerland (indicated by CH in Figure). Static GPS is able to detect motion larger than 1cm for duration larger than 10^4 seconds and then is naturally well supplemented by the Blum's silica inclinometer (Blum et al., 1959; Saleh et al., 1991; Llubes et al., 2008).

Bibliography Commission 3

- Clinton, J., Geiger, A., Häberling, S., Haslinger, F., Rothacher, M., Wiget, A., Wild, U. (2017): The Future of National GNSS-Geomonitoring Infrastructures in Switzerland. *Geodätisch-geophysikalische Arbeiten in der Schweiz*, Vol. 100. <http://www.sgc.ethz.ch/sgc-volumes/sgk-100.pdf>
- Dach, R., E. Brockmann, S. Schaer, G. Beutler, M. Meindl, L. Prange, H. Bock, A. Jäggi, L. Ostini (2009): GNSS Processing at CODE: status report. *Journal of Geodesy* (special Issue: The International GNSS Service (IGS) in a Changing Landscape of Global Navigation Satellite Systems, guest editor C. Rizos), vol. 83(3-4), pp. 353-366, DOI 10.1007/s00190-008-0281-2.
- Dach, R., Lutz, S., Walser, P., Fridez, P., editors (2015): Bernese GNSS Software, Version 5.2. Astronomical Institute, University of Bern, Bern, Switzerland, ISBN 978-3-906813-05-9. doi: 10.7892/boris.72297. User manual.
- Dach, R., S. Schaer, D. Arnold, L. Prange, D. Sidorov, P. Stebler, A. Villiger, A. Jäggi (2018): CODE final product series for the IGS. Published by Astronomical Institute, University of Bern. URL: <http://www.aiub.unibe.ch/download/CODE>; DOI: 10.7892/boris.75876.3.
- Hohensinn, R., Geiger, A., and Meindl, M. (2018a). Minimum detectable velocity based on GNSS Doppler phase observables. In *European Navigation Conference (ENC) in Gothenburg, Sweden, 2018. IEEE*.
- Hohensinn, R. and Geiger, A. (2018b). Stand-alone GNSS sensors as velocity seismometers: Real-time monitoring and earthquake detection. *Sensors*, 18(11):3712.
- Hohensinn, R., Geiger, A., Willi, D., and Meindl, M. (2019). Movement detection based on high-precision estimates of instantaneous GNSS station velocity. *Journal of Surveying Engineering* (forthcoming).
- Houlié, N., Funning, G. and R. Bürgmann, (2016), Use of a GPS-derived troposphere model to improve InSAR deformation estimates in the San Gabriel Valley, California, *IEEE Trans. Geosc. Rem. Sens.*, 54, 9, 10.1109/TGRS.2016.2561971
- Houlié, N. and T. A. Stern, Vertical tectonics at an active continental margin, (2017), *EPSL*, 457, 292-301, 10.1016/j.epsl.2016.10.018
- Kelevitz, K., Houlié, N., Giardini, D. and M. Rothacher, (2017), Performance of high-rate GPS waveforms at long periods: Moment tensor inversion of the 2003 Mw8.3 Tokachi-oki earthquake, *BSSA*, 107(4), 1891-1903, 10.1785/0120160338
- Lutz, S., P. Steigenberger, R. Dach, S. Schaer, K. Sošnica; 2015: Reprocessing activities at CODE. Swiss National Report on the Geodetic Activities in the years 2011-2015, Section 1 (Reference Frames), Swiss Geodetic Commission, A. Wiget (Ed), pp. 17-18, XXVI General Assembly of the IUGG, Prague, Czech Republic, 22 June - 2 July 2015, ISBN 978-3-908440-39-0.
- Meindl, M (2011): Combined analysis of observations from different global navigation satellite systems. *Geodätisch-geophysikalische Arbeiten in der Schweiz*, vol 83, Eid. Technische Hochschule Zürich, Switzerland
- Meindl, M, Beutler, G, Thaller, D, Dach, R, Jäggi, A (2013): Geocenter coordinates estimated from GNSS data as viewed by perturbation theory. *Adv Space Res* 51(7):1047–1064. doi: 10.1016/j.asr.2012.10.026
- Michel, C., Kelevitz, K., Houlié, N., Edwards, B. Psimoulis, P., Su, Z. Clinton, J.F. and D. Giardini, (2017), The potential of high-rate GPS for strong ground motion assessment, *BSSA*, 107(4), 1849-1859, 10.1785/0120160296

- Psimoulis, P., Houlié, N., Meindl, M. and Rothacher, M. (2015), Consistency of GPS and strong-motion records: case study of Mw9.0 Tohoku-Oki 2011 earthquake, *Smart Structures and Systems*, 16, 2, 347-366, preprint, 10.12989/sss.2015.16.2.347.
- Psimoulis, P., Houlié, N. and Y. Behr, (2018), Real-time magnitude characterization of large earthquakes using the predominant period derived from 1Hz GPS data, *GRL*, 45, 2, 517-526, 10.1002/2017GL075816
- Psimoulis, P., Houlié, N., Habboub, M., Michel, C. and M. Rothacher, (2018) Detection of ground motions using high-rate GPS time series, *Geophysical Journal International*, 214(2), 1237-1251, 10.1093/gji/ggy198
- Ray, J, Altamimi, Z, Collilieux, X, van Dam, T (2008): Anomalous harmonics in the spectra of GPS position estimates. *GPS Solut* 12(1):55–64. doi: [10.1007/s10291-007-0067-7](https://doi.org/10.1007/s10291-007-0067-7)
- Ray, J, Griffiths, J, Collilieux, X, Rebischung, P (2013): Subseasonal GNSS positioning errors. *Geophys Res Lett* 40(22):5854–5860. doi: [10.1002/2013GL058160](https://doi.org/10.1002/2013GL058160)
- Scaramuzza, S., Dach, R, Beutler, G, Arnold, D, Sušnik, A, Jäggi, A (2017): Dependency of geodynamic parameters on the GNSS constellation. *J Geod* 92(1):93-104. doi: 10.1007/s00190-017-1047-5
- Schaer S, Arnold D, Dach R, Prange L, Sidorov D, Stebler P, Sušnik A, Villiger A, Jäggi A (2019): CODE Contributions to the IGS; this volume.

4 Positioning and Applications

Dragon 4: Snow Depth and Snow Water Equivalent Estimation by Using Reflected and Refracted GPS Signals

L. Steiner¹, W. Li², M.Meindl¹, Y. Zhu², A. Geiger¹, D. Yongkai²

1 Institute of Geodesy and Photogrammetry, ETH Zurich

2 Department of Information and Communication Engineering, Beihang University, Beijing, China

This project is carried out in cooperation with the Department of Information and Communication Engineering at Beihang University within the ESA Dragon 4 framework. Dragon is a cooperation between ESA and the Ministry of Science and Technology (MOST) of the P.R. China. Dragon 4 focuses on the scientific exploitation of ESA, ESA Third Party Missions, Copernicus Sentinels and Chinese EO data for geo-science and applications development. Accurate and reliable in situ data is needed for calibration and validation of remote sensing data. GNSS remote sensing techniques could provide reliable, accurate, efficient, and continuous observations independent of weather conditions.

The project aims on the combination of GPS-reflectometry (GPS-r) for snow depth estimation with GPS-refractometry for snow water equivalent (SWE) determination, leading to additional snow characteristics as the bulk snow density. The snow depth and SWE distribution is strongly heterogeneous, whereas the bulk density is observed to be more stable in terms of its spatial distribution. Snow depth retrievals are validated against reference data observed by a sonic ranger. SWE results are validated against SWE data converted from Snow Micro Pen (SMP) observations within the test-site, based on the observed bulk snow density and snow depth. A GPS snow monitoring system is installed at the narrow Grimsel mountain pass located in the Swiss Alps and is surrounded by high mountains.

The GPS-r retrieved snow depth shows a certain correlation to the reference snow depth. However, compared with the situation with simple terrain (single reflector, no obvious obstructions around), the correlation value is significantly lower. Especially in mountainous areas the reflectors (e.g. flanks of a Peak) lead to difficult interpretations of the measurements. The terrain influences thereby the precision of the retrieved snow depth seriously. The model has thus to be further developed to account for multiple reflections. Sub snow GPS with low cost equipment enables accurate estimation of SWE when the station coordinates are known and fixed. GPS refractometry is able to correct the influence of the snow pack above the buried antenna. The systematic and stochastic snow induced effects in the GPS residuals are significantly reduced by estimating the SWE above the antenna. The presented method is promising as the snowpack is not destroyed or disturbed due to the automated, continuous, self-sustainable observation method and the effort for installation is relatively small. The combination of snow depth and snow water equivalent observations by the use of reflected and refracted GPS signals allows further parameter retrieval, e.g. bulk snow density.

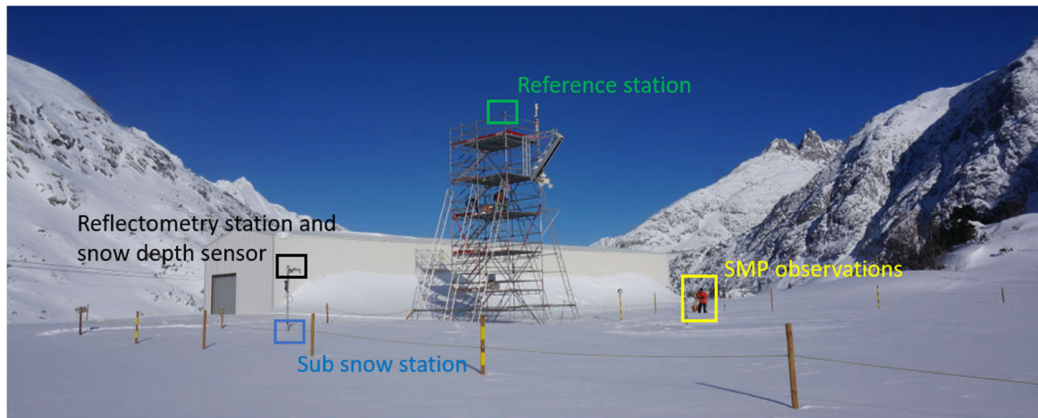


Figure 4. 2: Grimsel test-site equipped with the GPS snow monitoring system and a snow depth sensor. Manual Snow Micro Pen (SMP) observations are carried out sporadically at the North East side. Tower construction enabling Snow-Scat radar experiment (Gamma Remote Sensing AG, ESA).

Snow Water Equivalent Observations Using Refracted GPS Signals

L. Steiner¹, M. Meindl¹, C. Marty², C. Fierz², A. Geiger¹

1 Institute of Geodesy and Photogrammetry, ETH Zurich

2 WSL Institute for Snow and Avalanche Research SLF

Knowledge of snow characteristics is an important basis for climatology, natural hazards forecasting, early-warning systems, and hydro-energy industries. An extensive amount of water is stored in snow covers, which has a high impact on flood development during snow melting periods. Early assessment of the snow water equivalent (SWE) in mountain environments enhances early-warning and thus prevention of major impacts. Extensive observations of SWE are challenging due to the heterogeneity of snow distribution caused by mountainous terrain and environment. Global navigation satellite system (GNSS) remote sensing techniques are capable to provide reliable, accurate, efficient, and continuous observations independent of weather conditions.

This project was funded by the Swiss National Science Foundation was carried out in collaboration with the WSL Institute for Snow and Avalanche Research SLF. The main objective of this project was a thorough investigation of the contribution of geodetic GNSS remote sensing techniques to observe and quantify mountainous SWE. This investigation is based on differential GPS processing using refracted GNSS phase signals received by commercially available off-the-shelf GNSS antennas buried underneath a typical Alpine snowpack. The main tasks have been: a) Identification of the theoretical and empirical characteristics and limitations of GPS L1 single-frequency observations using submerged GPS antennas, as well as the development of a mathematical model for SWE estimation; b) Application of the developed model to an Alpine seasonal snowpack and investigation of the potential for SWE quantification; c) Identification of the main impacts of GPS processing on the accuracy of the derived SWE estimates when using refracted GPS signals. Further evaluation is based on the possibility of using low-cost GPS equipment for SWE quantification. Liquid water is expected theoretically to exert the largest influence on a GPS signal propagation through a snowpack. An experimental setup has been established to investigate the influence of liquid water on the GPS observations by testing water levels up to the signal penetration depth of 35mm above the antenna. Results correspond well with theory and the water level above the submerged antenna could be estimated using the derived model with sub-millimeter accuracy.

The potential of using refracted GNSS signals for SWE estimation has been evaluated based on an experimental setup at a seasonal Alpine snowpack. The study is carried out at the WSL Institute for Snow and Avalanche Research SLF test-site “Weissfluhjoch” above Davos, Switzerland (Figure 4. 3). A measurement network has been installed, consisting of a GPS reference station above the snowpack and a GPS antenna mounted on the ground underneath the snowpack. The empirical SWE results are validated against the state-of-the-art reference sensors snow pillow, snow scale, and manual observations over three seasons (2015/16 - 2017/18). The comparison shows a high level of agreement with a relative bias below 5% (RMSE of 38 mm w.e.) over all three seasons, including the melting periods (Figure 4. 4). SWE could be accurately estimated with a high temporal resolution of every hour. The applied ambiguity resolution strategy and the selection of an elevation cut-off angle and weighting function could be identified as the three most important GPS processing options influencing the quality of the resulting SWE estimates.



Figure 4. 3: SLF test-site "Weissfluhjoch" above Davos, Switzerland.

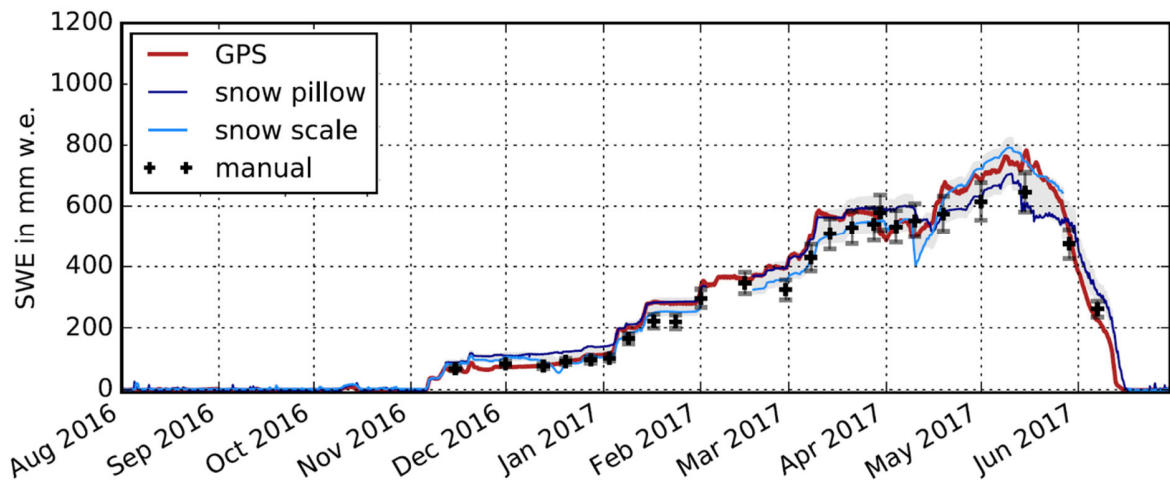


Figure 4. 4: GPS derived SWE time series for the 2016/17 season. A relative bias of 10% of the mean of the snow pillow and snow scale (gray background) visualizes the uncertainty of the reference snow pillow and snow scale values. Gray bars indicate a 10% relative bias for the manual observations.

Space Environmental Tests of Low-Cost GNSS receivers

M. Meindl, M. Rothacher

Institute of Geodesy and Photogrammetry, ETH Zürich, Switzerland

The Institute of Geodesy and Photogrammetry has made considerable efforts to up-screen the low-cost commercial-off-the-shelf (COTS) GNSS receiver u-blox M8T for space usage. The procedure encompasses space environmental tests, in particular radiation, temperature, and vacuum tests.

Radiation tests

The radiation tests have been conducted at the proton irradiation facility (PIF) of the Paul Scherrer Institute (PSI) in Villigen, Switzerland (Senn and Hügi, 2017). Two different experiments have been carried out at the PSI:

- a total ionizing dose (TID) test to assess the positioning performance of the receivers after being exposed to irradiation and to detect any non-reversible hardware failures;
- an analysis of single event effects (SEE) to characterize the receiver behavior during irradiation.

During the TID experiments, the devices under test (DUT) have been irradiated for 60 minutes with the total dose expected in a three-year mission run time (20 krad). The second experiment was designed to provoke and analyze single event effects. The receivers have been exposed to radiation at a constant flux at three different energy levels (50, 100, 150 MeV) for 15 minutes each. Four receivers have been exposed to the radiation during each experiment; a different set of receivers was used for the TID and SEE tests. During the full test procedure, a simulated antenna signal as received by a low Earth orbiting satellite was fed to the receivers. The quality of the receiver provided position, velocity and time (PVT) has been evaluated for all DUT before and after the irradiation to identify possible quality degradations caused by the radiation.

The most important result of the TID test is that all four receivers were still fully functional after the experiments. The performance of the receivers seems unaltered by the exposure to the radiation; the quality of the PVT solutions is the same before, during and after the irradiation. The receiver clock drift increased significantly when exposed to radiation. However, the increased clock drift values all stayed within a completely uncritical range (about a factor of 1000 smaller than the critical limit) and do not prevent the receivers from functioning. These findings confirm a basic suitability of the u-blox M8T receivers for space in accordance to the satellite mission parameters.

The SEE tests showed that one might expect a single event effect every 4 days in orbit. These SEEs usually lead to a quite harmless soft reset of the receiver and finally to only a few seconds without a PVT solution. Every 20 days, a severe SEE must be expected leading to a hard reset of the receiver, which in turn leads to missing PVT solutions for up to a minute. In all cases, however, the receivers reinitialized themselves without any interaction from the operator. This is quite important for an autonomous operation in space.

Thermal and vacuum tests

Equipment suitable for space operations must not only function well in a harsh radiation environment but is also subject to vacuum and high temperature variations. The u-blox GNSS receivers are built for Earth-bound applications. Especially the high vacuum in space might cause problems by outgassing of the components, which, e.g., might lead to broken solder joints or even to the physical destruction of the receiver. A series of environmental tests in a thermal vacuum chamber (TVC) have been conducted at the RUAG space facilities in Zurich, Switzerland.

Three receivers have been tested in vacuum during a repeating series of five temperature cycles covering -40° up to $+80^{\circ}$. A simulated GPS signal was fed to the receivers during the test. The resulting PVT solutions during the

vacuum/temperature tests, as well as before and after the experiments have been recorded to evaluate the correct functioning of the DUTs. The chamber temperature and pressure have been recorded, as well.

The most important result of the TVC experiments is that none of the three receivers was destroyed neither from vacuum nor from temperature. For the temperature, this is not surprising as the receivers are officially specified for a temperature range of -40°C to 80°C (u-blox, 2016). Moreover, the PVT solution of the receivers did not suffer during the experiments, i.e., the receivers performed equally well under vacuum as under normal conditions. No resets or extraordinary events like loss of locks could be observed. An interesting behavior can be observed, when looking at the estimated drifts of the internal temperature controlled crystal oscillator (TCXO). Figure 4. 5 shows the estimated clock drift for receiver 1 over the full 5 temperature cycles as a function of temperature. Heating phases are indicated in red color, cooling phases in blue. The clock drift increases if the temperature falls and vice versa. The drift changes show a similar behavior between cooling and heating phases but with an offset. This effect may result from the clock steering.

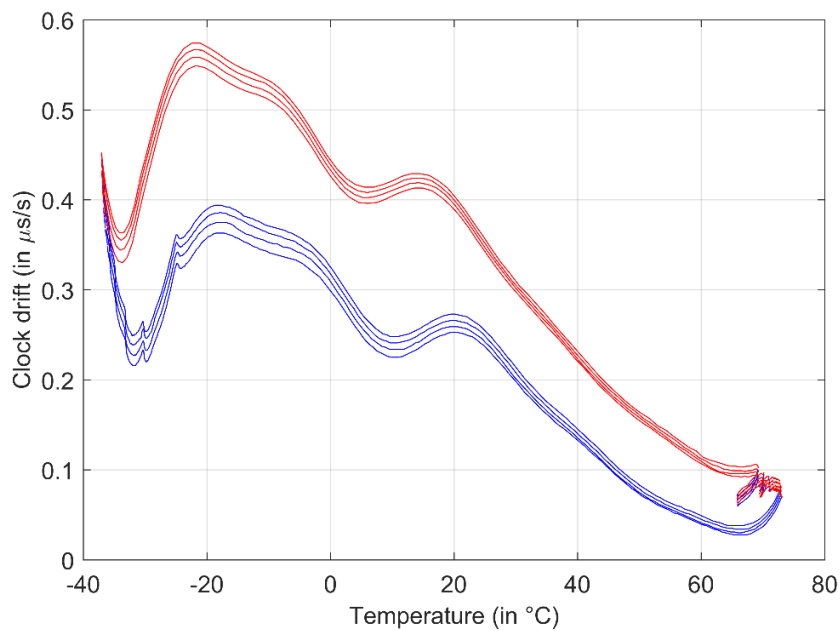


Figure 4. 5: Estimated clock drift (red: heating phase, blue: cooling phase)

The radiation tests as well as the temperature and vacuum tests showed that the receiver hardware is quite resistant to harsh space environmental influences. All devices worked equally well before, during and after the tests. All estimated parameters remain easily within uncritical limits. This is very encouraging as it demonstrates that this type of receiver may very well be used for space applications.

A GNSS Payload with Low-Cost Commercial-Of-The-Shelf Receivers

M. Meindl, F. Kreiliger, K. Chen, M. Rothacher

Institute of Geodesy and Photogrammetry, ETH Zürich, Switzerland

Motivation

Global Navigation Satellite Systems (GNSS) are nowadays one of the standard techniques for orbit and attitude determination. With the increasing popularity of small satellites like, e.g., the CubeSat standard, the need for an adapted small orbit determination payload increases. Therefore, we developed a small-sized versatile GNSS payload board (see Figure 4. 6, left) based on commercial-of-the-shelf GNSS receivers with extremely small weight (2 g), size (12 x 16 x 2.4 mm), power consumption (100 mW) and costs (€ 100). The board features two separate antenna connectors and four GNSS receivers—two per antenna. This redundancy lowers the risk of total payload failure in case one receiver should malfunction.

On December 3, 2018, a prototype of the GNSS positioning board was successfully launched to space onboard the Astrocast-01 (www.astrocast.com) 3-unit cube satellite (Figure 4. 6, right). In addition to the GNSS payload, the satellite is equipped with an array of three laser retro-reflectors allowing the validation of the orbit with satellite laser ranging. A second satellite (Astrocast-02)—also carrying the GNSS board—was launched on April 1, 2019.

A special feature of the integrated receivers is their multi-GNSS capability allowing the concurrent tracking of satellites from the four major systems GPS, GLONASS, BeiDou and Galileo. Moreover, the raw observation data can be recorded for a precise orbit determination in post-processing.



Figure 4. 6: GNSS payload board (left) and Astrocast-01 satellite (right) with GNSS antennas located on top and on front face.

Up-screening of receivers for space

As the receivers are, initially, not intended to be used in space applications, they have been tested for vacuum, temperature variations and irradiation. Hardware status, receiver performance and power consumption were monitored closely during all the tests. During the vacuum experiments, the receivers had to pass temperature cycles from +80°C to -40°C for several hours. The radiation hardness of the receivers was tested by putting the samples under a proton beam. A total ionizing dose of 20 krad was applied over 1 hour corresponding to about 3 years of lifetime at an orbital height of 575 km. In a dedicated irradiation experiment, the frequency of single event effects (SEE) has been assessed. The most severe SEEs forced the receivers in a hard reset state, which resulted in a cold start. After about one minute, the GNSS receiver again provided reliable navigation solutions. No receivers have been damaged or even been destroyed during the up-screening procedure.

In-orbit tests and validation

Three weeks after the launch of Astrocast-01, the first payload data was received including position, velocity and time (PVT) computed on-board by the receiver. This first data allowed the assignment of the satellite to a specific set of two-line elements provided by USSPACECOM and thus a definite identification of the satellite. The Astrocast-02 satellite could also be easily identified a few days after the launch by using the PVT solution.

To date we have continuous receiver PVT solutions available for both satellites but no raw observations yet. First orbit determination results indicate that the receivers perform very well. Figure 4. 7 shows that the orbit fit RMS for daily arcs is on the level of 2 meters. As we are restricted to the single frequency receiver solution, however, the results are biased by a systematic error caused by the ionosphere.

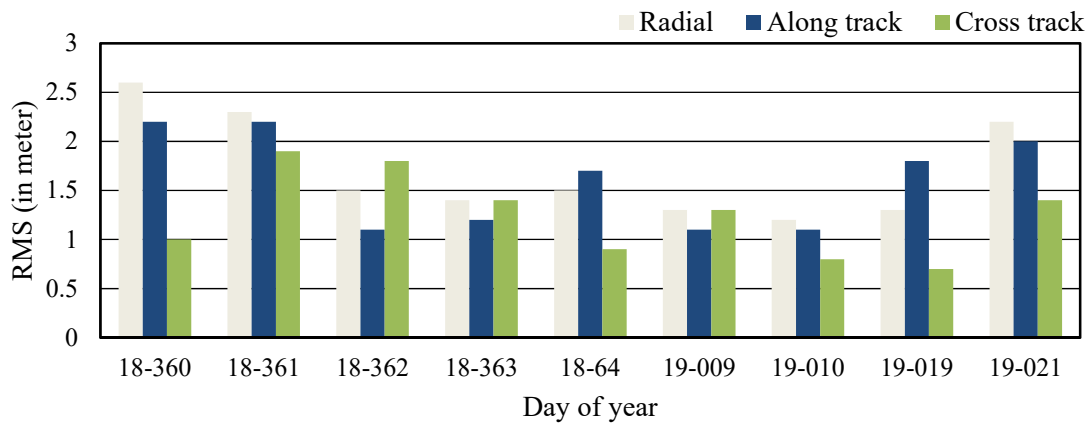


Figure 4. 7: Orbit fit RMS for various one-day arcs

Once raw observation data and long continuous observation arcs will be available, we will start an extensive quality assessment and orbit validation phase based on a precise orbit determination post-processed on ground. The tests will especially include

- an assessment of the achievable orbit quality and an overall performance estimation;
- an improvement of the orbit quality by eliminating the ionosphere effect based on a linear combination of phase and code observations;
- the evaluation of the quality of orbit predictions over one and more days (which will be especially important for scheduling SLR observation campaigns);
- orbit validations based on inter-technique comparisons with SLR observations;
- comparison of various single-system and multi-GNSS solutions.

Visibility Based Attitude Determination for Satellites

M. Meindl, G. Tagliaferro, M. Rothacher

Institute of Geodesy and Photogrammetry, ETH Zürich, Switzerland

Attitude determination is a requirement for many satellite missions. Besides star tracking camera systems, global navigation satellite systems (GNSS) may be used for that purpose. If the satellite is equipped with at least three different antennas and GNSS receivers, the attitude may be recovered by forming two baselines between the antennas and estimating Eulerian rotation angles between a body-fixed and the inertial reference frame. One such algorithm using low-cost receivers is described by Willi et. al (2017).

If only one receiver/antenna pair is available on the satellite, an approximate attitude may be derived based only on the visibility of the GNSS satellites. Note, however, that only a reduced attitude can be estimated: the rotation around the zenith direction of the satellite's antenna cannot be determined. If a second antenna/receiver pair is available pointing in a different direction (ideally in a perpendicular direction like a side-mounted antenna), the two separately estimated boresight vectors may be combined yielding the full satellite attitude.

The proposed algorithm (Tagliaferro, 2017) is basically a two-step procedure:

1. For each visible GNSS satellite, the allowed location (represented as a polygon on a unit sphere centered at the satellite) of the antenna boresight vector is computed. If more than one epoch is taken into account, the allowance region may be further reduced by incorporating rising or setting constraints for the satellites.
2. The union of all single satellite areas of allowance computed in step 1 is created. The final attitude is then estimated as the center of mass of the resulting unified area. Before this step is carried out, the shadowing effect of the Earth (blocking the visibility of certain GNSS satellites) must be taken into account.

If a second (side-looking) antenna is available, two polygons result restricting the possible pointing directions of both antennas. The full attitude can now be derived by finding perpendicular vectors lying in the plane spanned by the two single boresight vectors (including a weighting of the single vectors). The third vector completes a right-hand system. Figure 4. 8 shows a graphical representation of this combination step. All parts of the attitude determination procedure involve quite intricate geometrical computations.

The algorithm was tested based on various simulated observation scenarios. Altogether 72 low Earth orbits have been simulated using nine different inclinations (from 0° to 90°) and eight different altitudes (from 100 km up to 6000 km). The attitude determination was based on GPS, GLONASS, and Galileo.

The tests showed that the attitude may be determined with a root mean square error between 5° (if the satellite has nominal attitude) and 9° (if the satellite has a random attitude) if all GNSS are used in the algorithm. Figure 4. 9 shows the error distribution for the nominal case using all three GNSS. For single-system cases, e.g., GPS-only, the attitude error increases by a factor of about 1.5. The computation time for the attitude for one single epoch is below 100 ms on a standard personal computer.

The proposed algorithm is able to determine the attitude using only information on the visibility of GNSS satellites at a level below 10° . It profits in particular from the availability of multiple GNSS. A possible application might be to generate approximate solutions as input for other attitude determination algorithms.

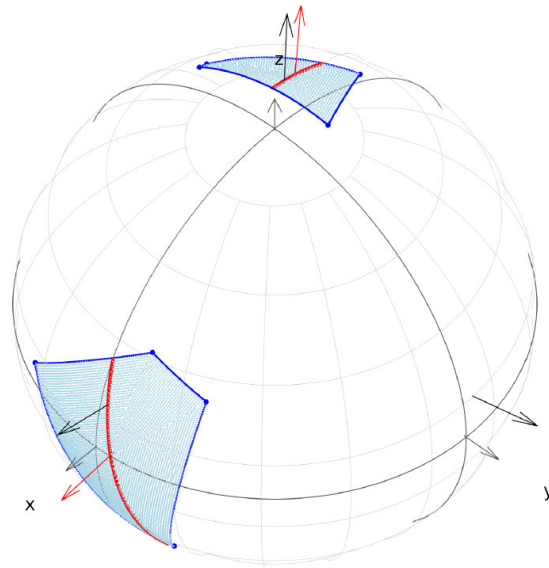


Figure 4. 8: Combination of two boresight vectors. Red: single antenna boresight vector, black: final attitude vectors; blue: polygons of allowance for each boresight vector.

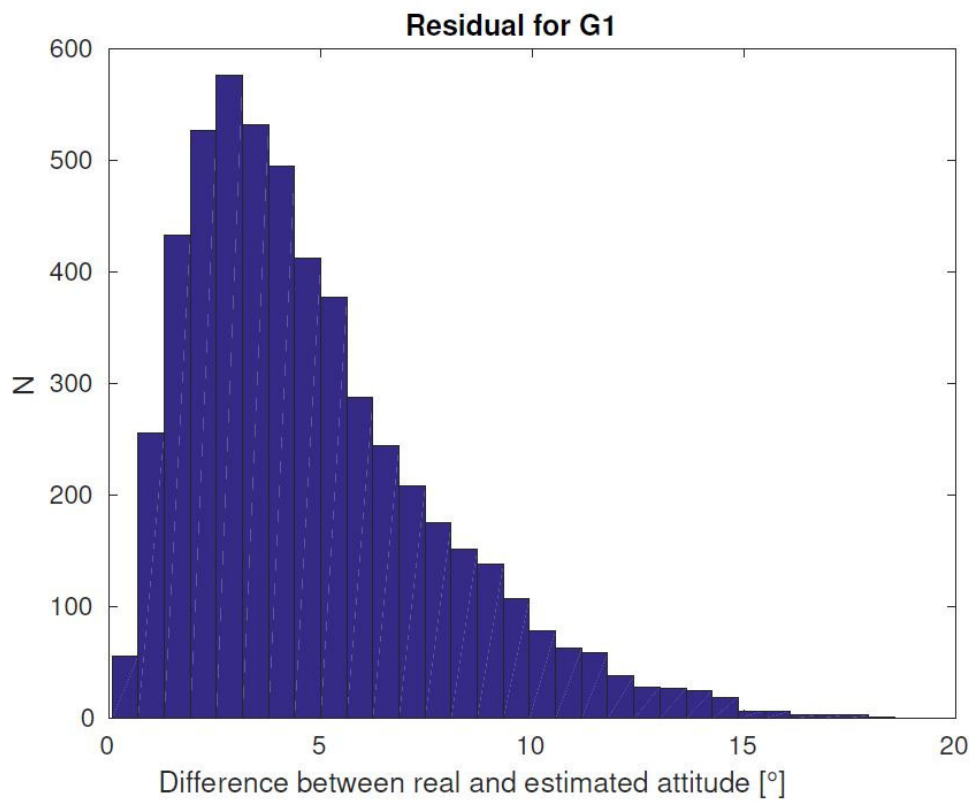


Figure 4. 9: Difference between ground truth and estimated attitude.

Attitude determination for cube satellites

D. Willi^{1,2}, M. Rothacher¹

¹Institute of Geodesy and Photogrammetry, ETH Zurich, Switzerland

²Now at Federal Office of Topography swisstopo, Switzerland

CubETH (see *Figure 4. 10*) is a 10 x 10 x 10 cm³ cube satellite study. The main goal of the mission is to deliver the proof of concept for precise orbit determination and attitude determination with low-cost, commercial off-the-shelf GNSS receivers. The spacecraft is equipped with 10 tiny GNSS receivers manufactured by the Swiss company u-blox. The u-blox receivers are predestinated for space applications, because of their small size (16 mm), small weight (1.6 g) and small power consumption (80 mW).

Every pair of receivers is connected to one GNSS patch antenna. Du to this redundancy concept, several receivers could be lost without endangering the mission goals. Having two receivers connected to the same antenna allow for zero-baseline tests.

Since the spacecraft is equipped with four antennas on its upper face, attitude determination becomes possible. The u-blox receivers are not synchronized and measure at different times within a window of 1 ms. In order to estimate the attitude, the measurements have to be extrapolated. The extrapolation is based on the receiver Position, Velocity and Time (PVT) estimation. The magnitude of the extrapolation term ranges from approximately -6 m to +6 m, which is due to the high velocity of the spacecraft in orbit. A filter algorithm for attitude determination, including the extrapolation term, is presented in Willi and Rothacher (2017). The attitude representation is based on quaternions. The advantage over a classical Euler-sequence parametrization is the absence of singularities.

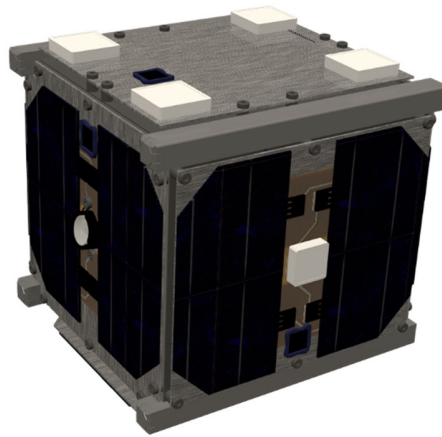


Figure 4. 10: A computer generated image of CubETH. The four white pads on the top and the white pad on the front are the GNSS antennas.

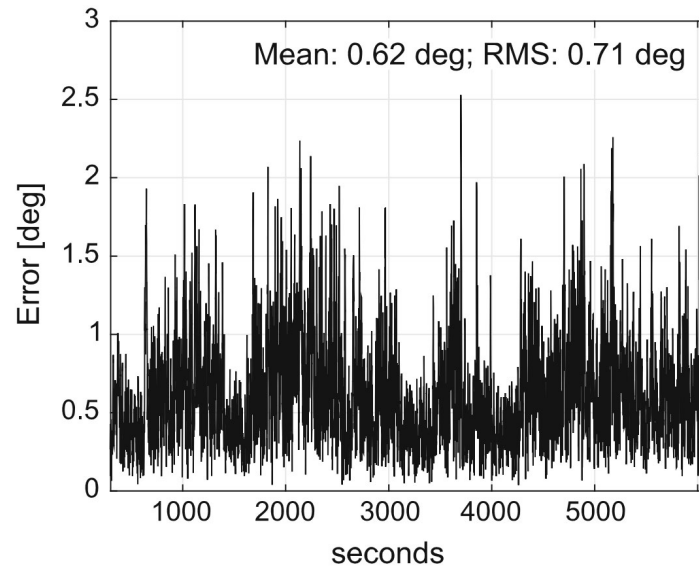


Figure 4. 11: Accuracy of the attitude estimation obtained with the Kalman-filter prototype in the GNSS signal simulator study. Source: Willi and Rothacher (2017)

The newly developed algorithm was validated in a signal simulator study using a Spirent GNSS Signal Simulator. The data was recorded using u-blox NEO-M8 receivers. Three orthogonal baselines of 10 cm were simulated, at an orbital height of 450 km. The root mean square error of the attitude estimated during the validation is 0.71 degrees, with an maximal error around 2.5 degrees (see Figure 4. 11). This validation proved the concept of the extrapolation of the measurements to work. Furthermore, this study demonstrated that attitude determination on 10 cm baselines reaches sub-degree accuracy, assuming that the antenna phase centre variations are perfectly modelled.

Estimation of Antenna Height Above Snow-Covered Glacier Surface Using GNSS-reflectometry

L. Steiner¹, M. Baumann¹, M. Huss², A. Geiger¹

¹ Institute of Geodesy and Photogrammetry, ETH Zurich

² Laboratory of Hydraulics, Hydrology and Glaciology VAW, ETH Zurich

Observing and monitoring glaciers is of great importance for natural disaster prevention and risk reduction. An important component is the mass balance of a glacier. Changes in glacier mass balance due to snow accumulation and ice melt over a glacier surface are important parameters to better understand glacier response to climatic forcing. The glacier mass balance is conventionally determined using in-situ measurements of poles. GNSS-reflectometry can be used to determine the pole height above a glacier surface.

This project was carried out in collaboration with the Laboratory of Hydraulics, Hydrology and Glaciology at ETH Zurich (VAW-ETHZ). Besides the position estimation by differential GPS processing, the project focuses on the potential contribution of GPS-reflectometry for automatically determining the pole height above a snow-covered glacier surface, and thus the glacier surface height change. A self-sustaining GPS station was installed on the Glacier de la Plaine Morte (Figure 4. 12) in the Bernese Alps, which is a well-accessible glacier with a flat and smooth surface and almost no GNSS line-of-sight obstruction due to clear sky visibility. A sonic ranger served as an independent reference and was provided by the VAW-ETHZ.

The feasibility of the GPS reflectometry SNR-analysis and phase-delay analysis to derive changes in the antenna height above the (snow-covered) glacier surface and the resulting ice melt has been evaluated. The SNR-analysis is based on the interference of the reflected satellite signals with the directly received signals. The frequency of the multipath oscillations depends on the antenna height above the reflective surface, the glacier surface. The phase-delay analysis uses two antennas, one nadir looking (low-cost) antenna for receiving the reflected signals and one zenith looking (geodetic) antenna for the direct satellite signals. The zenith looking antenna serves as the reference station and the nadir looking antenna as rover, using standard GPS double difference processing.

The change in antenna height above the (snow-covered) glacier surface was successfully estimated with the GNSS reflectometry SNR method (Figure 4. 13). The SNR method performed very well with an accuracy of a few centimeters and the results are highly correlated with the reference data. Due to the smooth glacier surface and clear sky visibility in the most directions, no complex multipath from heterogeneous reflective surfaces was present in the snow-covered period. Different scenarios were analyzed by using one track of a specific satellite to the use of all satellites or different azimuth or time bins. The solution which excluded the azimuth directions of high mountains (elevation angle of more than 10 degrees) performed best, followed by the result which included all satellites in view. The GNSS reflectometry phase method yielded no significant results. This was due to the use of a low-cost nadir-looking antenna, which did not allow the separation of direct and reflected GNSS signals. The alternative would be to use a special geodetic left-hand-circularly-polarized (LHCP) antenna which is much more expensive.



Figure 4. 12: GPS-reflectometry station at the Glacier de la Plaine Morte.

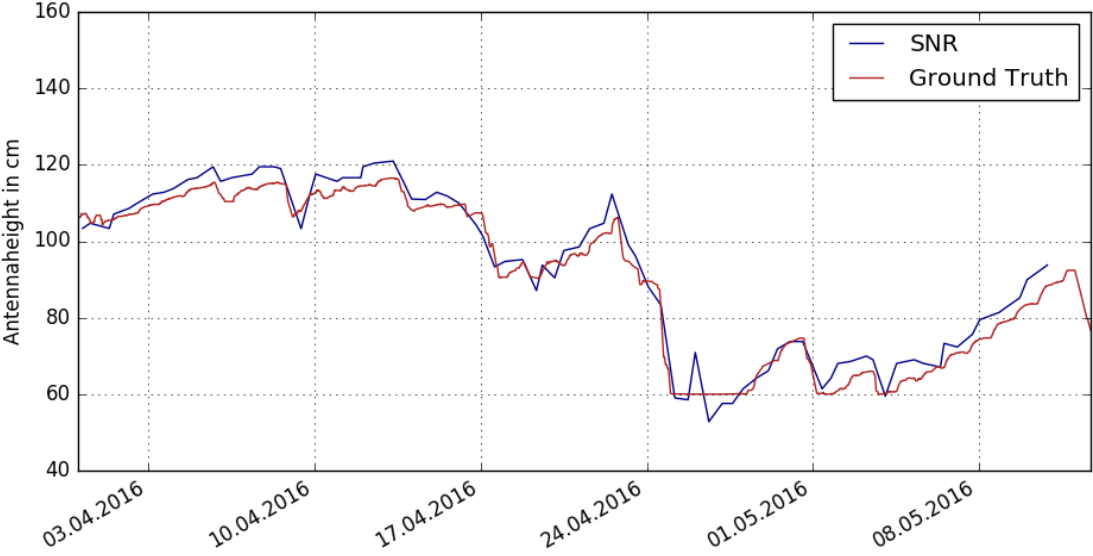


Figure 4. 13: Comparison of GNSS-reflectometry SNR results compared to the independent reference sensor.

GNSS Flight Performance Assessment of Enhanced Rotorcraft Operations

M. Troller¹, M. Scaramuzza¹, H. Wipf¹, M. Nyffenegger¹, H. Leibundgut², M. Bertschi³

¹ skyguide, Swiss Air Navigation Services

² Swiss Air Rescue – Rega

³ Swiss Air Force

In the frame of the Swiss-wide implementation program to promote GNSS procedures and applications in Switzerland, several projects have been launched allowing for a smooth integration of the new technologies. One of these, the project Helicopter Recording Random Flights (HRRF), aimed at recording randomly collected data from 35 helicopters of the Swiss Air Force and the Swiss HEMS operator REGA on their daily missions. Helicopters were operating under visual and instrument meteorological conditions, on different flight levels and in different topographies. All helicopters have been equipped with a mini quick access recording unit (mQAR). In total, data of more than 40'000 flight hours have been recorded. This powerful dataset allowed manifold investigations and analyses.

In one study, the horizontal and vertical protection levels have been assessed and statistically analyzed. Differences between the helicopter types and GPS/ EGNOS receivers have been taken into account. The analyses showed that the protection level histograms of the three different helicopter types are in the same order of magnitude. Overall, a homogeneously high protection level performance was observed in the whole Swiss airspace.

To assess the trajectory accuracy, the Swiss low-level flight network for helicopter operations has been used. Furthermore, additional dedicated routings have been designed in the frame of the present project. Several trajectory analyses have been carried out. The resulting total system error usually remained below 0.02 NM. In summary, the investigation showed that the RNP navigation accuracy requirement of 0.3 NM have been reached with a large margin and that a potential for more advanced rotorcraft operations exist.

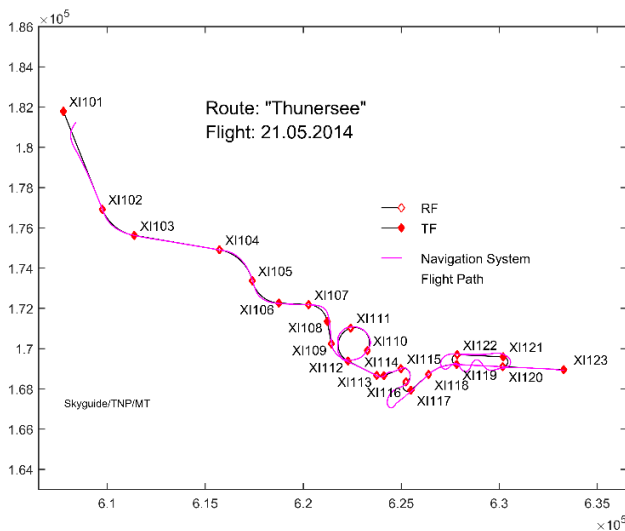


Figure 4. 14: Navigation System Flight Path of the dedicated "Thunersee" routing. The routing is highly challenging, significantly exceeds the ICAO standards and even the performance specified by the helicopter manufacturer.

Impact of the Navigation Performance in Mountainous Area due to the GPS Constellation Variation

M. Troller¹, M. Scaramuzza¹, P. Truffer¹, A. Geiger²

¹ Skyguide Swiss Air Navigation Services, Switzerland

² ETH Zürich, Switzerland

In mountainous area, terrain masking may significantly degrade the GNSS performance. A detailed performance and availability analysis is usually required before implementing a new GNSS flight procedure. The GPS Standard Positioning Service (SPS) performance standard commits to a GPS constellation of 24 satellites only. Consequently, applying a conservative approach, the 24-satellites constellation should be used for the performance assessment. This would lead to a considerable availability degradation for mountainous environments. Therefore, a more realistic constellation is usually considered for availability simulations of approach operations in mountainous areas and the possible variation of the GPS constellation with time is not taken into account.

A study has been carried out to assess this risk. It has been analysed whether the GPS constellation variation has a performance impact on the approach operations availability. The analysis considered the approach procedure of an airport in a mountainous environment (Meiringen), which already has partly degraded GNSS performance under today's 31 satellites constellation. Key numbers such as the dilution of precision (DOP), the horizontal protection levels (HPL) based on the receiver autonomous integrity monitoring (RAIM) concept as well as the horizontal (HPL) and vertical (VPL) protection levels based on SBAS augmentation have been determined and its variation with time have been assessed. Furthermore, a comparison with the situation of an airport in the Swiss flat area (Zürich) has been carried out.

Overall, the study showed that the reduction of operational satellites of the GPS constellation only has a minor effect on the performance. A degradation is mainly visible for the maximum protection levels resulting in an increased probability of availability outages, in particular for the RAIM performance.

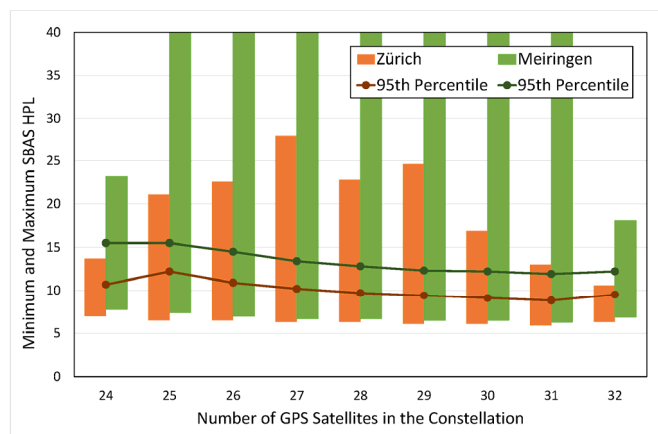


Figure 4.15: SBAS HPL based on the number of GPS satellites in the constellation. The bars are indicating the range between the minimum and maximum values (maximum often cut for better readability). The curves are showing the 95th percentile. The orange colour indicates results for Zürich airport, green colour indicates the results for the Meiringen scenario.

Assessment of environmental-friendly GNSS-based curved approach flight procedure

M. Troller¹, M. Scaramuzza¹, M. Nyffenegger¹, S. Rämi², M. Bertschi²,

¹ Skyguide Swiss Air Navigation Services, Switzerland

² Swiss Air Force, Switzerland

In the present study, the use of innovative flight procedures has been assessed along with a considerable reduction the environmental impact, i.e. fuel, noise and CO₂ emissions. In a project carried out at the military airfield of Dübendorf (close to Zürich), three GNSS-based curved approach procedures have been implemented in 2014 and 2015. One of the approach procedures was designated for arrivals from the west, one from the south and one from the northeast. The procedures are among the first world-wide containing RF (radius-to-fix) curved legs that connect directly to the final approach fix in a procedure based on RNP APCH. This new option was added to the ICAO PANS-OPS design criteria in November 2014 only. The navigation sensors used are GPS augmented with EGNOS, which enables approaches to the LPV minima, and GPS with RAIM to the LNAV minima respectively.

A detailed trajectory analysis of more than 200 approaches has been carried out. Roughly half of approaches were arriving from the west and south respectively and only a few from the northeast. Radar data was used to analyse the accuracy of the approach trajectories. The statistical analysis showed an excellent 95% total system error (TSE) of less than 0.1NM for the initial and intermediate RNP APCH segments with a 95% accuracy requirement of 1NM. By comparing the different aircraft types, only marginal differences were visible.

The comparison of the new approach track to the existing one showed a significant track reduction. Arriving from the west, the track miles were reduced by 17NM or 27%. Consequently, the implementation at the military airfield of Dübendorf is a successful example how innovative flight procedure concepts may reduce the environmental impact.

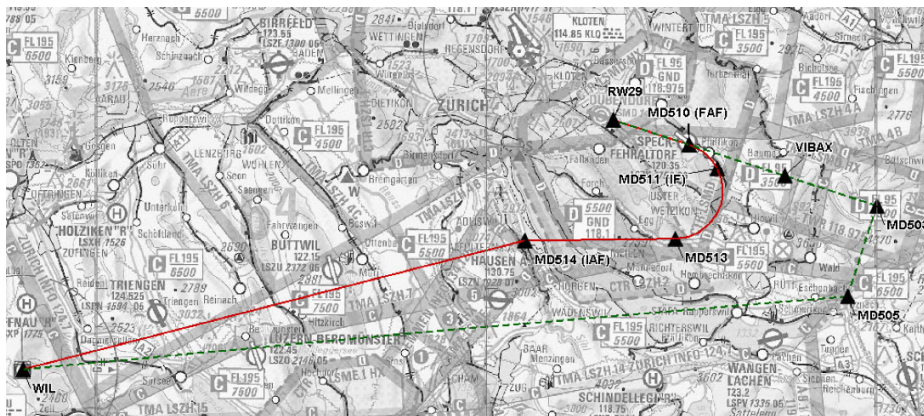


Figure 4. 16: Comparison of the track with a conventional Instrument Landing System (ILS) final (green dashed) and one of the new GNSS procedures (red).

Jamming of Aviation GPS Receivers: Investigation of Field Trials Performed with Civil and Military Aircraft.

P. Truffer¹, M. Scaramuzza¹, M. Troller¹, M. Bertschi²,

¹Skyguide Swiss Air Navigation Services, Switzerland

²Swiss Air Force, Switzerland

Tests of civil and military aircraft have been performed in live jamming scenarios. The analysis of the recorded aviation GPS and flight management system (FMS) data reveal the effects of the jamming signals on different aviation receivers and aircraft types. An equivalent isotropically radiated power of 200 mW has been chosen for the jamming signal. This is comparable to low power jamming devices. Four different types of interference signals were radiated from a biconical broad bandwidth antenna during predefined times, namely a pseudo random noise (PRN) sequence, a continuous wave (CW), a frequency hopping (FH) and a radar like signal with high pulse repetition frequency (PRF). The bandwidth of the interference signals was limited to 2 MHz around the center frequency of the GPS L1 band.

From the known transmit power of a jammer the calculation of the field strength at the aircraft in distance d is straightforward. The directional gain of the GPS antenna with its low noise amplifier and the cable that is connected to the GPS receiver are specified. However, the total receiver gain, which includes the influence of the fuselage of the aircraft, is unknown. This is because the GPS antenna is normally mounted on top of the aircraft, whereas the interference is transmitted from the ground. Without the total receiver gain, the calculation of the interference power at the GPS receiver, and thus the interference-to-signal ratio (J/S) or the carrier-to-noise ratio (C/N_0) is not feasible. By laboratory experiments, the critical thresholds of C/N_0 , where the tracking of the C/A code is lost, has been determined for different types of interference signals for the aviation receiver CMA-5024. Comparing those results to the ones of field trials reveal critical distances to the interference source and thus reliable values for the total receiver gain.

Civil and military organizations participated with fighters, helicopters and business aircraft. Three helicopters and one of the business aviation aircraft are equipped with specific data recorder units that collect data from the aviation GPS receiver, the FMS and attitude data of the aircraft. In addition, independent multiband GNSS receivers record reference tracks in the GPS and GLONASS bands. Several flights have been conducted while the four interference signals were successively radiated. As results, most of the GPS L1 receivers were susceptible to three of the four transmitted jamming signals, namely the PRN sequence, the CW and the FH. The high PRF signal seemed not to impact the GPS reception. Data of the four aircraft equipped with additional data recorder units is analyzed in the position and range domain. GPS tracks are compared to the FMS position solution and the track retrieved from an independent multiband GNSS receiver. Performance parameters like the horizontal integrity level (HIL), number of used satellites and position differences are evaluated. As one of the results reliable values for the total receiver gain for one specific receiver type are found. Analyses of further recorded data show that the detection of jammer events by monitoring C/N_0 is generally reliable. The field trials complement findings of theoretical calculations and laboratory experiments and support the understanding of realistic jamming scenarios.

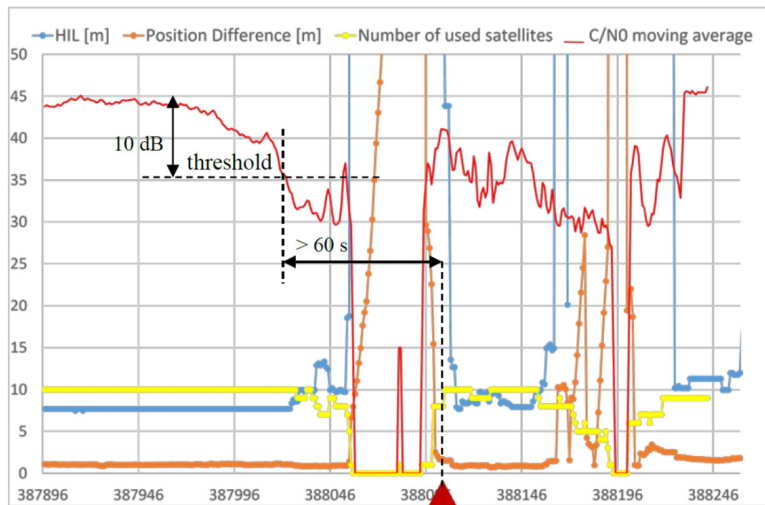


Figure 4. 17: Position and range domain compared and detection of jammer PRN with 10 dB threshold. The red triangle indicates the position of the jammer.

C/No Based GNSS RFI Detection On-Board of Helicopters

M. Scaramuzza¹, H. Wipfl¹, M. Troller¹, H. Leibundgut², S. Rami³, R. Wittwer⁴

¹ skyguide, Swiss Air Navigation Services

² Swiss Air Rescue – Rega

³ Swiss Air Force

⁴ armasuisse

A method has been developed to detect Radio Frequency Interference (RFI) on-board of helicopters. In a first step, mini quick access recorders (mQAR) were installed on-board of two dozen helicopters operated by REGA, the main Swiss Helicopter Emergency and Medical Service (HEMS), and by the Swiss Air Force, and collecting data during a period of several years. Daily missions of the two operators were used to record these data. The low flight altitude is common to all helicopter missions. Therefore, it was expected, that the probability having the aerial vehicles exposed to ground based RFI would be higher compared to commercial fixed wing operations.

In a second step, based on recorded Carrier to Noise Ratio (C/No), GPS satellite azimuth and elevation angles as well as roll, pitch and yaw angles of the helicopters, the GPS signals were normalized with use of an empirical derived GPS antenna pattern.

Application of this RFI detection method to several thousand flight hours had revealed different potential low power RFI sources. Few of them were stationary sources, but not permanently emitting signals. An increased number of sporadic RFI events were detected in proximity of cities and along of highways.

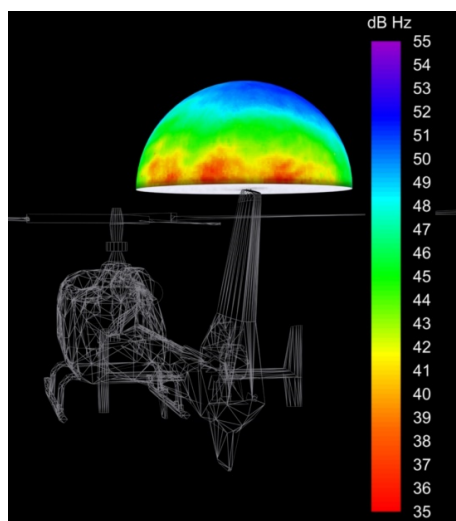


Figure 4. 18: GPS antenna pattern on top of a helicopter fin.

Assessment of RFI Impact on Aviation GPS/SBAS Receiver Performance

M. Scaramuzza¹, P. Truffer¹, M. Troller¹, H. Wipf¹, H. Leibundgut², M. Bertschi³, S. Rami³

¹ skyguide, Swiss Air Navigation Services

² Swiss Air Rescue – Rega

³ Swiss Air Force

Radio frequency interference (RFI) on L-band affecting GNSS receivers might lead to unacceptable performance degradations when operating with GNSS only. Flights using GNSS based procedures and operated under Instrument Meteorological Conditions (IMC), are particularly concerned about such a threat. Therefore, the impact of RFI on GPS/SBAS receivers is analyzed.

Based on a recorded RFI event during a flight, the behavior of the receivers' estimated Horizontal Protection Level (HPL) is analyzed. It is observed, that the HPL alters only slightly despite Carrier to Noise Ratio (C/No) degradations on all tracked satellites of 18dB. The HPL mainly begins to increase when signal tracking of satellites is lost and is recovered when satellite tracking is resumed.

In order to understand the behavior of the HPL, the corresponding algorithm is analyzed in depth. It is shown, that RFI impacts only few HPL algorithm input parameters. The size of HPL is only dictated by the increased pseudorange noise as well as the number of tracked satellite signals. The latter is directly related to the receivers' antenna pattern describing the expected C/No. Hence, the vehicles' attitude plays a relevant role, too.

Different simulations are performed to describe the HPL behavior in a more general way. It results that even under strong RFI influence the HPL rarely reaches values of 0.1NM or more. On the other hand, position solutions are not possible at C/No degradations of more than 26dB. This finding varies depending on the receiver, antenna and helicopter type.

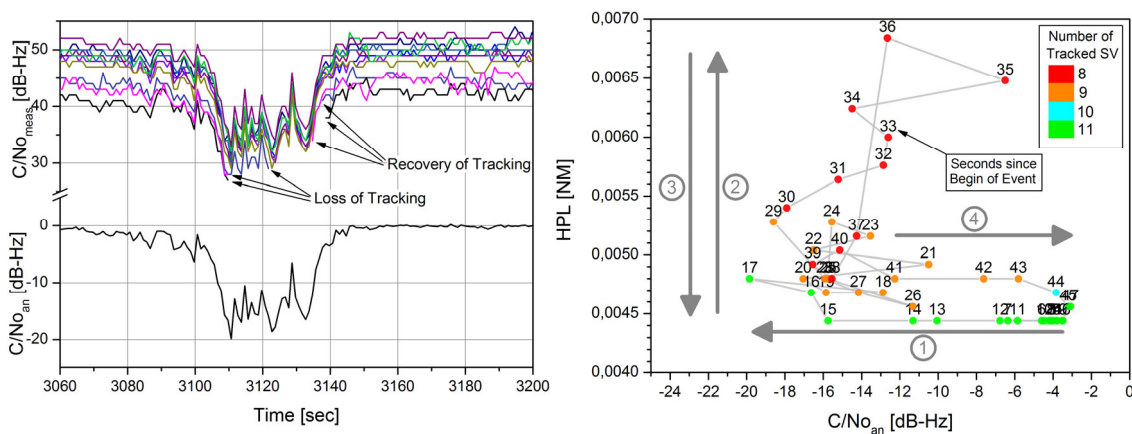


Figure 4.19: Left: Normalized C/No degradation on all satellites (top) and mean of normalized C/No (bottom) during an RFI event recorded on flight and lasting roughly one minute. Tracking of three satellites were lost. Right: Trajectory in C/No – HPL space during the RFI event shown in the left figure. Colored dots indicate one epoch where the color references to the number of tracked satellites. The numbers related to the dots show the elapsed time in seconds since beginning of the RFI event. The gray arrows show in a generalized way the behavior of HPL depending on C/No degradation.

Comparison of GNSS Performance Simulation Results with Data Recorded Onboard of Helicopters

M. Scaramuzza¹, P. Truffer¹, M. Troller¹, H. Leibundgut², M. Bertschi³

¹ skyguide, Swiss Air Navigation Services

² Swiss Air Rescue – Rega

³ Swiss Air Force

Implementation of new satellite-based flight procedures in Switzerland are always accompanied by simulations in order to assess the positioning solution performance and the resulting availability. This approach is even more important when procedures are designed in mountainous environment such as the Swiss Alps, where terrain masking of more than 20 degrees may be present.

These simulations cover the desired flight path or relevant points in space where the most critical terrain masking is expected. A software tool was developed at skyguide to perform these studies. A Digital Elevation Model (DEM), the designed flight procedure, and GPS almanacs at different epochs are loaded and simulations covering a period of a sidereal day are carried out. Availability of satellite signals are finally derived from these calculations.

Data recorded onboard of helicopters of the Swiss Air Force and REGA is used to compare real performance with simulated ones. Different areas of influence are analyzed including the required DEM resolution and sampling rate, signal masking caused by the helicopter and flight attitude.

It has been shown that accurate simulation results can be achieved with relatively simple approaches such as use of Line of Sight for signal propagation, exclusion of helicopter airframe masking and setting helicopter roll angle always to zero. However, few basic principles have to be respected. These includes the dimension of the DEM, the DEM type, and the DEM sampling rate.

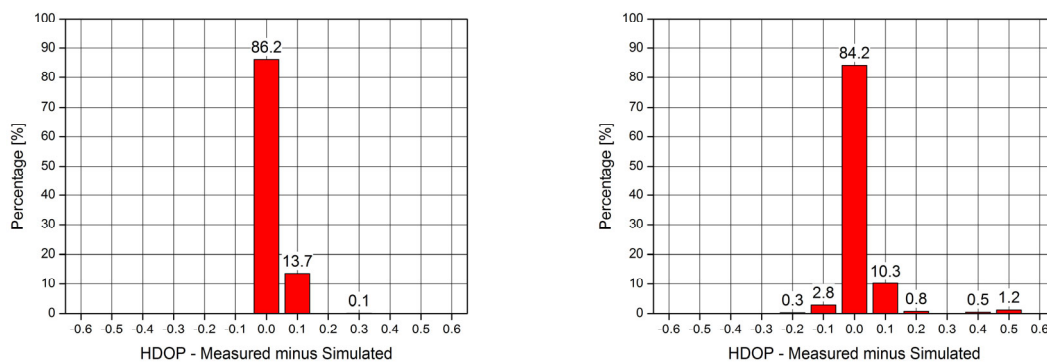


Figure 4. 20: Comparison of simulated HDOP with recorded ones on-board of helicopters. Left figure refers to an approach procedure in the Swiss Midland while the right figure refers to an approach procedure in the Swiss Alps.

Contributions of swisstopo to GNSS Meteorology and GNSS Climatology

E. Brockmann, D. Ineichen, S. Lutz

Federal Office of Topography swisstopo

GNSS Meteorology

Since 1999, swisstopo has been active in different projects covering the area of GNSS meteorology. swisstopo contributed on a routine basis to the European projects COST-716, TOUGH and E-GVAP I + II (with a product availability of more than 98%). Under the umbrella of EUMETNET, estimated troposphere parameters of more than 5400 permanent GNSS sites (3400 active sites on April 24, 2019) are provided by 19 analysis centers (totally 38 different solutions) with an averaged time delay of 1:30 hours (status April 2019; see Figure 4. 21).

In October 2014 the number of processed sites was considerably increased (Figure 4. 22) – this was motivated by having a quick monitoring of stations which are processed with a time delay in post-processing (especially re-processing). All these analyses use the Bernese GNSS Software (BSW). To keep the deadlines, several optimizations were implemented (e.g. clustering). Furthermore, results of the real real-time system used for the Swiss positioning system swipos (only Swiss stations, see Figure 4. 21 on the right) are provided since many years to the meteo community. This solution is already submitted few minutes after the full hour.

Due to a memorandum of understanding between EUREF and EUMETNET, signed in 2007, radiosonde data of more than 200 stations can be provided also to the geodetic community. Many of them are closer than 20-30 km to the next GNSS site, allowing comparisons between these collocated sites. Totally 61 sites out of the GNSS sites processed at swisstopo have collocations with radiosonde data. swisstopo's final troposphere parameters are derived from a reprocessing using GPS and GLONASS data between 1996 and 2014. After that, the operational solutions are used. They were enhanced to a complete GPS, GLONASS, Galileo and BeiDou processing mid of 2016.

From Switzerland, the so-called super site Payerne (PAYE) is processed by all analysis centers. Comparisons of troposphere parameters are also displayed on swisstopo's monitoring web pages (see Figure 4. 23 for comparison of radio sonde data with the post-processed GNSS solutions). Due to GNSS antenna changes and also due to changes on the radio sonde side, a linear fit for the entire interval is problematic. Figure 4. 24 shows comparisons with radio sonde values from station LDB2, which produces measurements more frequently. The corresponding estimates from near real-time are still based on GPS and GLONASS.



Figure 4. 21: GNSS permanent sites processed by all analysis centers (left), processed at swisstopo in near real-time (middle) and processed in real real-time (right). Status of April 24, 2019 monitored within the E-GVAP project of EUMETNET.

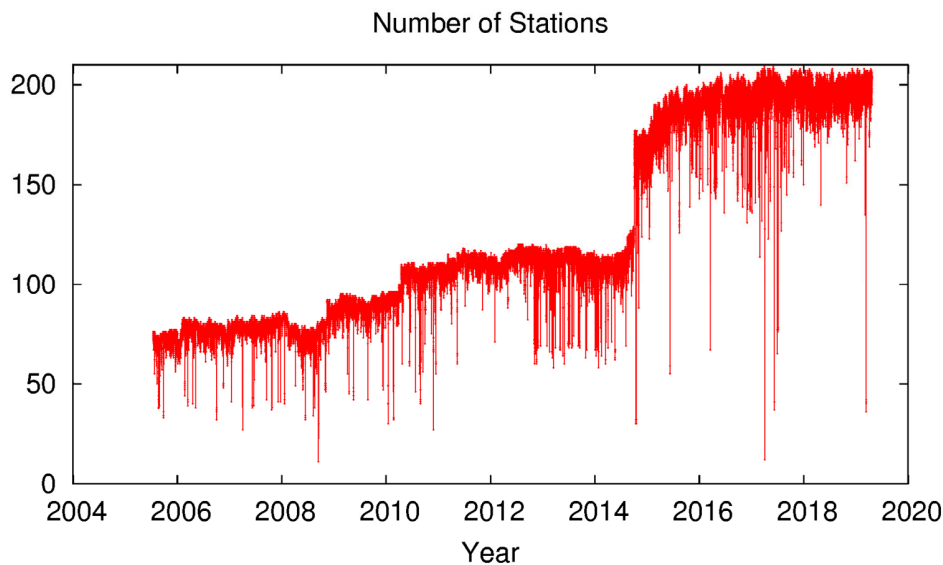
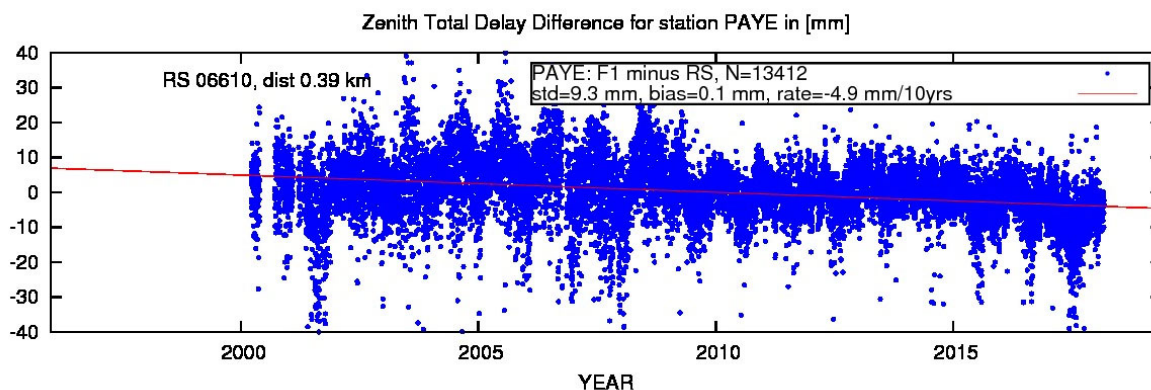


Figure 4. 22: Number of GNSS sites processed by swisstopo in near real-time.



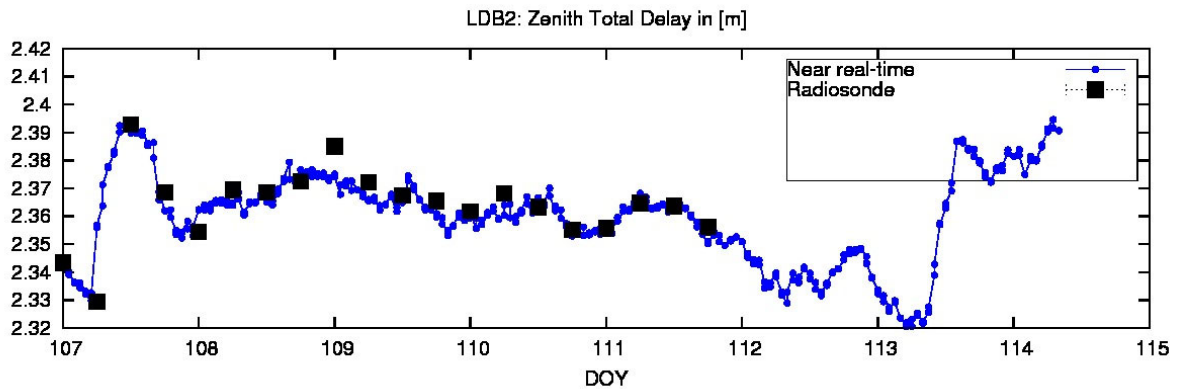
24/04/2019 04:43

Figure 4. 23: Difference between troposphere parameters estimated from GNSS post-processing and troposphere parameters derived from radiosonde data for station PAYE. A new humidity sensor was used for radiosonde launches after May 2009. Radio sonde data of a new model used since beginning 2018 are not yet available. Three GNSS antenna changes took place (September 2000, June 2007, April 2015).

The final troposphere parameters are also provided to the STARTWAVE database maintained by the Institute of Applied Physics (IAP) at the University of Bern, where results are compared with water vapor radiometers installed at the University of Bern and in Zimmerwald.

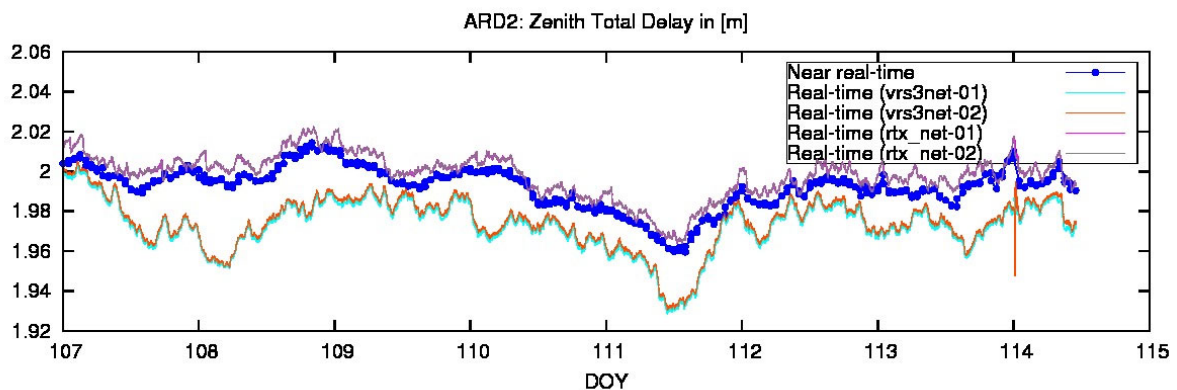
In 2015, the complete Swiss GNSS network AGNES was enhanced to GPS+GLO+GAL+BDS capable receivers. Since mid 2016, most operational post-processing computations are based on multi-GNSS data already. The complete data flow was switched from RINEX-2 to RINEX-3 and the analysis is performed with a multi-GNSS development version BSW5.3. The near real-time analysis remained on GPS and GLONASS due to missing high-quality ultra rapid multi-GNSS orbit products.

With the enhancement from GPS to full multi-GNSS analyses, also the real real-time system was updated. Galileo and BeiDou are fully supported in Trimble's new RTXNet processor, which now is based on PPP instead of a differential analysis. Version 3.10 was installed in June 2017 and from then on available for clients using MSM3.2 messages for real-time positioning. In parallel, the old system, based on GPS and GLONASS, still operates and serves the majority of our surveying clients. The corresponding troposphere parameters from both real real-time systems are archived. From Figure 4. 25 it becomes obvious that the results of the RTX processor generates zenith total delay estimates which are much closer to the near real-time results from BSW. Since January 21, 2019, the RTX-based results are submitted to EUMETNET under the name "LPTX", continuing the LPTR series after a longer validation phase (from week 2000; May 2018).



24/04/2019 10:42

Figure 4. 24: Comparison of near real-time zenith total delays with high resolution radio sonde values (example Lindenberg, Germany, LDB2, time span April 17-24, 2019). Radio sonde data are available with a delay of 2 days for comparisons).



24/04/2019 13:50

Figure 4. 25: Comparison of near real-time zenith total delays with real real-time values from BSW (example Ardez, ARD2, time span April, 17-24, 2019). VRS3NET results are based on the older GPS/GLONASS processor, RTX results are based on full multi-GNSS.

Figure 4. 26 shows an averaged statistics of differences of different troposphere estimates with respect to the post-processed solution (PP) for the time interval Jan. 1 until Apr. 7, 2019. The bias of the RTX solution (“RX”) is with about 5 mm significant, but much reduced compared to the VRS3NET results (“RR”, bias - 15 mm and, not shown here, a strong annual signal). Obvious is the small standard deviation of RX w.r.t. PP, which is partly even smaller than for the NRT solution. This might be due to the fact, that PP and RX use multi-GNSS data. More probable is the explanation that in case of RX only Swiss sites located in the center of the processed network are compared whereas for NRT all sites covering whole Europe, including those at the network borders, are compared. The slightly better agreement of the near real-time solution NRT of the last 3 weeks may be attributed to a lowering of the relative ztd weights from 1 mm to 2 mm (activated March 18, 2019; post-processed solutions don’t apply a relative troposphere weighting scheme).

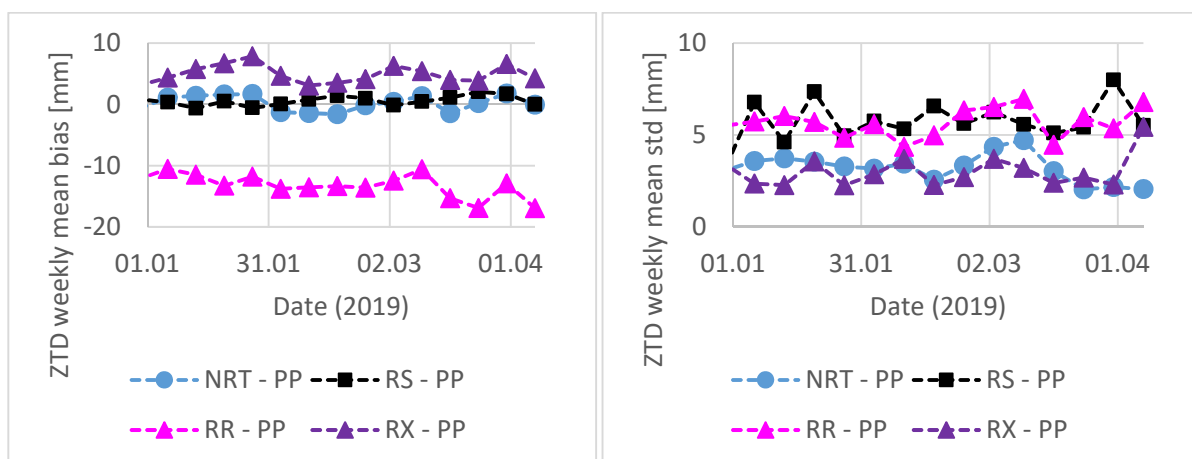


Figure 4. 26: Comparison of zenith total delays with post-processed values (PP) as reference. Time span 1.1. – 7.4.2019: Mean weekly bias left, mean weekly standard deviation right. NRT is the near real-time product (about 190 stations in common to PP), RS are the radio sonde results (about 37 sites), VRS3NET results are labeled with “RR”, RTX results with “RX” (both with 35 Swiss sites).

GNSS Climatology

swisstopo was joining the COST project GNSS4SWEC which started in 2013 after several years of preparation. It was successfully finished 2018. The final report is currently in preparation.

Main focus of the project is:

1. Severe weather forecasting: new GNSS products are required to provide more information on the spatial heterogeneity and rapid temporal variability of humidity in the troposphere.
2. Nowcasting: providing rapid updates in the analysis of the atmospheric state requires a transition from near real-time GNSS network processing (as implemented in E-GVAP) to real-time PPP processing.

3. Multi-GNSS analysis combining data from GPS, GLONASS and Galileo in the future is expected to provide improved tropospheric products. Processing algorithms need to be modified and impact of use of additional observations needs to be assessed.
4. Climate monitoring through the evaluation of trends and variability in Integrated Water Vapor (IWV) for which the quality of reprocessed GNSS data and homogenized IWV estimates need to be assessed. The goal is to establish a new climate data record, taking benefit of more than 15 years of reprocessed ZTD estimates from hundreds of global and regional GNSS stations.

swisstopo is basically interested in all of the project objectives. The main contribution was on topic 4 – the climate monitoring based on the swisstopo re-processing activities. The homogeneously processed time series allow investigating the development of the troposphere and especially the greenhouse gas “water vapor” on the long-term. swisstopo finished a reprocessing in 2014 covering a homogeneous processing of a time span starting at the beginning of 1996 until almost the end of 2014 and using GPS and GLONASS data. Some key parameters are given in Figure 4. 27. The number of stations increased over time from 20 to 170. The stations are mostly located in central Europe. Some boundary stations were included to enable a better decorrelation between troposphere parameters and station height. The number of satellites increased from 25 in 1996 to 65 in 2014. Since 2004, the number of satellites increased due to the improved GLONASS constellation. A ZTD standard series, based on GMF mapping, was submitted to EUREF on October 23, 2014 (as “LP0” series). A second series, based on Vienna Mapping function and individual receiver antenna phase center models was provided on March 20, 2015 (as “LP1” series). The reprocessing was performed with the Bernese GNSS Software BSW5.2 using most up-to-date models in a homogeneous way. Orbit and earth rotation parameters were used from the CODE repro2 products. More details are given in Table 4. 1: Basic processing options used for swisstopo repro2..

Overlapping 3-day solutions (using only the middle day) were calculated to optimize the ZTD estimates at midnight (see Figure 4. 28).

Figure 4. 29 shows that daily solutions are even more stable in view of the Helmert transformation parameters than the previous weekly solutions.

At the Thessaloniki workshop (May 11-13, 2015) the idea was born to analyze the impact of additional satellite systems on the long-term trends in ZTD. In June 2015, a reprocessed solution, identical to the previously described, but based on GPS-only data, was generated. It could already be shown at the Wroclaw Meeting (Sep. 29 – Okt.1, 2015) that the influence of GLONASS on the long-term trend is small. See especially Pacione et al. (2017) for further information.

Further conclusions can be drawn from the comparisons between different ZTD time series:

- Formal errors of ZTD estimates are smaller with more GLONASS observations (max. 10%) included
- Influence of GMF versus VMF: no significant rate, standard deviation 0.5 – 2.5 mm ZTD (109 sites with long time series)
- Difference to CODE’s global reprocessing: no significant rate, standard deviation 2.0 – 5.0 mm ZTD (39 sites with long time series)
- Influence of additional GLONASS observations: no significant rate, standard deviation: 0.4 – 1.5 mm (111 sites). This is in fact little higher (also GPS-only time is counted), but strongly dependent on the used a-priori ZTD constraints; there is only a statistical effect but no significant bias.

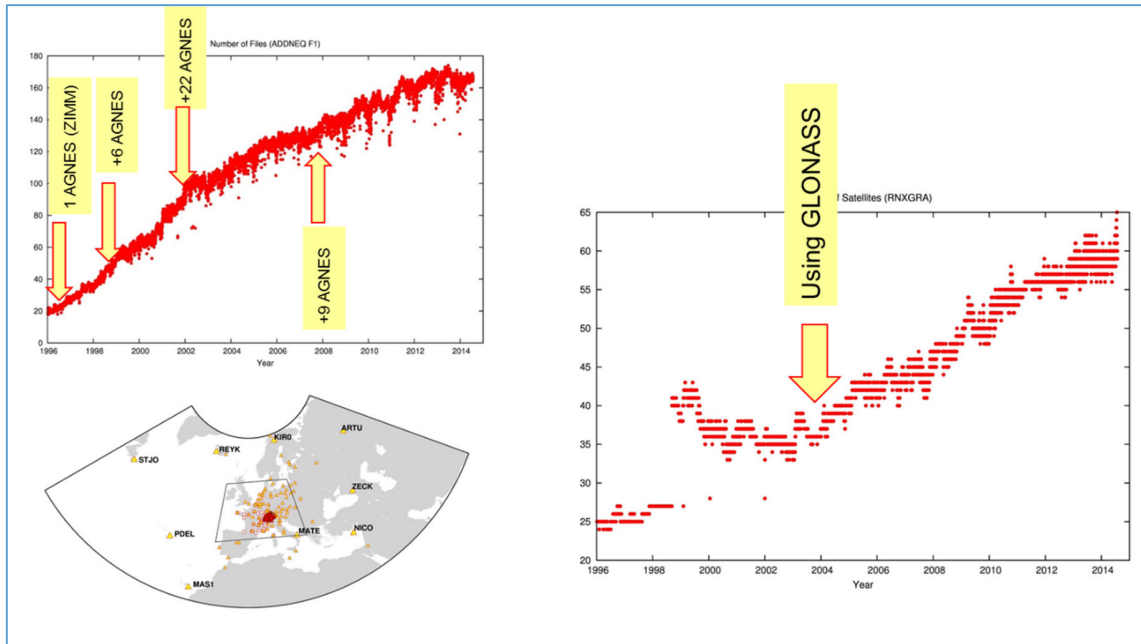


Figure 4.27: Key parameters of swisstopo's repro2.

Table 4. 1: Basic processing options used for swisstopo repro2.

Software	Bernese BSW5.2 (+)
Satellite systems	GPS+GLO (since 2004)
Elevation cutoff angle	3 deg
Observation weighting	COSZ elevation-dependent weighting
Antenna	I08 absolute antenna model (group values)
Troposphere	GMF and DRY GMF mapping for the a priori values and while estimating hourly ZPD parameters using WET GMF
Troposphere gradients	Chen Herring for tropospheric gradient estimation
Tides	Atmospheric tidal loading applied
Conventions	IERS2010
Ocean tides	FES2004
Gravity field	EGM08
Ionosphere	CODE 2-hour resolution; including higher order terms
Reference frame	IGb08
Network	Max. 180 stations
Time span	DOY 007, 1996 until DOY 207, 2014
Orbits/EOP	CODE reprocessing series 2011 (until DOY 106, 2011) and CODE reprocessing series 2013 (until DOY 362, 2013), CODE operational series in 2014

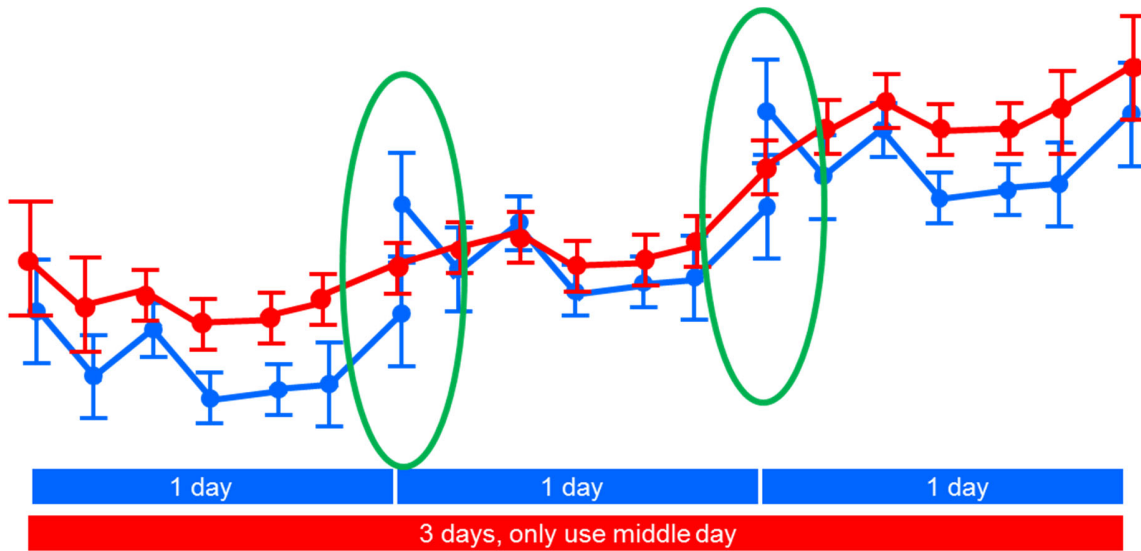
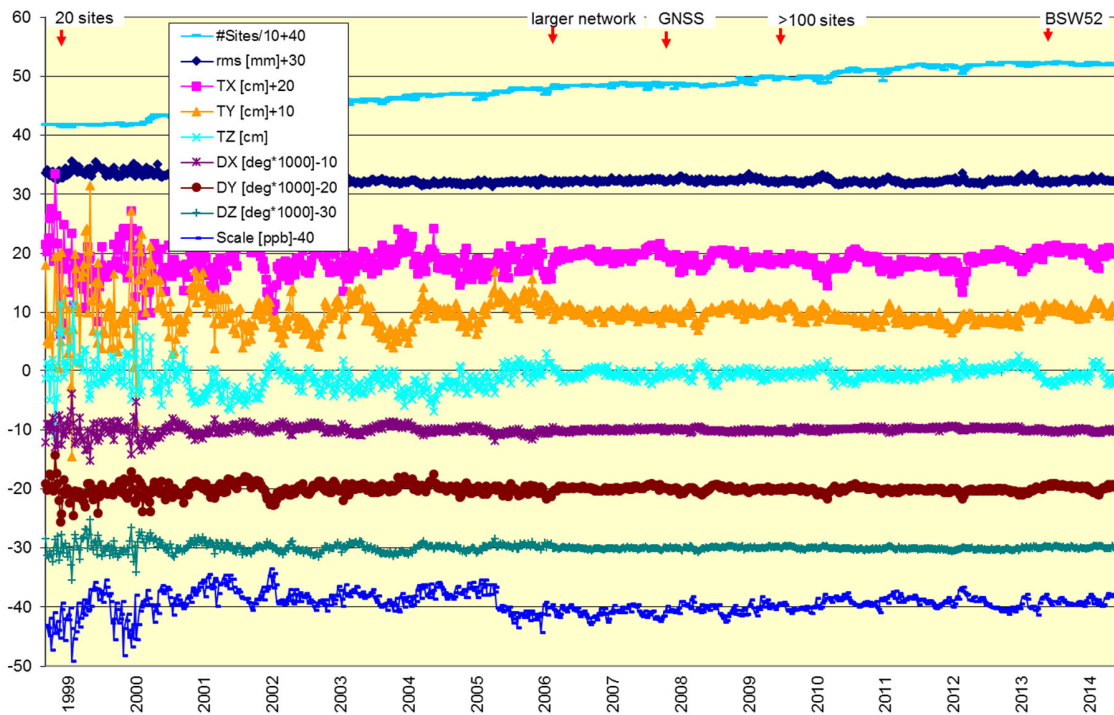


Figure 4. 28: 3-day solutions to optimize the ZTD estimates at midnight.



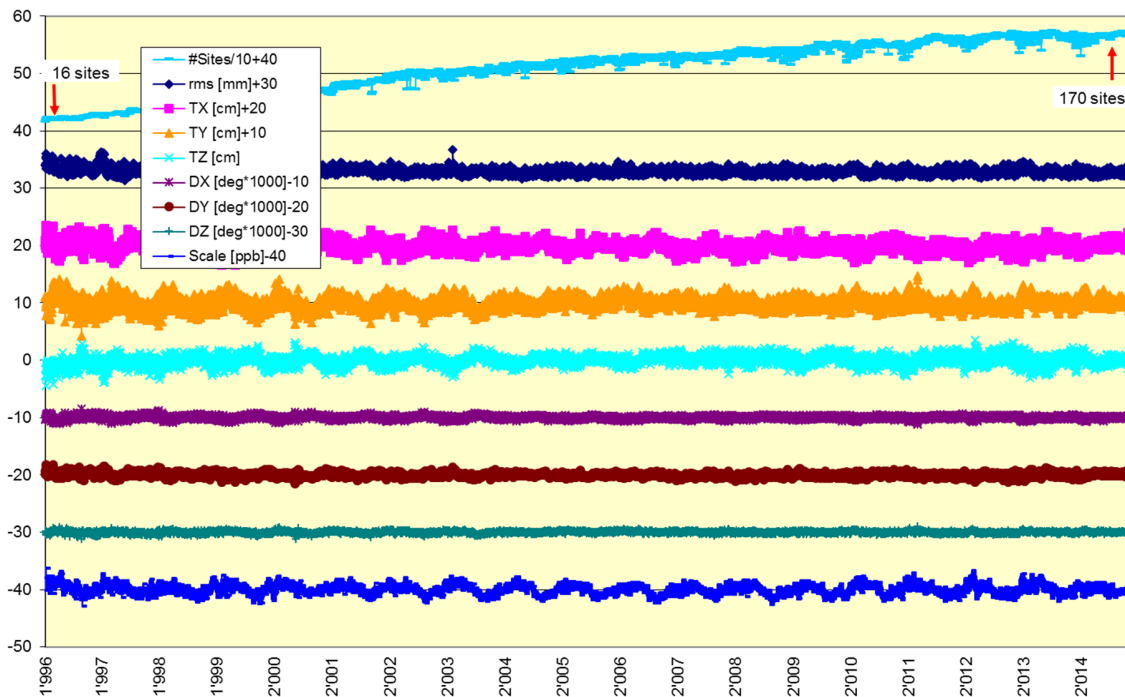
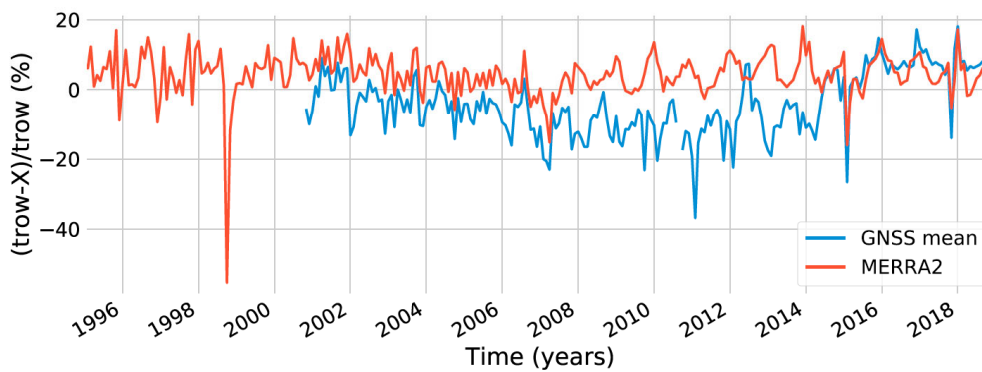


Figure 4. 29: Stability of the solutions expressed in Helmert parameters between each individual solution with respect to the combined solution (operational older weekly solution top, swisstopo repro2 daily solution bottom).

The advantages of a consistently reprocessed data series can also be seen from the comparison with the derived Integrated Water Vapor (IVW) of the TROWARA microwave radiometer, located on the rooftop of the University of Bern, in Figure 4. 30.

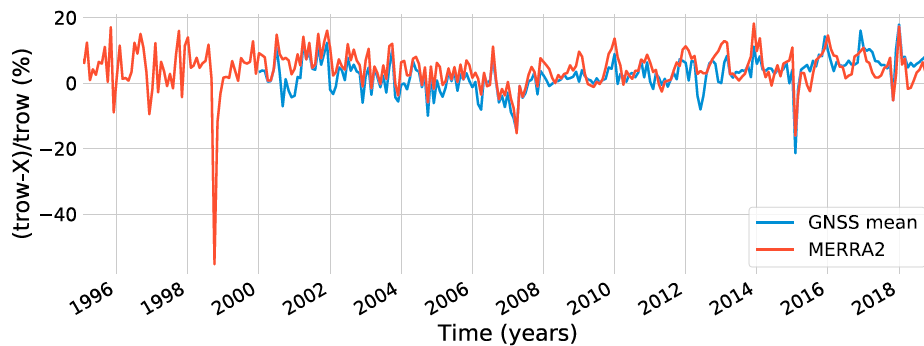
Integrated water vapour

Relative differences to TROWARA



Integrated water vapour

Relative differences to TROWARA (GNSS reprocessed data)



Change in GNSS processing: tropospheric apriori model, mapping function (MF), antenna model
↳ global mapping function ↳ Herring MF ↳ relative model

Figure 4. 30: Comparison of IWV of the TROWARA microwave radiometer with GNSS (operational GNSS solution top, swisstopo repro2 solution bottom).

Reprocessed GNSS Time Series of Troposphere Zenith Wet Delays for Climate

H. Su and M. Rothacher

Chair of Mathematical and Physical Geodesy, Institute of Geodesy and Photogrammetry, ETH Zürich

Evidence from sea level rise, shrinking ice sheets, etc. shows that global warming is occurring roughly since the mid-20th century. Water vapor is one of the important meteorological quantity that scientists care about because it influences Earth's weather pattern. Several techniques have been developed to record meteorological data. Radiosonde balloons are rising in the atmosphere and measure various atmospheric parameters. Moderate Resolution Imaging Spectroradiometer (MODIS) is a payload onboard the Terra and Aqua satellites. They can provide global meteorological data with a resolution from 250km to 1000km. In 1970s, GPS was developed. Besides its PNT service, it can also be used to determine troposphere zenith total or wet delays. And more GNSS constellations will be fully operational in the near future.

The troposphere zenith total delay derived from GNSS observations can be divided into a hydrostatic part caused by the dry gases in the atmosphere and a wet part caused by the refractivity due to water vapor. Due to the consistent data analysis in terms of strategy, parameterization and models and due to the growing length of the time series, ground-based GNSS is becoming an independent and more and more important data source for climate monitoring. This report tries to carefully analyze and assess the quality of the long GNSS time series for their potential use in climatology.

For this study here, 11 years of global GNSS data, from 2002 to 2012, was reprocessed generating three kinds of solutions, namely GPS-only, GLONASS-only and combined GPS/GLONASS solutions. A total of 320 global tracking stations recording GPS measurements, 154 thereof tracking both, GPS as well as GLONASS satellites. In the parameter estimation, 6-hourly ECMWF-based hydrostatic delays mapped with the VMF1 mapping function have been used as a priori troposphere delays. No a priori troposphere gradients have been used. Two-hourly piece-wise linear wet troposphere zenith delays, mapped with the wet VMF1 mapping function, and 24-hourly troposphere gradients have been estimated for each station. Much care has been taken to model all the station motion effects such as solid Earth tides, pole tides, ocean and atmospheric pressure loading in order to avoid a propagation of these effects into the troposphere zenith wet delay estimates (ZWDs).

We studied the long-term drifts in the ZWDs. In order to avoid an influence of periodic signals on the ZWD drift estimation, six main periodic terms were determined together with the drift. The six main periodic terms are annual (S_a), semi-annual (S_{sa}), 24h (S1), 23h56m (K1), 12h25m (M2) and 12h (S2), respectively. In order to assess, whether the same drifts are obtained from GPS, GLONASS and GPS/GLONASS observations, the mean of the drift differences between GPS-only and combined GPS/GLONASS solutions, amounting to tiny 0.01mm, and the mean of the drift differences between GPS-only and GLONASS-only, also at the sub-millimeter level, were computed. In addition, we compared drifts of ZWDs coming from all the GPS sites with temperature trends available from NASA's GISS analysis results. The temperature trends were only taken into account, if more than 66% of the records to be expected were available.

From Figure 4. 31 and Figure 4. 32 we can see that in most regions changes in water vapor coincide with changes in temperature. But this is not the case everywhere: in the area near the equator, the climate is characterized by two rainfall peaks, one in spring and one in summer and the Mediterranean Climate Zone is characterized by a rainy winter and a dry summer. Data gaps, in addition, may be responsible for biases between the two types of quantities.

Figure 4. 31 shows the ZWD trends from 2002 to 2012 and Figure 4. 32 from 2009 to 2012. Temperature trends are represented by the interpolated background color, whereas the ZWD drifts are displayed as individual colored points. Both quantities were normalized to range from -1 to +1, since ZWD and temperature have different unit.

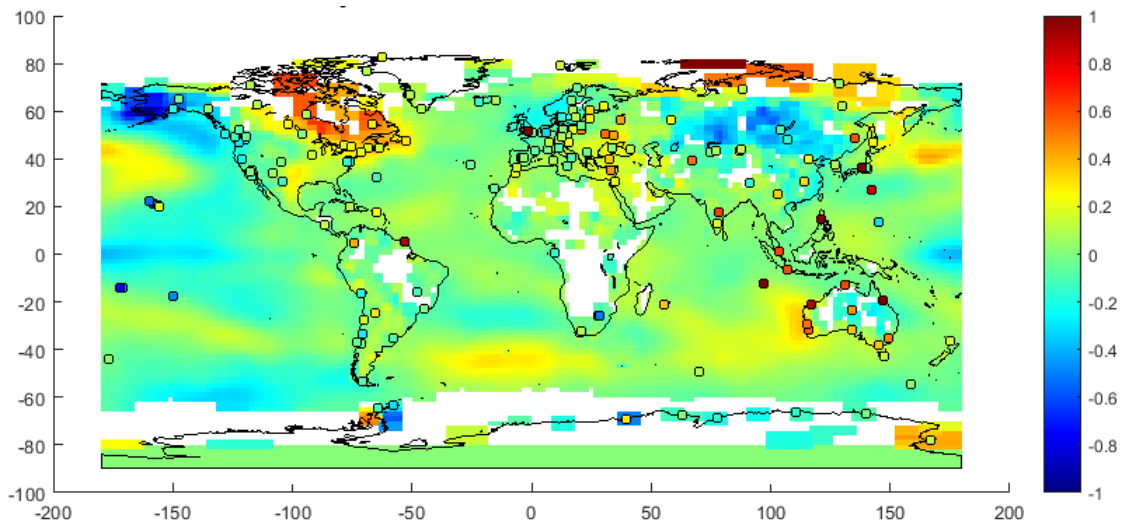


Figure 4. 31: ZWD drifts derived from GNSS data during the period 2002 to 2012 (dots) and corresponding temperature drifts represented as colored background

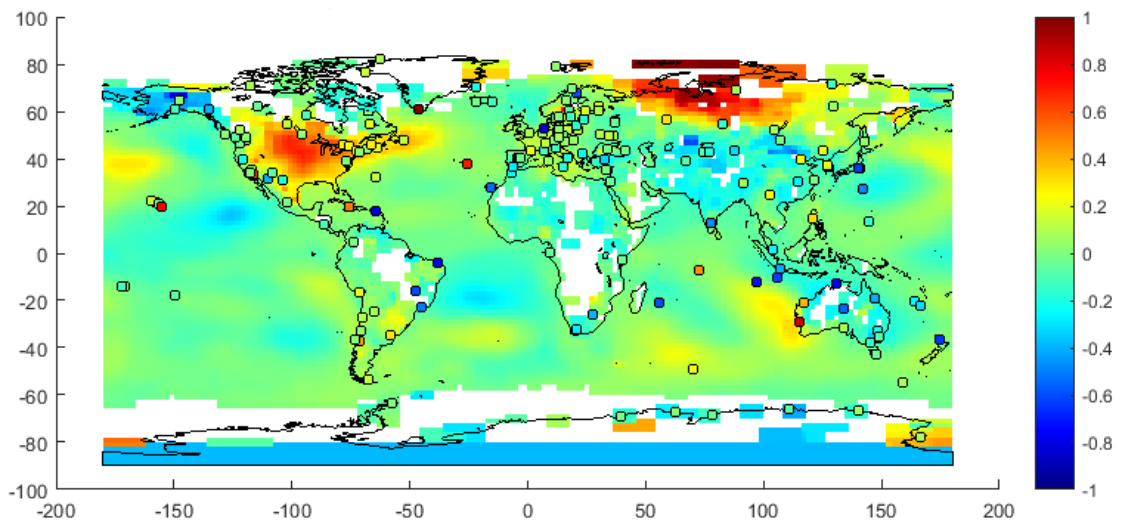


Figure 4. 32: ZWD drifts derived from GNSS data during the period 2009 to 2012 (dots) and corresponding temperature drifts represented as colored background

Figure 4. 33 is showing the mean of the maximum, minimum, mean and median ZWDs over all stations belonging to a certain class (classification according to latitude) from 2002 to 2012.

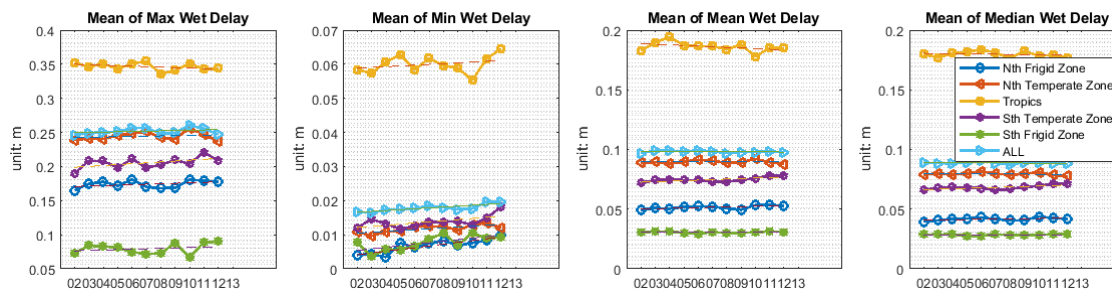


Figure 4. 33: Mean of the maximum, minimum, mean and median ZWDs over all stations belonging to a certain class

From Figure 4. 31, Figure 4. 32 and Figure 4. 33 we can see that, in general, water vapor is increasing from 2002 to 2012 but not for every year and every region. In particular, the drift in the mean of the minimum water vapor values shows a trend that is significantly increasing.

Due to the comparatively irregular and sparse distribution of the GNSS observations, the results are only covering certain regions. As the number of GNSS tracking stations is growing, GNSS will be an effective technique for climate monitoring and forecasting in the future.

Swiss Positioning Service (swipos)

U. Wild, D. Andrey, C. Biberstein-Pedroni, L. Kislig and J. Liechti

Swiss Federal Office of Topography

The years 2015 – 2019 were designated to the enhancement of the Automated GNSS Network Switzerland (AGNES) and the Swiss Positioning Service (swipos) to «Multi GNSS». The project AGNES-III (indicating the third technical generation of the network), which was already started in 2013, had the aims to replace the existing GNSS receivers (Trimble Net R5) with the newer Trimble Net R9 receivers and to install and test the new multi-GNSS capable software versions of the Trimble Pivot Platform.

The roll-out of the new GNSS receivers and antennas was completed in May 2015. Simultaneously with the replacement of the receivers at some stations older Trimble Zephyr antennas have been replaced by Trimble GNSS choke ring antennas. The installation of the new antennas was the opportunity to introduce new station coordinates, which are consistent with the absolute antenna calibration models of the AGNES stations.

The server infrastructure of the AGNES/swipos control center has been moved in late 2014 to the new Swisscom computing center. In order to be able to use the new Galileo and BeiDou signals from the AGNES stations, different new versions of the Trimble Pivot Platform software (Version 3.8 / Version 3.10 and Version 4.10) have been installed and tested.

The main new feature of all these versions was the new multi-GNSS capable network processor RTXNET. This processor uses the method of Precise Point Positioning (PPP) and combines the data of the AGNES stations with high-precision clock and orbit data, which are delivered as real-time data streams from a world-wide Trimble reference station network. The resulting geometric and ionospheric error models are used to compute the Virtual Reference Stations (VRS).

After the official declaration of the “Initial Services” for Galileo by the European Commission (EC) in December 2016 the first Galileo orbit data were available in the RTXNET processor.

For the transmission of real-time multi-GNSS corrections within swipos a new format version RTCM 3.2 MSM (=Multiple Signal Message) had to be introduced. This format includes different new record types for Galileo and BeiDou observations. Furthermore the format contains different information levels, ranging from 1 (= pseudoranges) to 7 (= pseudoranges/phase/doppler/signal-to-noise). For swipos the information level 4 was chosen. Because not all customer rovers were able to work with this new RTCM format version, the new multi-GNSS mountpoints (RTCM 3.2 MSM) were established in parallel to the existing ones (RTCM 3.1).

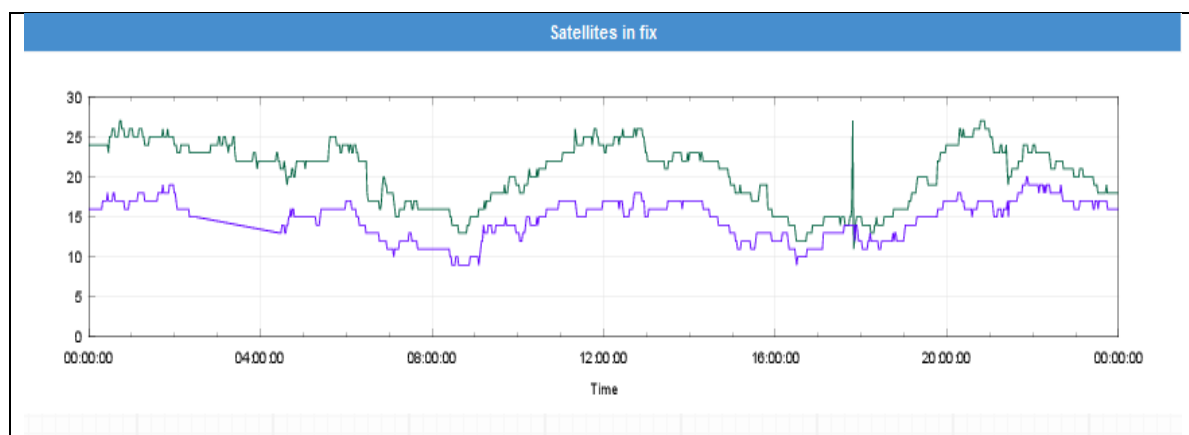


Figure 4. 34: Fixed in RTCM 3.1 (blue) and RTCM 3.2 MSM (green) [01.04.2019]

One major issue of swipos during the last years was the height accuracy. Especially during the summer season large variations (up to 1 – 2 dm in worst case situations) during the day were observed. The reason of these variations is the special topography within Switzerland, with huge altitude differences between the reference stations and also between the swipos users and the nearest reference station. In these cases the tropospheric interpolation scheme of the RTKNET processor seems not to work properly.

The new RTXNET processor however seems to give better results as can be seen in Figure 4. 34. The figure depicts the differences between different ZTD estimates for the AGNES station Ardez (ARD2). It becomes obvious the estimates of the new RTXNET processor (Real-time rtx_net-01 and rtx_net-02) show a much higher agreement with the reference solution (Near-real-time) of the Permanent Network Analysis Center (PNAC) of swisstopo than the estimates of the processor RTKNET (vrs3net-01 and vrs3net-02).

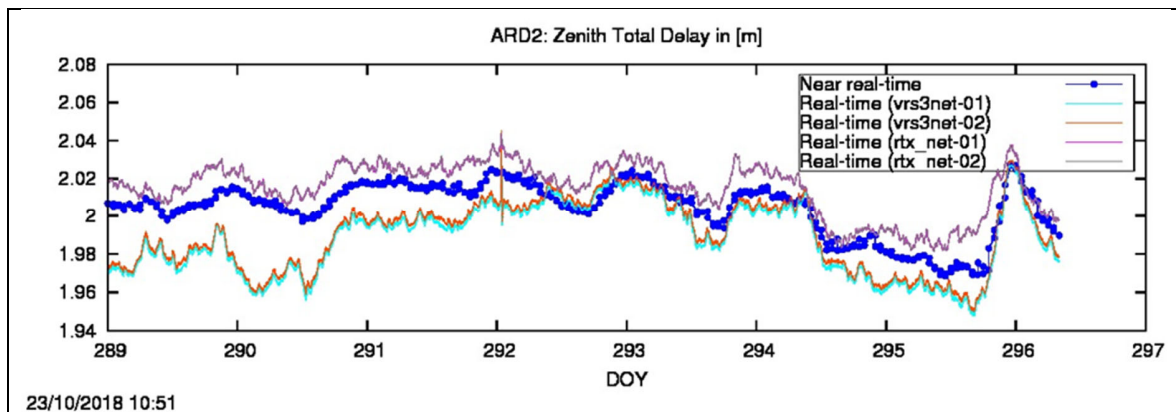


Figure 4. 35: Comparison of ZTD estimates from RTKNET and RTXNET

A major step ahead in the quality of service of AGNES/swipos could be reached in October 2017, when the communication between the stations and the AGNES/swipos central could significantly be improved by introducing a new direct routing on the communication network of the federal administration. The new routing lasted in smaller delays and higher reliability of the station communication.

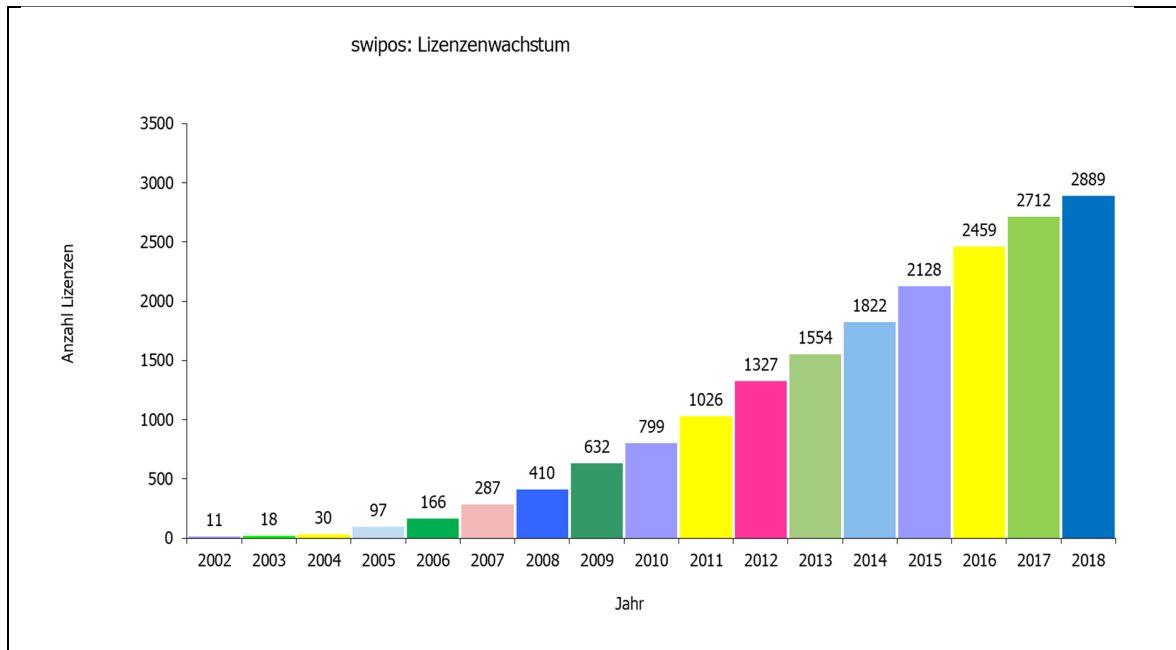


Figure 4. 36: Number of swipos licences 2002 - 2018

The number of licensed swipos users has increased in the period 2015 – 2019 by more than 50% from 1822 to 2889 users. Whereas at the beginning of swipos the major application was cadastral surveying, nowadays 36% of the users are in construction and machine guidance, followed by network information systems with 20% and cadastral surveying with 18%. In the last 2 years new market segments like precision farming and snow management could be acquired by introducing new business-to-business (B2B) price and reseller models.

AIUB contribution to the Copernicus POD Service

D. Arnold, V. Girardin, A. Jäggi

Astronomical Institute, University of Bern

The European Earth Observation Programme Copernicus (Aschbacher and Milagro-Pérez, 2012) is based on the fleet of the Sentinel Earth observation satellites. Table 4. 2 shows the Sentinels currently in orbit. All of them are equipped with GPS receivers and star cameras, allowing for GPS-based Precise Orbit Determination (POD). The Sentinel-3 altimetry satellites are as well equipped with a Doppler Orbitography and Radiopositioning Integrated by Satellite (DORIS) receiver, as well as Satellite Laser Ranging (SLR) retroreflectors for the independent orbit validation.

Table 4. 2: List of Sentinel satellites currently (March 2019) in orbit, together with their launch date and orbital altitude.

Satellite	Launch date	Altitude
Sentinel-1A	3 April 2014	693 km
Sentinel-1B	25 April 2016	693 km
Sentinel-2A	23 June 2015	786 km
Sentinel-2B	7 March 2017	786 km
Sentinel-3A	16 February 2016	815 km
Sentinel-3B	25 April 2018	815 km
Sentinel-5P	13 October 2017	824 km

The operational POD of the Sentinel-1/2/3 satellites is performed by the Copernicus POD (CPOD) Service (Fernández et al., 2014, 2015, 2016), developed and operated by a GMV-led consortium from Tres Cantos, Spain. The accuracy requirements for the Non-time Critical (NTC) orbits are 5 cm in 3D for Sentinel-1 and 2-3 cm in radial direction for Sentinel-3. External orbit validation is regularly performed by comparing the CPOD Service orbits to orbit solutions provided by POD expert members of the Copernicus POD Quality Working Group (QWG). AIUB, as a regular member of the POD QWG, is computing the orbits for all six Sentinel-1/2/3 satellites from GPS data on an operational basis and delivers them three times per year for the CPOD Regular Service Reviews (RSRs). The diversity of processing software packages and orbit modelling details among the different members of the POD QWG allows for a validation of the official Sentinel orbits, as well as for investigations regarding systematic orbit deficiencies. E.g., the RSRs have revealed systematic orbit offsets mainly in radial direction for Sentinel-1, which could be attributed to erroneous geometrical information on the satellites (Peter et al., 2017).

For all Sentinel orbits AIUB employs a rather reduced-dynamic orbit parametrization with no explicit modelling of non-gravitational forces (air drag, solar and planetary radiation pressure). Since RSR #11 (28 January 2018 – 26 May 2018) AIUB is also delivering a second orbit product for Sentinel-3, for which a state-of-the-art modelling of non-gravitational accelerations is employed, allowing to constrain the empirical orbit parameters much more towards a dynamic solution. As an example, Figure 4. 37 shows the 3D orbit differences of individual external solutions w.r.t. a combined orbit solution for Sentinel-3A for the time span covered by RSR #11. The solution labelled “AIUB” corresponds to the standard reduced-dynamic AIUB solution, while “AING” refers to the solution with more dynamic stiffness. It can be seen that the AING solution performs well, yielding among the smallest 3D orbit differences.

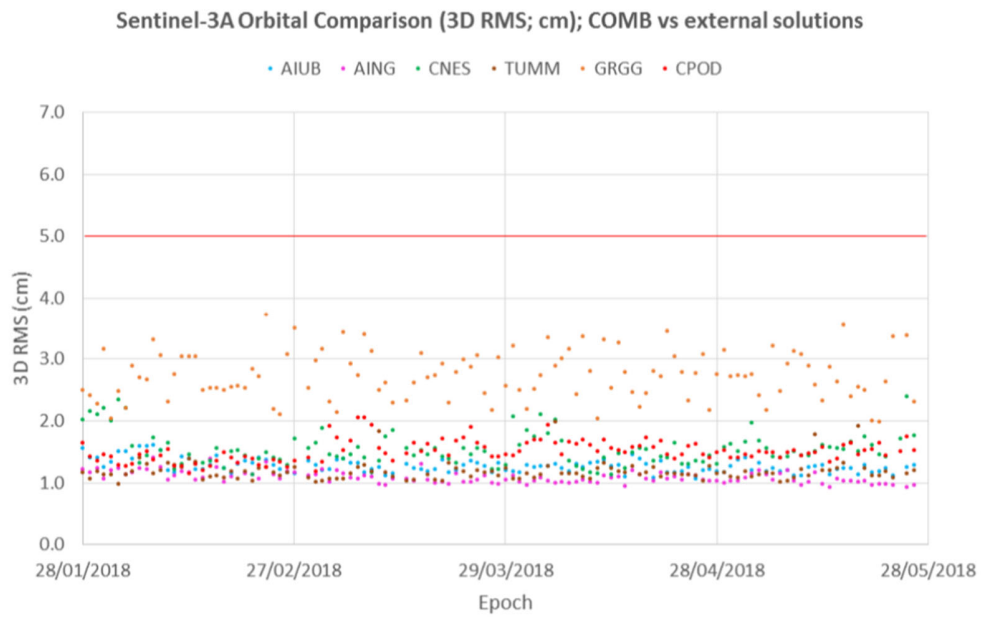


Figure 4. 37: Sentinel-3A orbit comparison conducted in the frame of RSR #11. “AIUB” denotes the standard reduced-dynamic orbit solution without non-gravitational force modelling, while “AING” labels the AIUB solution including non-gravitational force modelling and stronger constrained empirical orbit parameters

Reprocessing of the GOCE Precise Science Orbits

D. Arnold¹, V. Sterken¹, Th. Grombein², L. Schreiter¹, A. Jäggi¹

¹ Astronomical Institute, University of Bern, Switzerland

² Geodetic Institute, Karlsruhe Institute of Technology, Karlsruhe, Germany

The Gravity field and steady-state Ocean Circulation Explorer (GOCE, Floberghagen et al. 2011) satellite was launched on 17 March 2009 and orbited Earth until end of 2013 at exceptionally low orbital altitude of 224-254 km to measure the static part of Earth's gravity field with unprecedented accuracy. In the frame of the GOCE high-level processing facility (HPF) AIUB was responsible for the operational generation of the official GOCE Precise Science Orbits (PSOs) from the processing of GPS and star camera data (Bock et al. 2014). Both reduced-dynamic and kinematic orbits were delivered in 30 hour overlapping batches.

Using the kinematic GOCE orbits as pseudo-observations for GPS-only gravity field recovery, it became soon evident that the orbit quality was affected by high ionospheric dynamics, resulting in systematic artifacts in the gravity field solutions along the geomagnetic equator (Jäggi et al. 2015), see Figure 4. 38.

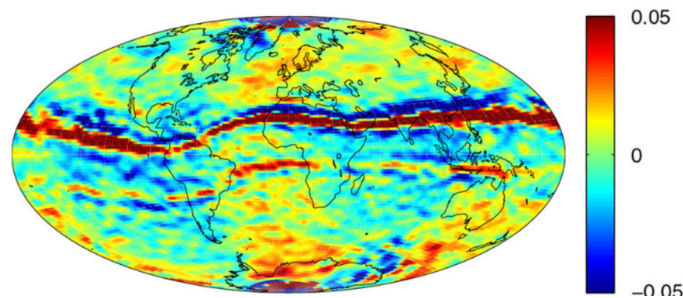


Figure 4. 38: Filtered geoid height differences in m of a GOCE GPS-only gravity field solution for November/December 2011 w.r.t. ITG-GRACE2010

Attempts were made in Jäggi et al. (2015) to mitigate these artifacts by modeling of higher order ionospheric (HOI) terms, but the success was only relatively marginal. An empirical approach involving the omission of all GPS phase data with $|\Delta L_{gf}/\Delta t| > 5$ cm/s, where $L_{gf} = L_1 - L_2$ is the geometry-free linear combination of the GPS carrier phase measurements L_1 and L_2 , turned out more efficient. While this strategy allowed to remove large parts of the equatorial artifacts in the gravity field solutions, it degraded the quality of the orbit solutions in terms of Satellite Laser Ranging (SLR) residuals, and it was, therefore, decided not to apply this data screening strategy to the generation of the official PSOs.

Since the end of the GOCE mission in 2013 the understanding of remaining artifacts (especially in gradiometer data) has improved. Due to this, ESA initiated a complete reprocessing of the entire GOCE mission data with improved processors, enabling significant improvements of the resulting gravity field solutions over the original solutions. In the frame of this reprocessing effort, AIUB had the task to reprocess the PSOs using the latest version of the Bernese GNSS Software (Dach et al. 2015), the homogeneously reprocessed GNSS products of the EGSIM reprocessing campaign (Sušnik et al. 2019), as well as with an improved strategy to mitigate ionosphere-induced artifacts in the orbit and gravity field solutions. The major steps towards the PSO reprocessing were 1) the generation of 30 hour GNSS products from the 24 hour EGSIM products and 2) the development of improved data handling strategies to address the artifacts.

The requirement of 30 hour orbit arcs for GOCE (starting at 21:00 GPS time of the previous day and ending at 03:00 GPS time of the next day) makes necessary to concatenate the 24 hour GNSS products (satellite orbits and clock corrections) to 30 hour batches. While this is straightforward for the satellite orbits, the proper concatenation of satellite clock corrections requires some dedicated procedures to avoid inconsistencies at the day boundaries (Bock et al., 2007). These procedures need the clock corrections of all GNSS satellites at the midnight epoch of the subsequent day, and since the 5s clock corrections of the EGSIM reprocessing stopped at 23:59:55, the corresponding midnight epoch had first to be added by means of a proper clock densification using GPS data including the midnight epoch.

To find more optimal data handling strategies addressing ionosphere-induced artifacts numerous different tests have been conducted, involving either the omission or the downweighting of GPS data according to different criteria. The resulting orbits were validated by means of SLR and the kinematic orbit positions were used for subsequent gravity fields recoveries to test the efficiency of the data handling strategy at hand. For the reprocessing of the GOCE PSOs the following GPS data downweighting strategy was finally chosen:

For every epoch and each GPS phase observation:

1. If $|d^2L_{\text{gr}}/dt^2| > 0.0004 \text{ m/s}^2$ and the absolute value of the geographic latitude of GOCE is below 50° , set $\sigma_d = 5$, otherwise $\sigma_d = 1$
2. Set $\sigma_r = 6 \cdot \text{ROTI}$, where ROTI is the rate of TEC (total electron content) index over 30 s
3. Use $\sigma = \max(\sigma_d, \sigma_r)$ as uncertainty for the downweighting of the GPS observation.

This strategy allowed to produce GOCE reduced-dynamic and kinematic orbits of in general better quality compared to the original PSOs, and to efficiently remove ionosphere-induced artifacts along the geomagnetic equator in gravity fields derived from kinematic orbits. As an example, Table 4. 3 shows the average values of daily differences between reduced-dynamic and kinematic orbits and the averages of SLR residuals for the reduced-dynamic orbits, both for the original PSOs and the reprocessed orbits.

Year	Red.-dyn. vs. kin. orb. (3D) [cm]	Std. dev. of SLR residuals [mm]
2009	1.84/1.72	17.9/17.6
2010	2.16/2.04	15.9/15.8
2011	3.11/2.84	15.2/15.2
2012	3.92/3.57	18.4/18.2
2013	4.81/4.37	24.9/23.0

Table 4. 3: *Quality measures of original/reprocessed GOCE orbits: 3D differences (in terms of RMS) between the reduced-dynamic and kinematic orbits and standard deviations of SLR residuals for the reduced-dynamic orbits*

Figure 4. 39 shows the impact of the downweighting strategy on the yearly gravity field solution of 2011, the worst year regarding ionosphere-induced artifacts (due to high solar activity). Notice that the shown gravity field solutions were obtained without making use of the common mode accelerometer data. Using this data significantly improves the spherical harmonic coefficient S_{22} and removes the obvious blue and yellow longitudinal pattern in the geoid height plots (Jäggi et al. 2015).

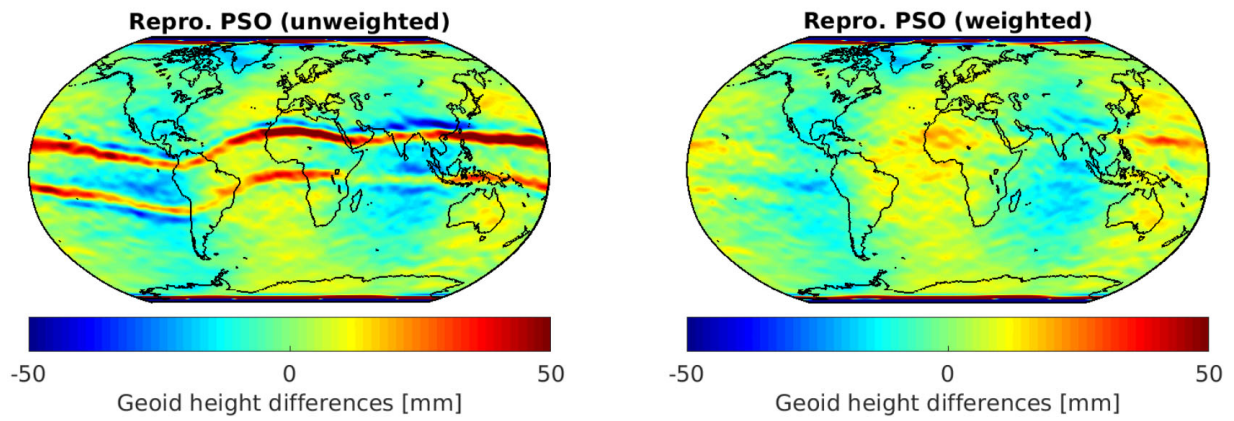


Figure 4. 39: Geoid height differences of yearly GOCE GPS-only solutions for 2011 w.r.t. ITG-GRACE2010 (300 km Gauss filter applied). The gravity field solutions were derived from reprocessed GOCE kinematic orbits obtained without (left) and with (right) applying the GPS data downweighting strategy

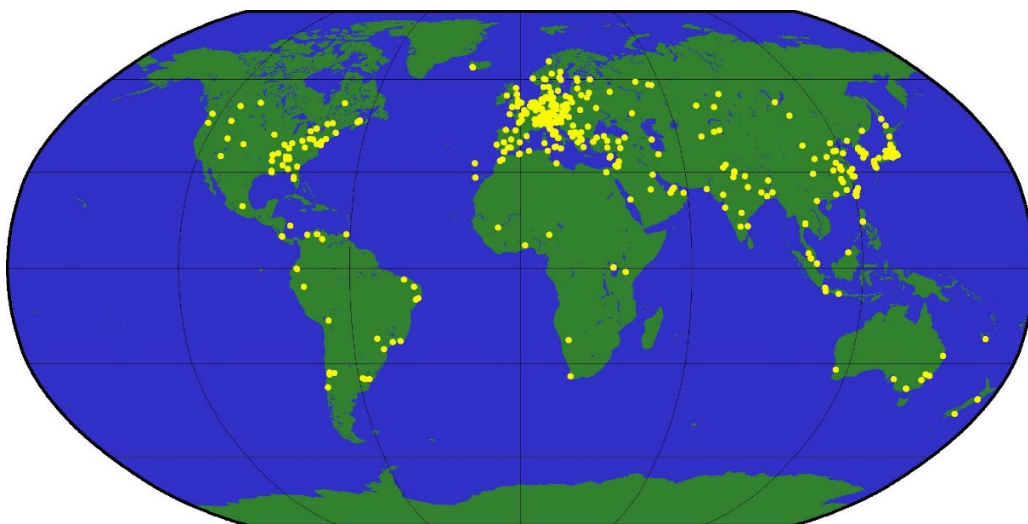
Bernese GNSS Software

R. Dach, P. Fridez, F. Andritsch, D. Arnold, S. Bertone, A. Grahl, V. Girardin, Y. Jean, M. Lasser, S. McNair, L. Mervart, U. Meyer, L. Prange, S. Scaramuzza, S. Schaer, L. Schreiter, D. Sidorov, P. Stebler, A. Sušnik, A. Villiger, A. Jäggi

Astronomical Institute, University of Bern, Switzerland

The Bernese GNSS Software (BSW, Dach et al., 2015) is the backbone for all activities of the satellite geodesy research group at AIUB: high performance processing of measurements, obtained by GNSS (Global Navigation Satellite Systems) and SLR (Satellite Laser Ranging), precise orbit determination for GNSS as well as Low Earth Orbiting satellites (LEOs), and even gravity field determination. The software is also applied in the context of operational processing schemes, e.g., in the context of CODE (Center for Orbit Determination in Europe) since more than 20 years. CODE is a consortium of four institutions, namely the Astronomical Institute of University of Bern (AIUB, Switzerland), the Swiss Federal Office of Topography (swisstopo, Switzerland), the Bundesamt für Kartographie und Geodäsie (BKG, Germany), and the Ingenieurinstitut für Astronomische und Physikalische Geodäsie, Technische Universität München (IAPG/TUM, Germany). CODE's main functions are its activities as an Analysis Center (AC) of the International GNSS Service (IGS, Schaer et al. 2019a), AC of the European Permanent Network (EPN, Schaer et al. 2019b), and as an Associated AC of the International Laser Ranging Service (ILRS, e.g., Meyer et al. 2019).

The BSW is a high performance, high accuracy GNSS and SLR post-processing software package primarily used in the space-geodetic community. It is supported, maintained, and regularly updated by AIUB, considering the latest recommendations and models (e.g., according to the IGS standards and IERS Conventions, Petit and Luzum, 2010) as well as technological advancements (e.g., new satellite systems and observables), offering the user a maximum of flexibility in customizing processing strategies and options. The BSW comes with a user-friendly interface, an online help system, and an extensive user manual. The so-called Bernese Processing Engine (BPE) allows for automated processing, which is especially useful for large network processing and reprocessing efforts. Nowadays the BSW consists of more than 100 programs and about 1300 modules and subroutines, is platform-independent, and is used by several hundred customers throughout the world (see Figure 4. 40).



GMD 2019 Jan 24 15:59:25 Geographical Distribution of Institutions using the Bernese GNSS Software

Figure 4. 40: Worldwide distribution of the Bernese GNSS Software users as of March 2019.

Since the release of the version 5.2 of the BSW in 2012, 8 maintenance releases have been made available to the users. These updates not only correct software bugs, but also implement improvements based on our own research activities and developments in the area of GNSS, thus keeping the BSW version 5.2 as an efficient and useful tool for GNSS data analysis.

Important improvements concerned the following:

- The implementation of the new extended CODE orbit model (ECOM-2, Arnold et al., 2015) which takes better into account the varyingly illuminated cross section of elongated satellite bodies.
- Full implementation of the new ITRF2014 (Altamimi, et al., 2016), which takes into consideration the post-seismic deformation, along with the IGS realisation IGS14 together with documentation and processing examples.
- Adapting the software to handle also the new RINEX v3 standard for improved handling of different observation types not only from enhanced GPS but also for other GNSS, like Galileo (Prange et al., 2016).
- Galileo processing capabilities, which are documented in examples and are part of the material covered in the BSW course held twice a year at AIUB.
- Implemented compatibility with the new Standard Product Orbit Format 3 (SP3d), which is prerequisite to be able to produce solutions based on combined observations to the multiple GNSS available today, as explored and promoted in the MGEX project (Prange et al., 2019a).
- Improved support of individually calibrated receiver antennas including the full multi-GNSS/multi-frequency calibrations from an anechoic chamber (Villiger et al, 2019a).

For the daily research at AIUB and the routine processing tasks for CODE, the development version of the BSW is used and many additional developments are being implemented there. This version serves as the base for future versions of the BSW that will be made available to the user community. Major new developments are described in other sections of this volume and include:

- Further advances in the orbit model for eclipsing satellites (Sidorov et al., 2019) and the SRP model for orbit normal attitude (Prange et al., 2019b)
- Full support of additional GNSS besides GPS, GLONASS, and Galileo, namely BeiDou and QZSS (Prange, et al., 2016, 2019)
- Ambiguity resolution in zero-difference solutions and PPP (Schaer et al., 2019c)
- Improved code bias handling in terms of observation specific bias setup allowing for a flexible processing of multi-GNSS data (Villiger et al., 2019b).

CODE Contributions to Global Ionosphere Monitoring

S. Schaer^{1,2}, A. Villiger¹

¹ Astronomical Institute of the University of Bern, Switzerland

² Swiss Federal Office of Topography (swisstopo), Wabern, Switzerland

CODE has been extracting information of the total electron content (TEC) from the International GNSS Service (IGS) tracking data since 1995. Since June 1998, related global ionosphere maps (GIM) have been generated in IONEX (Ionosphere Exchange) format and provided to the IGS to support variable applications, e.g., dealing with the ionosphere induced short-term signal variations or strong horizontal gradients.

In addition to this primary IONEX product, which is a product of the final analysis line, also corresponding rapid and predicted GIMs are generated at CODE on an operational basis. All GIM products are made available in form of IONEX and as ionosphere files in the internal format of the Bernese Software (Dach et al. 2015). Since July 2000, CODE has additionally been providing RINEX-formatted Klobuchar-style ionosphere coefficients (best fitting CODE's IONEX data).

In November 2014, the time resolution has been increased (from 2 hours) to 1 hour for all CODE GIM product lines (Schaer 2014).

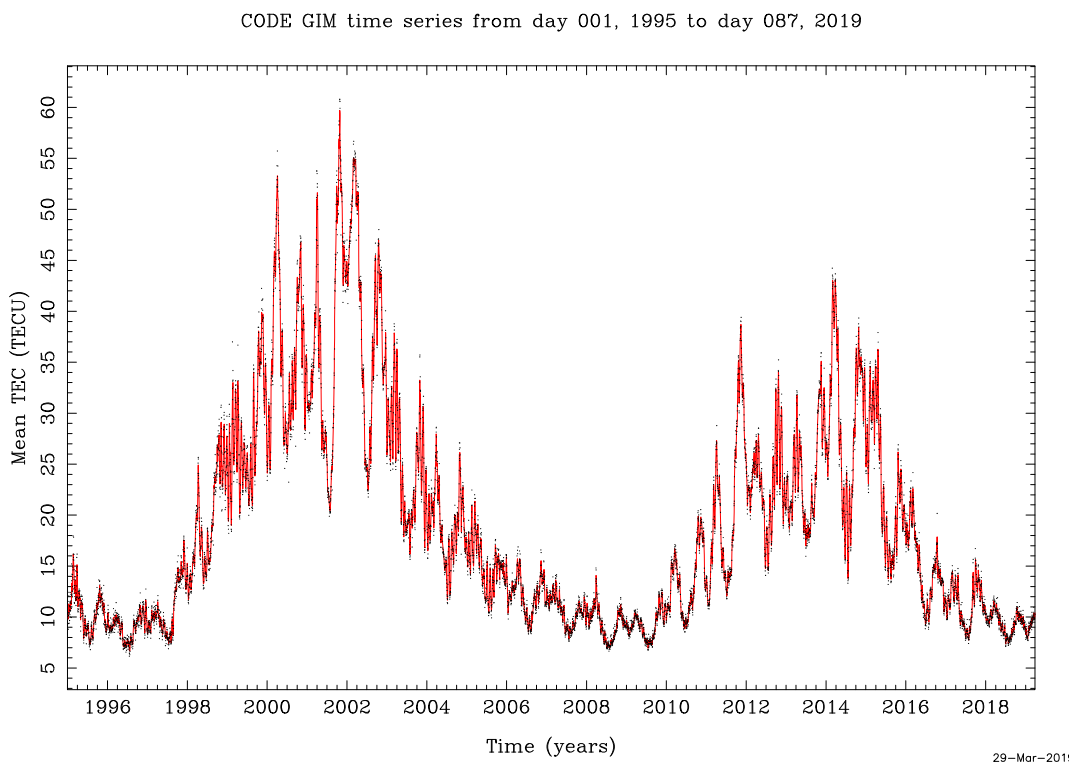


Figure 4. 41: The time series of global mean TEC values extracted from the GIMs produced by CODE covers, with 24 years, more than two (11-year) solar cycles. Daily averaged mean TEC values, namely the zero-degree coefficients of the spherical harmonic expansion used to represent the global TEC, are shown. Annual and semi-

annual variations are visible. The ionospheric signal also includes very pronounced 27-day variations, caused by distinctive groups of sunspots co-rotating with the Sun.

C1W-C2W and C1P-C2P DCBs (differential code biases) for GPS and GLONASS (satellites and receivers) are an essential by-product of the ionosphere analysis. In 2016, CODE switched from a differential to pseudo-absolute observable-specific signal bias (OSB) parametrization (Schäfer et al. 2019; Villiger et al. 2019). Figure 4. 42 shows corresponding code bias results for the GPS satellite constellation and Figure 4. 43 for the GLONASS constellation.

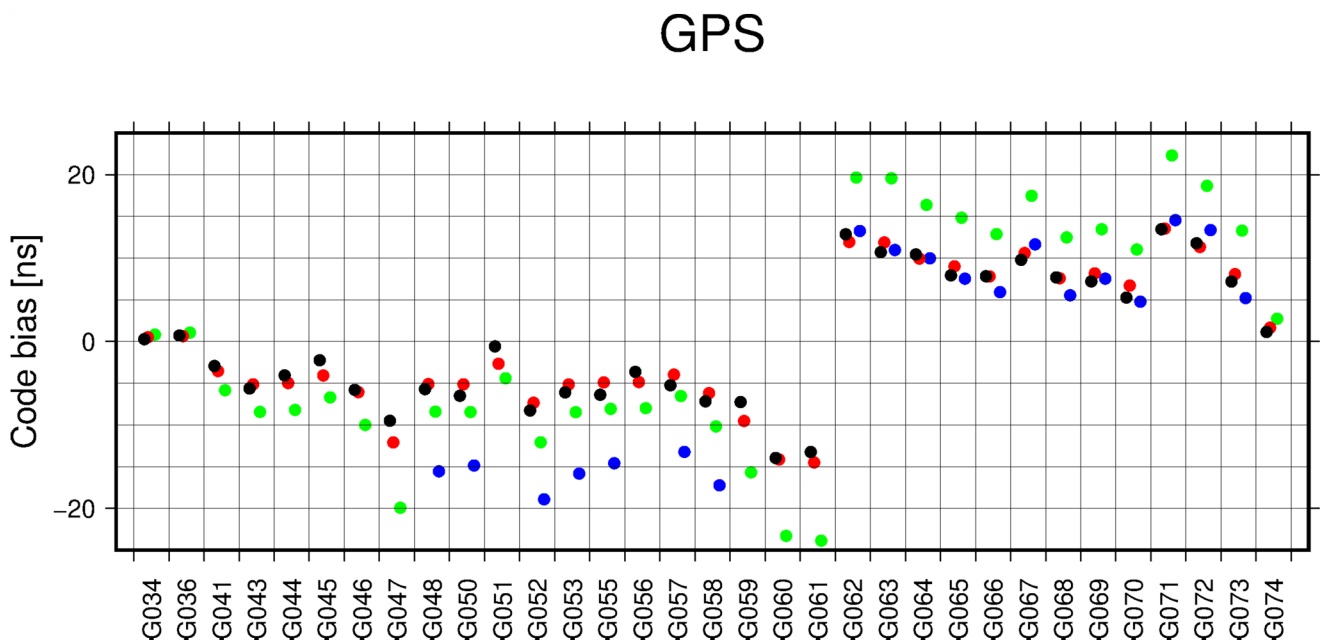


Figure 4. 42: Observable-specific code bias (OSB) estimates for GPS code observable types (using the RINEX3 nomenclature) and GPS SV numbers, computed at CODE, for January 2019. Note that G034–G036 correspond to Block IIA; G041–G061 correspond to Block IIR, IIR-M; G062–G073 correspond to Block IIF satellite generations and G074 corresponds to the first Block IIIA.

GLONASS

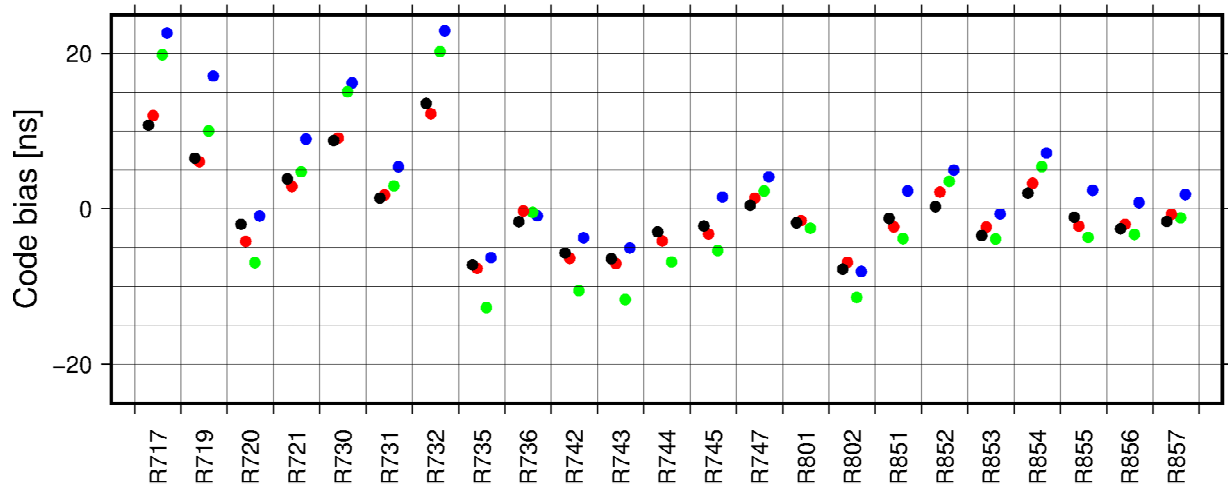


Figure 4. 43: Observable-specific code bias (OSB) estimates for GLONASS code observable types (using the RINEX3 nomenclature) and GLONASS SV numbers, computed at CODE, for January 2019.

Since the beginning of 2010, CODE has considered not only first-order but also higher-order ionosphere (HOI) and ray bending correction terms for the analysis of space geodetic observations in the operational contributions as well as for a future reanalysis of the data from IGS (Lutz et al. 2009, 2010). It should be mentioned that the previously introduced GIM products are of fundamental importance for computation of these higher-order ionosphere correction terms.

Ambiguity Resolution in Zero-Difference Solutions and for PPP

S. Schaer^{1,2}, A. Villiger¹, D. Arnold¹, L. Prange¹, R. Dach¹, A. Jäggi¹

¹ Astronomical Institute, University of Bern, Switzerland

² Swiss Federal Office of Topography (swisstopo), Wabern, Switzerland

The Center for Orbit Determination in Europe (CODE) IGS analysis center has established the generation of a high-quality signal-specific phase bias product and a fully consistent ambiguity-fixed clock product within its rapid and final IGS-related processing. The new clock products have been submitted to the IGS starting with GPS week 2004 (June 3, 2018) for our IGS rapid and final product lines and starting with GPS week 2006 (July 17, 2018) for our multi-GNSS clock product contribution to MGEX. The MGEX

clock product does include ambiguity fixing not only for GPS but also for Galileo.

This quantum leap in GNSS clock analysis at CODE could be accomplished due to successful between-satellite ambiguity resolution using undifferenced observation data of IGS receiver network. The new CODE clock products reveal a notably improved quality and, in the end, allow for single-receiver ambiguity resolution, thus enabling integer-PPP (IPPP). Our new clock and bias products are conditioned in a way that maximum consistency may be ensured for ambiguity-float, ambiguity-fixed, and pseudorange-supported, or pseudorange-only PPP applications. In any case, the clock product has to be used in conjunction with the associated phase and pseudorange bias product in order to achieve best possible performance.

The ambiguity resolution concept that was implemented into the rapid, final and MGEX clock solutions provided to the IGS is illustrated in Figure 4. 44. It consists of the following steps:

- A clock solution without ambiguity resolution is carried out.
- Wide-lane (WL) phase biases for the Melbourne-Wübbena (MW) linear combination are computed.
- Using these WL phase biases, the Melbourne-Wübbena linear combination is analyzed to resolve the WL ambiguities.
- Narrow-lane (NL) phase biases are computed based on the clock solution (and resolved WL integers).
- Using these NL phase biases (and resolved WL integers), the ionosphere-free linear combination of phase observations is analyzed to resolve the NL ambiguities.
- The phase biases for the original frequencies (L1 and L2) are derived from the WL and NL phase biases.
- A clock solution with fixed L1 and L2 phase ambiguity integers is generated.
- The NL ambiguity resolution steps could be repeated by continuing at step 4 in order to start a NL phase bias determination and NL ambiguity resolution already with an ambiguity-fixed clock solution. Additional iterations turned out to be not necessary.

The phase biases in step 6 are represented following the principle of Observation-Specific Biases (OSBs). This allows a flexible combination of results based on observations from different frequencies.

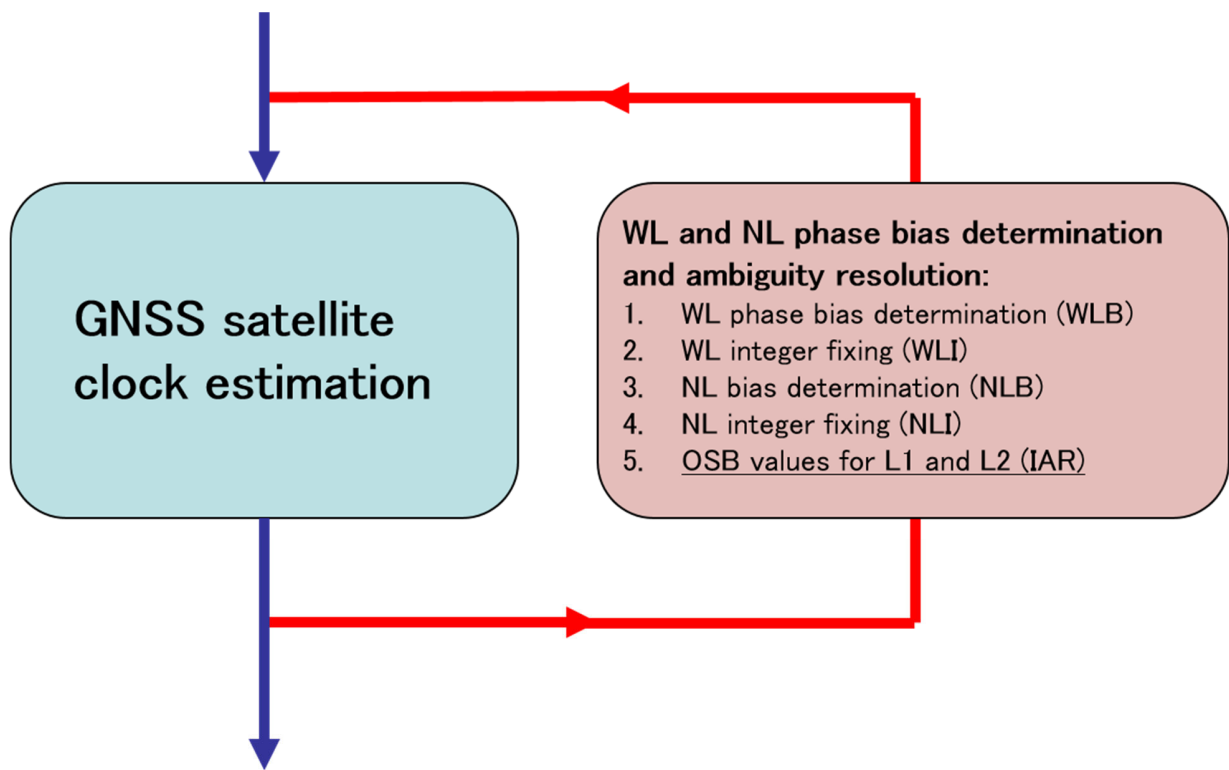


Figure 4. 44: Principle of the single-receiver ambiguity resolution as performed in the clock analysis for the IGS at AIUB.

The positive impact of the introduced ambiguity resolution scheme on the CODE contribution (red line) can be seen in Figure 4. 45. It shows the clock standard deviations as they are computed in the clock combination procedure by the analysis center coordinator (ACC, <http://acc.igs.org>). The zoomed part is related to the epoch in June 2018 when the single-receiver ambiguity resolution was enabled.

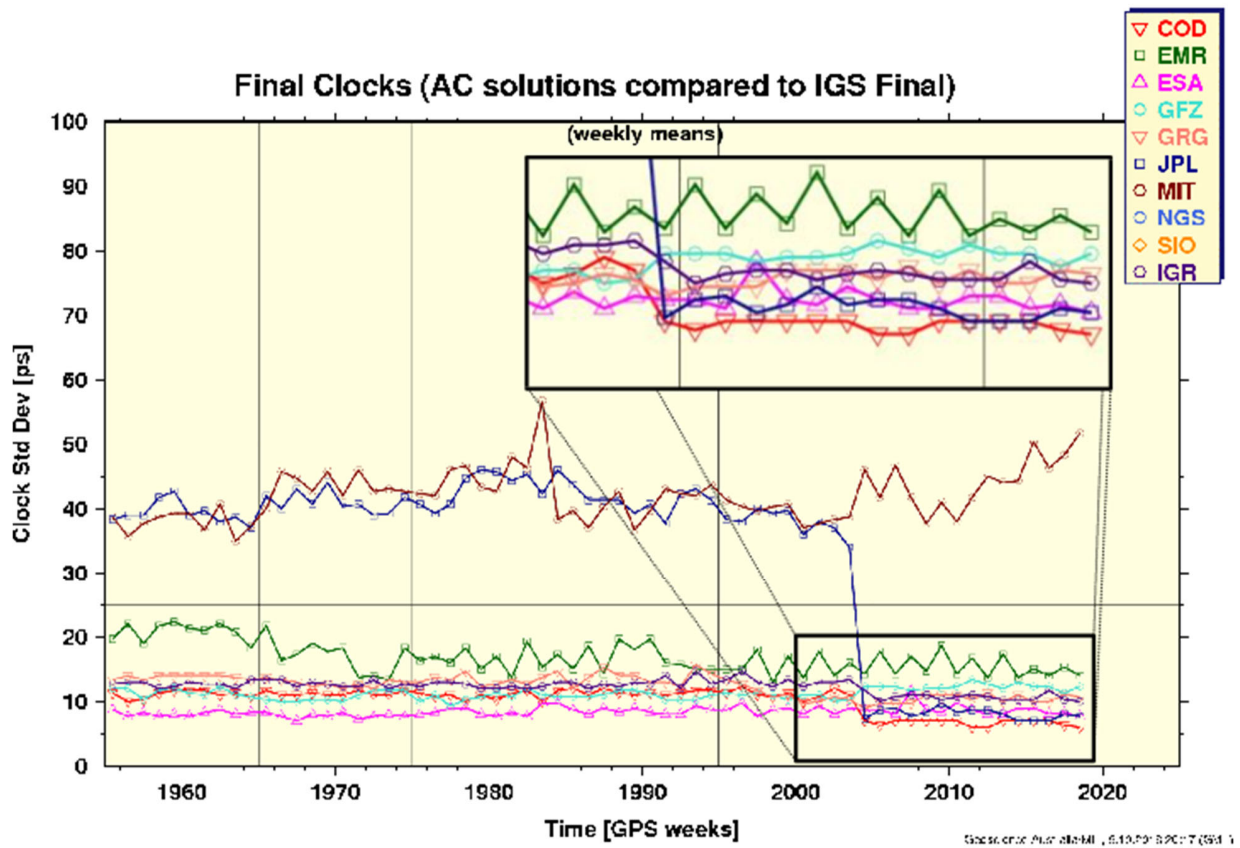


Figure 4. 45: Impact of introducing undifferenced ambiguity resolution at CODE on the IGS final clock combination as provided by <http://acc.igs.org>.

Determination of GNSS Pseudo-Absolute Code Biases and Classification of Receiver Tracking Technology

A. Villiger¹, S. Schaer^{1,2}, R. Dach¹, L. Prange¹, A. Sušnik^{1,3}, A. Jäggi¹

¹ Astronomical Institute, University of Bern

² Federal Office of Topography (swisstopo)

³ Now with: School of Civil Engineering and Geosciences, Newcastle University, Newcastle NE1 7RU, UK.

The code bias estimation is crucial for GNSS data processing when code measurements are used, e.g., for clock analysis or ambiguity resolution strategies relying on code measurements. They describe the time delay between the signal generation and the actual emission from the satellite antenna and the receiver delay between the actual reception time in the antenna and the clock reading within the receiver. These delays are highly correlated to the clock parameters and cannot be separated (unless absolute calibrations are available which is typically not the case). In order to overcome this correlation one can define the bias of an observable type as zero (defining the clock) or a linear combination thereof. In the IGS this is typically a C1W/C2W ionosphere free linear combination (IF) clock ($C1W=C2W=0$).

With the increasing number of GNSS and observation types, the classical differential parametrization of the code biases becomes more and more cumbersome as one needs to keep track of the used signals and define the desired clock definition in advance to setup the remaining code biases. A more direct approach, which offers much more flexibility, is the observable-specific signal bias (OSB) approach where each observable type gets its own code bias parameter. After processing the available data and storing the results into normal equations (NEQs) – without any code bias datum definition. Only before the actual inversion of the NEQ, the content can be analyzed and an optimal set of constraints applied (e.g. defining C1W/C2W IF clock). One benefit from the new parameterization approach is that it has the potential to easily change the datum according to the current needs, e.g. to redefine the C1W/C2W IF to a C1C/C2C IF clock for GPS or even to C1C/C5Q from Galileo.

Observable-specific code biases (OSB)

With setup of OSBs in the NEQ without introducing any datum, it is possible to combine the NEQs from multiple sources, namely from the clock and ionosphere analysis, resulting to a multi-purpose set of OSB values which can be used for any applications. This can also be done for the phase biases extracting the L1 and L2 bias values from the wide and narrow lane biases (Schaer et al., 2019). In addition to the combination of NEQs from different sources, it is also possible to stack NEQs over longer time periods (e.g. 1 or even 20 years). The main advantage is, that with the stacking of multiple days one can unify the datum definition and align all daily code biases to one common bias datum definition. Figure 4. 46 shows the result of such a code bias combination (combination of NEQs from clock and ionosphere) which are aligned to one common code bias datum over a time span of one year (2017) for GPS.

Figure 4. 47 shows the time series for C1W OSB values of GPS satellite G046 which have been aligned to a common datum over the whole time span (2000-2018). The satellite has two jumps in the shown time period but otherwise has a remarkably stable behavior. Figure 4. 48 shows the biases for station WTZR (GPS: top, GLONASS: bottom) for the tracked OSBs. Note that during the time series from 2000 to 2018 several equipment change happened and even the tracked signals have changed. The biases are much more stable over time for GPS than for GLONASS, however, GLONASS has been treated the same way as GPS (system-wise) and not as satellite-receiver code biases which would be beneficial because GLONASS uses a frequency dependent signal modelling.

Receiver tracking technology classification

In context of the switch from a differential to an observable-specific bias approach, the traditional DCB multiplier estimation from CODE has been extended to support the OSBs. The main idea behind the multiplier approach is to introduce a known set of satellite OSBs (formerly DCBs) and search for the best fitting match of the satellite OSBs.

The satellite OSBs are obtained from a previously bias estimation run using as many stations as possible. Therefore, the satellite biases are basically the values as seen from the receivers using the assumption that the given observation type in the RINEX data is true. Thus, the multiplier approach search for receiver groups which have the same satellite bias patterns indicating that for all those receivers the same pattern can be used. This is done by introducing for each observable type an individual multiplier and during their estimation all but one set of OSB should be zero and the match come out with values corresponding to the factors of the used linear combination (e.g. 2.55 for P1 and 1.55 for P2 in case of the ionosphere free linear combination). Tests have shown that this approach works rather well for GPS. For Galileo the situation is not as good as for GPS. One of the main obstacles is, that especially the code bias values for E5, E6 and E7 are close together (as they frequencies are similar) and it is not possible to separate them using the multiplier approach as their OSB pattern cannot be distinguished between each other.

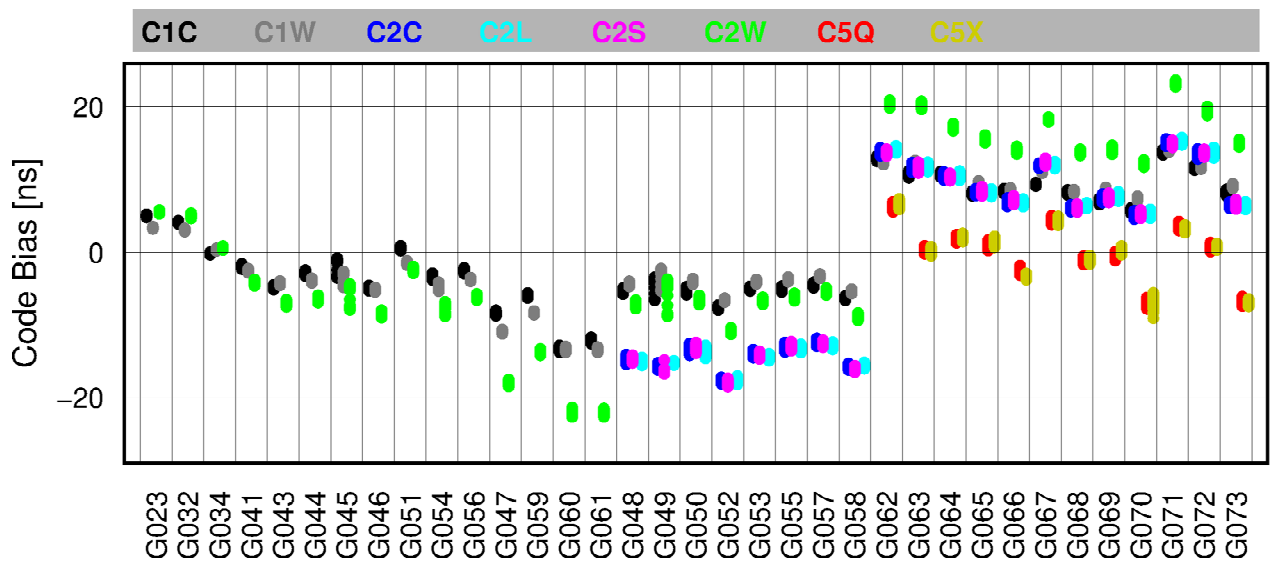


Figure 4. 46: OSB values, obtained from the combination of clock and ionosphere analysis, for GPS from a dedicated study over one year (2017). The OSB values are re-aligned to one common datum over the entire time span.

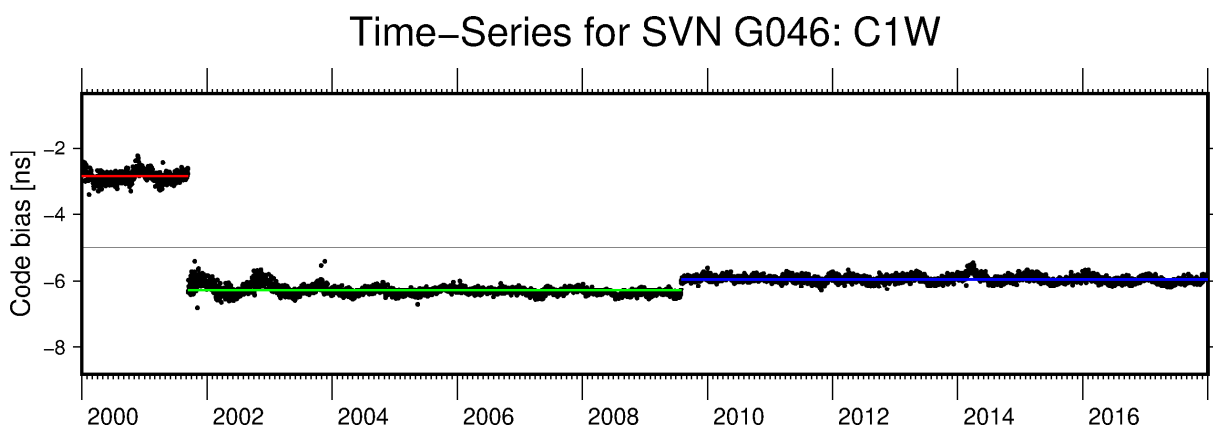


Figure 4. 47: C1W OSB values for GPS satellite (space vehicle number) G046 using a common datum over the entire time span.

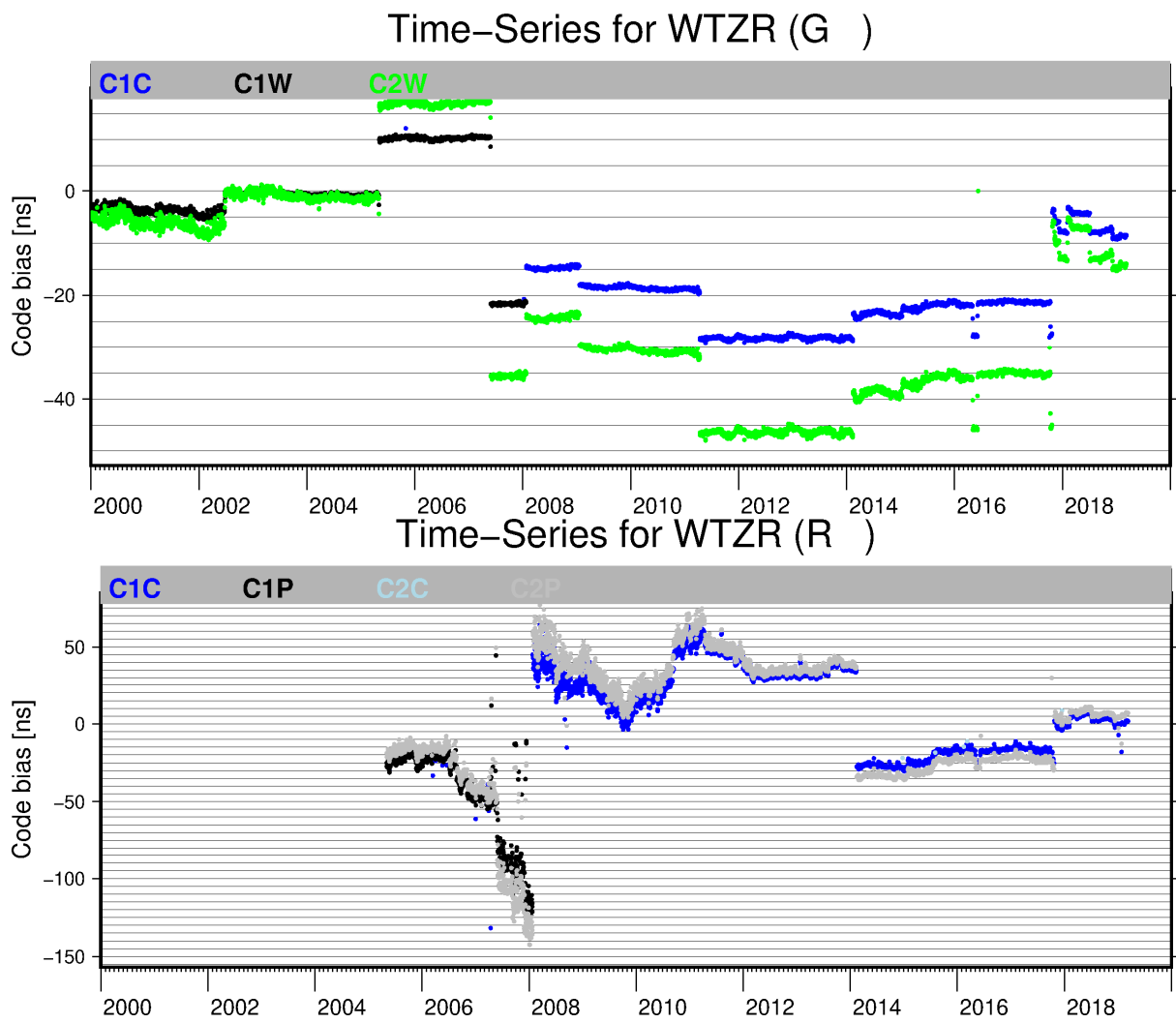


Figure 4. 48: OSB values for station WTZR using a common datum over the entire time-span.

Consistency of antenna products in the MGEX environment

A. Villiger¹, L. Prange¹, R. Dach¹, F. Zimmermann², H. Kuhlmann², A. Jäggi¹

¹ Astronomical Institute, University of Bern

² Institut für Geodäsie und Geoinformation, Universität Bonn, Bonn, Germany

Since many years the International GNSS Service (IGS, Johnston et al. 2019) is relying on absolute robot calibrations for receiver antennas (Schmid et al. 2008). The corresponding satellite antenna phase center offsets (PCO) and nadir dependent variations (PV) were not disclosed for GPS and GLONASS and were estimated based on the IGS network taking the latest international terrestrial reference frame (ITRF) scale into account. With the modernization of GPS and GLONASS and the launches of new GNSS, namely Galileo, BeiDou, and QZSS, new frequencies were introduced for the transmitting of the signals. Currently the IGS is using robot calibrations for the ground side including GPS L1/L2 and GLONASS L1/L2 calibrations without covering the newer frequencies due to the lack of available calibrations.

In 2017 the chamber calibrated satellite antenna calibrations were released by the European GNSS Agency (GSA 2016a, 2016b; in the case of Galileo) and by the Cabinet Office, Government of Japan (CAO 2018; in the case of QZSS). This lead to the current situation illustrated in Figure 4. 49. For QZSS the situation is as desired were calibrations are available for the satellite and receiver antennas. This is because QZSS uses the same frequencies as GPS and they can be used when processing QZSS signals. On the other hand, for Galileo and BeiDou the ground antenna calibrations for those two systems are not available and are substituted by the GPS L1/L2 frequencies. This is a better approximation than using no patterns, but it is only a rough approximation.

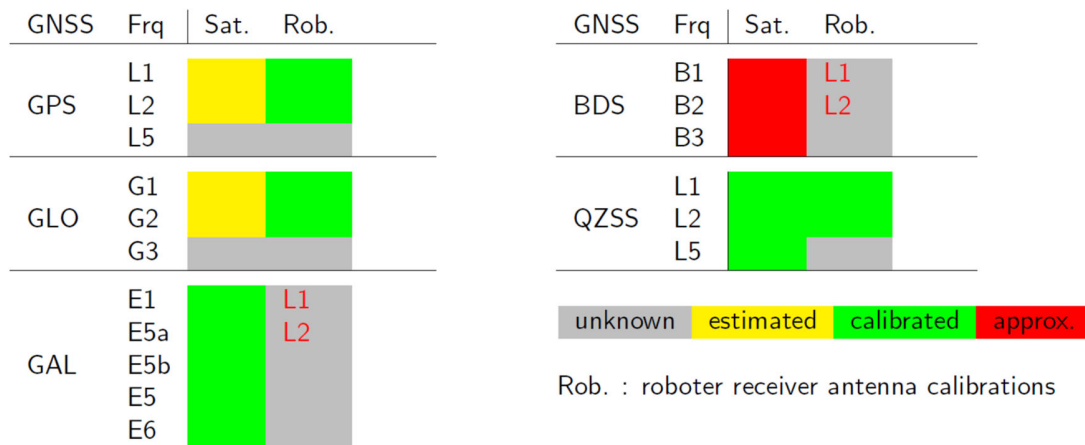


Figure 4. 49: Situation of the antenna calibrations by the end of 2018.

From Figure 4. 49 it becomes obvious that for multi-GNSS solutions the lack of calibrations for the newer signals, in particular Galileo where the satellite patterns are available, is a major drawback.

Chamber calibrations

In order to study the impact of missing calibrations a dedicated study was done using chamber calibrations for the receiver antennas from the University of Bonn. More than 250 individual antenna calibrations are available and allow to create type-mean antenna calibrations. With the available dataset it was possible to create calibrations for more than 35 antenna/random combinations. Those calibrations cover almost 50% of the used antennas within the IGS network. The difference between the phase center offsets derived from robot and chamber calibrations vary for the horizontal components between +2 mm and between 4 and -6 mm for the vertical component. As the chamber calibrated type-mean pattern cover most of the antennas used within the processing line of the Multi-GNSS Extension (Montenbruck et al., 2013) it is possible to switch from the robot to the chamber calibrations. This allows to test the impact of using either robot or chamber calibrations and reveal the impact of their differences on precise orbit determination (POD). Figure 4. 50 shows the difference between the phase variations of the ionosphere free linear combination of L1/L2 (GPS) derived from robot and chamber calibrations for the LEIAR20 LEIM antenna. The difference in the PCOs are -1.2 mm in x, -0.9 mm in y and -6.1 mm in z.

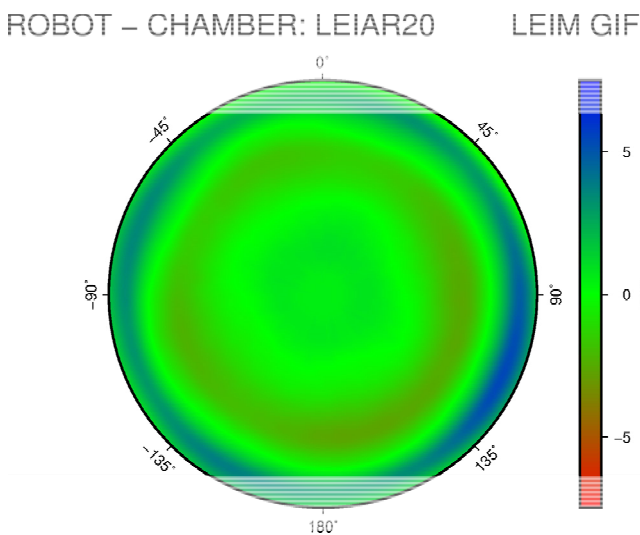


Figure 4. 50: Difference between robot and chamber phase variations (robot – chamber) for the ionosphere free linear combination of L1 and L2 (GPS)

Scale determination

Up to now the providers of GPS and GLONASS have not released their chamber calibrations. Therefore, it was so far not possible to estimate a scale for the terrestrial reference frame using GNSS. Their PCO estimations basically reflect the ITRF scale which was used to obtain those values. With the usage of the chamber calibrations the scale determination becomes feasible as on both side, on ground and in space, calibrated patterns are available. The test scenario consists of 60 days in 2018 using 90 stations. Four different test scenarios were created using different calibration combinations. On one hand, for the satellite pattern, either the estimated values (Steinberger et al., 2016) for Galileo or the actual chamber calibrations as provided by GSA were used (GSA 2016a, 2016b). On the other hand, for the receiver antenna either robot calibrations (using L1/L2 pattern from GPS also for Galileo) or using chamber calibrations.

The tests, using CODE's Multi-GNSS processing scheme (Prange et al., 2019), show that the best consistency between GPS and Galileo could be achieved by using chamber calibrations on the receiver side and the estimated values for the satellites. In order to test the different calibrations an offset between Galileo and GPS is introduced and estimated. It basically represents the offset between the coordinate which would be estimated using either GPS or Galileo only.

Table 4. 4 gives an overview over the four different test scenarios using either the PCOs provided by the GSA or the PCOs from the estimation in 2016 (Steigenberger et al., 2016).

Table 4. 4: Offset between GPS and Galileo in the up-component. Satellite antenna: Estim = estimated PCOs for Galileo (Steigenberger et al. 2016), GSA = Chamber calibrated pattern for Galileo. Ground antenna: robot: robot calibrations, currently used within the IG IGS, Chamber: chamber calibrated pattern including E5.

Satellite antenna	Ground antenna	Offset Galileo - GPS (up component)
Estim	Robot	-2.6 mm
Estim	Chamber	+0.4 mm
GSA	Robot	+7.3 mm
GSA	Chamber	+9.4 mm

When using the chamber calibrations for the Galileo satellites, the difference between a GPS vs a Galileo coordinate is, on average, almost 1 cm. The explanation for this offsets is quite simple: the estimated Galileo PCOs are based on the ITRF2014 scale, which is also valid for GPS. Changing to the chamber calibrated satellite antenna pattern for Galileo, will introduce a Galileo scale which is not consistent with the ITRF scale (a result of the combination between SLR and VLBI). This results in a difference in scale of about -1.2 ppb.

Future tests will show whether Galileo can contribute to a future ITRF scale. It would be for the first time that GNSS can contribute for the scale instead of relying on other techniques (very long baseline interferometry and satellite laser ranging).

Contributions of the National Geodetic Survey (swisstopo) and of the GGL/MPG of ETH Zürich to the AlpTransit Gotthard Base Tunnel

A. Wiget¹, B. Bürki², A. Geiger², S. Guillaume², U. Marti¹ and A. Schlatter¹

¹*Federal Office of Topography swisstopo, Wabern*

²*Institute of Geodesy and Photogrammetry, ETH Zurich*

On October 15, 2010, the final breakthrough in the east tube of the Gotthard base tunnel was realized, with a horizontal (transverse) deviation of 8 cm and a vertical (height) offset of 1 cm (see e.g. in *Ingenieur-Geometer Schweiz*, 2016, p. 21). On June 1, 2016 the world longest railway tunnel was officially inaugurated. This event was a reason to look back and to appreciate the contributions of the surveyors to this “most complex construction site of the century“. The articles published in *Geomatik Schweiz* describing these contributions, the challenges as well as the solutions and the great success were all collected in a special edition published by the professional organisation *Ingenieur-Geometer Schweiz (IGS)* (2016).

The Institute of Geodesy and Photogrammetry (IGP) of the ETH Zürich as well as the Federal Office of Topography swisstopo were involved in many ways in the surveying work of the Gotthard base tunnel, i.e. by counselling and expertises, by services as well as with reference datasets and own geodetic, gravimetric and astronomical observations. In this short referencing article we concentrate on measurements, datasets and consulting done by experts of two federal institutions swisstopo and the Geodesy and Geodynamics Lab GGL (today Chair of Mathematical and Physical Geodesy MPG) of ETHZ.

The New National Geodetic Survey 1995 (LV95) and its components, the Automated GNSS Network for Switzerland (AGNES), the GPS-based national control network LV95, the national height network LHN95 and the geoid models CHGeo98/2004 allowed the construction of base tunnels through the Alps (such as Lötschberg, Gotthard and Ceneri) with only minimal additional control surveys needed.

In two papers (Wiget, Marti and Schlatter, 2016; Schlatter, Marti and Wiget, 2016) these contributions are described in detail, with special focus on the gravity field, the national height network and recent movements of the earth’s surface. These influences had to be taken into consideration for a successful breakthrough, especially in the vertical component. For instance it was shown how a harmless, potentially theoretical and academic field trial led surprisingly to the discovery of a massive subsidence on the Gotthard Pass along the axes of the Gotthard road tunnel (Geiger and Schlatter, 2016). This was a warning example of the order of magnitude of subsidence that could be expected on the earth’s surface above tunnels with a large vertical covering, which may be caused by the drainage of rock masses. And it was the reason to establish the continuous geodetic monitoring of the surface above the base tunnel in the area of large dams and the intensified automatic monitoring of the large dams during the construction of the Gotthard base tunnel, since damages especially due to differential subsidence or other impacts of the tunnel construction had to be taken into account (Salvini and Studer in *Ingenieur-Geometer Schweiz*, 2016, p. 58).

A separate article describes the astrogeodetic control surveys (vertical deflections and azimuths) that were carried out by the IGP/ETHZ in order to verify the values of the corrections applied to the gyroscopic measurements and to validate the official geoid models CHGeo98 and CHGeo2004 with actual vertical deflection surveys (Bürki and Guillaume, 2016).

Integrated Sensor Orientation on Micro Aerial Vehicles

M. Rehak, J. Skaloud

EPFL – TOPO

Mapping with Micro Aerial Vehicles (MAVs whose weight does not exceed 5 kg) is gaining importance in applications, such as corridor mapping, road and pipeline inspections, or mapping of large areas with homogeneous surface structure, e.g. forest or agricultural fields. When cm-level accuracy is required, the classical approach of sensor orientation does not deliver satisfactory results unless a large number of ground control points (GCPs) is regularly distributed in the mapped area. This may not be a feasible method either due to the associated costs or terrain inaccessibility.

This thesis addresses such issues by presenting a development of MAV platforms with navigation and imaging sensors that are able to perform integrated sensor orientation (ISO). This method combines image measurements with GNSS or GNSS/IMU (Global Navigation Satellite System/Inertial Measurement Unit) observations. This innovative approach allows mapping with cm-level accuracy without the support of GCPs, even in geometrically challenging scenarios, such as corridors. The presented solution also helps in situations where automatic image observations cannot be generated, e.g. over water, sand, or other surfaces with low variations of texture.

The application of ISO to MAV photogrammetry is a novel solution and its implementation brings new engineering and research challenges due to a limited payload capacity and quality of employed sensors on-board. These challenges are addressed using traditional as well as novel methods of treating observations within the developed processing software. The capability of the constructed MAV platforms and processing tools is tested in real mapping scenarios. It is empirically confirmed that accurate aerial control combined with a state-of-the-art calibration and processing can deliver cm-level ground accuracy, even in the most demanding projects.

This thesis also presents an innovative way of mission planning in challenging environments. Indeed, a thorough pre-flight analysis is important not only for obtaining satisfactory mapping quality, but photogrammetric missions must be carried out in compliance with state regulations.

Vehicle Dynamic Model Based Navigation for UAVs

M. Khaghani, J. Skaloud

EPFL – TOPO

The dominant navigation system for small civilian UAVs today is based on integration of inertial navigation system (INS) and global navigation satellite system (GNSS). This strategy works well to navigate the UAV, as long as proper reception of GNSS signal is maintained. However, when GNSS outage occurs, the INS-based navigation solution drifts very quickly, considering the limited quality of IMU(s) employed in INS for small UAVs. In beyond visual line of sight (BVLOS) flights, this poses the serious danger of losing the UAV and its eventual falling down.

Limited payload capacity and cost for small UAVs, as well as the need for operating in different conditions, with limited visibility for example, make it challenging to find a solution to reach higher levels of navigation autonomy based on conventional approaches.

This thesis aims to improve the accuracy of autonomous navigation for small UAVs by at least one order of magnitude. The proposed novel approach employs vehicle dynamic model (VDM) as process model within navigation system, and treats data from other sensors such as IMU, barometric altimeter, and GNSS receiver, whenever available, as observations within the system.

Such improvement comes with extra effort required to determine the VDM parameters for any specific UAV. This work investigates the internal capability of the proposed system for estimating VDM parameters as part of the augmented state vector within an extended Kalman filter (EKF) as the estimator. This reduces the efforts required to setup such navigation system that is platform dependent.

Multiple experimental flights using two custom made fixed-wing UAVs are presented together with Monte-Carlo simulations. The results reveal improvements of 1 to 2 orders of magnitude in navigation accuracy during GNSS outages of a few minutes' duration/

Monte-Carlo simulations were performed to assess the effects of random changes in sensor errors, initialization errors, and even wind velocity, which came from real measurement in all simulations. The uncertainty levels were also predicted consistently, which the observability discussions were based on.

Computational cost for the proposed VDM-based navigation does not exceed 3~times that of conventional INS-based systems, which establishes its applicability for online application.

A global sensitivity analysis is presented, spotting the VDM parameters with higher influence on navigation performance. This provides insight for design of calibration procedures.

The proposed VDM-based navigation system can be interesting for professional UAVs from at least two points of view. Firstly, it adds little to no extra hardware and cost to the UAV. Secondly and more importantly, it might be currently the only way to reach such significant improvement in navigation autonomy for small UAVs regardless of visibility conditions and electromagnetic signals reception. Possibly, such environmental condition independence for navigation system may be needed to obtain certifications from legal authorities to expand UAV applications to new types of mission.

Calibration aspects of INS Navigation

P. Clausen, J. Skaloud

EPFL - TOPO

The use of a Bayesian filter (e.g., Kalman filter) for the fusion of information from satellite positioning and inertial navigation is a common approach in many applications, where the knowledge of position, velocity, and attitude in space are of great interest. The correctness of these estimates depends on many factors, among others the quality of the sensor measurements and the errors within, which are directly reflected in the filter design. A calibration process allows compensating for deterministic influences (which in return improve for instance qualitatively the attitude initialization) and their inherent stochastic error signals required for filtering.

This thesis presents in the first part the development of methods to perform a thorough calibration of different sensors in-lab under controlled conditions and in-field for a simplified calibration with limited resources and equipment. The stochastic properties of error signals are analyzed in the second part. A novel approach called Generalized Method of Wavelet Moments (GMWM) allows investigating the error structure using wavelets, which is similar to the Allan variance. An intuitive online tool is presented, which grants simplified access to the GMWM framework that provides a consistent, identifiable, and computationally efficient estimation of stochastic model parameters. The parameters of these error models are then made dependent on an external covariate such as temperature or motion. Indeed, it is experimentally confirmed that these properties shape the stochastic behavior of the measurements and how the stochastic parameters relate functionally to the influence of the covariate. Later, such knowledge is included in the filter for the correct estimation of confidence levels.

The successful implementation of these proposed concepts is validated in a fully functional drone-system for mapping purposes. A real-time calibration scheme is applied first in-lab, later in-field to initialize the navigation processor. Apart from the benefit of achieving considerably better estimates of the attitude, and in case of satellite signal outage also of the position, the calibration allows for a simplified fusion of redundant inertial sensors. The improved performances through calibration and sensor redundancy are attractive to drone mapping applications relying on an accurate direct or integrated orientation such as lightweight airborne laser scanning systems or frame-cameras, which are utilized in the experiments.

Optimized Low Level Trajectories for Instrument Flight Rules in Alpine Areas

R. Pott¹, S. Guillaume^{1,2}, A. Geiger¹, and H. Wipf^{3,4}

¹⁾ Institute of Geodesy and Photogrammetry, ETH, Zürich, Switzerland

²⁾ Institut d'ingénierie du territoire, heig-vd, Yverdon-les-Bains, Switzerland

³⁾ Airnav Consulting, Switzerland

⁴⁾ Skyguide, Switzerland

In the framework of establishing ICAO's Performance Based Navigation (PBN) in Switzerland a number of special issues have been identified, especially for mountainous regions. The GNSS performance on aerial vehicles operating is of central importance for flight safety and operation efficiency, because the rugged topography might easily jeopardize the performance. Especially low-level operations in alpine areas need careful assessment of the protection levels and the GNSS performance. For the near future Switzerland's lower air space will primarily be operated based on PBN.

This work focuses onto the implementation of Instrument Flight Rules (IFR) predefined tracks for low-level transfer flights of helicopters through mountainous valleys. One of the main stakeholders of this ongoing research are Helicopter Emergency Medical Services (HEMS), which have to transfer patients in medical emergency from secondary hospitals in the Alps to primary ones in urban centers. Another domain of application is the military helicopter air transportation e.g. for disaster relief. Theoretical studies were conducted to assess the feasibility from the point of view of the GNSS performance. We devised a mathematical model, which allows assessing GNSS performance avoiding tedious simulations or expensive in-flight measurements. The use of continuous satellite distributions rather than discrete satellite positions leads to closed formulae describing the impact of erroneous or obstructed measurements. It becomes possible to quantify in a generalized manner the decrease of position's accuracy caused by descending into a valley.

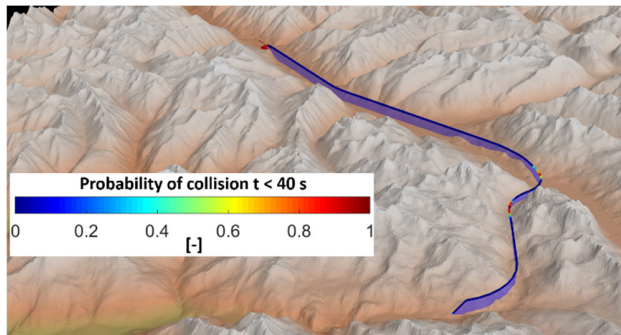


Figure 4.51: Optimized trajectory

Additionally an optimization algorithm was developed to automatically create the IFR low-level trajectory through a given valley. Different optimization parameters are taken into account such as height, which has to be low enough to avoid icing on the rotor blades. At the same time, the trajectory shall be constrained by an upper bound of collision probability with terrain and obstacles. These constraints of utmost importance asked for a rigorous probabilistic calculation. Not only the position's uncertainty is taken into consideration, but also the anticipated ground/obstacle collision probabilities, given the aircraft speed.

Traditionally, instrument flight procedures build on instructions from ICAO's Required Navigation Performance (RNP) documentations. This leads to geometrically rigid primary and secondary protection surfaces, a most conservative design. In consequence, for a flight path following a valley, the established RNP 0.3 designing procedure results in a non-optimal trajectory above the surrounding mountain peaks, prone for waste of time and fuel while running the chance of collecting ice. The probabilistic considerations enable the design of procedures without rigid protection areas. Currently, no method exists, which uses terrain and obstacle collision probabilities together with aircraft speed to devise an optimized flight path.

The computation of a field of collision probabilities is the basis of the trajectory optimization process, which takes into account the maximum tolerable terrain and obstacle collision probabilities, and creates the lowest and fastest flight path possible. The method is flexible when it comes to optimization parameters like smoothness (of importance for HEMS flights) and the terrain collision probabilities.



*Figure 4. 52: Full simulator at REGA's training center: A path, resulting from this optimization process, was entered into a full flight helicopter simulator. First simulator test flights proved the practicability of the results.
Foto: R. Pott*

The theoretical method devised gives a generic insight into error propagation within a satellite navigation system. Further, the development of optimization methods enables an automated process, and eliminates the need to delineate protection surfaces and allows for optimally adapting trajectories.

Bibliography Commission 4

- Altamimi, Z., P. Rebischung, L. Metivier, and X. Collilieux (2016). ITRF2014: A new release of the International Terrestrial Reference Frame modeling nonlinear station motions. *Journal of Geophysical Research, Solid Earth*, 121. doi:10.1002/2016JB013098
- Arnold, D., M. Meindl, G. Beutler, R. Dach, S. Schaer, S. Lutz, L. Prange, K. Sośnica, L. Mervart, A. Jäggi (2015). CODE's new solar radiation pressure model for GNSS orbit determination. *J Geod*, vol. 89(8), pp. 775-791. doi: 10.1007/s00190-015-0814-4.
- Aschbacher, J., Milagro-Pérez, M. (2012) The European Earth monitoring GMES programme: Status and perspectives. *Remote Sensing of Environment*, 120:3-8, doi:10.1016/j.rse.2011.08.028, 2012
- Bernet L., Mätzler L., Brockmann E., Kämpfer N., Hocke K. (2019): "Atmospheric water vapour trends in Switzerland based on data from ground-based microwave radiometry and GNSS ground stations", 16th European Geosciences Union – General Assembly, Vienna, Austria, 04/08 - 04/12/2019
- Bock, H., Jäggi, A., Švehla, D., Beutler, G., Hugentobler, H., Visser, P (2007): Precise orbit determination for the GOCE satellite using GPS. *Adv Space Res*, vol. 39(10), pp. 1638-1647, [DOI 10.1016/j.asr.2007.02.053](https://doi.org/10.1016/j.asr.2007.02.053)
- Bock, H., Jäggi, A., Beutler, G., Meyer, U. (2014): GOCE: Precise orbit determination for the entire mission. *J Geod*, vol. 88(11), pp. 1047-1060. [DOI 10.1007/s00190-014-0742-8](https://doi.org/10.1007/s00190-014-0742-8)
- Brockmann E., et al. (2015): "Multi-GNSS activities at EPN and at swisstopo", EUREF-TWG in Warsaw, March 23-24, 2015.
- Brockmann E. et al. (2015): "National Report of Switzerland", EUREF-Symposium in Leipzig, June 3-5, 2015.
- Brockmann E. (2015): "Reprocessed GNSS tropospheric products at swisstopo", GNSS4SWEC workshop, Thessaloniki, May 11-14, 2015.
- Brockmann E. et al. (2015): "Multi-GNSS activities at EPN and at swisstopo", EUREF-Symposium in Leipzig, June 3-5, 2015.
- Brockmann E. (2015): "Impact of GLONASS on reprocessed Zenith Total Delay Estimates", GNSS4SWEC workshop, Wrocław, September 29 – 30, 2015.
- Brockmann E. (2015): "swisstopo Report for EGVAP 2015", EGVAP expert meeting, Wrocław, October 1, 2015.
- Brockmann E., et al. (2015): "Multi-GNSS activities at EPN and at swisstopo", EUREF-TWG in Bern, October 13, 2015.
- Brockmann E., D. Andrey, D. Ineichen, L. Kislig, J. Liechti, S. Lutz, C. Misslin, S. Schaer and U. Wild (2016): "Automated GPS Network in Switzerland (AGNES)", International Foundation HFSJG, Activity Report 2016, University of Bern, 2016.
- Brockmann E. et al. (2016): "National Report of Switzerland", EUREF-Symposium in SanSebastian, Spain, 25-27 May, 2016
- Brockmann E. (2016): "swisstopo Report for EGVAP 2016", EGVAP expert meeting, Copenhagen Dec 6-7, 2016.
- Brockmann E., D. Andrey, D. Ineichen, L. Kislig, J. Liechti, S. Lutz, S. Schaer and U. Wild (2017): "Automated GPS Network in Switzerland (AGNES)", International Foundation HFSJG, Activity Report 2017, University of Bern, 2017.

- Brockmann E. et al. (2017): “National Report of Switzerland”, EUREF-Symposium in Wroclaw, Poland, May 17-19, 2017
- Brockmann E., S. Lutz, D. Ineichen, S. Schaer (2017): “Multi-GNSS developments for the EPN and for the Swiss networks”, EUREF-Symposium in Wroclaw, Poland, May 17-19, 2017
- Brockmann E., S. Lutz, D. Ineichen, S. Schaer (2017): “Impact of Multi-GNSS analysis on precise geodetic applications”, IAG-IASPEI scientific Assembly in Kobe, Japan, July 30 – August 4, 2017
- Brockmann E. (2017): “swisstopo Report for EGVAP 2017”, EGVAP expert meeting, DeBilt Nov. 28-29, 2017.
- Brockmann E., D. Andrey, D. Ineichen, L. Kislig, J. Liechti, S. Lutz, and U. Wild (2018): "Automated GPS Network in Switzerland (AGNES)", International Foundation HFSJG, Activity Report 2018, University of Bern, 2018.
- Bürki, B., Guillaume, S. (2016): Astrogeodätische Lotabweichungs- und Azimutmessungen für AlpTransit / Mesures astro-géodésiques des déviations de la vertical et des azimuts pour AlpTransit / Astro-geodetic measurements of vertical deflections and azimuths for AlpTransit. In the Special Edition of *Geomatik-Schweiz* for the AlpTransit Gotthard Base Tunnel (in german, french and english). S. 82 - 89 (dt.), p. 79 - 85 (fr.), p. 77 - 83 (engl.).
- Cabinet Office (CAO), Government of Japan (2017). QZSS Satellite Information. URL: <http://qzss.go.jp/en/technical/qzssinfo>
- Clinton, J., Geiger, A., Häberling, S., Haslinger, F., Rothacher, M., Wiget, A., Wild, U. (2017): The Future of National GNSS-Geomonitoring Infrastructures in Switzerland. *Geodätisch-geophysikalische Arbeiten in der Schweiz*, Vol. 100. <http://www.sgc.ethz.ch/sgc-volumes/sgk-100.pdf>
- Dach, R., Lutz, S., Walser, P., Fridez, P. (Eds); 2015: Bernese GNSS Software Version 5.2. User manual, Astronomical Institute, University of Bern, Bern Open Publishing. DOI: 10.7892/boris.72297; ISBN: 978-3-906813-05-9
- Dach, R., Schaer, S., Arnold, D., Prange, L., Sidorov, D., Stebler, P., Villiger, A., Jäggi, A. (2018): CODE final product series for the IGS. Published by Astronomical Institute, University of Bern. URL: <http://www.aiub.unibe.ch/download/CODE>; DOI: 10.7892/boris.75876.3.
- Fernández, J, Escobar, D., Águeda, F. et al. (2014) Sentinels POD Service Operations, SpaceOps 2014 Conference, SpaceOps Conferences, AIAA 2014-1929, doi:10.2514/6.2014-1929, 2014
- Fernández, J, Escobar, D, Peter, H, Féménias, P (2015) Copernicus POD service operations – Orbital accuracy of Sentinel-1A and Sentinel-2A. Proc. Int. Symp. Space Flight Dyn, pp 1-14
- Fernández, J, Fernández C, Féménias, P, Peter, H. (2016) The Copernicus Sentinel-3 mission. ILRS workshop, p. 1-4
- Floberghagen R., Fehringer M., Lamarre D., Muzi D., Frommknecht B., Steiger C., Pineiro J., da Costa A., 2011, Mission design, operation and exploitation of the gravity field and steady-state ocean circulation explorer mission. *J Geod*, 85(11), 749-758; DOI 10.1007/s00190-011-0498-3.
- Geiger, A., K. Wang, M. Meindl, M. Rothacher, M. Scaramuzza, M. Troller, P. Truffer (2015): Non-ionosphere biases in the single-difference ionospheric residuals, Proc.: European Navigation Conference, ENC2015, Bordeaux.

- Geiger, A., Schlatter, A. (2016): Von der Potenzialtheorie zu den Senkungen am Gotthardpass / De la théorie du potential aux tassements déclinés au col du Sainth-Gothard / From potential theory to the subsidences at the Gotthard Pass. In the Special Edition of *Geomatik-Schweiz* for the AlpTransit Gotthard Base Tunnel (in german, french and english). S. 90 - 91 (dt.), p. 86 - 87 (fr.), p. 84 - 85 (engl.).
- GSA (2016a) Galileo IOV and FOC Satellite Antenna Calibrations, SINEX code GSAT_1934, URL https://www.gsc-europa.eu/sites/default/files/sites/all/files/ANTEX_GAL_FOC_IOV.atx (accessed 18/01/26)
- GSA (2016b) Galileo IOV and FOC satellite metadata, URL <https://www.gsc-europa.eu/support-to-developers/galileo-iov-satellite-metadata> (accessed 18/01/26)
- Hügi, F. (2017): Strahlungstests für den Weltraumeinsatz der u-blox NEO-M8T GNSS-Empfänger am PSI. Bachelor thesis, Institute of Geodesy and Photogrammetry, ETH Zürich.
- IERS Conventions (2010). Petit, G. and Luzum, B. (eds.). (IERS Technical Note ; 36) Frankfurt am Main: Verlag des Bundesamts für Kartographie und Geodäsie, 2010. 179 pp., ISBN 3-89888-989-6
- Ineichen D., E. Brockmann, S. Lutz, S. Schaer (2015): “Reprocessing activities at swisstopo (LPT)”, EUREF-LAC Workshop in Bern, October 14-15, 2015.
- Ingenieur-Geometer Schweiz (IGS) (2016): Ingenieur-Geometer im längsten Tunnel der Welt / Les ingénieurs-géomètres dans le plus long tunnel du monde / The surveyors in the longest tunnel of the world. Special Edition of *Geomatik-Schweiz* for the AlpTransit Gotthard Base Tunnel (in german, french and english).
- Jäggi, A., Bock, H., Meyer, U., Beutler, G., van den Ijssel, J. (2015): GOCE: assessment of GPS-only gravity field determination. *J Geod*, vol. 89(1), pp. 33-48. DOI [10.1007/s00190-014-0759-z](https://doi.org/10.1007/s00190-014-0759-z)
- Januth, T. (2017) Robot validation with the QDaedalus system: Integration of a robot in a global reference frame». Master Thesis, HES-SO, Yverdon, Switzerland.
- Johnston, G., Riddell, A., Hausler, G. (2017). The International GNSS Service. In Teunissen, Peter J.G., & Montenbruck, O. (Eds.), *Springer Handbook of Global Navigation Satellite Systems* (1st ed., pp. 967-982). Cham, Switzerland: Springer International Publishing, DOI: [10.1007/978-3-319-42928-1](https://doi.org/10.1007/978-3-319-42928-1)
- Lutz S., S. Schaer, D. Ineichen, E. Brockmann (2015): “Multi-GNSS analysis at swisstopo: Developments and first results”, EUREF-LAC Workshop in Bern, October 14-15, 2015.
- Lutz, S., Schaer, S., Meindl, M., Dach, R., Steigenberger, P. (2009): Higher-order ionosphere modeling for CODE's next reprocessing activities. AGU 2009 Fall Meeting, San Francisco, CA, USA, December 14-18, 2009.
- Lutz, S., Schaer, S., Meindl, M., Dach, R., Steigenberger, P. (2010): Higher-Order Ionosphere Modeling for CODE's Next Reprocessing Activities. IGS Workshop 2010, Newcastle upon Tyne, England, 28 June-2 July, 2010.
- Meyer, U., Grahsl, A., Dach, R., Jäggi, A. (2019): Low-degree time-variable gravity fields from satellite laser ranging; this volume.
- Montenbruck O, Rizos C, Weber, R, Weber G, Neilan RE, Hugentobler U (2013). Getting a Grip on Multi-GNSS: The International GNSS Service MGEX Campaign, *GPS World*, 24(7), pp. 44–49, 2013
- Pacione, R.; Araszkievicz, A.; Brockmann, E.; Douša, J. (2017) EPN-Repro2: A reference GNSS tropospheric data set over Europe, *Atmos. Meas. Tech.*, 10, 1689-1705. doi:10.5194/amt-10-1689-2017.

- Peter, H, Jäggi, A., Fernández, J, Escobar, D, Ayuga, F, Arnold, D, Wermuth, M, Hackel, S, Otten, M, Simons, W, Visser, PN (2017) Sentinel-1A – First precise orbit determination results. *Adv Space Res*, 60(5): 879-892; doi 10.1016/j.asr.2017.05.034
- Prange, L. R. Dach, S. Lutz, S. Schaer, A. Jäggi; 2016: The CODE MGEX orbit and clock solution. In *IAG 150 years, IAG Symposia*, edited by Chr. Rizos and P. Willis, pp 767-773. doi: 10.1007/1345_2015_161
- Prange, L., Orliac E., Dach R., Arnold D., Beutler G., Schaer S., Jäggi A.; 2017: CODE five-system orbit and clock solution – the challenges of multi-GNSS data analysis. *J Geod*, vol 91(4), pp345-360. doi:10.1007/s00190-016-0968-8t
- Prange, L., Arnold, D., Dach, R., Schaer, S., Sidorov, D., Stebler, P., Sušnik, A., Villiger, A. Jäggi, A. (2019a): CODE five system solution for the IGS MGEX; this volume.
- Prange L, Beutler G, Dach R, Arnold D, Schaer S, Villiger A, Jäggi A (2019b): An empirical SRP model for the orbit normal attitude mode; this volume.
- Scaramuzza, M. (2016): Localization of GNSS RFI Transmitters Using Digital Surface Models, Proc.: IFIS 2016, 13.-17. June 2016, Belgrade, Serbia.
- Scaramuzza, M., P. Truffer, M. Troller, H. Leibundgut, M. Bertschi (2017): Quality Assessment of GNSS Simulations for Flight Procedures based on Onboard Recorded Flight Data. Proceedings of the 30th International Technical Meeting of The Satellite Division of the Institute of Navigation (ION GNSS+ 2017), Portland, Oregon, September 2017, pp. 1633-1643.
- Scaramuzza, M., P. Truffer, M. Troller, H. Wipf, H. Leibundgut, M. Bertschi, S. Rämi (2016): Empirical Assessment and Modelling of RFI Impact on Aviation GPS/SBAS Receiver Performance. Proceedings of the 29th International Technical Meeting of The Satellite Division of the Institute of Navigation (ION GNSS+ 2016), Portland, Oregon, September 2016, p. 3063 – 3069.
- Scaramuzza, M., H. Wipf, M. Troller, H. Leibundgut, S. Rämi, R. Wittwer (2015): GNSS RFI Detection: Finding the Needle in the Haystack, Proceedings of the 28th International Technical Meeting of The Satellite Division of the Institute of Navigation (ION GNSS+ 2015), Tampa, Florida, September 2015, pp. 1617-1624.
- Schaer S, Arnold D, Dach R, Prange L, Sidorov D, Stebler P, Sušnik A, Villiger A, Jäggi A (2019a): CODE Contributions to the IGS; this volume.
- Schaer S, Arnold D, Dach R, Prange L, Sidorov D, Stebler P, Sušnik A, Villiger A, Jäggi A (2019b): EUREF Activities at CODE; this volume.
- Schaer S, Villiger A, Arnold D, Prange L, Dach R, Jäggi A (2019c): Ambiguity Resolution in Zero-Difference Solutions and for PPP; this volume.
- Schaer, S. (2014): CODE GIM products with 1-hour resolution, IGSMail-6993, IGS Central Bureau Information System.
- Schaer, S., A. Villiger, R. Dach, L. Prange, A. Jäggi (2018): New ambiguity-fixed IGS clock analysis products at CODE. IGS Workshop 2018, Wuhan, China, 29 October – 2 November 2018.
- Schaer S, Villiger A, Arnold D, Prange L, Dach R, Jäggi A (2019): Ambiguity Resolution in Zero-Difference Solutions and for PPP; this volume.

- Schlatter, A., Marti, U., Wiget, A. (2016): AlpTransit-Gotthard-Basistunnel – Aspekte zu den Themen Schwerefeld, Höhe und Geodynamik / AlpTransit Gotthard base tunnel – Aspects of gravity field, heights and geodynamics. *Allgemeine Vermessungs-Nachrichten AVN 123* (2016) 7, S. 199 – 206.
- Schmid R., Dach R., Collilieux X., Jaeggi A., Schmitz M., Dilssner F. (2016) Absolute IGS antenna phase center model igs08.atx: status and potential improvements. *J Geod* 90(4): 343-364, doi: 10.1007/s00190-015-0876-3
- Sidorov, S., Dach, R., Prange, L., Jäggi, A. (2019): Advancing the orbit model for Galileo satellites during the eclipse seasons; this volume.
- Steigenberger P., Fritsche M., Dach R., Schmid R., Montenbruck O., Uhlemann M., Prange L. (2016): Estimation satellite antenna phase center offsets for Galileo, *J Geod* 90(8): 773–785, doi: 10.1007/s00190-016-0909-6
- Steiner, L., M. Meindl, and A. Geiger (2018), Characteristics and Limitations of GPS L1 Observations from Submerged Antennas, *Journal of Geodesy*, vol. 93, no. 2, pp. 267 - 280.
- Steiner, L., M. Meindl, C. Fierz, and A. Geiger (2018), An assessment of Sub-Snow GPS for Quantification of Snow Water Equivalent, *The Cryosphere*, vol. 12, pp. 3161 - 3175.
- Steiner, L., M. Meindl, C. Fierz, C. Marty, and A. Geiger, Monitoring Snow Water Equivalent Using Low-Cost GPS Antennas Buried Underneath a Snowpack (2019), *Proceedings of the 13th European Conference on Antennas and Propagation*, Krakow, Poland, April 2019.
- Steiner, L., M. Meindl, C. Marty, and A. Geiger (2019), Impact of GPS Processing on the Estimation of Snow Water Equivalent Using Refracted GPS Signals, *IEEE Transactions on Geoscience and Remote Sensing*, in review.
- Steiner, L., W. Li, Y. Zhu, M. Meindl, D. Yang, and A. Geiger, Snow Depth and Snow Water Equivalent Monitoring by Using Reflected and Refracted GPS Signals, *Journal of Remote Sensing*, 2019, in review.
- Sušnik, A., Grahsl, A., Arnold, D., Villiger, A., Dach, R., Jäggi, A., Beutler, G. (2019): GNSS reprocessing results in the framework of the EGSIM project, this volume.
- Troller, M., M. Scaramuzza, H. Leibundgut, M. Bertschi (2017): Assessment and Modelling of Avionics EGNOS Protection Levels. *Proceedings of the European Navigation Conference, ENC2016, Lausanne, May 2017.*
- Troller, M., M. Scaramuzza, H. Leibundgut, M. Bertschi (2018): Assessment and Modelling of Avionics EGNOS Protection Levels., *European Journal of Navigation*, 16(1):11-18.
- Troller, M., M. Scaramuzza, P. Truffer, A. Geiger (2017): Assessment of the GPS Constellation Variation and its Impact to the Navigation Performance in Mountainous Area. *Proceedings of the International Symposium on Precision Approach and Performance Based Navigation, ISPA 2017, DGON, Munich, November 2017.*
- Troller, M., M. Scaramuzza, M. Nyffenegger, S. Rämi, M. Bertschi (2016): Performance of environmental-friendly GNSS-based curved approach flight procedure, *European Journal of Navigation*, 14(5):21-30.
- Troller, M., M. Scaramuzza, M. Nyffenegger, S. Rämi, M. Bertschi (2016): Performance of environmental-friendly GNSS-based curved approach flight procedure, *Proc.: European Navigation Conference, ENC2016, Helsinki.*

- Troller, M., M. Scaramuzza, H. Wipf, M. Nyffenegger, H. Leibundgut (2016): Flight Performance Investigations of Enhanced Rotorcraft Operations in Mountainous Areas – Towards a More Ambitious RNP Performance, Proceedings of the 29th International Technical Meeting of The Satellite Division of the Institute of Navigation (ION GNSS+ 2016), Portland, Oregon, September 2016, pp. 3660-3668.
- Truffer, P., M. Scaramuzza, M. Troller (2017): Assessment of the susceptibility of pseudo range to RF interference. Abstract of the International Symposium on Precision Approach and Performance Based Navigation, ISPA 2017, DGON, Munich, November 2017.
- Truffer, P., M. Scaramuzza, M. Troller (2017): Field Test of Susceptibility of Aviation GPS Receivers to Radio Frequency Interference. Proceedings of the European Navigation Conference, ENC2016, Lausanne, May 2017.
- Truffer, P., M. Scaramuzza, M. Troller (2017): Field Test of Susceptibility of Aviation GPS Receivers to Radio Frequency Interference. European Journal of Navigation, 15(2):4-10.
- Truffer, P., M. Scaramuzza, M. Troller, M. Bertschi (2017): Jamming of Aviation GPS Receivers: Investigation of Field Trials Performed with Civil and Military Aircraft. Proceedings of the 30th International Technical Meeting of The Satellite Division of the Institute of Navigation (ION GNSS+ 2017), Portland, Oregon, September 2017, pp. 1258-1266.
- u-blox (2016): NEO/LEA-M8T u-blox M8 concurrent GNSS timing modules – data sheet. u-blox, Switzerland.
- Villiger, A., Prange, L., Dach, R., Zimmermann, F., Kuhlmann, H., Jäggi, A. (2019a): Consistency of antenna products in the MGEX environment; this volume
- Villiger, A., Schaer, S., Dach, R., Prange, L., Sušnik, A., Jäggi, A. (2019b): Determination of GNSS pseudo-absolute code biases and classification of receiver tracking technology; this volume
- Villiger, A., Schaer, S., Dach, R., Prange, L., Sušnik, A., Jäggi, A. (2019): Determination of GNSS pseudo-absolute code biases and their long-term combination, J Geod (in review)
- Wiget, A., Marti, U., Schlatter, A. (2016): Beiträge der Landesvermessung zum AlpTransit Gotthard Basistunnel / Contributions de la mensuration nationale au tunnel de base du Saint-Gothard, coeur du projet AlpTransit / National Surveying contributions to the AlpTransit Gotthard Base Tunnel. In the Special Edition of *Geomatik-Schweiz* for the AlpTransit Gotthard Base Tunnel (in german, french and english). S. 43 - 49 (dt.), p. 41 - 47 (fr.), p. 39 - 45 (engl.).
- Willi, D (2019): GNSS receiver synchronisation and antenna calibration. Doctoral Thesis, ETH Zurich, Zurich, Switzerland, <https://doi.org/10.3929/ethz-b-000308750>.
- Willi, D, Guillaume S. (2019): Calibration of a six-axis robot for GNSS antenna phase center estimation. Journal of Surveying engineering. Accepted for publication.
- Willi, D., Koch, D., Meindl, M., Rothacher, M. (2018): Absolute GNSS Antenna Phase Center Calibration with a Robot. In: Proceedings of the 31st International Technical Meeting of The Satellite Division of the Institute of Navigation (ION GNSS+ 2018), Miami, FL, USA, pp. 3909-3926.
- Willi, D., Rothacher, M. (2017): GNSS attitude determination with non-synchronized receivers and short baselines onboard a spacecraft, GPS Sol, <https://doi.org/10.1007/s10291-017-0639-0>